Aurora-A prevents transcription-replication conflicts in *MYCN*-amplified neuroblastoma

Aurora-A verhindert Transkriptions-Replikationskonflikte in *MYCN*-amplifizierten Neuroblastomen

Doctoral thesis

for a doctoral degree

at the Graduate School of Life Sciences

Julius-Maximilians-Universität Würzburg,

Section: Biomedicine

submitted by

Isabelle Röschert

from Ober-Hilbersheim

Würzburg 2021

Members of the thesis committee:

Chairperson:	Prof. Alexander Buchberger
Primary supervisor:	Prof. Martin Eilers
Second supervisor:	Prof. Manfred Gessler
Third supervisor:	Prof. Stefan Knapp

Submitted on:

Date of Public Defense:

Date of Receipt of Certificates:

Substantial part of this thesis was published in the following article:

Roeschert I.*, Poon E.*, Henssen A.G., Dorado-Garcia H., Gatti M., Giansanti C., Jamin Y., Ade C.P., Gallant P., Schülein-Völk C., Beli P., Richards M., Rosenfeldt M., Altmeyer M., Anderson J., Eggert A., Dobbelstein M., Bayliss R., Chesler L., Büchel G. & Eilers M. (2021): Combined inhibition of Aurora-A and ATR kinases results in regression of *MYCN*-amplified neuroblastoma. *Nature Cancer,* https://doi.org/10.1038/s43018-020-00171-8

* authors contributed equally

Content

Summary

Neuroblastoma is the most abundant, solid, extracranial tumor in early childhood and the leading cause of cancer-related childhood deaths worldwide. Patients with high-risk neuroblastoma often show *MYCN*-amplification and elevated levels of Aurora-A. They have a low overall survival and despite multimodal therapy options a poor therapeutic prognosis. *MYCN*-amplified neuroblastoma cells depend on Aurora-A functionality. Aurora-A stabilizes MYCN and prevents it from proteasomal degradation by competing with the E3 ligase SCF^{FBXW7}. Interaction between Aurora-A and MYCN can be observed only in S phase of the cell cycle and activation of Aurora-A can be induced by MYCN *in vitro*. These findings suggest the existence of a profound interconnection between Aurora-A and MYCN in S phase. Nevertheless, the details remain elusive and were investigated in this study.

Fractionation experiments show that Aurora-A is recruited to chromatin in S phase in a MYCN-dependent manner. Albeit being unphosphorylated on the activating T288 residue, Aurora-A kinase activity was still present in S phase and several putative, novel targets were identified by phosphoproteomic analysis. Particularly, eight phosphosites dependent on MYCN-activated Aurora-A were identified. Additionally, phosphorylation of serine 10 on histone 3 was verified as a target of this complex in S phase. ChIP-sequencing experiments reveal that Aurora-A regulates transcription elongation as well as histone H3.3 variant incorporation in S phase. 4sU-sequencing as well as immunoblotting demonstrated that Aurora-A activity impacts splicing. PLA measurements between the transcription and replication machinery revealed that Aurora-A prevents the formation of transcription-replication conflicts, which activate of kinase ATR.

Aurora-A inhibitors are already used to treat neuroblastoma but display dose-limiting toxicity. To further improve Aurora-A based therapies, we investigated whether low doses of Aurora-A inhibitor combined with ATR inhibitor could increase the efficacy of the treatment albeit reducing toxicity. The study shows that the combination of both drugs leads to a reduction in cell growth as well as an increase in apoptosis in *MYCN*-amplified neuroblastoma cells, which is not observable in *MYCN* non-amplified neuroblastoma cells. This new approach was also tested by a collaboration partner *in vivo* resulting in a decrease in tumor burden, an increase in overall survival and a cure of 25% of TH-MYCN mice. These findings indicate indeed a therapeutic window for targeting *MYCN*-amplified neuroblastoma.

Zusammenfassung

Das Neuroblastom ist der häufigste, solide, extrakranielle Tumor der frühesten Kindheit und die häufigste mit Krebs verbundene Todesursache von Kleinkindern weltweit. Patienten mit geringerer Überlebenswahrscheinlichkeit und schlechterer Therapieprognose zeigen oft eine *MYCN*-Amplifikation und erhöhte Mengen von Aurora-A. Aurora-A ist eine Serin/Threonin-Protein Kinase, die wichtige mitotische Prozesse reguliert. Aurora-A stabilisiert MYCN und verhindert dadurch den proteasomalen Abbau von MYCN. Die Interaktion zwischen Aurora-A und MYCN ist S Phasen-spezifisch und MYCN ist *in vitro* in der Lage, durch seine Bindung Aurora-A zu aktivieren.

Die Funktionen und Prozesse, die von Aurora-A in der S Phase reguliert werden, sind noch nicht hinreichend untersucht und daher Gegenstand dieser Dissertation.

Zell-Fraktionierungen zeigen, dass Aurora-A in der S Phase in einer MYCN-abhängigen Weise an das Chromatin gebunden ist. Phosphoproteom-Analysen mittels Massenspektrometrie identifizierten zahlreiche neue Substrate von Aurora-A, sowie acht Substrate von MYCN-aktiviertem Aurora-A. Zusätzlich konnte gezeigt werden, dass Histon 3 Serin 10 von Aurora-A in Abhängigkeit von MYCN in S Phase phosphoryliert wird. ChIP-Sequenzierungen zeigen, dass Aurora-A die Elongation der Transkription und den Einbau der Histone Variante H3.3 in S Phase beeinflusst. 4sU-Sequenzierung sowie Immunoblots zeigen einen Zusammenhang zwischen der Aktivität von Aurora-A und dem Spleißosom in der S Phase. Zusätzlich konnte mittels PLA nachgewiesen werden, dass Aurora-A die Entstehung von Transkriptions-Replikationskonflikten verhindert, die andernfalls die Kinase ATR aktivieren würden.

Aurora-A Inhibitoren wurden unter anderem zur Therapie von Neuroblastomen eingesetzt, allerdings ist die Dosis des Aurora-A Inhibitors durch die hohe Toxizität limitiert, was die Effizienz der Therapie stark beeinträchtigt. Daher wurde untersucht, ob die gleichzeitige Gabe von geringeren Mengen Aurora-A Inhibitor in Kombination mit einem ATR Inhibitor zur Therapie geeignet ist. *In vitro* konnte gezeigt werden, dass die Kombination beider Inhibitoren das Zellwachstum reduziert und das *MYCN*-amplifizierte Zellen im Vergleich zu *MYCN* nicht-amplifizierten Zellen verstärkt durch Apoptose sterben. Durch einen Kollaborationspartner konnte die Kombination der beiden Inhibitoren an Mäusen getestet werden. Die mit der Kombination behandelten Mäuse, zeigen ein deutlich reduziertes Tumorwachstum, sowie längeres Überleben. Somit stellt diese Kombination ein therapeutisches Fenster dar und könnte zur Behandlung von Neuroblastompatienten genutzt werden.

1 Introduction

1.1 Neuroblastoma

Cancer is, after cardiovascular diseases, the second most common cause of death for people worldwide. In 2018, 18 million new cancer cases occurred and about 9.5 million people died because of cancer (WHO, 2020).

Cancer is a disease with various subtypes, each characterized by an abnormal cell growth due to an unlimited number of cell divisions. It is a very heterogeneous disease and the probability to get cancer varies with age, gender, and genetic factors. There are characteristic risk factors for different kinds of tumors.

More than 11,000 children have been diagnosed with cancer in 2019 in the US. Pediatric cancer is, after accidents, the second most common reason for children to die (Siegel et al., 2019). The most common cancer types in children under the age of 14 years are shown in Figure 1.1. Acute lymphocytic leukemia (26%) is the most abundant type of cancer in children, followed by cancers developing in the brain and central nervous system (CNS; 21%). The third most common type of cancer in childhood is neuroblastoma with 7% of all childhood tumor cases. Neuroblastoma is most commonly diagnosed in the first year of life (American Cancer Society, 2014).

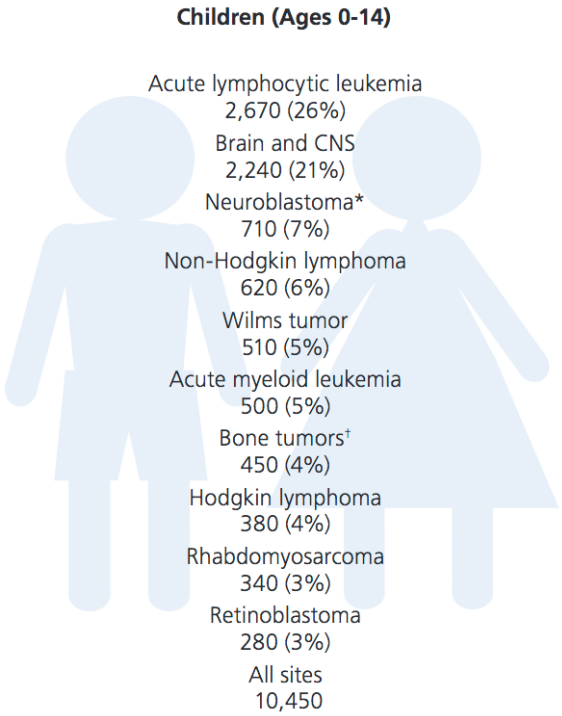

Figure 1.1: The most abundant cancer types in children under the age of 14.
This Figure was published in similar form by the American Cancer Society, 2014.

Neuroblastoma accounts for 15% of cancer related deaths of children and is therefore the most common, deadly, solid, extracranial tumor in early childhood (Schulte & Eggert, 2015).

Additionally, neuroblastoma is with 97% of the cases the most common tumor of the sympathetic nervous system. Neuroblastoma derives from a developing and incompletely committed precursor cell from the neuronal crest tissue, which is called neuroblast (Hoehner et al., 1996). The tumor arises along the sympathetic nervous system mainly at the adrenal glands and the paraspinal ganglia, but it can also occur in the nervous tissues of neck, chest, and abdomen (Ries et al., 1999). At the time of diagnosis, around 50% of the tumors already have metastasized (Maris et al., 2007). Metastases mainly occur in the bone marrow, bone, lymph nodes, liver, and brain (DuBois et al., 1999).

Neuroblastomas are clinically as well as biologically very heterogeneous tumors. Their cellular heterogeneity is suggested to cause the wide range of clinical indications and the diverse response to treatment. On one hand neuroblastomas have the highest proportion of spontaneous and complete regression especially in very young patients. On the other hand, there are high-risk neuroblastomas which have a poor prognosis despite multimodal therapy (Ngan, 2015; Yamamoto et al., 1998; Carlsen, 1990).

Therapy leading to survival of children improved over the last decades. The 5-year survival increased from 58% in the mid-1970s to 83% in 2014 (Schulte & Eggert, 2015).

1.1.1 Classification systems

Since the mid-1990s, the International Neuroblastoma Staging System (INSS) is used to classify neuroblastoma. Depending on the localization and the spreading of the primary tumor the patients can be divided in six stages (1, 2A, 2B, 3, 4, 4S). The staging which only relies on the localization and spread of the tumor cannot give reliable prognosis for individual patients. Therefore, additional factors are essential like age of the patient, as well as tumor-specific markers.

For that reason, a second classification system made by the Children´s Oncology Group is commonly used to define risk of neuroblastoma patients. Patients are classified into three groups (low, intermediate, or high) according to age, tumor histology, DNA ploidy, and *MYCN*-amplification status (American Cancer Society).

The outcome of neuroblastomas largely depends on their stage. Low-risk tumors often regress spontaneously or differentiate into benign ganglioneuroma. High-risk neuroblastomas almost-always relapse despite therapy. 50% of high-risk neuroblastoma show a *MYCN*-amplification which is therefore considered as an adverse prognostic factor (Seeger et al., 1985).

1.1.2 Prognostic features

As mentioned above there are further prognostic features which define the outcome and thereby the risk group of neuroblastoma patients. The categories which are used as prognostic features are age, tumor histology, mutations, DNA ploidy, or chromosomal anomalies. They are further explained and discussed:

Age

The age of the patient at diagnosis is the best predictor for the therapy outcome (Moroz et al., 2011). 88% of children survive when the age at diagnosis is less than 18 months. When the patient is older than 18 months and younger than 12 years the survival probability is 49% which further decreases to 10% in patients older than 12 years (Cohn et al., 2009; Franks et al., 1997). According to the neuroblastoma study NB97 performed in 2002, patients younger than one year are most often found in classes with better prognosis (1, 2A, 2B, 3, or 4S), whereas the majority of patients older than one year are found in the unfavourable class (4). This is also reflected in the five-year survival, were children younger than one year (85%) survive more often compared to patients older than one year (42%; NB97, 2002).

Tumor histology

Tumor histology is used by the International Neuroblastoma Pathology Classification (INPC) to classify neuroblastomas based on the Shimada Index (Sano et al., 2006; Shimada et al., 1999; Shimada et al., 1984). The Shimada Index is a tool for histopathological classification to define clinical aggressiveness of peripheral neuroblastic tumors. The Index is based on the patient age, degree of differentiation, and Mitosis-Karyorrhexis Index (defined as percentage of the sum of mitotic cells and cells with fragmented nuclei; Sano et al., 2006). Based on recent findings, it is suggested to stratify patients according to the immunohistochemistry (IHC) staining of MYCN-, TERT-, and ALT-status since these staining give insights about the survival benefits (Ikegaki et al., 2019). Patients with *MYCN*-amplification, TERT-overexpression, or ALT-loss are considered as high-risk patient with unfavourable histology, whereas all other patients would be considered as low-risk patients with favourable histology. IHC staining of MYC family members is already incorporated into some pathologic analyses (Wang et al., 2015).

Heritable germline and somatic mutations

The majority of neuroblastoma arises spontaneously. Only a small subset of neuroblastoma is familial and is usually related to mutations in paired-like homeobox 2b (*PHOX2B*) and anaplastic lymphoma kinase (*ALK*) genes.

The first discovered genetic predisposition regards mutations in *PHOX2B* which either lead to a truncation of the protein or are found in the homeobox resulting in a loss of DNA binding (Bourdeaut et al., 2005; Mosse et al., 2004; Trochet et al., 2004). The transcription factor

enables cell cycle exit and regulates differentiation of neuronal progenitors (Pattyn et al., 1999). Mutations in *PHOX2B* are found in 6-10% of familial neuroblastoma cases (Raabe et al., 2008; Mosse et al., 2004).

The second known genetic predisposition was found in *ALK* in 2008 (Janoueix-Lerosey et al., 2008; Mosse et al., 2008). Mainly three missense mutations (R1192P, R1275Q, and G1128A) occur within the kinase domain of ALK, found in the majority of familial as well as in up to 12% of the sporadic cases (Chen et al., 2008; George et al., 2008). The membrane bound receptor regulates several important signalling pathways like PI3K, JAK/STAT, and MAPK pathways (reviewed in Hallberg & Palmer, 2016). Crosstalk between ALK and other proteins involved in neuroblastoma has been observed, since overexpression of *PHOX2B* increases the expression of *ALK* (Bachetti et al., 2010) and ALK has also been identified to cooperate with MYCN in tumorigenesis (Schnepp et al., 2015).

Besides the germline mutations also somatic mutation have been identified in neuroblastoma patients. Somatic mutations often found in neuroblastoma involve the tumor suppressor *ATRX* (Cheung et al., 2012). 19 different mutations in *ATRX* have been found in neuroblastoma patients. The mutations can occur on various sites, although 15 of those mutations result in a truncation of the protein (Zeineldin et al., 2020). Patients with *ATRX* mutation are usually older than five years and therefore have an unfavourable prognosis. ATRX recognized guanine-rich stretches in DNA, often occurring at telomeres. Additionally, it positions the histone variant H3.3 to prevent the formation of G-quadruplex (G4) structures, known to interfere with replication and transcription (Clynes et al., 2013; Clynes & Gibbons, 2013). Loss of ATRX results in homologous recombination at telomeres which in turn results in the alternative lengthening of telomeres (ALT; Clynes et al., 2015). *ATRX* mutations are mutually exclusive with *MYCN*-amplification (Zeineldin et al., 2020).

Besides *ATRX* mutations, also mutations or focal deletions in AT-rich interactive domain 1A gene (*ARID1A*) and/or 1B gene (*ARID1B*) have been observed in 11% of neuroblastoma cases. Those alterations result in a truncated protein with loss in two domains required for DNA binding and interaction with topoisomerase II (TOP2; Sausen et al., 2013).

Additionally, mutations in *TIAM1* have been identified to frequently (3%) occur in neuroblastoma cases (Molenaar et al., 2012). TIAM1 is a guanine regulatory exchange factor for the GTPase Rac and is a regulator of cytoskeleton organization and neuritogenesis (Matsuo et al., 2003; Leeuwen et al., 1997). The mutations identified in neuroblastoma result in a truncation of the protein or are predicted as damaging for the protein (Molenaar et al., 2012).

<u>DNA ploidy</u>

Eckenschlager et al., performed a study to correlate DNA ploidy with prognosis in neuroblastoma patients not yet treated. Aneuploidy of DNA was correlated with low clinical

stage, young patients, as well as no *MYCN*-amplification and the overall survival was increased in those patients (Eckschlager et al., 1996).

Chromosomal anomalies

Some chromosome aberrations have been correlated with a poor prognosis. Loss of the chromosome arms 1p, 11q, and gain of 17q are used as genetic markers for high-risk neuroblastoma (Bown et al., 1999; Guo et al., 1999; Fong et al., 1989).

Short arm of chromosome 1 is deleted in 20% of all neuroblastoma cases and is correlated with *MYCN*-amplification (Fong et al., 1989). A gene identified on chromosome 1 which could be involved in the poor prognosis is the tumor suppressor Cadherin-5 (*CDH5)*. Low levels of *CDH5* correlate with worse prognosis and higher staging of neuroblastoma patients. Additionally, *MYCN*-amplification results in a hypermethylation of the promoter of *CDH5* (Koyama et al., 2012; Fujita et al., 2008).

The deletion of the long arm of chromosome 11 occurs in 35 – 45% of all neuroblastoma cases (Caren et al., 2010) and is mutually exclusive with *MYCN*-amplification (Vandesompele et al., 2005). Deletion of this chromosome arm correlates with less expression of the cell adhesion molecule 1 (*CADM1)* gene. CADM1 is an adhesion protein which is also involved in the regulation of cell proliferation (Nowacki et al., 2008). Besides CADM1, also ataxia-telangiectasia mutated (*ATM*; Mandriota et al., 2015), or *PHOX2A* (Wilzen et al., 2009) were suggested to be responsible for driving tumorigenesis upon deletion of chromosome 11.

Gain of the distal part of the long arm of chromosome 17 is often associated with loss of the chromosomes 1p or 11q. The gene associated with gain of chromosome 17q might be protein phosphatase 1 D (*PPM1D)*, since downregulation of *PPM1D* lead to suppressed growth of neuroblastoma cells (Saito-Ohara et al., 2003).

Besides the aberration of chromosome arms, some amplifications (e.g., *MYCN*) or rearrangements (e.g., TERT) are also known to result in a reduced survival and a classification into high-risk neuroblastoma.

The most important marker for risk-stratification of neuroblastoma patients is the amplification status of the *MYCN* gene. Amplification of the *MYCN* gene, usually localized on chromosome 2, is found in more than 20% of all neuroblastoma cases (Roderwieser et al., 2019). Amplifications of the *MYCN* gene are frequently located at different chromosomes, and the expression rate is usually 100 x fold higher than in non-amplified cells (Maris & Matthay, 1999; Schwab et al., 2003). All cases with *MYCN*-amplification belong to the high-risk group (Huang & Weiss, 2013). In mice transgenic expression of MYCN using a tyrosine hydroxylase (TH) promoter in neuronal crest cells leads to the development of neuroblastic tumors (Weiss et al., 1997).

Telomerase reverse transcriptase (*TERT*) is rearranged in 10% and overexpressed in additional 5% of all neuroblastoma cases (Roderwieser et al., 2019). The rearrangement results in the proximity of a super-enhancer to the *TERT* promoter, leading to an increased expression of TERT (Peifer et al., 2015; Valentijn et al., 2015). TERT overexpression results in the activation of several signalling pathways like E2F, WNT, MYC, and DNA repair pathways. MYCN overexpression also results in upregulation of TERT (Peifer et al., 2015). The effect on survival probability is reflected in Figure 1.2. Low-risk neuroblastoma (LR) show no TERT expression which results in no telomere elongation and is associated with better survival prognosis. High-risk neuroblastoma with mutations in *ATRX*, show low TERT expression but results in an alternative lengthening of telomeres which decreased survival probability. However, TERT rearrangement as well as *MYCN*-amplification which results in upregulation of TERT, results in telomerase activation which further decreases the survival probability.

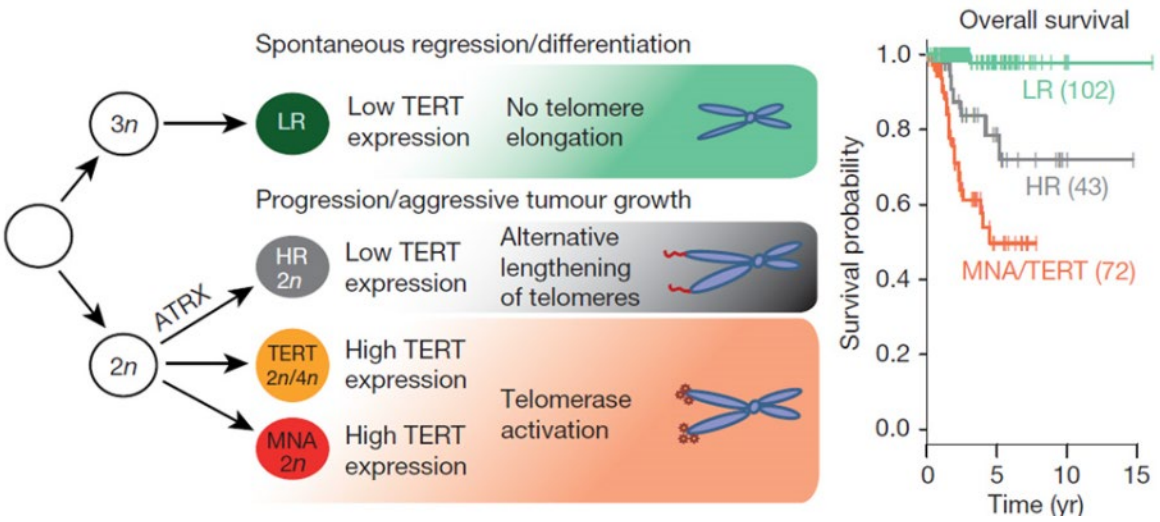

Figure 1.2: Survival probability of neuroblastoma patients depending on TERT expression.
Additional factors like *MYCN*-amplification (MNA), and ATRX mutations contributing to differential expression of TERT.
This Figure was published in similar form by Peifer et al., 2015.

1.1.3 Molecular differences in neuroblastoma

Neuroblastoma consists of two cellular subtypes: undifferentiated mesenchymal and committed adrenergic cells. They derive most likely from different cell lineages (van Groningen et al., 2017). The subtypes show different chromatin landscapes, associated with certain transcription factors resulting in different gene expression patterns, known as core regulatory circuitries (CRCs; Figure 1.3). The adrenergic cells are driven by transcription factors like HAND1, PHOX2A, and GATA3, whereas mesenchymal cells are driven by different transcription factors like ELK4, SMAD3, and PRRX1. Additionally, it has been shown that cells are able to convert from adrenergic towards mesenchymal state. Expression of PRRX1 in an

adrenergic cell leads to a reprogramming towards a mesenchymal state (van Groningen et al., 2017).

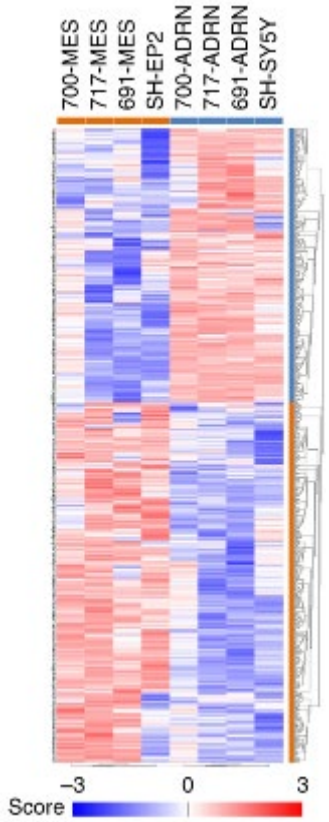

Figure 1.3: Heatmap showing the clustering of mRNA expression profiles of four mesenchymal (MES) and corresponding adrenergic (ADRN) cell lines.
This Figure was published in similar form by van Groningen et al., 2017.

Those cell states are co-occurring, meaning that one tumor can consist of adrenergic as well as mesenchymal cells. Those cell populations differ in their response to treatment. Chemotherapy results in a decrease of adrenergic cells, whereas mesenchymal cells remain largely unaffected. This results in an enrichment of mesenchymal cells after therapy and in relapsed tumors (Boeva et al., 2017; van Groningen et al., 2017).

Later data identified that those CRCs might even result in four different epigenetic subtypes. Three subtypes reflect the clinical groups *MYCN*-amplified, *MYCN* non-amplified with high-risk, *MYCN* non-amplified with low-risk, whereas the fourth group shows mesenchymal characteristics and may arise from a multipotent Schwann precursor cell (Gartlgruber et al., 2020).

1.2 Cell cycle

The cell cycle of eukaryotes is divided in four distinct phases: G1, S, G2, and mitosis (M). Additionally, there is a quiescent state called G0 phase. The first cell cycle stage is G1 phase, in which the cells increase the number of organelles, the supply of proteins required for cell growth, and the capacity of protein synthesis. In S phase DNA replication occurs, aiming at the duplication of all chromosomes. In G2 phase - which has similar aspects as G1 phase - the cells are prepared for mitosis. During the M phase the chromosomes are separated into two identical sets. The M phase is further subdivided into prophase, metaphase, anaphase, and telophase. At the end of telophase, cytokinesis occurs enabling the distribution and separation of all components into two identical daughter cells (reviewed in Batty & Gerlich, 2019).
If there are no external growth stimuli it is also possible for a cell, after mitosis is completed, to go into G0 phase. Most cells with diploid DNA content in adults are in the G0 state, either transiently (quiescent) or permanently (terminal differentiated or senescent; Ding et al., 2020). The cell cycle needs to be tightly controlled since the genetic integrity as well as aberrant and unscheduled cell division could lead to malignancies like cancer, autoimmunity, and degenerative disorders (Zubiaga, 2020).

1.2.1 Cell cycle checkpoints

There are cell cycle checkpoints to ensure that all important processes for one cell cycle phase are successfully completed before entering the next cell cycle phase (Hartwell & Weinert, 1989). Key regulators of checkpoints are heterodimers composed of cyclins and cyclin-dependent kinases (CDKs). Binding of the regulatory subunit (cyclins) to the catalytic subunit (CDKs) lead to the activation of the latter (Nigg, 1995). The heterodimers can then phosphorylate proteins and consecutively orchestrate the entry into the next cell cycle phase. Mitogenic signals (e.g., hormones and growth factors) can induce activation of cyclins/CDKs (Otto & Sicinski, 2017). The regulation possibilities of the cell cycle checkpoints are illustrated in Figure 1.4.

The transition from G0 or G1 phase into S phase is regulated by activation of CDK4 or CDK6. These CDKs can be activated by cyclin D proteins (cyclin D1, cyclin D2, or cyclin D3) and repressed by interaction with proteins of the INK4 family (p15, p16, p18, or p19; Malumbres & Barbacid, 2001). The activated cyclin D/CDK4 or CDK6 complex hyper-phosphorylates the RB protein RB1 as well as two closely related proteins RBL1 and RBL2. When unphosphorylated, RB proteins interact with the E2F transcription factors and thereby keep them inactive. Upon phosphorylation this interaction is abolished, releasing E2F proteins, and enabling transcription of their targets (Asghar et al., 2015).

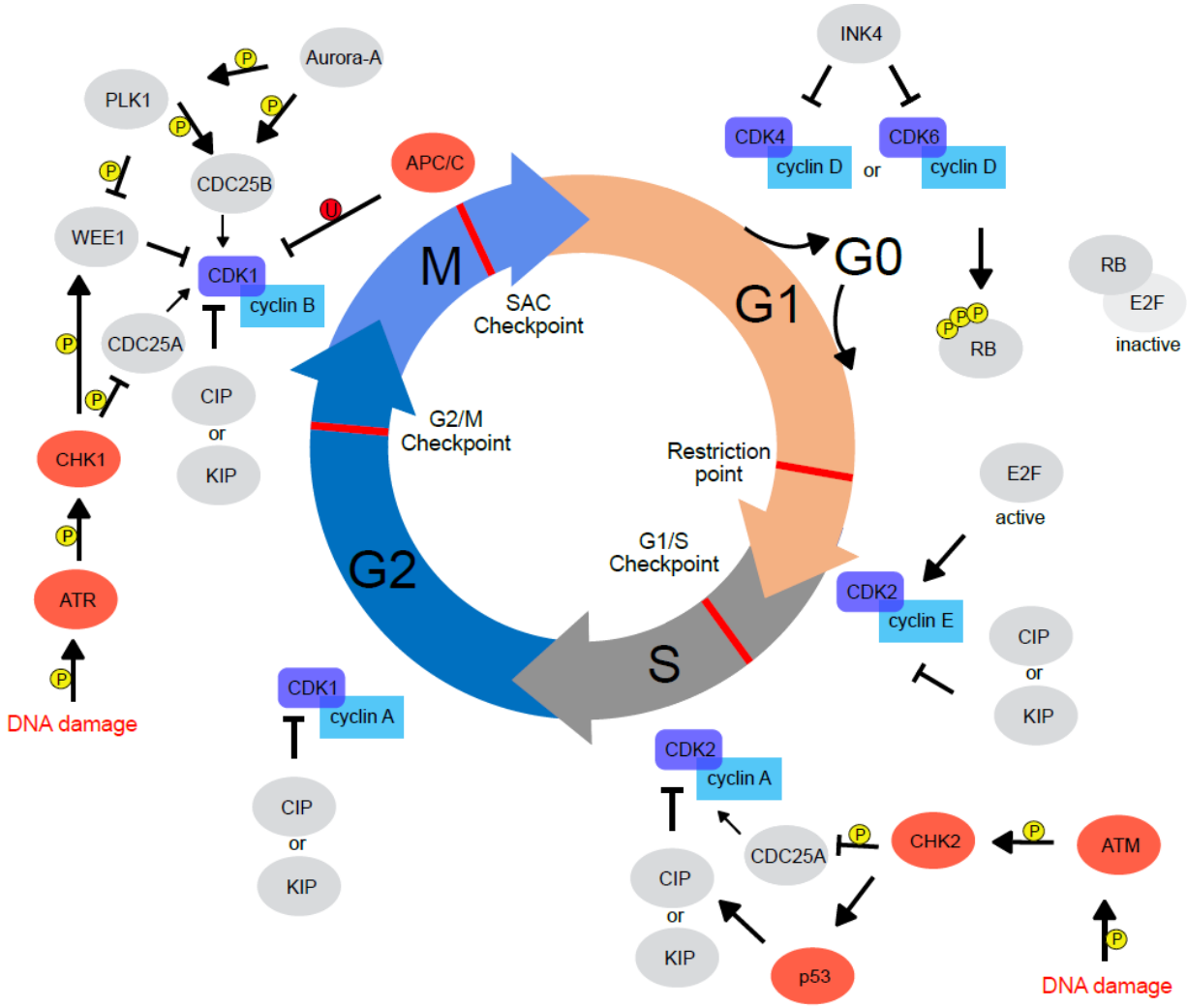

Figure 1.4: Regulation of cell cycle checkpoints in eukaryotic cells.
Cyclins and CDKs are depicted in light blue and dark blue, respectively. Proteins which regulate cyclins and CDKs are shown in grey. Proteins involved in checkpoints are depicted in red. Regulation induced by phosphorylation (indicated by yellow circle with P) or ubiquitination (indicated by red circle with U) are shown on the arrow.

To progress from G1 to S phase the E2F target genes cyclin E1 and cyclin E2 need to form a complex and thereby activate CDK2. CDK2 is usually inhibited due to sequestration by $p21^{CIP1}$ and $p27^{KIP1}$ (Cheng et al., 1999). The active cyclin E/CDK2 complex can phosphorylate multiple proteins involved in DNA replication (RPA and RPC), cell cycle progression (E2F, RB, p27), centrosome duplication (NPM), and histone synthesis (NPAT; Sever-Chroneos et al., 2001; Ma et al., 2000; Okuda et al., 2000). At the end of S phase, cyclin E is degraded by the E3 ligase SCF^{FBXW7} (Grim et al., 2008). Cyclin A, another E2F target, takes over the function of cyclin E, forming a complex with activated CDK2 (Schulze et al., 1995). The cyclin A/CDK2 complex phosphorylates CDC6 and E2F1 and thereby terminates S phase and enables the transition from S to G2 phase (Petersen et al., 1999).

To transit between G2 and M phase, an active complex between cyclin B/CDK1 needs to form. CDK1 is inhibited due to phosphorylation on T14 and T15 by the kinase WEE1 (Watanabe et al., 2005). The phosphatase CDC25B can dephosphorylate and reactivate cyclin B/CDK1, therefore promoting cell cycle progression (Izumi & Maller, 1993). Interestingly, the kinase Aurora-A has a pivotal role in this as it can both activate CDC25B by phosphorylating S353 (Dutertre et al., 2004) and PLK1 by phosphorylating T210 (Seki et al., 2008; Jang et al., 2002). Importantly, PLK1 also promotes cyclin B/CDK1 function by CDC25B activation due to phosphorylation on several sides including S353 and WEE1 inhibition due to phosphorylation on S53 (Sur & Agrawal, 2016; Watanabe et al., 2005). All in all, a lot of steps regulate the activity of CDK1 to allow cells to enter mitosis. The active cyclin B/CDK1 complex phosphorylates proteins required for nuclear envelope breakdown, condensation of chromosomes, and the assembly of mitotic spindle. The spindle assembly checkpoint (SAC), controlling the metaphase to anaphase transition, is activated upon the loss of cyclin B/CDK1 activity due to the degradation of cyclin B by the APC/C complex (reviewed in Gavet & Pines, 2010).

Cells can also arrest in the cell cycle mainly due to two checkpoints responding to DNA damage. Prior and after DNA synthesis in G1 and G2 phase several kinases are involved in arresting cells when sensing problems in DNA replication (Ding et al., 2020).
One sensor is the serine/threonine kinase Ataxia telangiectasia and Rad3-related (ATR). ATR is activated upon DNA damage in S phase, can detect stalled replication forks, and thereby induce a cell cycle arrest in S or G2 phase to ensure maintenance of genome integrity (Saldivar et al., 2017). Upon activation, ATR establishes the block mainly by phosphorylating and activating CHK1. CHK1 can phosphorylate and inactivate CDC25A, a related family member of CDC25B with similar functions in cell cycle progression. This phosphorylation results in proteasomal degradation of CDC25A, thereby inducing G2 arrest. Additionally, CHK1 can stimulate WEE1, thereby facilitating the inhibitory phosphorylation on CDK2 and CDK1 also resulting in G2 arrest (Otto & Sicinski, 2017).
Another factor which detects DNA damage is the serine/threonine kinase ATM, which can in turn phosphorylate and thereby activate the checkpoint kinase 2 (CHK2; Matsuoka et al., 2000). CHK2 can activate p53, inducing p53-dependent early G1 phase arrest allowing DNA repair prior to DNA synthesis (Schwartz & Rotter, 1998). This arrest occurs due to the p53-mediated transcription of $p21^{CIP1}$, an inhibitor of cyclin E/CDK2 (Benson et al., 2014). When repair cannot be successfully completed, cells undergo p53-induced apoptosis (Koniaras et al., 2001).

1.2.2 Transcription, replication, and their coordination

DNA replication takes place only in the S phase and its outcome is tightly controlled by the systems described above. Another process using DNA as a template is transcription, which is not restricted to a specific cell cycle phase. This poses a challenge to cells, considering that DNA and RNA polymerases can interfere with each other during S phase. Therefore, the basics concerning transcription and replication and how the two processes are coordinated are described below.

1.2.2.1 Transcription

Transcription is a process where information of the DNA is transcribed into messenger RNA (mRNA). mRNA is subsequently processed, exported from the nucleus, and translated into proteins by ribosomes. Transcription is mainly coordinated by a multiprotein complex generally dubbed “transcription machinery” and is regulated by CDKs and cyclins.

Transcription by RNA Polymerase II (RNAPII) can be divided in three phases: initiation, elongation, and termination. The various steps of RNAPII can be investigated by different phosphorylation pattern of the heptameric repeat of the C-terminal domain (CTD) of the largest subunit of RNAPII. The sequence of the CTD is conserved whereas the number of repeats increases from yeast (26 repeats) to human (52 repeats; Eick & Geyer, 2013).

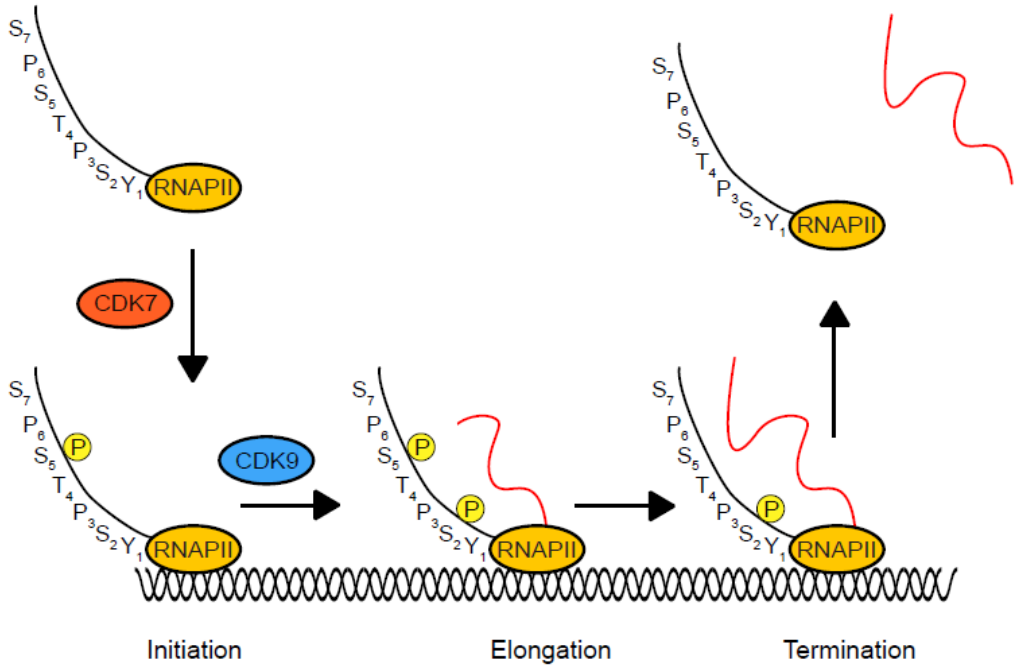

Figure 1.5: Different stages of transcription are associated with differential RNAPII phosphorylation patterns.
Initiation is marked by phosphorylation on Ser5 by CDK7. Upon CDK9 phosphorylation on Ser2, RNAPII is elongating and termination of RNAPII results in an unphosphorylated RNAPII. Nascent RNA is depicted in red.

Transcription initiation starts with the assembly of the pre-initiation complex (pre-IC) which consists of general transcription factors, co-regulators and the RNAPII complex (Grunberg & Hahn, 2013). The general transcription factor TFIIH comprises ten subunits, including XPB and CDK7 (Compe & Egly, 2012). XPB is a helicase which unwinds the double-stranded DNA (dsDNA) a process referred as promoter melting, allowing the RNAPII to access the template strand (Kim et al., 2000). CDK7 is the kinase phosphorylating the CTD on Ser5 (Akhtar et al., 2009; Glover-Cutter et al., 2009). The phosphorylation on Ser5 is established during initiation and is gradually removed as productive elongation proceeds (Harlen & Churchman, 2017). It is used as a marker for promoter-proximal pausing of RNAPII. This phosphorylation is also needed to recruit RNA capping enzymes, which are regulating the capping of the 5´end of nascent RNA (Bentley, 2014).

After transcription initiation, most genes undergo a regulatory step called promoter-proximal pausing (Muse et al., 2007), which happens 50 – 70 nucleotides downstream of the transcription start site (TSS). Negative elongation factor (NELF) and DRB-sensitive induced factor (DSIF) are factors contributing to the pausing of RNAPII (Yamaguchi et al., 1999). CDK9 - a kinase which is part of the positive transcription elongation factor B (pTEFB) - is then required to release RNAPII from promoter-proximal pausing (Peng et al., 1998). CDK9 phosphorylates NELF, DSIF and the CTD of RNAPII on Ser2 (Sanso et al., 2016). Upon phosphorylation, NELF is dissociated from chromatin and replaced by the elongation factor RNA Polymerase II-associated factor 1 (PAF1; Vos et al., 2018; Fujinaga et al., 2004). DSIF in contrast remains on chromatin upon phosphorylation and switches functions from being a pausing factor to a positive elongation factor (Yamada et al., 2006). The Ser2 phosphorylation of RNAPII (RNAPII pSer2) is considered as the elongating form of RNAPII.

For transcription termination, the polyadenylation signal (PAS) is needed. Up to 30 nucleotides downstream of the PAS the cleavage and polyadenylation specific factor (CPSF) complex cuts the nascent RNA. Polyadenylation of the 3´ end of the nascent transcript occurs favoring the export to the cytoplasm. The 5´end of the nascent RNA which is still transcribed by RNAPII is processed by XRN2, a 5´ to 3´ endonuclease, resulting in the dissociation of RNAPII from chromatin (reviewed in Porrua & Libri, 2015).

1.2.2.2 Replication

DNA replication is a conserved mechanism throughout evolution and has the aim to duplicate the genetic information of a cell. The dsDNA is duplicated by unwinding the double helix and using each strand as a template for a new, complementary DNA strand. The replication process after origin licensing can be as transcription divided in three different phases: initiation,

elongation, and termination. The basic factors involved in origin licensing, initiation, and elongation of replication are shown in Figure 1.6.

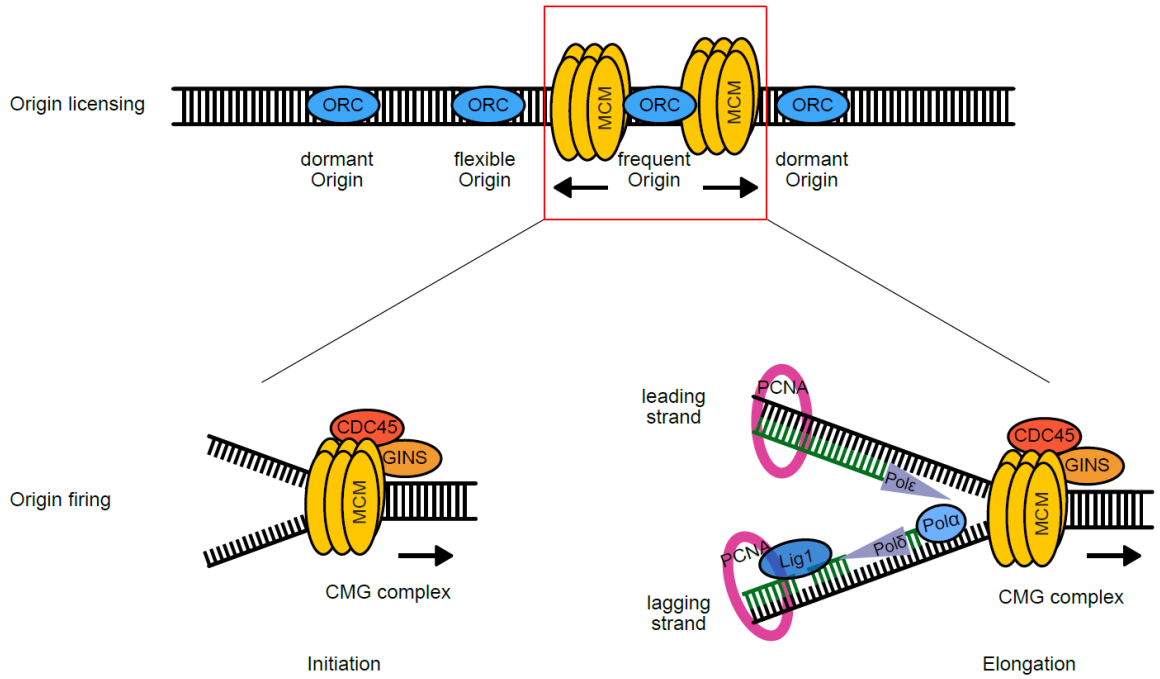

Figure 1.6: Schematic overview of origin licensing, initiation, and elongation of replication in eukaryotic cells.

The initiation of DNA replication starts with the pre-replication complex (pre-RCs) formation at thousands of origins (Marahrens & Stillman, 1992). The pre-RCs are formed by association of the origin of replication (ORC) complex to the origins, followed by recruitment of CDT1 and CDC6. Those two proteins load the inactive mini-chromosome maintenance (MCM) complex to DNA, which is composed of six subunits. This process is called origin licensing and already takes place in G1 phase of the cell cycle. Activation of origins, which is also called origin firing, is not happening on all licensed origins (DePamphilis, 1993). This enables to distinguish three classes of origins: frequent, flexible, and dormant origins (Callan, 1974).

Inactive MCM is phosphorylated by DDK and CDKs, resulting in two activated MCM complexes within two bidirectional functioning replisomes (Abid Ali et al., 2017; Heller et al., 2011). This phosphorylation additionally recruits GINS, Treslin, TOPBP1, and CDC45, resulting in the formation of the pre-IC. MCM has a DNA helicase activity and forms together with GINS and CDC45 the CMG complex required to unwind the dsDNA (Ilves et al., 2010; Masai et al., 2010). CMG complex formation enables the assembly of the replisome and bidirectional DNA synthesis can occur (Boos et al., 2012). The replisome consists of the CMG complex, the primase polymerase α, DNA polymerase δ or ε, the sliding clamp PCNA (proliferating cell nuclear antigen), the clamp loader RFC, and single strand binding protein RPA as well as several not yet characterized factors (Waga & Stillman, 1998).

The unwinding of the DNA results in strands with different orientations. Only one DNA strand will be continuously synthesized (leading strand) whereas the other strand is synthesized in short fragments (Okazaki fragments) in the direction opposing the fork movement (lagging strand; reviewed in Zheng & Shen, 2011).

The replisome of the leading strand is composed by the CMG helicase associated with Pol ε (Langston et al., 2014).

The lagging strand instead needs to be primed by polymerase α, a primase creating RNA-DNA primers (MacNeill, 2012), used as start for the replication by polymerase δ. The RNA primers will be removed by nucleases like FEN1 (Harrington & Lieber, 1994), gaps will be filled with nucleotides and the DNA ligase I joins the Okazaki fragments to achieve an intact lagging strand.

The function of RFC is to load PCNA onto the DNA. The ring-shaped sliding clamp (PCNA) minimizes the dissociation of the newly synthesized strand from the polymerases (Krishna et al., 1994). Additionally, PCNA is a platform for the recruitment of FEN1, DNA ligase I, and to coordinate sequential actions of the polymerases (Sporbert et al., 2005).

When two replication forks meet on the same DNA stretch, the DNA replication is terminated. Therefore, the forks converge, all remaining gaps are filled, and the proteins involved in replication are unloaded from DNA (reviewed in Dewar & Walter, 2017).

1.2.2.3 Transcription-replication coordination

Replication and transcription are independent processes. However, in S phase where both replication and transcription occur, they need to be regulated to protect genome stability. Ways to regulate those processes is to control them in time or space.

The number and timing of fired origins is a way to regulate replication. Fired origins are usually found in intergenic regions and not within genes (Gilbert et al., 2010). Origins can be activated in early, middle, or late S phase (Dimitrova & Gilbert, 1999). Origin activation depends also on the chromatin environment as nucleosome positioning has been implicated in the efficiency of origin firing (Lipford & Bell, 2001). Additionally, replication from early activated origins correlates with GC-rich regions, active chromatin marks, and gene expression, whereas replication of late activated origins correlate with AT-rich regions, repressive chromatin marks, and gene-poor regions, suggesting a mechanistic link (Lipford & Bell, 2001). Besides this, also the three-dimensional localization of the chromosomes within the nucleus is crucial for timing of replication. Replication of early activated origins occurs mainly within the inner part of the nucleus, whereas activated origins in late S phase are usually found in the periphery of the nucleus or close to nucleoli (Lipford & Bell, 2001).

It was shown that the timing of transcription and replication is coordinated, as early replicating genes increase their transcription late in S phase and late replicating genes show increased

transcription early in S phase (Meryet-Figuiere et al., 2014). However, the exact mechanisms and proteins accounting for that observations are yet unclear. Furthermore, active transcription as well as the resulting topology at 3´ends of genes can displace ORC or other pre-RC complex members and therefore abolish origin firing (Cadoret et al., 2008; Mori & Shirahige, 2007). Additionally, active origins are often found close to promoters of actively transcribed genes. This mechanism can allow the regulation of replication by transcription factors or chromatin remodelers. Transcription factors or chromatin remodelers can regulate access, recruitment, or sequestration of proteins involved in replication, thereby coordinating those processes (Knott et al., 2009).

If those processes happen unregulated in S phase, RNAPII and the replication machinery can collide, leading to transcription-replication conflicts (Hamperl & Cimprich, 2016). Two types of transcription-replication conflicts can occur, depending on the orientation of transcription and replication machinery when colliding. Head-on collisions occur when the two machineries move into opposite direction. They lead to stalled replication forks, followed by the activation of ATR, and showing the distinctive feature of accumulation of DNA/RNA hybrids called R-loops. Co-directional collisions occur instead when the two machineries collide while moving in the same direction. These conflicts result in fork progression, ATM activation, but no R-loops (Hamperl et al., 2017).

1.3 The transcription factor MYC

The oncogene MYC and its related family members are overexpressed or amplified in many human tumors (Nesbit et al., 1999). Amplification often occurs due to chromosomal translocations or copy number changes of *MYC*. Overexpression of MYC is mainly caused by deregulation of signaling pathways which result in elevated MYC expression. High MYC levels often correlate with poor prognosis and survival outcome. Induction of MYC *in vitro* can change a normal cell into a cell with tumor cell properties. Additionally, manipulation of MYC *in vivo* changes incidence and development of tumors (Soucek et al., 2008). Therefore, MYC proteins are considered as major drivers of tumorigenesis. And indeed, more than 70% of cancers show MYC family member related amplification or overexpression. Patients with tumors of the nervous system like neuroblastoma (25%) and medulloblastoma (10%) show *MYCN*-amplification or overexpression (Massimino et al., 2016).

1.3.1 The family of MYC transcription factors

The family of MYC proteins comprises the three members MYC, MYCN, and MYCL. MYC was identified first as the cellular homolog of viral oncogenic protein v-myc promoting myelocymatosis in chicken (Sheiness & Bishop, 1979). MYCN and MYCL were discovered later in neuroblastoma (Kohl et al., 1983) and in small cell lung cancer (Nau et al., 1985), respectively. Those three proteins have slightly different sizes: MYCN is with 464 amino acids the largest family member, followed by MYC with 439 amino acids, and MYCL which is the smallest family member with 364 amino acids. They share very conserved sequences, named MYC-boxes (MB) and basic region helix-loop-helix-leucine zipper (BR-HLH-LZ). More details about these regions are provided below (see 1.3.2).

As shown in mouse embryos, MYC proteins have different expression patterns depending on developmental stage and investigated tissue and typically responding to different developmental cues (Zimmerman et al., 1986).

MYCN is mainly expressed during early stages of development in the forebrain, kidney, and hindbrain, whereas it is absent in adults. MYCN was found to be essential for the development of the central nervous system (Knoepfler et al., 2002).

MYC is ubiquitously expressed throughout the body of a mouse, but most abundant in thymus, spleen, and liver in early development and in the adrenal glands and the thymus in late development (Zimmerman et al., 1986).

MYCN and MYC are required for maintaining hematopoietic stem cells (Trumpp et al., 2001) and for development of early organogenesis. Deletion of both showed embryonic lethality in midgestation at E10.5 (Davis et al., 1993; Charron et al., 1992; Stanton et al., 1992), most

probably due to placental insufficiency (Dubois et al., 2008). MYC was shown to be necessary for development and growth of crypt progenitor cells in the intestine (Muncan et al., 2006), skin keratinocytes, and other cell lines where it is expressed. Besides the essentiality of MYC proteins, it could be shown that replacing MYC by MYCN can rescue the growth and development phenotypes observed with knockdown of MYC (Malynn et al., 2000). This indicates that, despite the relevant differences among the homologs, the essential protein functions could be similar.

1.3.2 Structural and functional domains of the MYC protein

MYC proteins are intrinsically disordered which makes it difficult to assess their crystal structure. Co-crystallization of MYC or MYCN is only possible when bound in a complex, for example shown for MAX (Nair & Burley, 2003), Aurora-A (Richards et al., 2016), and WDR5 (Chacon Simon et al., 2020). The architecture of MYC proteins as well as their canonical function and interaction partners are displayed in Figure 1.7.

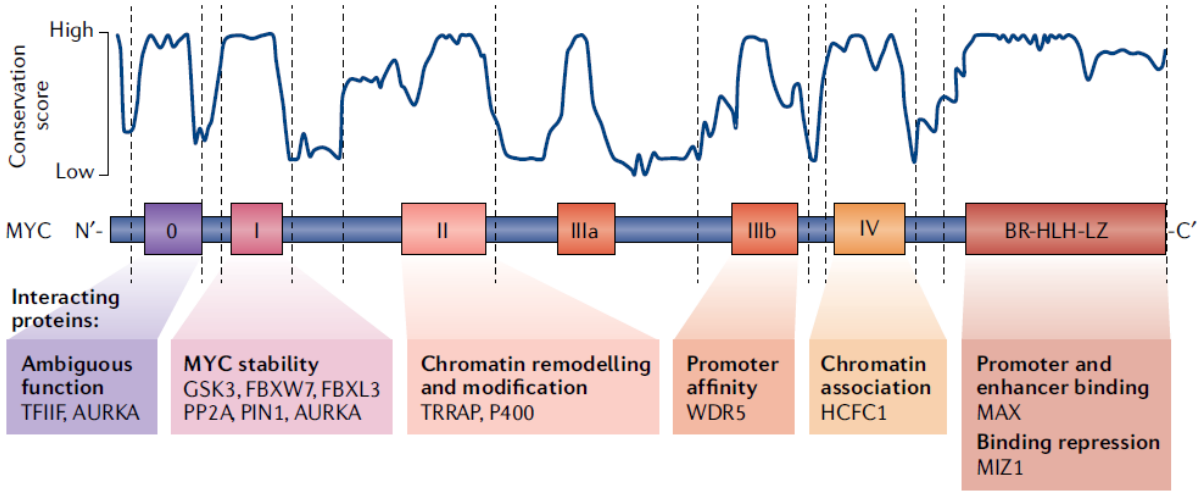

Figure 1.7: Domains of MYC protein and their canonical function and interaction partner.
Schematic representation of the MYC structure from amino-terminus (N´) to carboxy-terminus (C´). Above the structure the Conservation score is shown, high indicating highly conserved throughout evolution, whereas low meaning highly diverse. The highly conserved regions correlate with the occurrence of MYC-boxes (MB) named from 0 to IV and the basic region helix-loop-helix-leucine zipper (BR-HLH-LZ). Below the sequence the interaction partner of this MB as well as the processes regulated by this MB are displayed.
This Figure was published in similar form by Baluapuri et al., 2020.

All MYC family members share common features at the carboxy-terminus as well as six highly homologous stretches, the MBs (Atchley & Fitch, 1995). Otherwise, the sequence homology between the three MYC family members is not very similar, which is also reflected in the conservation score (Figure 1.7). The six currently described MBs are numbered MB0, MBI, MBII, MBIIIa, MBIIIb, and MBIV. The amino-terminus of the MYC proteins display a

transcriptional activation domain (Kato et al., 1990) spanning the MB0 and MBI (Zhang et al., 2017).

MB0 has ambiguous functions. It could be shown that it interacts with the transcription factor II F (TFIIF; Kalkat et al., 2018). Additionally, it harbors a sequence allowing – at least partially - the interaction required for association with Aurora-A (Büchel et al., 2017). Another function of MB0 is the MYC-induced p53-independent function in apoptosis, although the exact mechanisms of MB0 in this context remains elusive (Zhang et al., 2017).

MBI is the most studied of the MYC-boxes and known for its regulation of proteasome-dependent MYC degradation. It harbors several serine/threonine residues which are known to serve as a phosphodegron. The phosphorylation of those residues – namely T58 and S62 - is required for recruitment of the E3 ligases SCF^{FBXW7} and SCF^{FBXL3}, leading to MYC degradation (Fujii et al., 2006), as in more detailed described below (see 1.3.4). This MYC-dependent degradation by E3 ligases can be antagonized by binding of Aurora-A (Dauch et al., 2016; Richards et al., 2016). MBI is also associated with pTEFb interaction (Eberhardy & Farnham, 2001) which is a positive elongation factor of RNAPII (see 1.2.2.1).

The MBII contains a stretch required for interaction with the MYC-coactivator transformation/transcription domain-associated protein (TRRAP; McMahon et al., 1998). TRRAP is the scaffolding subunit for several large multi-protein complexes including NuA4 complex involved in histone acetylation to remodel chromatin (Zhang et al., 2014) enabling euchromatin formation (McMahon et al., 2000). Ultimately, euchromatin formation promotes transcription of MYC target genes (Frank et al., 2003).

MBIIIb is known to regulate promoter affinity by interaction with WDR5 (Lorenzin et al., 2016). The interaction of WDR5 with MYC is essential for H3K4 tri-methylation. WDR5 is a presenter of H3K4 methylation (Thomas et al., 2015) and can serve as platform for the recruitment of chromatin remodelers, transcription factors, and long non-coding RNAs (Lu et al., 2018). H3K4 methylation can be found on all open and active promoters (Bernstein et al., 2002), enhancing the affinity of MYC for its promoters (Nie et al., 2012).

MBIV was shown to interact with host cell factor 1 (HCF-1). The disruption of MYC-HCF-1 interaction results in a decreased tumorigenesis in mice (Thomas et al., 2016). Other interaction partners for this MB are not described yet, although functions for MBIV have been discovered. Loss of MBIV results in a G2 arrest, whereas cells show a reduction in MYC-induced apoptosis as well as transformation ability. Additionally, loss of MBIV results in a decreased DNA binding ability which is not as prominent as seen for loss of MBIII (Cowling et al., 2006).

At the CTD MYC proteins have a BR-HLH-LZ serving as DNA-binding domain (Blackwell et al., 1990). Necessary for the DNA binding of MYC is its interaction and thereby formation of a

heterodimer for example with MYC associated factor X (MAX). When MYC and MAX are in a complex, they can bind to consensus sequences CAC(G/A)TG on DNA called Enhancer-boxes (E-boxes; Blackwell et al., 1990). Although, E-boxes are enriched where MYC-binding occur, this motif is not mutually exclusive (Guo et al., 2014). Therefore, it is suggested that other interaction factors could influence the association with chromatin. Another factor which can interact with the CTD of MYC at the BR-HLH-LZ is the zinc finger protein MIZ1. MIZ1/MYC heterodimers form repressive complexes (Vo et al., 2016), preventing MYC-dependent transcription and thereby also enabling a regulation step (Walz et al., 2014).

1.3.3 Transcriptional functions of MYC

There are numerous publications studying the role of MYC proteins as transcription factors. Those studies have been recently grouped in three major categories which are depicted in Figure 1.8 (reviewed in Baluapuri et al., 2020).

The gene-specific regulation model refers to the classical interpretation of MYC including the expression of a specific set of target genes (Sabò et al., 2014; Staller et al., 2001). This view, although in conflict with recent chromatin-occupancy studies (i.e., employing ChIP-sequencing techniques) that identified MYC binding to virtually all open promoters (Walz et al., 2014), is still rather popular in the field and theorizes that the role of MYC in tumorigenesis is the specific expression of certain genes.

The “global amplifier” model is mainly driven from the observation that MYC enhances the rate of transcription genome-wide (Lin et al., 2012). Experiments in primary B cells revealed that transcription following mitogenic stimuli of early B cells is MYC-dependent (Nie et al., 2012) which results in increased mRNA levels and correlates with cell growth (Lewis et al., 2018). This is in line with the observation that tumors with increased MYC levels highly depend on the transcriptional kinases CDK7 and CDK9 (Chipumuro et al., 2014; Huang et al., 2014). Therefore, the global amplifier model posits that the role of MYC in tumorigenesis is to enhance general expression of all genes. However, the increase in total mRNA levels cannot be observed in all conditions (Tesi et al., 2019; Lewis et al., 2018; Sabó et al., 2014; Walz et al., 2014).

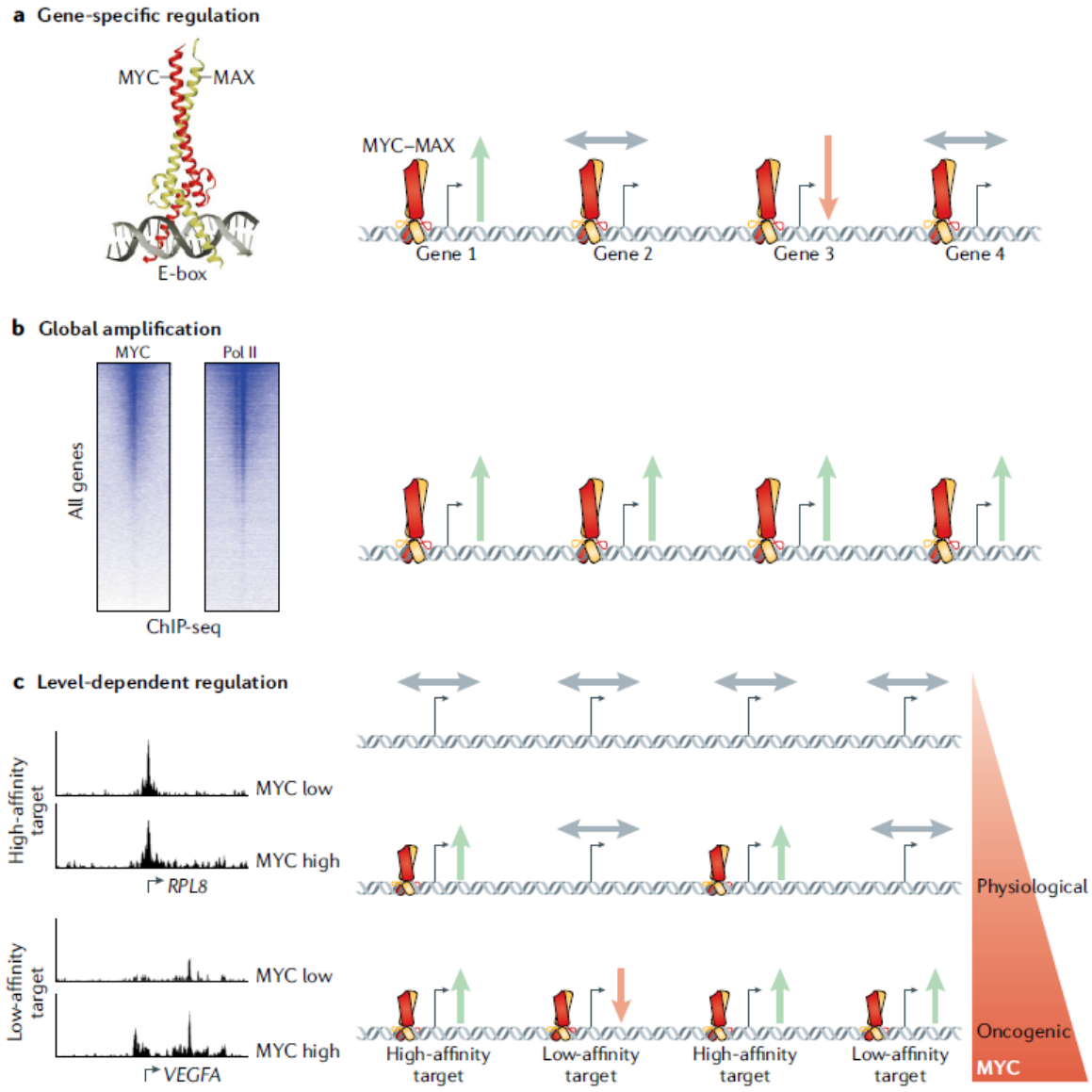

Figure 1.8: Scheme of different models how MYC regulate transcription.
Three different models can be distinguished: (a) gene-specific regulation, (b) global amplification, and (c) level-dependent regulation.
This Figure was published in similar form by Baluapuri et al., 2020.

The third model reported is the gene-specific affinity model. This model is based on the observations that cells show different expression patterns depending on the amount of MYC (Staller et al., 2001). Therefore, high-affinity and low-affinity targets can be distinguished. High-affinity targets show MYC binding already under physiological MYC levels, whereas low-affinity target genes show MYC binding only upon oncogenic expression of MYC (Lorenzin et al., 2016). According to this view tumorigenesis is driven by oncogenic, elevated MYC levels through the transforming expression of low-affinity target genes.

These postulated models highly depend on the experiment performed and the cellular context (Lewis et al., 2018). An additional difference might be the normalization algorithm used for

high-throughput sequencing methods like RNA-sequencing. Therefore, global increase in mRNA levels could be underestimated according on the algorithms used (Lovén et al., 2012). Several other possibilities like direct and indirect effects are additionally under debate. Whether one of the models is correct, a mixture of all, or each model in certain cells or under specific conditions remains elusive and needs to be further investigated.
However, recent publications also indicate that MYC might context-dependently change the recruitment of accessory proteins and/or stress responders and thereby modulating the RNAPII behavior which might account for the changes in gene expression (Herold et al., 2019).

1.3.4 Regulation of MYC

Since MYC is a key regulator of transcription, it needs to be tightly regulated under physiological conditions. Therefore, MYC binding to chromatin as well as MYC protein stability are under constant control of several independent proteins. To understand this regulation is also beneficial to disturb oncogenic functions of MYC and thereby target MYC-driven tumors.

One possibility to regulate MYC is the dependence on its interaction partners which are needed for DNA binding. Since MYC is not able to homo-dimerize at physiological concentrations (Prendergast & Ziff, 1991), it needs a partner protein for DNA binding, for example MAX. MAX can also form homodimers as well as hetero-dimerize with one of the four MAX dimerization (MXD) proteins. MAX interaction with MGA1 or MNT suppresses cell growth (Hurlin et al., 2003). Since all the interactions within this network are mediated via the BR-HLH-LZ region, this enables a variety of mechanisms to control MYC-dependent transcription in untransformed cells which is frequently perturbed in cells with oncogenic MYC level (Schaub et al., 2018).
Another means of MYC regulation is its degradation which is controlled by the ubiquitin proteasome system (UPS). The UPS primes proteins for degradation by the addition of ubiquitin molecules. The specificity of the system is ensured by E3 ligases which are required for substrate selectivity. One E3 ligase known to degrade MYC is SCF^{FBXW7}. For the recognition by this E3 ligase, MBI of MYC needs to be post-translationally modified by cyclin B/CDK1, which phosphorylates MYC on S62 (Sjostrom et al., 2005), subsequently, GSK3-β targets T58 (Pulverer et al., 1994); later protein phosphatase 2A (PP2A) dephosphorylates S62 (Arnold & Sears, 2006), finally SCF^{FBXW7} recognizes the protein phosphorylated on T58 only (Welcker et al., 2004a; Welcker et al., 2004b) and this leads to MYC proteasomal degradation (Otto et al., 2009).
Phosphorylation-independent degradation pathways have also been observed. TRUSS has been shown to interact with the BR-HLH-LZ and with amino acids close to the amino terminus of MYC proteins, resulting in their ubiquitination and degradation (Choi et al., 2010). Another E3 ligase which is known to ubiquitinate MYC followed by proteasomal degradation is UBR5

(Schukur et al., 2020). Additionally, SCF^{SKP2} was shown to interact with MBII and BR-HLH-LZ motif and to ubiquitinate MYC, leading to its proteasomal degradation (Kim et al., 2013; von der Lehr et al., 2003).

MYC function is key for both normal and oncogenic tissues. This renders the protein a difficult target, as MYC-driven therapies were expected to yield massive side-effects. This was suggested *in vivo* for mice in which deletion of either *MYCN* or *MYC* was lethal at embryonic day 10.5 due to consequences of organ and tissue growth failure (Soucek & Evan, 2010).

In addition, MYC proteins have no active site and their surface does not allow the binding of small molecules. Therefore, MYC proteins are considered as "*undruggable*" (Gustafson et al., 2014) and direct targeting of MYC remains difficult. However, several strategies have been identified to target MYC proteins indirectly, as summarized in Figure 1.9.

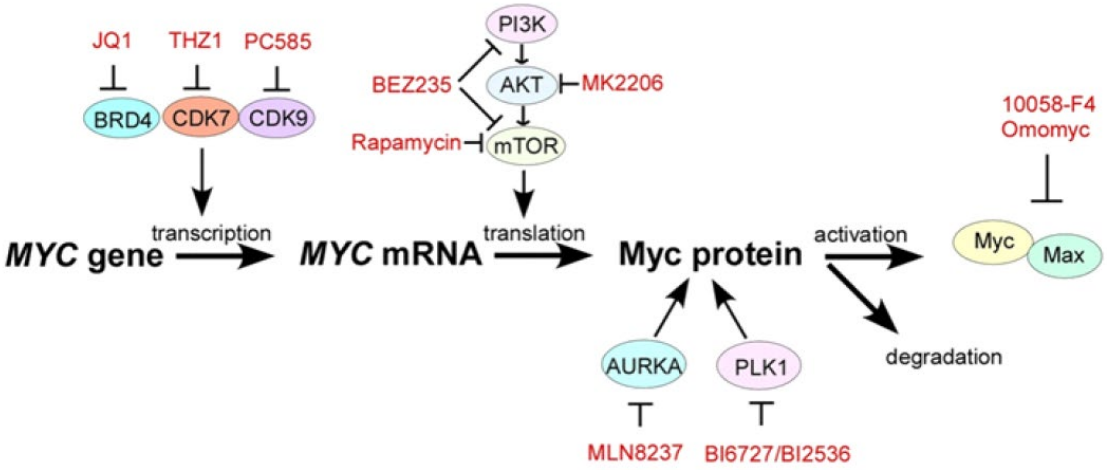

Figure 1.9: Approaches to target MYC proteins.
This Figure was published in similar form and is modified from Chen et al., 2018.

It is possible to target MYC function at different levels, as the transcription of *MYC* mRNA, the translation of MYC protein, the stability of MYC protein, or the ability of MYC to bind to chromatin.

The inhibition of transcription of MYC mRNA can be pursued by targeting key regulatory transcriptional proteins like CDK7, CDK9, or BRD4. For example, the JQ1 compound competes with BRD4 for the binding to acetylated lysine and thereby displaces BRD4 from super-enhancers regulating the expression of MYC (Delmore et al., 2011; Filippakopoulos et al., 2010). However, this strategy is not specific for MYC mRNA but interferes with the transcription of all (e.g., CDK7 or CDK9 inhibition) or a lot (e.g., BRD4 inhibition) of genes (Shi & Vakoc, 2014).

The same is true for the targeting of MYC translation by inhibiting the PI3K/AKT/mTOR pathway. Inactivation of this pathway reduces the transcription of RNAPI and RNAPIII target genes. RNAPI and RNAPIII regulate the transcription of components of the protein-synthesis machinery and are therefore required for the translation of all proteins in a cell (Martin et al., 2004; Mahajan, 1994).

More specific targeting approaches for MYC proteins have been proposed through the identification of proteins that lead to the stabilization of MYC proteins. Therefore, discovering MYC-interaction partner as potential targets for drug treatment of MYC-driven tumors is still an approach to treat these cancer types. Several pathways have been identified as competing with or inactivating the MYC-targeting E3 ligases. Aurora-A was shown to stabilize MYC by competing with SCF^{FBXW7} and thereby preventing the proteasomal degradation (Otto et al., 2009). Inhibition of Aurora-A results in a decrease in MYC protein levels (see 1.4.5). PLK1 phosphorylates the E3 Ligase SCF^{FBXW7} and thereby inactivates it, which also leads to the stabilization of MYC (Xiao et al., 2016).

Finally, two approaches have successfully in reducing the ability of MYC to associate with chromatin. The strategies are the inhibitor 10058-F4 and Omomyc. 10058-F4 blocks the hetero-dimerization of MYC and MAX and thereby prevents MYC´s association with chromatin (Follis et al., 2009; Yin et al., 2003). However, since the blocking in hetero-dimerization also prevents other BR-HLH-LZ proteins to dimerize, also this approach can yield side-effects and high doses of the inhibitor are needed.

Omomyc is a dominant negative variant of MYC that forms heterodimers with MYC, thereby preventing its interaction to MAX and their DNA-binding (Soucek et al., 2002; Soucek et al., 1998). Omomyc induction does not show any side-effects in healthy tissues, whereas it reduces tumor burden in several tested MYC-driven cancers (Jung et al., 2017; Soucek et al., 2013; Soucek et al., 2008; Soucek et al., 2004), suggesting the existence of a therapeutic window.

1.4 The kinase Aurora-A

Aurora-A is a serine/threonine kinase with essential roles in mitosis and general cell proliferation. Consistently, Aurora-A knockout is embryonic lethal, due to defects in mitotic spindle assembly as well as chromosome orientation (Lu et al., 2008; Sasai et al., 2008). The ortholog of Aurora-A (Ipl1, known as increase-in-ploidy-1) has been discovered in 1993 in *Saccharomyces cerevisiae* as a mitotic protein required for chromosome segregation (Chan & Botstein, 1993). Since then, two further related serine/threonine kinases (Aurora-B and Aurora-C) were identified in higher eukaryotes. While the members of the Aurora kinase family have multiple established roles during mitosis and meiosis, it became evident more recently that they could also fulfil non-mitotic functions.

1.4.1 The family of Aurora kinases

The family of Aurora kinases consists of three members: Aurora-A (*AURKA*), Aurora-B (*AURKB*), and Aurora-C (*AURKC*; Figure 1.10). The expression of the family members differs, since Aurora-A and Aurora-B are ubiquitously expressed in all cell types, whereas Aurora-C is mainly expressed in testis (Hu et al., 2005; Nigg, 2001).

Aurora-A is with 403 amino acids (AA) and 46 kDa the largest family member. All family members share a conserved catalytical domain (shown in green) but differ in their amino- as well as carboxy-terminus (shown in grey). KEN box, activation box (A box), and destruction box (D box) are structures which facilitate the proteasomal degradation of Aurora family members by the Cadherin-1/APC/C complex (Taguchi et al., 2002). The binding of the anaphase promoting complex/cyclosome (APC/C) is mediated by the D box, present in the catalytic domain of all Aurora family members. Multiple degrons are present to enhance this interaction (Lindon et al., 2015). Additional conserved motifs are the KEN motif and the A box with the AA sequence QRVL which can be found in the amino-terminus of Aurora-A and Aurora-B. Interestingly, it was demonstrated that intact KEN and A boxes are necessary for the proteasomal degradation of Aurora-B (Nguyen et al., 2005).

Additionally, the catalytic domain contains the so-called activation loop. Aurora family members are inactive, but when bound to a coactivator they change their conformation towards an active state. Additional activation can occur due to the auto-phosphorylation of the kinase on a threonine [T288 (Aurora-A), T232 (Aurora-B), and T195 (Aurora-C)] within the activation loop. The auto-phosphorylation site can be dephosphorylated by protein phosphatase 1 (PP1) *in vitro* and *in vivo* (Eyers et al., 2003; Tsai et al., 2003, Sen et al., 2002). Another known phosphatase demonstrated to regulate T288 phosphorylation when Aurora-A is activated by TPX2 is PP6 (Zeng et al., 2010).

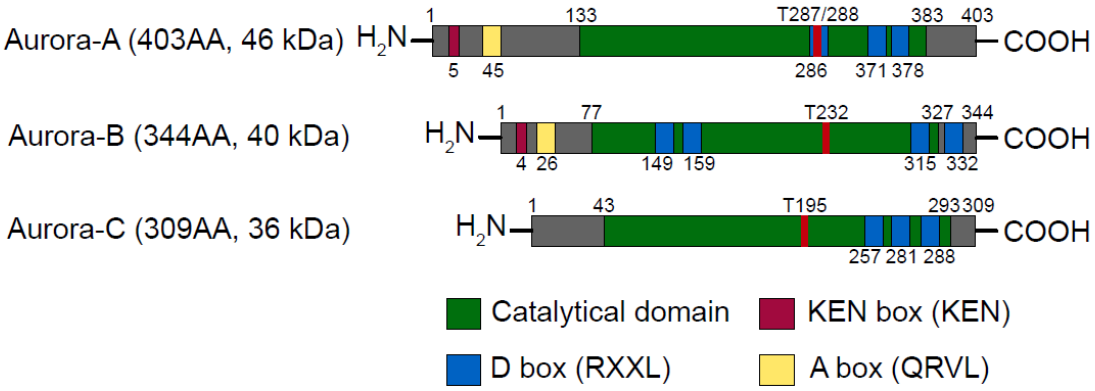

Figure 1.10: Schematic view of Aurora family members.
The structure of Aurora-A (AURKA), Aurora-B (AURKB), and Aurora-C (AURKC) including their amino acid (AA) length and their molecular weight is depicted. Conserved regions as catalytic domain (green), KEN box (red), A box (yellow) and D box (blue) are shown (modified from Tang et al., 2017).

The function of Aurora family members is tightly controlled and correlated with their distribution throughout the cell cycle. Aurora-A is required for centrosome maturation, separation, bipolar spindle assembly, and entry into mitosis. Aurora-B localizes to kinetochore and the spindle midzone, where it is required for chromosome condensation, alignment, segregation, and cytokinesis. Aurora-C is expressed in meiosis and is thought to have analogous functions to Aurora-B in mitosis, still its function is least understood (Marumoto et al., 2005).

Aurora-A harbors a mitochondrial targeting sequence (MTS) at the amino-terminus. This MTS allows the targeting and import into the mitochondrial matrix independently of cell cycle phases (Bertolin et al., 2018). The kinase is considered to play important roles in maintenance of mitochondrial morphology as well as mitochondrial dynamics (Bertolin et al., 2018; Grant et al., 2018; Kashatus et al., 2011).

Aurora-A and Aurora-B share parts of their consensus motif which is the favored sequence to be phosphorylated on their target proteins. The Aurora-A motif has a positively charged amino acid on -2 and/or -3 positions in front of the serine or threonine (R/K R/K X S/T). The Aurora-B motif instead has a positively charged residue on -2 position in front of the serine or threonine (R/K X S/T). Additional positive residues on -1 or -5 positions are enriched in Aurora-B consensus motifs. Both kinases prefer no proline after the phosphorylated amino acid (Kettenbach et al., 2011).

1.4.2 Canonical, mitotic functions of Aurora-A

The function of Aurora-A is regulated by its protein level as well as its subcellular localization and both parameters change throughout the cell cycle. At the end of S phase, Aurora-A localizes to duplicated centrosomes. Its localization shifts to the bipolar spindle during mitosis.

At the end of mitosis, Aurora-A moves to the perinuclear material of the daughter cell (Sugimoto et al., 2002). Concomitantly, Aurora-A expression increases during late G2 phase and peaks at the transition from G2 to M phase. At the end of mitosis Aurora-A is degraded by the APC/C complex (Taguchi et al., 2002) and its coactivator subunits CDC20 and CDH1 (Alfieri et al., 2017).

Aurora-A controls and regulates several processes like centrosome maturation, centrosome separation, mitotic entry, bipolar spindle assembly, chromosome alignment on metaphase plates as well as cytokinesis (Hirota et al., 2003; Marumoto et al., 2003; Roghi et al., 1998).

Centrosome maturation

Aurora-A activity at centrosomes is regulated by the LIM protein AJUBA (Hirota et al., 2003). Centrosome maturation is a step where large amounts of pericentriolar material (PCM) is recruited to centrosomes. The PCM consists of an interaction network of many proteins with high molecular weight building a platform to anchor γ-tubulin (Reboutier et al., 2012; Muller et al., 2010). Active Aurora-A can recruit γ-tubulin, NDEL1 as well as TACC/MAP215 to microtubule organizing centers (MTOCs; Mori et al., 2007; Bellanger & Gonczy, 2003; Giet et al., 2002). MTOCs facilitate the maturation of centrosomes as well as enhance the nucleation of microtubules required to ensure bipolarization as well as correct mitotic spindle assembly (Tillery et al., 2018; Pinyol et al., 2013).

Centrosome separation

The centrosome separation happens before the breakdown of the nuclear envelope (Hannak et al., 2001). Aurora-A localizes to the unseparated centrosome asters during spindle assembly (Marumoto et al., 2003). In *Xenopus laevis* the Aurora-A homologue phosphorylates the kinesin-like protein XIEg5 (Eg5 in human). This protein has an essential role in separation of centrosomes after nuclear-envelope breakdown (Giet et al., 1999).

Mitotic entry

Aurora-A also regulates the mitotic entry by phosphorylating CDK1, as further discussed above (see 1.2.1).

Bipolar spindle formation

Aurora-A localizes to the mitotic spindle, as soon as spindle assembly starts to coordinate bipolar spindle formation. At the spindle Aurora-A is activated by TPX2 (Wittmann et al., 2000; Wittmann et al., 1998). Active Aurora-A phosphorylates NEDD1, which is required for the targeting of centrosomes to the mitotic spindle as well as for microtubule nucleation, overall regulating bipolar spindle formation (Haren et al., 2006; Luders et al., 2006).

Chromosome alignment on metaphase plates

Aurora-A and Aurora-B work cooperatively to define chromosome alignment on metaphase plates. Aurora-A as well as Aurora-B are shown to phosphorylate the kinetochore-specific

histone H3 variant CENP-A on S7 (Marumoto et al., 2003; Zeitlin et al., 2001). Aurora-A performs this phosphorylation during prophase, which enables the localization of Aurora-B to the inner centromere (Kunitoku et al., 2003). Aurora-B maintains this phosphorylation from late prophase through metaphase. This phosphorylation enables proper attachment of microtubules to kinetochores and is therefore required for kinetochore structure and the regulation of proper chromosome alignment and segregation (Cheung et al., 2000).

Cytokinesis

Aurora-A levels affect cytokinesis, as suggested by the injection of Aurora-A antibodies as well as overexpression of Aurora-A, which impaired cytokinesis by leading to multinucleated or binucleated cells, respectively (Marumoto et al., 2003; Meraldi et al., 2002). This indicates that the timing of activation and subsequential inactivation is crucial for proper cytokinesis.

1.4.3 Aurora-A in cancer

The *Aurora-A* gene is localized on the fragile chromosome region 20q13.2 (Isola et al., 1995). This region is amplified in a great number of epithelial cancers (Nikonova et al., 2013) as well as haematological malignancies (Farag, 2011). Besides amplification, also overexpression of Aurora-A is found in several cancers including ovarian, skin, pancreatic, and breast cancer (Vader & Lens, 2008; Zhang et al., 2004; Meraldi et al., 2002; Isola et al., 1995). The amplification or overexpression can lead to checkpoint disruption (Marumoto et al., 2002), tetra-ploidy due to cytokinesis failure (Meraldi et al., 2002) and abnormal spindle formation (Minn et al., 1996).

In cancer cells, it was observed that overexpression of Aurora-A negatively correlates with DNA damage response genes, indicating a role in DNA repair. In urothelial cell carcinoma samples or ovarian cancer cells Aurora-A expression correlates with Breast Cancer 1 (BRCA1) and CHK2 or BRCA2 levels, respectively (Yang et al., 2010; Veerakumarasivam et al., 2008). Additionally, Aurora-A regulates the activity of poly (ADP-ribose) polymerase 1 (PARP1), an enzyme controlling the balance between non-homologous end joining (NHEJ) and homologous recombination (Du et al., 2016). Aurora-A inhibition regulates PARP1 activity and results in an increased double-strand break repair with NHEJ which is the more error prone form of DNA repair. Therefore, Aurora-A has an additional role in DNA repair in cancer cells by controlling the expression of BRCA1 (mainly in G1 and S phase) and the activation of PARP1-dependent NHEJ (mainly in G1 phase; Ray Chaudhuri & Nussenzweig, 2017; Ruffner & Verma, 1997; Vaughn et al., 1996).

Additionally, Aurora-A was shown to interact with the RAS effector RALA, thereby enhancing oncogenesis utilizing the RAS pathway (Lim et al., 2010; Wu et al., 2005).

1.4.4 Mechanisms of regulation

As mentioned above, Aurora-A is amplified or overexpressed in a great number of tumors leading to genomic instability. This suggests the need for a tight regulation of Aurora-A activity and expression during cell cycle under physiological circumstances.

Aurora-A activity and expression is regulated by three distinct mechanisms illustrated in Figure 1.11.

Transcription is enhanced by MYC family members and suppressed by p53 (Figure 1.11 a). In cancer cells MYC as well as MYCN are often overexpressed, leading to an increase in Aurora-A transcription (den Hollander et al., 2010; Shang et al., 2009). Consistently, the tumor suppressor p53 is often lost in tumor cells, leading to an increase in Aurora-A transcription (Liu et al., 2004). Additionally, Aurora-A can auto-regulate its transcription by phosphorylation of p53 on S215 and S315 (Katayama et al., 2004; Liu et al., 2004). These phosphorylations lead to an inhibition of p53 transcriptional activity as well as MDM2-mediated degradation of p53.

Besides transcriptional regulation, Aurora-A protein stability is tightly regulated (Figure 1.11 b). Degradation of Aurora-A is taking place at the end of mitosis through the APC/C complex (Taguchi et al., 2002) and its coactivator subunits CDC20 and CDH1 (Alfieri et al., 2017). Whether Aurora-A degradation is ubiquitin-dependent is currently a matter of debate. On one hand, it is known that the E3 ligase CHFR is interacting with the amino-terminus thereby ubiquitinating Aurora-A (Yu et al., 2005). Aurora-A degradation mainly relies on ubiquitination on K5 (Min et al., 2013). Additionally, Aurora-A is dephosphorylated on S51 by the phosphatase PP2A (Littlepage et al., 2002), an event considered a hallmark of mitotic exit. These steps allow the APC/C complex to degrade Aurora-A. On the other hand, the Aurora-A kinase interacting protein 1 enhances binding of Aurora-A with Antizyme 1 (AZ1; Lim & Gopalan, 2007b). AZ1 is an enzyme involved in polyamine biosynthesis pathway but has also a function in regulating ubiquitin-independent protein degradation pathways (Qiu et al., 2017). Therefore, AZ1 could promote the degradation of Aurora-A in a ubiquitin-independent manner (Lim & Gopalan, 2007a).

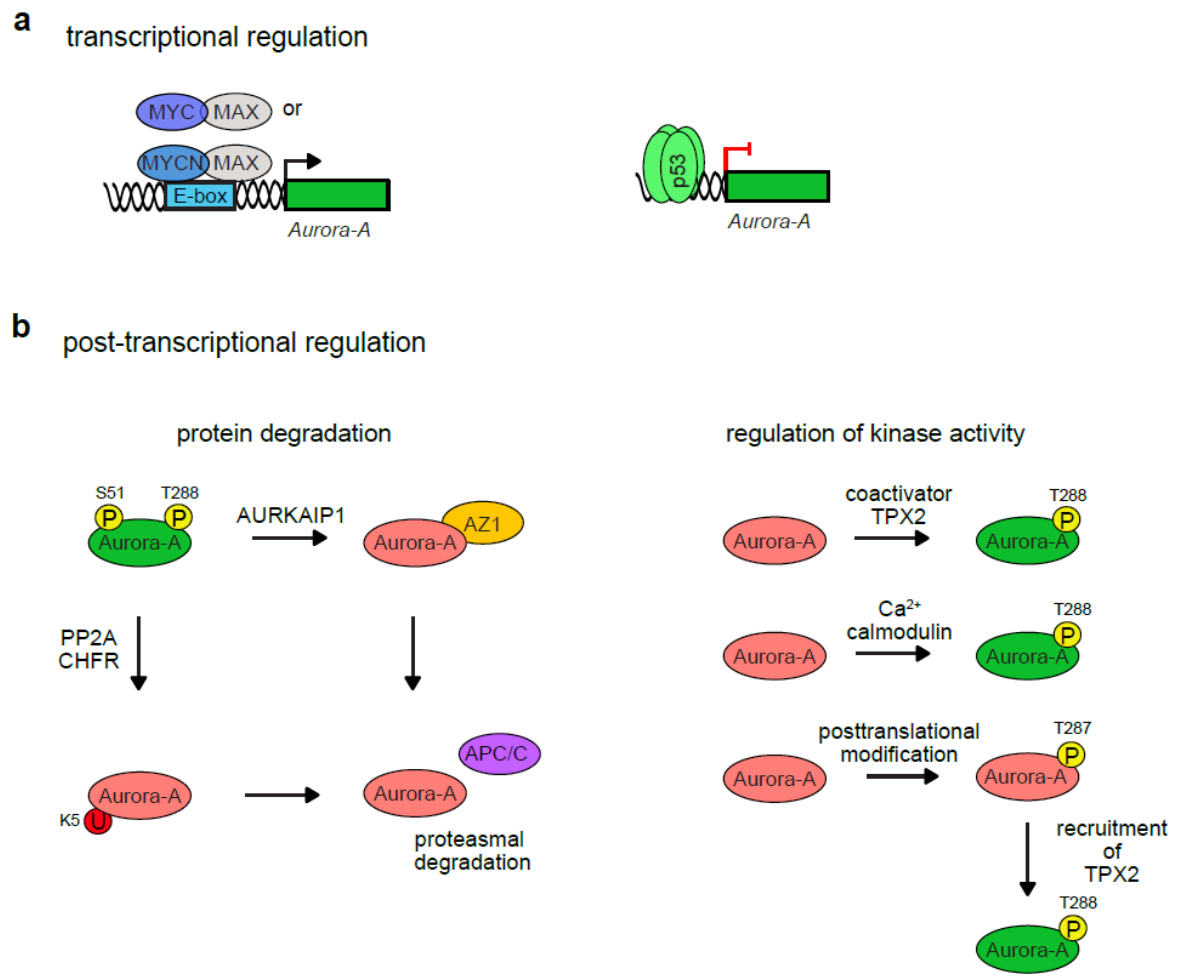

Figure 1.11: Mechanisms illustrating the regulation of Aurora-A expression and activity.
a. Aurora-A transcription is enhanced by MYC or MYCN and repressed by p53.
b. Post-transcriptional regulation of Aurora-A either depends on protein degradation or regulation of the kinase activity.

A further regulation point aims at balancing Aurora-A kinase activity which structurally relies on the orientation of the so-called DFG motif at the beginning of the T-loop. Depending on the DFG motif direction towards the ATP binding pocket, Aurora-A can exist in two states, named DFG-in or DFG-out state. The function of the DFG motif is the stabilization and coordination of the Mg^{2+} ion, required for the ATP-dependent phosphorylation of the substrate. If the T-loop is in a DFG-out state, the kinase can be considered as inactive, since Mg^{2+} is not stabilized. When bound to a coactivator, Aurora-A can change its conformation towards an DFG-in state. When in the DFG-in state, Aurora-A can auto-phosphorylate itself which further enhances its activity (Gilburt et al., 2017). The best characterized coactivator is TPX2 (Eyers et al., 2003) but also other coactivators like MYCN (Richards et al., 2016), AJUBA (Hirota et al., 2003), and PIFO (Kinzel et al., 2010) were identified. Additionally, calmodulin can activate Aurora-A in a Ca^{2+}-dependent manner (Plotnikova et al., 2012; Plotnikova et al., 2010). Protein kinase C was reported to phosphorylate T287, thereby enhancing Aurora-A´s interaction with TPX2 which can in turn activate Aurora-A (Mori et al., 2009).

1.4.5 Aurora-A and MYCN

Aurora-A was identified in a synthetic lethality screen as a protein required for the growth of *MYCN*-amplified neuroblastoma cells (Otto et al., 2009). Neuroblastoma have increased expression of Aurora-A protein, due to MYCN-mediated transcription (Shang et al., 2009). One possible explanation for the synthetic lethality could be that Aurora-A leads to the stabilization of MYCN (Figure 1.12).

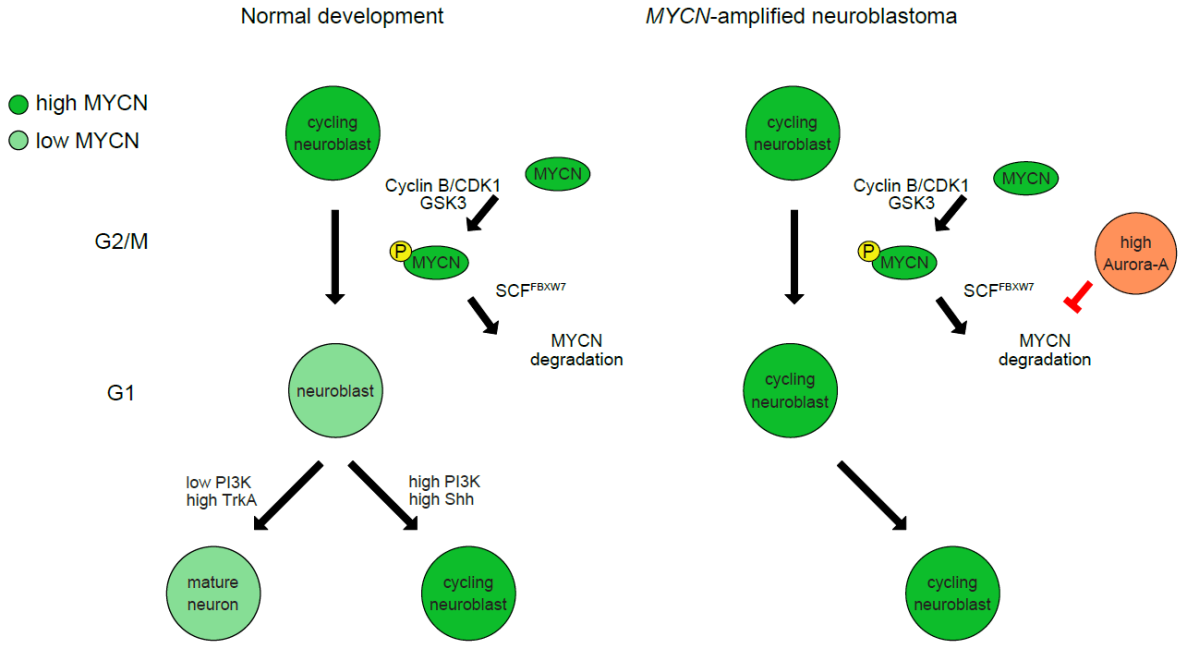

Figure 1.12 Model of the stabilization of MYCN by Aurora-A in neuroblastoma cells.
On the left, MYCN degradation under physiological conditions in a neuroblast is shown. On the right, it is shown that in neuroblastoma cells high Aurora-A level prevents MYCN from proteasomal degradation (as Otto et al., 2009).

During normal development MYCN is degraded in G2/M phase after the subsequent phosphorylation by cyclin B/CDK1 and GSK3-β. The phosphorylation on its degron primes it for the recognition by the ubiquitin ligase SCF^{FBXW7}. The ubiquitination of the E3-ligase leads to proteasomal degradation and to differentiation and development of the nervous system. In *MYCN*-amplified neuroblastoma cells the high level of Aurora-A leads to an association with MYCN and prevents its proteasomal degradation. Therefore, cycling neuroblasts always have high MYCN levels which allow them to remain in a proliferative state regardless of external signals (Otto et al., 2009).

Interestingly, while the kinase domain of Aurora-A is required for the dimerization with MYCN (Dodson et al., 2010), Aurora-A does not need to be catalytically active for the association to occur (Otto et al., 2009).

A peptide of MYCN spanning the residues 28 – 89 is sufficient to induce the auto-phosphorylation of Aurora-A *in vitro*, indicating a role of MYCN as coactivator of Aurora-A (Richards et al., 2016). Additionally, using proximity ligation assay (PLA), it was possible to

determine that the proximity between Aurora-A and MYCN is cell cycle-regulated and occurs in S phase (Büchel et al., 2017). This finding indicates that the Aurora-A/MYCN interaction in S phase is not only required for the stabilization of MYCN, but also leads to an activation of Aurora-A, suggesting the existence of a novel role for Aurora-A in S phase.

1.4.6 Inhibition of Aurora-A

Considering the role of Aurora-A in cancer, a lot of medicinal chemistry efforts aimed at the development of Aurora-A inhibitors. Currently, there is a broad range of Aurora-A inhibitors available that generally exploit three different targeting strategies. Catalytic inhibitors, conformation-disrupting (CD) drugs, or inhibitors performing both tasks are available.

MK5108 belongs to the class of catalytic Aurora-A inhibitors without any CD activity. This inhibitor has a 220-fold higher selectivity for Aurora-A (IC_{50} = 0.064 nM) compared to Aurora-B. MK5108 induces cell cycle arrest in G2/M phase (Shimomura et al., 2010). It was already used in Phase I clinical trial in patients with solid tumors showing a remarkably low toxicity (Amin et al., 2016).

Since it was considered that the conformation of Aurora-A is important for the stabilization of MYCN, Gustafson et al. analyzed 32 drugs with CD activity, among which CD532 was identified to be the most potent Aurora-A inhibitor. Treatment with CD532 leads to a stabilization of Aurora-A in an inactive conformation, unable to associate with MYCN. Therefore, MYCN is degraded by the proteasome. Treatment with CD532 leads to a cell cycle arrest in S phase and can be used to indirectly target MYCN. However, the pharmacological properties of the inhibitor are not suitable for clinical use and therefore still need to be optimized (Gustafson et al., 2014). So far, no clinical trial using CD532 was conducted.

MLN8237 (Alisertib) is the most studied Aurora-A inhibitor (Hong et al., 2014). MLN8237 is a partly CD compound and is also a catalytic inhibitor of Aurora-A. It has a 200-fold higher selectivity for Aurora-A (1.2 nM) compared to Aurora-B. Additionally, MLN8237 has negligible off-target effects towards other structurally related kinases (Manfredi et al., 2011). However, MLN8237 is not as effective as CD532 in reducing MYCN protein level. Cancer cells treated with MLN8237 show an accumulation in G2/M phase (Brockmann et al., 2013). Treating cells with 100 nM MLN8237 results in a catalytic inhibition of Aurora-A whereas it has no impact on the complex formation of Aurora-A and MYCN. Increasing doses of Aurora-A inhibitor (e.g., 1 µM or more) results in an abolishment of the catalytic activity as well as in a reduced complex formation of Aurora-A with MYCN (Brockmann et al., 2013).

Several Aurora-A inhibitors are already used in clinical trials for breast cancer, prostate cancer, leukemia, neuroblastoma, and other malignancies (Mosse et al., 2019; Bavetsias & Linardopoulos, 2015; Kollareddy et al., 2012). MLN8237 is the only Aurora-A inhibitor included

in a Phase III clinical trial (Barr et al., 2015; Melichar et al., 2015). This clinical trial was interrupted due to non-significant survival effects on patients with relapsed or refractory peripheral T-cell lymphoma (Bertolin & Tramier, 2020). Additionally, treating patients with MLN8237 showed dose-limiting toxicities (DLTs) as neutropenia, nausea and fatigue appears as side-effects after treatment (Durlacher et al., 2016).

Aurora-A inhibitors are not only used as monotherapies. A combination with a microtubule targeting agent (docetaxel) showed a significant increased survival of mice xenograft for mantle cell lymphoma. Therefore, this combination could be a beneficial treatment of B cell non-Hodgkin lymphomas (Qi et al., 2011). Besides this, also a combination with the proteasome inhibitor bortezomib was used in clinical trials for the treatment of multiple myeloma and showed a beneficial outcome (Rosenthal et al., 2016).

Aurora-A was also suggested to contribute to cisplatin-based chemotherapy resistance in non-small cell lung cancer (Xu et al., 2014). Therefore, simultaneous inhibition could enhance anti-tumor effects as well as overcome drug resistance (Tang et al., 2017).

All in all, it can be concluded that Aurora-A is a promising target in cancer treatment. However, the treatment needs to be further improved.

Besides the use of inhibitors, recently also a PROTAC has been designed which is able to target Aurora-A (Adhikari et al., 2020). PROTACs have two moieties; one binding to a certain protein of interest and the other one, which is able to recruit an E3 ligase that is able to degrade the protein (Winter et al., 2015). Treating cells with an Aurora-A PROTAC resulted in a cell cycle arrest in S phase. Together with the identified novel interaction partner involved in RNA metabolism, indicating a non-catalytic scaffolding function for Aurora-A in S phase (Adhikari et al., 2020).

1.5 Aim of the thesis

The role of Aurora-A in mitosis is extensively studied under physiological conditions as well as in the cancer situation. However, little is known regarding the role and function of Aurora-A in other cell cycle phases, although Aurora-A is expressed and can be activated also beyond mitosis.

The aim of this project was to elucidate and understand the role of Aurora-A in S phase of *MYCN*-amplified neuroblastoma cells.

Therefore, the localization of the complex formation as well as the substrates phosphorylated by Aurora-A upon activation by MYCN were investigated. Furthermore, downstream processes regulated by Aurora-A activity in S phase were assessed.

From our previous results, we suggested to combine low doses of Aurora-A inhibitors with ATR inhibitors. This new therapeutic approach was tested by a collaboration partner, revealing a therapeutic window for *MYCN*-amplified neuroblastoma. Therefore, the underlying mechanism for this therapeutic window was elucidated *in vitro*.

2 Materials

2.1 Cell lines and bacterial strains

2.1.1 Human cell lines

Cell lines were validated using STR analysis and routinely tested for mycoplasma contamination.

Name	Description (Source)
HEK293T	Human embryonic kidney cell line, derived from HEK293 cells but stable expressing SV40 large T antigen (ATCC)
IMR-5	Human *MYCN*-amplified neuroblastoma cell line (Angelika Eggert)
IMR-32	Human *MYCN*-amplified neuroblastoma cell line (Manfred Schwab)
NGP	Human *MYCN*-amplified neuroblastoma cell line (Angelika Eggert)
SH-EP	Human *MYCN* non-amplified neuroblastoma cell line (Manfred Schwab)
SH-SY5Y	Human *MYCN* non-amplified neuroblastoma cell line (Angelika Eggert)
SK-NAS	Human *MYCN* non-amplified neuroblastoma cell line (Angelika Eggert)

2.1.2 Murine cell lines

Cell lines were validated using STR analysis and routinely tested for mycoplasma contamination.

Name	Description (Source)
NIH-3T3	Murine embryonic fibroblasts (ATCC)

2.1.3 Bacterial strains

Name	Description
DH5α	*Escherichia coli*, genotype: F^-, Φ80lacZΔM15, Δ(lacZYA-argF) U169, recA1, endA1, hsdR17 (rK^-, mK^+), phoA, supE44, λ^-, thi-1, gyrA96, relA1
XL1 blue	*Escherichia coli*, genotype: recA1, endA1, gyrA96, thi-1, hsdR17, supE44, relA1 lac [F´proAB lacIqZΔM15 Tn10 (Tetr)]

2.2 Cultivation media and supplements

All chemicals were obtained from Sigma-Aldrich and Roth, changes in company are indicated.

2.2.1 Cultivation media for cell culture

For cultivation of human neuroblastoma cell lines RPMI-1640 (Thermo Fisher Scientific) and for HEK293T and murine cells DMEM (Thermo Fisher Scientific) was used and supplemented with:

10% (v/v) heat-inactivated (30 min, 56 °C) fetal calf serum (FCS; Biochrom)
1% (v/v) Penicillin/Streptomycin (100,000 U/ml, PAA)

Freezing medium	90% FCS 10% DMSO
Transfection medium	DMEM/RPMI-1640 2% (v/v) heat-inactivated FCS
Trypsin/EDTA	0.25% Trypsin (Thermo Fisher Scientific) 5 mM EDTA 22.3 mM Tris, pH 7.4 125 mM NaCl

2.2.2 Supplements and inhibitors for cell lines

Following supplements were used in cell culture by directly adding to the media.

Compound (Source)	Stock concentration	Final concentration
Doxycycline	1 mg/ml in EtOH; stored at -20 °C	1 µg/ml
Thymidine	200 µM	200 nM (Cell cycle synchronization)
Nocodazole	0.1 mg/ml in medium	0.1 µg/ml (Cell cycle synchronization)

The following inhibitors were used in cell culture by directly adding to the media. All inhibitors were diluted in DMSO and the stock solutions were kept at -20°C.

Compound (Source)	Inhibitor	Stock concentration	Final concentration
MLN8237 (Selleckchem)	Aurora-A	10 mM	100 – 10,000 nM
MK5108 (Selleckchem)	Aurora-A	10 mM	1 µM
10058-F4 (Sigma-Aldrich)	MYC/MAX hetero-dimerization	100 mM	100 µM
AZD6738 (Hycultec)	ATR	10 mM	100 nM
Pladienolide B (PlaB; Santa Cruz)	Splicing	1 mM	1 µM
AZD1152 (Selleckchem)	Aurora-B	10 mM	1 µM
CHIR-124 (Selleckchem)	CHK1	10 mM	1 µM
NVP-2 (Tocris)	CDK9	1 mM	200 nM
Flavopiridol (FP; Sigma-Aldrich)	Multiple CDKs	1 mM	200 nM

2.2.3 Cultivation media for bacterial strains

Medium	Composition
Lysogeny broth (LB) medium	10% (w/v) Bacto tryptone 0.5% (w/v) Yeast extract 1% (w/v) NaCl
LB agar	LB medium with 1.2% (w/v) Bacto agar autoclaved, then heated in a microwave, cooled down to 50 °C; antibiotics were added, and a 10 cm dish was filled with 20 ml.

2.2.4 Supplements for bacterial strains

Supplements were obtained from Roth in powder formulations. Stock solutions were prepared in ddH_2O and sterile filtered before use.

Antibiotic	Concentration
Ampicillin	100 µg/ml
Carbenicillin	100 µg/ml
Kanamycin	30 µg/ml

2.3 Buffers and solutions

Buffers and solutions were prepared in ddH_2O and stored at room temperature (RT). All chemicals were obtained from Sigma-Aldrich and Roth. All changes in dissolving solution, storage temperature and company are indicated.

Buffers and solutions	Composition
Ammonium persulfate (APS; 10%)	100 mg/ml; aliquots stored at -20 °C
Annexin V binding buffer	10 mM HEPES, pH 7.4 140 mM NaCl 2.5 mM $CaCl_2$
BCA buffer A	1% (w/v) BCA-Na_2 2% (w/v) Na_2CO_3 x H_2O
BCA buffer B	4% (w/v) $CuSO_4$ x 5 H_2O
Bis-Tris (3.5 x)	1.25 M Bis-Tris
Bis-Tris stacking gel	4% (v/v) acrylamide/bisacrylamide 1 x Bis-Tris 0.03% (v/v) APS 0.05% (v/v) TEMED
Bis-Tris separation gel	8 – 10% (v/v) acrylamide/bisacrylamide 1 x Bis-Tris 0.03% (v/v) APS 0.05% (v/v) TEMED
Blocking solution for ChIP	5 mg/ml BSA in PBS; sterile filtered with 0.45 µm vacuum filter, stored at 4 °C
Bradford reagent	0.01% (w/v) Coomassie Brilliant Blue G250 8.5% (v/v) phosphoric acid 4.75% (v/v) EtOH
ChIP elution buffer	50 mM Tris, pH 8.0 1 mM EDTA 1% SDS 50 mM $NaHCO_3$; prepared immediately before use
ChIP swelling buffer	5 mM PIPES, pH 8.0 85 mM KCl 0.5% NP-40, stored at 4°C

ChIP wash buffer I	20 mM Tris/HCl, pH 8.0 150 mM NaCl 2 mM EDTA 0.1% SDS 1% Triton X-100, stored at 4 °C
ChIP wash buffer II	20 mM Tris/HCl, pH 8.0 500 mM NaCl 2 mM EDTA 0.1% SDS 1% Triton X-100, stored at 4 °C
ChIP wash buffer III	10 mM Tris/HCl, pH 8.0 250 mM LiCl 1 mM EDTA 1% NP-40 1% deoxycholic acid sodium salt, stored at 4 °C
Crystal violet solution	0.1% (w/v) crystal violet 20% (v/v) EtOH
Digestion buffer	10% TFA in 100 mM ammonium bicarbonate
DNA loading buffer (6 x)	10 mM EDTA, pH 8.0 0.2% (w/v) Orange G 40% (w/v) sucrose, stored at -20 °C
Mini lysis buffer	0.2 M NaOH 1% SDS
Mini neutralization buffer	3 M NaOAc, pH 4.8
Mini resuspension buffer	50 mM Tris, pH 8.0 10 mM EDTA 10 µg RNase A
MOPS running buffer (20 x)	1 M MOPS 1 M Tris 20 mM EDTA 2% (w/v) SDS
MOPS running buffer (ready to use)	1 x MOPS running buffer 5 mM sodium bisulfite
Nucleoplasmic lysis buffer	20 mM HEPES, pH 7.9 3 mM EDTA 10% glycerol 150 mM potassium acetate 1.5 mM $MgCl_2$
NuPAGE transfer buffer (20 x)	500 mM Bis-Tris 500 mM bicine 20.5 mM EDTA 0.1 mM Chlorobutanol, stored at 4 °C
NuPAGE buffer (ready to use)	1 x NuPAGE transfer buffer 20% (v/v) Methanol
Phosphatase inhibitor cocktail	Ser/Thr phosphatase inhibitor (Sigma-Aldrich, P0044) Tyr phosphatase inhibitor (Sigma-Aldrich, P5726)

	used 1:1,000, aliquots stored at -20 °C
Phosphate buffered saline (PBS; 1 x)	137 mM NaCl 2.7 mM KCl 10.1 mM Na_2HPO_4 1.76 mM KH_2PO_4 Solution was autoclaved
Polybrene stock	200 mg dissolved in 50 ml H_2O; sterile filtered with 0.2 µM syringe filter, aliquots stored at -20 °C
Propidium iodide (PI) stock solution	1 mg/ml in PBS
Protease inhibitor cocktail	Protease inhibitor cocktail (Sigma-Aldrich, P8340) used 1:1,000, aliquots stored at -20 °C
Proteinase K	10 mg/ml in ddH_2O, aliquots stored at -20 °C
RIPA lysis buffer	50 mM HEPES, pH 7.9 140 mM NaCl 1% (v/v) Triton X-100 0.1% (w/v) SDS 0.1% (w/v) sodium deoxycholate 10 mM sodium fluoride 10 mM sodium pyrophosphate 10 mM β-glycerophosphate
Sucrose buffer	10 mM HEPES, pH 7.9 0.34 M sucrose 3 mM $CaCl_2$ 2 mM magnesium acetate 0.1 mM EDTA
Sample buffer (6 x)	1.2 g SDS 6 mg bromophenol blue 4.7 ml 100% (v/v) glycerol 1.2 ml 0.5 M Tris, pH 6.8 2.1 ml ddH_2O 0.93 g DTT
Tris-Acetate-EDTA (TAE) buffer (50 x)	2 M Tris, pH 8.0 5.7% (v/v) acetic acid 50 mM EDTA
Tris buffered saline (TBS; 20 x)	500 mM Tris 2.8 M NaCl pH 7.4
TBS with Tween 20 (TBS-T)	1 x TBS 0.2% (v/v) Tween-20
TE	10 mM Tris, pH 7.0 1 mM EDTA, pH 8.0

2.4 Standards, Enzymes, and Kits

2.4.1 Standards

DNA marker	Gene Ruler 1 kb Plus DNA ladder (Thermo Fisher Scientific)
Protein marker	PageRuler Prestained Protein Ladder (Thermo Fisher Scientific)

2.4.2 Enzymes

Benzonase nuclease	Merck
DNase I	Thermo Fisher Scientific
Gateway BP clonase II	Life Technologies
Gateway LR clonase II	Life Technologies
M-MLV Reverse Transcriptase	Promega
Phusion Hot Start II HF DNA polymerase	Thermo Fisher Scientific
Proteinase K	Roth
Restriction enzymes	Thermo Fisher Scientific
RNase A	Roth
SYBR®Green qPCR Mastermix	Thermo Fisher Scientific
T4 DNA Ligase	Thermo Fisher Scientific
Trypsine (sequencing-grade modified)	Promega

2.4.3 Kits

Click-iT EdU Alexa Fluor Imaging Kit	Themo Fisher Scientific
CloneJET™ PCR Cloning Kit	Thermo Fisher Scientific
Duolink® In Situ PLA® Probe Anti-Rabbit PLUS	Sigma-Aldrich
Duolink® In Situ PLA® Probe Anti-Mouse MINUS	Sigma-Aldrich
Duolink® In Situ Detection Reagents Green	Sigma-Aldrich
GeneJET Gel Extraction Kit	Thermo Fisher Scientific
Immobilon Western HRP Substrate	Sigma-Aldrich
NEBNext® ChIP-Seq Library Prep Master Mix Set for Illumina®	NEB
NEBNext Multiplex Oligos for Illumina (Dual Index Set 1)	NEB
NEBNext® Poly(A) mRNA Magnetic Isolation Module	NEB
NEBNext® rRNA Depletion Kit	NEB
NEBNext® Ultra™ II Directional RNA Library Prep with Beads	NEB
NEBNext® Ultra™ II DNA Library Prep with Beads	NEB
NEBNext® Ultra™ RNA Library Prep Kit	NEB
MiniElute PCR Purification Kit	Qiagen
miRNeasy® MiniKit	Qiagen
PureLink™ HiPure Plasmid Maxiprep Kit	Thermo Fisher Scientific
QIAquick Gel Extraction Kit	Qiagen
QIAquick PCR Purification Kit	Qiagen
Quant-iT™ PicoGreen dsDNA Assay Kit	Life Technologies
Quant-iT™ RiboGreen RNA Assay Kit	Life Technologies
RNeasy® MinElute® cleanup kit	Qiagen

2.5 Nucleic acids

2.5.1 Primers

Unless otherwise indicated, all oligos were synthetized and obtained by Sigma-Aldrich at 0.025 µmol scale and purified by desalting (DST). Oligos longer than 50 bases were purified by HPLC. Each primer was resuspended in ddH_2O (Ampuwa) to a concentration of 100 µM and used at a final concentration of 10 µM. Stock and diluted primers were stored at -20 °C.

Primers for Cloning

Name of target	Sequence forward primer (5´to 3´)	Sequence reverse primer (3´to 5´)
mirE	TGAACTCGAGAAGGTATATTGC TGTTGACAGTGAGCG	TCTCGAATTCTAGCCCCTTGAAGT CCGAGGCAGTAGGC
attB H3.3	GGGGACAAGTTTGTACAAAAAA GCAGGCTTCAGTGCACGCGGA TCCGCGA	GGGGACCACTTTGTACAAGAAAG CTGGGTTTGCACTCCGGAATTCC GGTAA

Primers for qPCR

Name of target	Sequence forward primer (5´to 3´)	Sequence reverse primer (3´to 5´)
B2M	GTGCTCGCGCTACTCTCTC	GTCAACTTCAATGTCGGAT
SF3B2	CATCCATGGGGACCTGTACT	GGCTTCTTCTCCTTCAGTCG

Primers for ChIP qPCR

Name of target	Sequence forward primer (5´to 3´)	Sequence reverse primer (3´to 5´)
ACTB	GAGGGGAGAGGGGGTAAA	AGCCATAAAAGGCAACTTTCG
centrosome	TCATTCCCACAAACTGCGTTG	TCCAACGAAGGCCACAAGA
DRG2	CGTGGGCCAGTACAGCAT	CCGGAAGCCAAAGAGAACAG
EIF3B	TGGGTGTGCTGTGAGTGTAG	ATGGACAATTCTGAGGGGCA
GBA	AGCCCTTCCTCAAGTCTCAT	ACTGTGGGAATTCAATCGCC
intergenic	TTTTCTCACATTGCCCCTGT	TCAATGCTGTACCAGGCAAA
NCL	CTACCACCCTCATCTGAATCC	TTGTCTCGCTGGGAAAGG
NME1	GGGGTGGAGAGAAGAAAGCA	TGGGAGTAGGCAGTCATTCT
NPM1	TTCACCGGGAAGCATGG	CACGCGAGGTAAGTCTACG
POLG	CTTCTCAAGGAGCAGGTGGA	TCATAACCTCCCTTCGACCG
PPRC1	GTGAGGATTAGCGCTTGGAG	TGCTGTACGTTCCTTTCACC
RAN	CCGTGACTCTGGGATCTTGA	CAAGGTGGCTGAAACGGAAA
RCC1	AGTGGTCGCTTCTTCTCCTT	GCATTAGACCCACAACTCCG
RPS16	CCGAGCGTGGACTAGACAA	GTTAGCCGCAACAGAAGCC
TFAP4	CCGGGCGCTGTTTACTA	CAGGACACGGAGAACTACAG

2.5.2 shRNAs

Name	Sequence 5´to 3´
sh*SF3B2* #1	CAAGGAAAGAGATGAATATTTA
sh*SF3B2* #2	AACAGAAGACCATGAAGTCAAA
sh*DEK* #1	CCAGCTTCACGATTATGACTAA
sh*DEK* #2	AACCGATGAACTTAGAAATCTA
sh*DEK* #3	CCAGGCACTGTGTCCTCATTAA
sh*ATAD2* #1	TGCCGATGTTGATCCAATGCAA
sh*ATAD2* #2	AAAGGTGCTGATTGTCTAAGTA
sh*ATRX* #1	TCAGGAAGTTCCACAAGATAAA
sh*ATRX* #2	GAAGACAGAAGATAAAGATAAA
sh*ATRX* #3	GCAGCTAGACTACATTAGCAAA
sh*MSH6* #1	CTCCGAAGTTGTAGAGCTTCTA
sh*MSH6* #2	TAAGAGTGAAGAAGATAATGAA
sh*SMARCAD1* #1	GAAGGGTGATAGAGTTGTGTTA
sh*SMARCAD1* #2	CCAAGAAAGAGATGTAGTTATA
sh*DHX9* #1	AAACGATGTTGTTTATGTCATT
sh*DHX9* #2	AAAGGAAGAACAAGAAGTGCAA
sh*DHX9* #3	TCAGCTGCAAAACATCATTCAA
sh*CDK12* #1	TCAGCGACAAAGTGGTGTTGTA
sh*CDK12* #2	CCCGGGACTTACTAAAAGCTAA
sh*CDK12* #3	GAAGGAAATTGTCACAGATAAA
sh*CDK12* #4	CTCCGAGAAGCATCTTGTTAAA
sh*CDK12* #5	TAAAGAGAATAGTGTTCACAAA
sh*CCNK* #1	ATCCATACCAGTTCCTACTAAA
sh*CCNK* #2	TCCCGGTCGACGTTTTGGAAGA
sh*CCNK* #3	GCCCTTGCAGTCTGACTGTGTA
sh*CCNK* #4	CTGGATCTTTACTCACAAGGAA
sh*SUPT16H* #1	GCAGAAGAGTCAGACTATTCTA
sh*SUPT16H* #2	TTACGAGGAAGAAGAAGAACAA
sh*SUPT16H* #3	GCAAGTCTAATGTGTCCTATAA
sh*SUPT16H* #4	CAAGAAGTTCAAGAAAATTATA
sh*SSRP1* #1	TAAGCGAGAGCTTCAAGAGCAA
sh*SSRP1* #2	GCCGAGAGAAGATCAAGTCAGA
sh*SSRP1* #3	AAAGGTAAAGATGGAAAAGAAA
sh*SSRP1* #4	CAAAGAAGAAGAAGAAAGTAAA
sh*SSRP1* #5	ACAAGTCAAAGAAGAAGAAGAA
sh*ORC6* #1	CTAGCTGTACAGTTTAGCTGTA
sh*ORC6* #2	GAGCGAGACTTATAGATAGATA
sh*ORC6* #3	TTAGCTGTATAGAAGCAGTGAA
sh*PCF11* #1	ACAGGTTGATGAACATAGTAAA
sh*PCF11* #2	ACAGGAAAGAATTTCTAATGAA
sh*PCF11* #3	AGACGTTGGTACTACAGTTTAA
sh*PCF11* #4	AAAGCTGCTGTTGGATCTAGAA
sh*PCF11* #5	GAGCGACCACAAGAAACTACAA

2.5.3 siRNAs

si*NTC*	SMART pool RNAi library, Dharmacon; non-targeting control (NTC)
si*SF3B2*	SMART pool RNAi library, Dharmacon; cat. No 026599

2.5.4 Plasmids

All sequences cloned into the vectors refer to human sequences.

Verification of constructs by Sanger sequencing was carried out by LCG Genomics.

Empty vectors

pDONR221	Vector for generating entry clones for Gateway cloning
pInducer21	Doxycycline-inducible cDNA expression vector with IRES GFP (Meerbrey et al., 2011)
pJET2.1	Blunt cloning vector with T7-promoter (CloneJET™PCR Cloning Kit, Thermo Fisher Scientific)
pLT3GEPIR	pRRL vector backbone expressing Tet-ON mirE-based RNAi

Packaging vectors for lentiviral production

psPAX.2	Plasmid encoding virion packaging system
pMD2G	Plasmin encoding virion envelope

Plasmids available in the laboratory of Martin Eilers

pcDNA3.0 MYCN	pcDNA3.0 vector with coding sequence (CDS) of human MYCN WT; cloned by Tobias Otto
pcDNA3.0 MYCN T58A	pcDNA3.0 vector with CDS of human MYCN harboring a T58A mutation; cloned by Tobias Otto
pInd21 HA-RNase H1	pInducer21 vector with CDS of human RNase H1 tagged with HA, cloned by Jacqueline Kalb
pTRE2pur AURKA	pTRE2pur vector with CDS of human Aurora-A WT; cloned by Markus Brockmann
pTRE2pur AURKA T217D	pTRE2pur vector with CDS of human Aurora-A harboring a T217D mutation; cloned by Markus Brockmann

Plasmids generated during this study

pInd21 H3.3-HA	pInducer21 vector with CDS of human H3.3 tagged with HA
pInd21 H3.3	pInducer21 vector with CDS of human H3.3
pJET2.1 Repair template H3 WT	pJET2.1 vector with repair template of human H3 WT
pJET2.1 Repair template H3S10A	pJET2.1 vector with repair template of human H3 introducing a H3S10A mutation
pJET2.1 Repair template H3S10D	pJET2.1 vector with repair template of human H3 introducing a H3S10D mutation
pLT3GEPIR shSF3B2 #1	pLT3GEPIR shRNA targeting *SF3B2* #1

pLT3GEPIR shSF3B2 #2	pLT3GEPIR shRNA targeting *SF3B2* #2
pLT3GEPIR shDEK #1	pLT3GEPIR shRNA targeting *DEK* #1
pLT3GEPIR shDEK #2	pLT3GEPIR shRNA targeting *DEK* #2
pLT3GEPIR shDEK #3	pLT3GEPIR shRNA targeting *DEK* #3
pLT3GEPIR shATAD2 #1	pLT3GEPIR shRNA targeting *ATAD2* #1
pLT3GEPIR shATAD2 #2	pLT3GEPIR shRNA targeting *ATAD2* #2
pLT3GEPIR shATRX #1	pLT3GEPIR shRNA targeting *ATRX* #1
pLT3GEPIR shATRX #2	pLT3GEPIR shRNA targeting *ATRX* #2
pLT3GEPIR shATRX #3	pLT3GEPIR shRNA targeting *ATRX* #3
pLT3GEPIR shMSH6 #1	pLT3GEPIR shRNA targeting *MSH6* #1
pLT3GEPIR shMSH6 #2	pLT3GEPIR shRNA targeting *MSH6* #2
pLT3GEPIR shSMARCAD1 #1	pLT3GEPIR shRNA targeting *SMARCAD1* #1
pLT3GEPIR shSMARCAD1 #2	pLT3GEPIR shRNA targeting *SMARCAD1* #2
pLT3GEPIR shDHX9 #1	pLT3GEPIR shRNA targeting *DHX9* #1
pLT3GEPIR shDHX9 #2	pLT3GEPIR shRNA targeting *DHX9* #2
pLT3GEPIR shDHX9 #3	pLT3GEPIR shRNA targeting *DHX9* #3
pLT3GEPIR shCDK12 #1	pLT3GEPIR shRNA targeting *CDK12* #1
pLT3GEPIR shCDK12 #2	pLT3GEPIR shRNA targeting *CDK12* #2
pLT3GEPIR shCDK12 #3	pLT3GEPIR shRNA targeting *CDK12* #3
pLT3GEPIR shCDK12 #4	pLT3GEPIR shRNA targeting *CDK12* #4
pLT3GEPIR shCDK12 #5	pLT3GEPIR shRNA targeting *CDK12* #5
pLT3GEPIR shCCNK #1	pLT3GEPIR shRNA targeting *CCNK* #1
pLT3GEPIR shCCNK #2	pLT3GEPIR shRNA targeting *CCNK* #2
pLT3GEPIR shCCNK #3	pLT3GEPIR shRNA targeting *CCNK* #3
pLT3GEPIR shCCNK #4	pLT3GEPIR shRNA targeting *CCNK* #4
pLT3GEPIR shSUPT16H #1	pLT3GEPIR shRNA targeting *SUPT16H* #1
pLT3GEPIR shSUPT16H #2	pLT3GEPIR shRNA targeting *SUPT16H* #2
pLT3GEPIR shSUPT16H #3	pLT3GEPIR shRNA targeting *SUPT16H* #3
pLT3GEPIR shSUPT16H #4	pLT3GEPIR shRNA targeting *SUPT16H* #4
pLT3GEPIR shSSRP1 #1	pLT3GEPIR shRNA targeting *SSRP1* #1
pLT3GEPIR shSSRP1 #2	pLT3GEPIR shRNA targeting *SSRP1* #2
pLT3GEPIR shSSRP1 #3	pLT3GEPIR shRNA targeting *SSRP1* #3
pLT3GEPIR shSSRP1 #4	pLT3GEPIR shRNA targeting *SSRP1* #4
pLT3GEPIR shSSRP1 #5	pLT3GEPIR shRNA targeting *SSRP1* #5
pLT3GEPIR shORC6 #1	pLT3GEPIR shRNA targeting *ORC6* #1
pLT3GEPIR shORC6 #2	pLT3GEPIR shRNA targeting *ORC6* #2
pLT3GEPIR shORC6 #3	pLT3GEPIR shRNA targeting *ORC6* #3
pLT3GEPIR shPCF11 #1	pLT3GEPIR shRNA targeting *PCF11* #1
pLT3GEPIR shPCF11 #2	pLT3GEPIR shRNA targeting *PCF11* #2
pLT3GEPIR shPCF11 #3	pLT3GEPIR shRNA targeting *PCF11*#3
pLT3GEPIR shPCF11 #4	pLT3GEPIR shRNA targeting *PCF11* #4
pLT3GEPIR shPCF11 #5	pLT3GEPIR shRNA targeting *PCF11* #5

2.6 Antibodies

2.6.1 Primary antibodies for immunoblotting

Antibody	Species	Clone/Cat. No	Manufacturer
Actin	Mouse	AC-15	Sigma-Aldrich
Aurora-A	Rabbit	ab1287	Cell Signaling
Aurora-A pT288	Rabbit	D13A11	Cell Signaling
Chk1	Rabbit	sc-7898	Santa Cruz
Chk1 pS345	Rabbit	2348	Cell Signaling
γH2A.X	Rabbit	2577	Cell Signaling
H2B	Rabbit	ab1790	Abcam
H3	Rabbit	ab1791	Abcam
H3 pS10	Rabbit	06-570	Sigma-Aldrich
HA	Rabbit	16B12	Biolegend
KAP1	Rabbit	A300-274A	Bethyl Laboratories
KAP1 pS824	Rabbit	ab70369	Abcam
MYC	Rabbit	Y69	Abcam
MYCN	Mouse	NCM II 100	Santa Cruz
RPA32	Mouse	sc-53496	Santa Cruz
RPA32 pS33	Rabbit	A300-264A	Bethyl Laboratories
SF3B1	Mouse	D221-3	MBL
SF3B1 pT313	Rabbit	D8D8V	Cell Signaling
SF3B1 pT328	Rabbit	Lührmann lab	(Girard et al., 2012)
TOP2A	Rabbit	A300-054A	Bethyl Laboratories
TPX2	Mouse	sc-271570	Santa Cruz
Tubulin	Rabbit	sc-12462	Santa Cruz
Vinculin	Mouse	V9131	Sigma-Aldrich

2.6.2 Primary antibodies for immunofluorescence

Antibody	Species	Clone/Cat. No	Manufacturer	Dilution
ATAD2	Rabbit	HPA029424	Sigma-Aldrich	1:200
ATRX	Rabbit	HPA064684	Sigma-Aldrich	1:200
Aurora-A	Mouse	4G10	Biozol	1:200
Cyclin B1	Mouse	sc-245	Santa Cruz	1:500
DEK	Rabbit	HPA057799	Sigma-Aldrich	1:100
MSH6	Rabbit	HPA028376	Sigma-Aldrich	1:1,000
MYCN	Mouse	C-19	Santa Cruz	1:100
PCNA	Rabbit	ab92552	Abcam	1:1,000
pH3S10	Rabbit	06-570	Sigma-Aldrich	1:500
pH3T3	Rabbit	9714S	Cell Signaling	1:100
RPA pS33	Rabbit	A300-264A	Bethyl Laboratories	1:400
SF3B2	Rabbit	HPA045028	Sigma-Aldrich	1:100
SMARCAD1	Rabbit	HPA016737	Sigma-Aldrich	1:500
Total RNAPII	Mouse	F12	Santa Cruz	1:1,000

2.6.3 Antibodies for ChIP

Antibody	Species	Clone/Cat. No	Manufacturer
H3	Rabbit	ab1791	Abcam
H3.3	Rabbit	ab176840	Abcam
H3 pS10	Rabbit	ab177218	Abcam
MYCN	Mouse	B8.4.B	Santa Cruz
RNAPII total	Mouse	A10	Santa Cruz
RNAPII pS2	Rabbit	ab5095	Abcam

2.6.4 Secondary antibodies for immunoblotting

Antibody	Species	Clone/Cat. No	Manufacturer
Anti-mouse IgG-HRP	Goat	sc-2314	Santa Cruz
Anti-rabbit IgG-HRP	Goat	sc-2313	Santa Cruz
IRDye® 800CW anti-Mouse	Goat	C30109-03	LI-COR
IRDye® 800CW anti-Rabbit	Goat	C30409-07	LI-COR

2.6.5 Secondary antibodies for Immunofluorescence

Antibody	Species	Clone/Cat. No	Manufacturer
Alexa Fluor®488 anti-Mouse	Goat	A11017	Invitrogen
Alexa Fluor®568 anti-Rabbit	Goat	A11036	Invitrogen

2.7 Consumables

Consumables were purchased from Eppendorf, Greiner, Nunc, Sarstedt, Ibidi, Waters, GLScience, Thermo Scientific, and VWR and included disposable plastic items such as cell culture dishes, reaction tubes, cryotubes, syringes, cuvettes, pipettes, plates for Immunofluorescence or Proximity-Ligation Assay.

2.8 Equipment

Cell culture incubator	BBD 6220 (Heraeus)
Cell counter	Casy cell counter (Innovatis)
Centrifuges	Avanti J-26 XP (Beckman Coulter) Eppendorf 5417 R (Eppendorf) Eppendorf 5425 (Eppendorf) Eppendorf 5430 (Eppendorf) Galaxy MiniStar (VWR) Multifuge 1S-R (Heraeus)
Deep-sequencer	Illumina GAIIx sequencer (Illumina) NextSeq 500 (Illumina)
Flow cytometer	BD FACS Canto II (BD Biosciences) BD FACS Aria III (BD Biosciences)
Fragment analyzer system	Fragment analyzer (Agilent)
Heating block	Thermomixer® comfort (Eppendorf)
Immunoblot detection	LAS-4000 imager (Fujifilm Global) Odyseey ® CLx Imaging System (LI-COR)
Immunoblotting transfer chamber	PerfectBlue Tank Electro Blotter Web S (Peqlab)
Microscopes	Leica SP2 microscope Operetta® High-Content Imaging System (Perkin Elmer)
PCR thermal cycler	C1000 Thermal cycler (Bio-Rad) Mastercycler pro S (Eppendorf)
Photometer	Multiscan Ascent (Thermo Labsystems) Ultrospec™ 3100 pro UV/Visible (Amersham Biosciences) Spectrofluorometer NanoDrop 1000 (Thermo Fisher Scientific)
Plate Reader	Infinite M200 Pro (Tecan)
Power supply	Power Pac (Bio-Rad) Consort EV231/EV243 (Roth)
PVDF transfer membrane	Immobilon P transfer membrane (Millipore)
Quantitative RT-PCR machine	StepOne® plus (Applied Biosystem)
Sterile Bench	HeraSafe (Heraeus)
Ultrasonifier	Bioruptor® (Pico) CovarisM220 (Covaris)
UV fluorescence table	Maxi UV fluorescent table (Peqlab)
Vortex mixer	Vortex-Genie 2 (Scientific Industries)
Whatman filter paper	Gel Blotting Paper (Schleicher und Schuell)

2.9 Software and online programs

Acrobat	Adobe Inc.
Affinity	Serif
Ascent	Thermo Labsystem
ApE plasmid editor	By M. Wayne Davis
BD FACSDiva 6.1.2	BD Biosciences
hermo	(Chen et al., 2013)
EndNote X7	Clarivate Analytics
EnrichR	(Huang da et al., 2009)
Harmony® High-Content Analysis software version 4.6	Perkin Elmer
Image J	By Wayne Rasband
Image Studio™ version 5.2.5	LI-COR
Integrated Genome Browser	(Nicol et al., 2009)
LAS AF 2.0	Leica
MaxQuant version 1.5.7.4 and 1.5.2.8	MaxQuant
Multi Gauge	Fujifilm Global
Multiscan Ascent	Thermo Labsystems
NanoDrop 1000 3.8.1	Thermo Fisher Scientific
Office 2011 Mac	Microsoft Inc.
Prism6	GraphPad Software Inc.
Spotfire data visualization software	TIBCO
Stepone software v2.3	Applied Biosystem
UCSC Genome Bioinformatics	http://genome.ucsc.edu

3 Methods

3.1 Cell-biological methods

3.1.1 Cultivation of eukaryotic cell lines

The human neuroblastoma cell lines IMR-5, IMR-32, NGP, SH-EP, SH-SY5Y, and SK-NAS cells were cultivated in RPMI-1640. HEK293T and NIH-3T3 mouse cells were cultivated in DMEM. 10% FCS and 1% Penicillin/Streptomycin was added to RPMI-1640 or DMEM (from here on “medium”) and the cells were incubated at 37 °C with 5% CO_2.

3.1.1.1 Passaging of cells

To passage the cells, the medium was removed, and the cells were washed with PBS. Trypsin/EDTA was added to detach the cells. After 1 - 5 min incubation at 37 °C, medium was added to stop the reaction. The cells were individualized and split in an appropriate ratio for further cultivation. For seeding a specific number of cells, cells were counted using the CASY cell counter.

3.1.1.2 Freezing of cells

Cells were trypsinized, centrifuged for 5 min at 300 g and room temperature (RT), and resuspended in freezing medium. Cells were transferred into cryogenic vials and stored at -80 °C in a freezing container that ensures slow cell freezing (1 °C per min). For short-term storage, frozen cells were kept at -80 °C, for long-term storage cells were transferred to liquid nitrogen storage tanks.

3.1.1.3 Thawing of cells

Frozen cells were quickly thawed and transferred into a tube filled with medium. To remove residual traces of DMSO, the cells were centrifuged for 5 min with 300 g at RT. The cell pellet was resuspended in fresh medium and plated on a cell culture dish.

3.1.2 Transfection of cells

Transfection is a method to bring nucleic acids into mammalian cells. For the transfection of plasmids, the transfection reagents Lipofectamine 2000 or polyethylenimine (PEI) were used. For transfection of siRNA the transfection reagent RNAiMax was used.

3.1.2.1 Transfection of plasmids

Cells were seeded the day before. Shortly before transfection, cells were washed once with PBS and transfection medium was added. Two reaction tubes were prepared containing each 500 µl Opti-MEM. One was mixed with 30 µl Lipofectamine 2000 or PEI and the other one with appropriate amount of plasmid DNA (5 - 15 µg). After incubation for 5 min at RT separately, reactions were mixed and incubated for 20 min at RT. The mix was added dropwise to the cells.

3.1.2.2 Transfection of siRNA

Cells were seeded the day before and shortly before transfection, washed once with PBS and medium was changed to transfection medium. Two reaction tubes were prepared containing each 500 µl Opti-MEM. One was mixed with 10 µl RNAiMax and the other one with appropriate amount of siRNA. After incubation for 5 min at RT separately, reactions were mixed and incubated for 20 min at RT. The mix was added dropwise to the cells, leading to a final concentration of 20 nM siRNA and 0.2% RNAiMax. 12 - 16 h later the medium was removed, and cells were supplied with fresh medium.

3.1.3 Lentivirus production

$5x10^6$ HEK293T cells were seeded on a 10 cm cell culture dish. On the next day cells were transfected using PEI (see 3.1.2.1) Therefore, 10 µg of packaging vector psPAX2, 2.5 µg of the envelope vector pMD2G and 10 µg of the lentiviral expression plasmid (e.g., pInducer21) were used for transfection. 16 h after transfection, the medium was removed, and 6 ml fresh medium was added. Virus containing supernatant was harvested 48 h, 60 h, and 72 h after transfection. The pooled supernatant containing the virus was filtered with 0.45 µm filter using a syringe. For long-term storage, the virus was stored in aliquots at -80 °C or directly used for lentiviral infection of cells (see 3.1.4).

3.1.4 Lentiviral infection

For lentiviral infection, 4 ml transfection medium, 2 ml filtered virus and polybrene to a final concentration of 6 µg/ml were used to infect IMR-5 cells growing on a 10 cm cell culture dish. 16 h after infection, cells were washed with PBS and fresh medium was added. 48 h after infection cells were selected dependent on the used vector by appropriate antibiotics or at a FACSAria™III by color due to expression of a fluorescent protein.

3.1.5 Cell cycle synchronization of cells

To analyze processes in certain cell cycle phases, cells were synchronized using double thymidine block or nocodazole. To determine that cell populations accumulate in distinct cell cycle phases, cells were analyzed using PI FACS (see 3.1.8.1).

3.1.5.1 Cell cycle synchronization using thymidine

Thymidine in large excess causes an arrest of the cells at the border between G1 and S phase due to inhibition of DNA synthesis (Schvartzman et al., 1984). Cells were treated with 2 mM thymidine. After 16 h, the cells were released by washing with PBS and renewing the medium. After 8 h the thymidine block was repeated to improve efficiency of cell cycle synchronization.

16 h later the cells were released and harvested after different timepoints. IMR-5 cells were released for 4 h, 8 h, and 12 h - 14 h to harvest S, G2/M, and G1 phase, respectively.

3.1.5.2 Cell cycle synchronization using nocodazole

Nocodazole blocks cells in mitosis by preventing microtubule assembly (Ho et al., 2001). One day after seeding, cells were treated with 1 µg/ml nocodazole. After 16 h incubation cells were harvested.

3.1.6 Harvesting and lysis of cells

For immunoblotting analysis cell lysates were prepared. First, cells were washed with PBS and afterwards harvested in 1 x RIPA lysis buffer containing 1:1,000 protease- and phosphatase-inhibitor cocktail. The cells were scraped from the dish and transferred into a reaction tube. After 30 min incubation on ice the lysates were centrifuged for 5 min with 14,000 rpm at 4 °C to remove cell debris and insoluble cell components. Protein concentration in the lysate was measured using either Bradford assay (see 3.3.1.1) or BCA assay (see 3.3.1.2).

3.1.7 Fractionation of cells

Fractionation of cells was used to obtain proteins localized in cytoplasm, nucleoplasm, or bound to chromatin in separated fractions. The samples were prepared as previously described (Aygun et al., 2008). Briefly, cells were seeded and treated as indicated. Before harvest, cells were washed with TBS containing 1:1,000 protease- and phosphatase-inhibitor cocktails and harvested by scraping. Cells were pelleted by centrifugation (300 g, 20 min, 4 °C). Lysis was carried out in sucrose buffer containing 0.5% NP-40 for 20 min at 4 °C while rotating. Nuclei were pelleted by centrifugation for 20 min with 3,900 g at 4 °C and washed once with sucrose buffer. Lysis of nuclei was carried out in nucleoplasmic lysis buffer by performing 20 strokes with a dounce-homogenizer on ice. Lysed nuclei were incubated 30 min on ice and homogenized by performing 30 strokes using a dounce-homogenizer. Benzonase (25 U) was added to each sample and incubated for 1 h at 16 °C. Unsolubilized chromatin was pelleted by centrifugation for 30 min at 18,000 g and 4 °C, resuspended in 1 x Sample buffer containing 5 U Benzonase to release chromatin-bound proteins, incubated at RT for 1 h, and heated for 15 min at 95 °C.

3.1.8 FACS analyses

FACS analysis was used to investigate cell cycle (PI FACS) as well as measuring apoptosis of cells (Annexin V/PI FACS). All samples were measured with FACSCanto™II. The measured data was analyzed with the software BD FACSDiva 6.1.2.

3.1.8.1 PI FACS

DNA content changes during cell cycle due to the duplication of DNA in the S phase. The intercalating agent propidium iodide (PI) is therefore measured by FACS to quantify the amount of cellular DNA and infer cell cycle distribution.

PI FACS samples were washed with PBS, trypsinized for 5 min, and transferred to a 15 ml tube. After centrifugation for 10 min at 1,500 rpm and 4 °C, the cells were washed with 10 ml ice cold PBS, and centrifuged again for 5 min with 1,500 rpm at 4 °C. To fix the cells, the pellet was resuspended in 1 ml of ice-cold PBS and added drop wise to 4 ml ice cold 100% ethanol, while vortexing. Samples were kept at -20 °C for at least 10 h. At the day of FACS measurement the samples were centrifuged for 5 min at 1,500 rpm and 4 °C. The supernatant was discarded, and the pellet was washed with 10 ml of ice-cold PBS. The cells were centrifuged 5 min at 1,500 rpm and 4 °C and the supernatant was discarded. The pellet was resuspended in 400 µl PBS containing 36 µg/ml PI and 24 µg/ml RNase A and incubated for 30 min at 37 °C or overnight at 4 °C in the dark. Prior measurement, the samples were transferred to a FACS tube.

3.1.8.2 Annexin V/PI FACS

Cell apoptosis can be investigated by staining of cells with Annexin V and PI. Phosphatidylserine is a component of cell membranes that almost exclusively resides in the inner part of the cell membrane (i.e., facing towards the cytoplasm) under physiological conditions. Upon apoptotic induction, phosphatidylserine is exposed to the outside and can be bound by the ligand Annexin V. Additionally, in a late apoptotic stage, the membrane is disrupted allowing PI to enter cells and stain the DNA (Koopman et al., 1994).

Therefore, supernatant including floating cells was collected from the cell culture dish, adherent cells were trypsinized 5 min to ensure complete detachment and added to the supernatant. Cells were centrifuged for 5 min at 1,500 rpm and 4 °C. Pellet was washed with ice cold PBS and again centrifuged. The pellet was resuspended in 100 µl Annexin V binding buffer and incubated with 5 µl Pacific Blue-conjugated Annexin V (25 µg/ml). After incubation for 15 min at RT in the dark, 400 µl of Annexin V binding buffer was added. Samples were transferred to FACS tubes and 5 µl of PI (1 mg/ml) was added to each sample before the measurement.

3.1.9 Crystal violet staining

Crystal violet staining is a method to visualize the density of cells plated on a cell culture dish. Therefore, cells were seeded on 6-well dishes and subjected to different treatments. Upon treatment end, medium was removed, and cells were washed with PBS once. Crystal violet

stain solution was added for 1 h at RT. Afterwards, excess of dye was washed from the cell culture dish with desalted water. The plates were air dried overnight at RT.

3.2 Molecular biology methods

3.2.1 Transformation of competent bacteria with plasmid DNA and plasmid amplification

Transformation of chemically competent bacteria with plasmid DNA was used following ligation (see 3.2.6) or for plasmid amplification. Therefore, competent bacteria were thawed on ice. The ligation mix or 1 µg plasmid DNA was added. After incubation for 30 min on ice, a heat-shock was performed for 45 s at 42 °C. Afterwards, the mix was kept on ice for 2 min, followed by addition of 700 µl prewarmed Lysogeny broth (LB) medium without antibiotics and incubation for up to 1 h at 37 °C. The suspension was centrifuged and resuspended in 100 µl of LB medium and plated on LB agar plates containing the appropriate antibiotic for selection. The plate was incubated overnight at 37 °C.

3.2.2 Isolation of plasmid DNA from bacteria

3.2.2.1 Small-scale isolation of plasmid DNA from bacteria (mini-preparation)

Plasmid DNA isolation in small-scale was performed using alkaline lysis. 1.4 ml overnight culture was centrifuged, and the pellet resuspended in 150 µl Mini resuspension buffer. To denaturate protein components, 150 µl of Mini lysis buffer was subsequently added, inverted several times, and incubated at RT. The lysis was stopped after 5 min by addition of 150 µl Mini neutralization buffer. Samples were centrifuged for 5 min at 14,000 rpm at RT, the supernatant containing the DNA was incubated with 500 µl isopropanol to precipitate DNA. After incubation for 30 min at -20 °C, the precipitate was pelleted by centrifugation for 10 min with 14,000 rpm at 4 °C. The pellet was washed once with 1 ml 80% ethanol, air-dried, and solubilized in 20 µl TE buffer.

3.2.2.2 Large-scale isolation of plasmid DNA from bacteria (maxi-preparation)

For large-scale isolation of plasmid DNA from bacteria, 200 ml overnight culture was processed using the PureLink™ HiPure Plasmid Maxiprep Kit according to manufacturer´s protocol. The purified DNA was solubilized in TE buffer and the DNA concentration was adjusted to 1 µg/µl using the NanoDrop 1000 system.

3.2.3 Restriction analysis of DNA

Restriction analysis of DNA was used for analytical and preparative reasons. Sequence-specific hydrolysis of DNA was performed using restriction endonucleases from Thermo Fisher Scientific or New England Biolabs according to manufacturer´s protocol.

Analytical digestion was set up as follows and incubated for 1 h at 37 °C.

1 µg	plasmid DNA
0.5 µl	restriction endonuclease 1
0.5 µl	restriction endonuclease 2
1 µl	10 x reaction buffer
Ad 10 µl	ddH_2O

For preparative digestion, the amount of DNA and restriction endonucleases, digestion time, and reaction volume were adjusted.

3.2.4 Gel electrophoresis separating DNA fragments

Gel electrophoresis is a method to analyze the molecular weight of nucleic acids. According to the expected size of the DNA fragment, agarose gels between 1 - 2% were prepared. Therefore, agarose was dissolved by boiling in TAE buffer. After the solution cooled down to 60 °C, ethidium bromide was added to a final concentration of 0.3 µg/ml, and mixed. The solution was poured in a horizontal gel chamber with a comb. DNA loading dye was added to each sample, before loading to the well of the gel. To determine the size of the DNA fragments, the Gene Ruler 1 kb Plus DNA ladder was used. The separation of DNA according to size was performed at 120 V for 1 h. Ethidium bromide intercalates DNA, which makes it possible to detect DNA-bands in the gel with UV light (254/365 nm) at a UV transilluminator. For documentation, ImageJ was used.

3.2.5 Extraction and purification of DNA fragments

The DNA fragments of interest were cut out of the agarose gel and extracted, using either QIAquick PCR Purification Kit or GeneJET Gel Extraction Kit according to manufacturer's protocol.

3.2.6 Ligation of DNA fragments into plasmids

To clone DNA fragments into linearized vectors, the T4 DNA ligase was used. The insert was added in 3 x molar excess to the vector. A ligation control with water instead of insert was used as a negative control.

100 ng	linearized vector
x ng	insert
1 µl	T4 DNA ligase
2 µl	10 x ligation buffer
Ad 20 µl	ddH_2O

The reaction mix was incubated up to 1 h at RT and then transformed into competent bacteria (see 3.2.1).

3.2.7 Cloning

3.2.7.1 Cloning of shRNAs into pLT3GEPIR

Short hairpin RNAs (shRNAs) are used to knock down a protein of interest. Therefore, constructs to generate shRNAs targeting the protein of interest were cloned into pLT3GEPIR, which harbors a miR-E based backbone. Sequences optimized for the protein of interest were obtained from Fellmann et al., 2013.

As a first step the oligos were amplified by a polymerase chain reaction (PCR).

1 µl	miR-E primer
50 ng	oligo
10 mM	dNTPs
2%	DMSO
10 µl	5 x HF buffer
0.5 µl	Phusion DNA polymerase
Ad 50 µl	ddH_2O

This mix was heated for 3 min at 98 °C. Afterwards, the mix was denaturated (25 s, 98 °C), annealed (30 s, 54 °C), and elongated (60 s, 72 °C) for 25 cycles, followed by a final elongation step for 5 min at 72 °C. 5 µl of the PCR mix was loaded to a 2% agarose gel (see 3.2.4) to investigate the success of the amplification, verified by a band at 150 bp. Amplified DNA was purified (see 3.2.5) and eluted in 20 µl TE-buffer.

To clone the shRNA oligo into the pLT3GEPIR, both the pLT3GEPIR vector and the amplified shRNA sequence were digested with the restriction enzymes EcoRI and XhoI (see 3.2.3), loaded onto a 1% agarose gel, cut out, and purified (see 3.2.5), followed by ligation (see 3.2.6) and transformation into competent bacteria (see 3.2.1). Clones were picked and a mini-preparation was performed (see 3.2.2.1), followed by a restriction digestion with MluI and XhoI, to investigate if the oligo was inserted into the vector. If a band at 250 bp could be detected, the plasmid DNA was sequenced (LGC Genomics) to confirm the correct orientation of the inserted oligo. Positive clones were amplified with a maxi-preparation (see 3.2.2.2).

3.2.7.2 Gateway cloning

To clone cDNA into the pINDUCER21 vector, the Gateway® cloning technology was used. The attB1 and attB2 sequences were inserted, flanking the cDNA by PCR with specific primers. The cDNA was first cloned using the BP clonase enzyme into the pDONOR221 vector according to manufacturer´s protocol. After transformation (see 3.2.1) and mini-preparation (see 3.2.2.1), clones were sequenced (LGC genomics). The positive entry clone was transferred into pINDUCER21 according to manufacturer´s protocol using the LR clonase enzyme. A positive clone was verified by sequencing (LGC genomics) and amplified by maxi-preparation (see 3.2.2.2).

3.2.8 Concentration measurement of nucleic acids

Different methods were accessed for measuring concentration of nucleic acids. Usually, concentration of plasmid DNA or RNA was measured with Nanodrop system (see 3.2.8.1), low amount of DNA or RNA, usually before library preparation was measured with either Pico- or RiboGreen (see 3.2.8.2), and all DNA and RNA used for sequencing e.g., prepared libraries were measured with Fragment analyzer (see 3.2.8.3).

3.2.8.1 NanoDrop

The concentration of isolated plasmid DNA or RNA was measured at the NanoDrop 1000. The NanoDrop is a spectrophotometer, which measures the absorption at 260 nm, directly correlated to nucleic acid concentration. The aromatic rings of the bases contribute to the absorption. The purity of the sample was determined by the ratio between the absorption at 260 nm to 280 nm.

3.2.8.2 PicoGreen and RiboGreen

Concentration measurements of double-stranded DNA (dsDNA) were performed with the Quant-iT™ PicoGreen dsDNA reagent. Concentration measurements of RNA were performed with the Quant-iT™ RiboGreen RNA reagent. Both PicoGreen as well as RiboGreen intercalate into their respective nucleic acid and the fluorescence can be determined at a wavelength of 485/535 nm. The samples were measured at a Tecan Infinite M200 Pro plate reader. The preparation of the samples was performed according to the manufacturer´s protocol. Quantification with PicoGreen was used to determine DNA concentration of ChIP samples, that were used as input material for library preparation of ChIP-sequencing. Quantification with RiboGreen was used to determine RNA concentration of samples containing pulled-down 4-thio-uridine RNA. These samples were then used as input material for library preparation of 4sU-sequencing.

3.2.8.3 Fragment analyzer

Isolated RNA, used as input material for RNA-sequencing (see 3.4.2) as well as DNA-libraries for RNA-, 4-thio-uridine-, and ChIP-sequencing were quantified on the Fragment analyzer according to manufacturer´s protocol.

3.2.9 Nucleic acid isolation

3.2.9.1 RNA isolation with TriFAST

For total RNA isolation the medium was removed from the cells. 1 ml TriFast™ was added to each dish and the cells were scraped and transferred into a reaction tube. After incubation for 5 min at RT 200 µl chloroform was added, the suspension was thoroughly vortexed, and incubated for 3 min at RT. After centrifugation for 5 min at 14,000 rpm and 4 °C, the aqueous phase was transferred into a new tube. 1 µl GlycoBlue and 500 µl isopropanol were added.

After vortexing, the mix was incubated for 15 min at -20 °C and afterwards centrifuged for 10 min at 4 °C and 14,000 rpm. The supernatant was removed, and the RNA pellet was washed twice with 1 ml 75% ethanol. After centrifugation for 10 min at 14,000 rpm and 4 °C, the supernatant was removed, and the pellet was dissolved in 25 µl RNase-free water. The concentration was determined with the Nanodrop 1000. The samples were further used for cDNA synthesis (see 3.2.10) and stored at -80 °C.

3.2.9.2 RNA isolation with the RNeasy® Mini

For RNA-sequencing (see 3.4.2), the RNA isolation was performed using the RNeasy® MinElute® cleanup kit according to manufacturer´s protocol, including a DNase I digestion step.

3.2.9.3 RNA isolation with the miRNeasy® Mini Kit

For labelled, nascent RNA, which was further used for 4-thio-uridine-sequencing (see 3.4.3), the isolation of RNA was performed using the miRNeasy® Mini Kit according to manufacturer´s protocol.

3.2.9.4 DNA isolation with phenol-chloroform

DNA within the process of Chromatin immunoprecipitation (ChIP; see 3.2.8.2) was isolated using phenol-chloroform. Therefore, one volume phenol-chloroform-isoamyl alcohol (25:14:1) was added to the samples and mixed thoroughly by vortexing. Samples were centrifuged for 5 min at 14,000 rpm and RT. The upper phase containing the DNA was transferred into a new reaction tube and mixed with 1 ml 100% ethanol, 30 µl NaAc with pH 5.2, and 2 µl GlycoBlue. To precipitate the DNA, the sample was vortexed and incubated for at least 30 min at -20 °C, followed by a centrifugation for 30 min at 14,000 rpm and 4 °C. The pellet was washed twice with 80% ethanol, air-dried, and resuspended in TE buffer or ddH_2O.

3.2.10 Complementary DNA (cDNA) synthesis

For the expression analysis of individual genes, the extracted total RNA (see 3.2.9.1.) was reverse transcribed into cDNA. For cDNA synthesis, 0.5 - 2 µg RNA was added to a final volume of 10 µl with water and incubated for 1 min at 65 °C. After a short incubation on ice, 40 µl of the master mix was added containing component as followed:

10 µl	5 x first strand buffer
1.25 µl	10 mM dNTPs
2 µl	random hexanucleotide primer
0.2 µl	RiboLock RNase inhibitor
1 µl	M-MLV reverse transcriptase
Ad 50 µl	ddH_2O

The mix was incubated for 10 min at RT, followed by an incubation for 50 min at 37 °C, and a 15 min incubation at 70 °C. 200 µl ddH_2O was added and the cDNA was stored at -20 °C. 10 µl were used for qPCR analysis (see 3.2.11).

3.2.11 Quantitative PCR (qPCR)

qPCR is used to analyze gene expression by measuring the abundance of the corresponding mRNA or to analyze enrichment of DNA fragments after ChIP (see 3.3.4). Therefore, a fluorescent dye which intercalates into newly synthesized DNA during the amplification step was used. In this study, SYBR® Green was employed as a fluorescent dye which is already present in the SYBR® Green Master Mix.

10 µl of DNA were added to 3 µl H_2O, 5 µl 2 x SYBR® Green Master Mix, and 2 µl of forward and reverse primer (10 µM). The samples were pipetted with the master mix into a 96 well plate and initially denaturated for 15 min at 95 °C. Afterwards 38 cycles of 30 s denaturation at 95 °C, 20 s annealing at 60 °C, and 15 s extension at 72 °C were performed to amplify the cDNA on the StepOne® plus machine.

The comparative Ct method described by Schmittgen and Livak in 2008 was applied to compare the amounts of nucleic acids in different samples. First, every well associated to a threshold cycle ("Ct") and every Ct was subtracted to the respective Ct of a housekeeping gene, thus obtaining a ΔCt value. Per definition, a housekeeping gene is expected not to change upon the tested experimental conditions. In this study ß-2-microglobulin (*B2M*) was used as housekeeping gene. Secondly, ΔCt values were subtracted to the respective ΔCt value of the untreated control (thus obtaining the ΔΔCt value). Finally, a fold change (FC) value was obtained through the formula $FC = 2^{-\Delta\Delta Ct}$. For all DNA fragments after ChIP, 1% input was used to normalize the samples. For each sample, the average and standard deviation of technical triplicates was calculated and reported.

3.3 Protein biochemical methods

3.3.1 Quantification of protein using colorimetric methods

Colorimetric methods were used to determine the protein concentration in a sample after lysis of cells (see 3.1.6).

3.3.1.1 Bradford assay

Bradford assay uses the binding of the Coomassie-brilliant blue G250-dye to unpolar, hydrophobic, and cationic side chains of amino acids. The binding leads to a shift of the absorbent maxima from 465 nm to 595 nm.

To determine the protein concentration, 1 µl of each lysate was mixed with 1 ml Bradford reagent and incubated for 5 min at RT. The absorption of the samples was measured at 595 nm using the Ultrospec™ 3100 pro. Protein concentration was then calculated using a standard curve, defined by known, increasing concentrations of BSA.

3.3.1.2 Bicinchoninic acid (BCA) assay

BCA uses the ability of peptide bonds in proteins to reduce Cu^{2+} ions to Cu^{+} ions. The amount of Cu^{+} is proportional to the protein amount in the sample. Additionally, two BCA molecules build purple colored chelate complexes with each Cu^{+} ion, leading to absorption at a wavelength of 562 nm.

A bovine serum albumin (BSA) standard curve was pipetted using 0 mg/ml, 0.5 mg/ml, 1 mg/ml, 2 mg/ml, 4 mg/ml, 6 mg/ml, and 8 mg/ml BSA, to calculate the protein concentration of the sample. 4 µl of standards and samples were added to 150 µl BCA solution (BCA buffer A and B were mixed in a 50:1 ratio) to a flat bottom 96 well plate. After incubation for 30 min at 37 °C in the dark the 96 well plate was measured with the Multiscan Ascent plate reader at 550 nm.

3.3.2 Bis-Tris gel electrophoresis

With Bis-Tris gel electrophoresis proteins are separated according to their molecular weight, and therefore used to analyze the composition of protein lysates. 6 x sample buffer was added, and the samples were denaturated for 5 min at 95 °C. The temperature and the detergent properties of SDS disrupt secondary and tertiary structures of the proteins. Due to DTT in the sample buffer, disulfide-bonds are reduced and thereby disrupted. After applying a voltage between 80 - 120 V, proteins run through the gel in the direction of the anode. Due to the mesh-like structures of the gels, there is a size-dependent separation of the proteins. Large proteins run slower through the gel than small proteins do. Mesh-like structures can be changed according to the amount of acrylamide.

Equal protein amounts (15 - 30 µg) were loaded into wells of a Bis-Tris gel consisting of a separation gel overlaid with a stacking gel. To estimate the size of a protein, 3 µl of the PageRuler Prestained Protein Ladder, which has a distinct pattern at specific molecular weights, was also loaded.

3.3.3 Immunoblotting

Afterwards, proteins were transferred onto a PVDF membrane using a wet blotting system. The PVDF membrane was activated for 5 min in 100% methanol, then washed for 5 min in water and subsequently incubated in 1 x NuPAGE transfer buffer. The gel, two sponges and 8 Whatman filter papers were also equilibrated in the transfer buffer.

The gel was laid on the PVDF membrane covered by four Whatman filter papers and a sponge on each side and fixed in the transfer chamber, filled with 1 x NuPAGE transfer buffer. Due to the positive charge of the membrane, the negatively charged proteins are transferred from the gel to the membrane after applying 300 mA at 4 °C for 2.5 h. Afterwards the membrane was

incubated for 1 h with 1:5 blocking solution in TBS to block unspecific binding. Subsequently, the membrane was cut into pieces according to the size of the proteins of interest and the pieces were incubated with the respective primary antibodies overnight at 4 °C. To wash away unspecifically bound antibody, the membranes were washed 3 times with TBS-T for 5 min. Afterwards the membranes were incubated for 1 h with the secondary antibody coupled to an infra-red fluorophore or horseradish peroxidase (HRP). The membranes were washed again 3 times for 5 min with TBS-T. The infra-red signal was detected by Odyseey ® CLx Imaging System. The HRP-coupled secondary antibodies were visualized by chemiluminescence using the Immobilon Western Substrates according to manufacturer´s instruction and detected with the LAS-4000 imager.

3.3.4 Chromatin Immunoprecipitation (ChIP)

ChIP is used to investigate protein binding on DNA. At the end of treatment, formaldehyde was directly added to the medium to crosslink proteins with DNA. Formaldehyde had a final concentration of 1% and was incubated for 5 min at RT while shaking. The reaction was stopped by addition of 1 ml 1 M glycine and incubated for 5 min at RT while shaking. Afterwards, the medium was removed, and cells were washed twice with ice-cold PBS. Cells were scraped in 1 ml ice-cold PBS containing 1:1,000 protease- and phosphatase-inhibitor cocktails and collected in falcon tubes. Cells were centrifuged for 5 min at 4 °C and 1,500 rpm and pellets were lysed in ChIP swelling buffer. After incubation on ice for 20 min, nuclei were pelleted for 5 min at 4 °C and 1,500 rpm. The pellets were resuspended in RIPA buffer and incubated for 10 min on ice.

After cell lysis, the DNA was fragmented using the Covaris M220 (Peak Power = 75.0; Cycles/Burst = 200; Duty Factor = 10.0; Duration = 1800 s). Samples were kept at 4 °C while fragment size was verified. To investigate sample size 15 µl of sonicated samples were incubated with 15 µl 5 M NaCl, 2 µl RNase A (1 mg/ml), and brought to a final volume of 300 µl with TE buffer. The mix was incubated for 1 h at 37 °C to degrade RNA, followed by overnight incubation at 65 °C while shaking to revert the crosslink. On the next day 2 µl Proteinase K (1 mg/ml) was added and the mix was incubated for 2 h at 45 °C while shaking to degrade all proteins. DNA was isolated by phenol-chloroform purification (see 3.2.9.4), the pellets were resuspended in 20 µl TE, and DNA separation was performed on a 2% agarose gel (see 3.2.4). When verified that fragment size of chromatin is smaller than 500 bp, chromatin was cleared by centrifugation for 30 min at 4 °C and 14,000 rpm. The samples were distributed equally for immunoprecipitation (IP) and IgG control. 1% input samples were kept as a control reference. The primary antibody was coupled to a 50:50 Protein A:G Dynabeads mixture overnight at 4 °C on the rotating wheel. Therefore, 30 µl of beads per sample and number of IP were

washed 3 times with 1 ml 0.5% BSA in PBS. All washing steps were performed using the magnetic rack. After the last washing step, beads were resuspended in 1 ml 0.5% BSA in PBS and 3 µg antibody per IP were added. At the next day residual unbound antibody was washed away by washing the beads again 3 times with 0.5% BSA in PBS. After the last washing step, beads were resuspended in 30 µl per IP and added to the distributed chromatin. The mix was incubated overnight on the rotating wheel at 4 °C. The immunoprecipitated chromatin was washed 3 times with 1 ml ChIP washing buffer I, ChIP washing buffer II, and ChIP washing buffer III each. The beads were then washed once with TE and transferred into a new reaction tube. The DNA was eluted by adding 150 µl elution buffer and incubated 15 min on the rotating wheel at RT. The elution was performed twice, and the eluates were merged. 300 µl elution buffer was added to the input samples and chromatin decrosslinking was performed for all samples as described above. The DNA was purified using phenol-chloroform (see 3.2.9.4), the pellet was resuspended in 500 µl ddH_2O, and 10 µl were used for qPCR (see 3.2.11).

3.3.5 Immunofluorescence

Immunofluorescence enables the visualization of proteins to investigate amount and localization of the proteins of interest within the cell. Cells were plated in 18-well ibidi slides or on 96-well plates. Inhibitor treatment was performed for 8 h. For pulsed 5-ethynyl-2'-deoxyuridine (EdU) incorporation, cells were incubated for 30 min in medium containing 10 µM EdU. Upon EdU incorporation and inhibitor treatment, cells were fixed and permeabilized with ice-cold methanol for 20 min at RT. After removing the methanol, cells were blocked for 30 min with 5% BSA in PBS at RT to reduce unspecific binding of the primary antibody. The Click-iT EdU Alexa Fluor 647 Imaging Kit was used according to manufacturer´s protocol for visualization of EdU. After 30 min incubation, the samples were washed 3 times with PBS. The primary antibody was diluted to the desired concentration in 5% BSA in PBS and added to the sample overnight at 4 °C. At the next day, the sample was washed 3 times with PBS and then incubated for 1 h at RT with the secondary antibody. Nuclei were counterstained using Hoechst 33342. Afterwards the samples were again washed 3 times with PBS to remove residual unspecific bound secondary antibody or Hoechst 33342. The samples were analyzed with the Leica SP2 microscope (18-well ibidi slides) or with the Operetta® High-Content Imaging System (96-well plates).

3.3.6 Proximity ligation assay (PLA)

Cells were plated one day before the treatment in 384-well plates or 18-well ibidi slides. The cells were treated for 8 h with the indicated inhibitors. For pulsed EdU incorporation, cells were incubated in medium containing 10 µM EdU. After 30 min, cells were fixed and permeabilized

with ice-cold methanol for 20 min at RT. After removing the methanol, cells were blocked for 30 min with 5% BSA in PBS at RT to reduce unspecific binding of the primary antibody. The Click-iT EdU Alexa Fluor 647 Imaging Kit was used according to manufacturer´s protocol for EdU detection. After 30 min incubation the samples were washed for 3 times with PBS. The primary antibody was diluted to the used concentration in 5% BSA in PBS and added to the sample overnight at 4 °C. PLA was performed using Duolink® In Situ Kit according to the manufacturer´s protocol. Nuclei were counterstained using Hoechst 33342. Pictures from 384-well plates were taken with an Operetta® High-Content Imaging System and pictures from 18-well ibidi slides were taken with Leica SP2 microscope.

3.3.7 Phosphoproteomic analysis

Phosphoproteomic analysis and sample preparation was performed as previously described (Cossa et al., 2020). Phosphoproteomic analysis using mass-spectrometry (MS) is a method to investigate global changes in the phosphorylation status of proteins. Measurement of proteomic and phosphoproteomic data by MS was performed by Andreas Schlosser (Rudolf-Virchow-Center, Wuerzburg) and data analysis was carried out by Andreas Schlosser and Petra Beli (Institute of Molecular Biology, Mainz).

3.3.7.1 Sample preparation

The samples for phosphoproteomic analysis were cell cycle synchronized using double thymidine block (see 3.1.5.1) and treated for 4 h with indicated inhibitors. Proteins of chromatin-bound fraction were isolated (see 3.1.7). Samples were incubated for 10 min at 70 °C, 120 mM iodacetamide was added, and incubated for 30 min at RT in the dark. After adding 50 µl 1 M ABC buffer, 4 x acetone was added, and proteins were precipitated overnight. After centrifugation at 2,000 g for 15 min, pellets were washed 3 times with ice-cold acetone, and dried up. Pellets were resuspended in 750 µl digestion buffer and sonified in a Bioruptor® (5 cycles of 30 s). 1:100 LysC was added to each sample and incubated 1 h at 37 °C, followed by addition of 10 µg sequencing-grade modified trypsin, and incubation overnight at 37 °C upon shaking. Digested samples were centrifuged at 16,000 g for 20 min and lyophilized overnight. Samples were dissolved in 2% acetonitrile, 0.5% formic acid with the help 3 x 30 s Bioruptor cycles and 20 min shaking. After centrifugation for 5 min at 5,000 g, samples were cleaned up with Sep Pak C18 cartridges. 10 µl sample was collected for proteomic measurement, while the rest was used for lyophilization. Phosphopeptides were enriched with PhosphTio tips 3 mg/200 µl and eluted in 150 µl 15% acetonitrile, 5% ammonium hydroxide. After overnight lyophilization, samples were re-dissolved in a mixture of 100 µl 200 mM citric acid with 20 µl acetonitrile, and 1 µl formic acid shortly before NanoLC-MS/MS measurement.

3.3.7.2 Data analysis

NanoLC-MS/MS analyses were performed on an Orbitrap Fusion equipped with a PicoView Ion Source and coupled to an EASY-nLC 1000. Peptides were loaded onto self-packed capillary columns (PicoFrit, 30 cm x 150 µm ID) with ReproSil-Pur 120 C18-AQ, 1.9 µm and separated with a 90-min linear gradient from 3% to 40% acetonitrile and 0.1% formic acid and a flow rate of 500 nl/min.

An Orbitrap analyzer with a resolution of 60,000 for MS scans and 15,000 for MS/MS scans was used. HCD fragmentation with 35% normalized collision energy was applied. A top speed data-dependent MS/MS method with a fixed cycle time of 3 s was used. Dynamic exclusion was applied with an exclusion duration of 45 s and a repeat count of 1; single charged precursors were excluded from selection. Minimum signal threshold for precursor selection was set to 50,000.

Raw MS data files were analyzed with MaxQuant version 1.5.7.4 and 1.5.2.8. Andromeda, which is integrated in the utilized version of MaxQuant, was used to perform database search against the UniProt Human database. Additionally, a database containing common contaminants was used. The search was performed with tryptic cleavage specificity with 3 allowed miscleavages. Protein identification was under control of the false-discovery rate (1% false discovery rate (FDR) on protein and peptide level). The search was performed against following variable modifications: oxidation (Met), Gln to pyro-Glu formation (N-term. Gln), and Phospho (STY), in addition to MaxQuant default settings. Carbamidomethyl (Cys) was set as fixed modification. For protein quantitation, the LFQ intensities were used (Cox et al., 2014). Proteins with less than two identified razor/unique peptides were dismissed. Intensities from MaxQuant Phospho (STY) table were used for relative quantitation of phosphorylation sites. For Phosphoproteomics upon Aurora-A inhibition intensities from the MaxQuant Phospho (STY) table were quantile normalized and subsequently a moderate t-test (limma algorithm) was applied to identify significantly regulated phosphorylation sites (Ritchie et al., 2015; Bolstad et al., 2003).

3.4 Next generation sequencing

The libraries of all next generation sequencing experiments were sequenced on an Illumina NextSeq 500 system by Carsten Ade. The data analysis of ChIP-sequencing and RNA-sequencing was done by Peter Gallant. The data analysis of the 4sU-sequencing was done by Susanne Walz and the p-value was calculated by Peter Gallant. Carsten Ade, Peter Gallant, and Susanne Walz are employed at Theodor Boveri Institute, Department for Biochemistry and Molecular Biology, University of Wuerzburg.

3.4.1 ChIP-sequencing (ChIP-seq)

ChIP-seq was performed to analyze global DNA binding of a protein. To enable normalization all ChIP-seq experiments were spike-in experiments.

3.4.1.1 Sample preparation

ChIP was performed as described previously (see 3.3.4) using as starting material 30 – 50 million cells and 10% of fixed NIH-3T3 mouse cell for spike-in. 100 µl Protein 50:50 A:G Dynabeads and 10 µg antibody was used per sample. The purified DNA was solubilized in 40 µl ddH_2O and the amount was quantified using Quant-iT™ PicoGreen dsDNA Assay Kit (see 3.2.8.2).

3.4.1.2 Library preparation

Purified DNA was end-repaired, A-tailed, and ligated to Illumina adaptors using NEBNext® ChIP-Seq Library Prep Master Mix Set for Illumina® or NEBNext® Ultra™ II DNA library Prep. Size-selection was performed by agarose gel (200 bp) or with beads depending on the kit used for preparation. DNA fragments were amplified by 15 to 18 cycles of PCR. Library size and amount of library was measured with the Fragment analyzer. The library was subjected to Illumina NextSeq 500 sequencing according to the manufacturer's instructions.

3.4.1.3 Sequencing data analysis

Base calling was performed using Illumina's FASTQ Generation software v1.0.0. Sequencing quality was analyzed using the FastQC script. Reads were mapped independently to the human hg19 or murine mm10 genome (i.e., spike-in material), using Bowtie1 (Langmead et al., 2009) with default parameters. A normalization factor for the spike-in was calculated by dividing the number of mapped reads of the spike-in of the smallest sample to each sample. This factor was multiplied by the number of reads, for each sample, that map to the human genome. All bam files were adjusted to this read count for subsequent analysis.

Traveling ratios were calculated by counting reads with BEDtools "intersectBed" (Quinlan, 2014) around the TSS (-30 to +300 bp) and within gene bodies (+300 bp to TES) of Ensembl genes. Gene body counts were normalized to the gene length and TSS counts were divided by gene body counts. With help of ngs.plot.r. (Shen et al., 2014) metagene window plots were generated. Nucleosome coordinates were used from the published data sets: GSM1838910 and GSM1838911 (Devaiah et al., 2016). MYCN ChIP-seq reads from S phase-synchronized and DMSO-treated IMR-5 cells were used to stratify for MYCN affinity. Reads were counted in a 600 bp window centered at the TSS using BEDtools intersect. Lists of downstream pause sites belonging to the top 3,000 or bottom 3,000 MYCN-bound genes were obtained by intersecting the corresponding lists, restricted to genes with minimal expression in IMR-5 cells.

3.4.2 RNA-sequencing (RNA-seq)

RNA-seq can be used to investigate global changes in expression of mRNA.

3.4.2.1 Sample preparation

For RNA-seq total RNA was extracted using RNeasy® kit including on-column DNase I digestion (see 3.2.9.2). The quality of the RNA was determined with the Fragment analyzer. RNA quality indicator (RQI) was calculated and samples with RQI greater than 9 were further processed. 1 µg of total RNA was used to isolate mRNA using the NEBNext® Poly(A) mRNA Magnetic Isolation Module.

3.4.2.2 Library preparation

Library preparation was performed with the NEBNext® Ultra™ RNA Library Prep Kit for Illumina according to manufacturer´s instruction. Agencourt AMPure XP Beads were used for size-selection of the libraries, followed by amplification with 12 PCR cycles. Library quantification and size determination was performed with the Fragment analyzer.

3.4.2.3 Sequencing data analysis

For RNA-seq, Tophat2 (Kim et al., 2013) and Bowtie2 (Langmead et al., 2009) were used to map the reads to hg19 and samples were normalized to the number of mapped reads in the smallest sample. The “summarizeOverlaps” function from the R package “GenomicAlignments” using the “union”-mode and Ensembl genes were used to count the number of reads per gene. Genes with mean count over all samples <1, were considered as non- or weakly expressed genes, and therefore removed. Differentially expressed genes were called with edgeR and p-values were adjusted for multiple-testing using the Benjamini-Hochberg procedure. Gene set enrichment analysis (GSEA; Subramanian et al., 2005) were done with the “Hallmark” databases from MSigDB (Liberzon et al., 2011) using 1,000 permutations and default settings.

3.4.3 4-Thio-uridine (4sU)-sequencing (4sU-seq)

4sU-seq can be used to investigate global changes in nascent RNA transcription and splicing efficiency.

3.4.3.1 Sample preparation

IMR-5 cells were cell cycle synchronized using double thymidine block (see 3.1.5.1). At timepoint of release indicated inhibitors were added. 2 h before harvesting cells, 500 µM of 4sU was added to the medium to label nascent RNA. After 15 min medium was changed. 4 h after release, RNA was harvested using the miRNeasy® Mini Kit (see 3.2.9.3). After extraction and quantification of total RNA by Nanodrop (see 3.2.8.1), equal amount was labelled with biotin in presence of DMF-HPDP buffer. To remove free biotin a chloroform-isoamyl-alcohol extraction was carried out, after which RNA was resuspended with nuclease-free water.

Dynabeads™ MyOne™ Streptavidin C1 beads were used to enrich biotinylated RNA, which was then eluted by 100 mM DTT and cleaned by RNeasy® MinElute® cleanup kit. The concentration of nascent RNA was then measured using RiboGreen RNA assay kit (see 3.2.8.2) and equal amounts were used for library preparation.

3.4.3.2 Library preparation

Before library preparation, rRNA was depleted using NEBNext® rRNA Depletion Kit and then all eluted material was used for NEBNext® Ultra™ II Directional RNA Library Prep. Library was amplified using 14 PCR cycles and sequenced for 75 cycles using Illumina NextSeq 500 system.

3.4.3.3 Sequencing data analysis

4sU-seq was performed as previously described (Cossa et al., 2020). Briefly, reads were mapped using Tophat2 (Kim et al., 2013) and Bowtie2 (Langmead et al., 2009) to human genome hg19. Ribosomal reads, which were defined by UCSCs Repeat Masked table filtered for rRNA, were mapped, and removed. All samples were normalized to the sample with the smallest number of mapped reads. UCSC hg 19 RefGene table was used for filtering reads, which belong to certain regions of a gene. The following regions were defined: exons, the first intron of a gene, all introns, intron-spanning (‘‘spliced’’), exon-intron-overlapping, TES (defined as annotated transcriptional end site (TES) to TES+20kb), and TES overlapping (‘‘TES-RT’’). Reads falling into introns were normalized by the intron length and ‘‘spliced’’ reads were normalized for the number of exons per gene. For each gene and region analyzed, the mean from three replicates was calculated. To determine the significance of drug treatment on splicing efficiency, for each condition all biological replicates were combined, and for each gene the fraction of spliced reads relative to total reads was calculated. Each treatment was then compared to the DMSO control using both t-test and Wilcoxon matched-pairs signed rank test in GraphPad Prism.

4 Results

4.1 Binding of Aurora-A to chromatin in S phase is MYCN-dependent

Previous data showed that Aurora-A stabilizes MYCN and prevents it from proteasomal degradation (Otto et al., 2009), the interaction of the two proteins is S phase-specific (Büchel et al., 2017), and MYCN is able to activate Aurora-A *in vitro* (Richards et al., 2016). To understand the function of the Aurora-A/MYCN complex, the localization of this complex as well as the phosphorylation status of Aurora-A in S phase were investigated.

4.1.1 Binding of Aurora-A to chromatin changes during cell cycle

To investigate the localization of Aurora-A within the cell cycle, IMR-5 cells were synchronized using double thymidine block and released into different cell cycle phases. The efficacy of the thymidine block was assessed by PI FACS. Since during replication the DNA content is duplicated, G1 phase (2n), S phase (2n – 4n), and G2 or early stages of mitosis (M; 4n) can be robustly distinguished.

Asynchronous growing cells show a distribution of cells with mainly 2n DNA content, indicating that most cells are in G1 phase. Upon synchronization with thymidine (T0) cells are blocked at the border between G1 and S phase leading to an increase in cells with 2n content. Timepoints 4 h, 8 h, and 14 h after release (T4, T8, and T14, respectively) were carefully chosen to obtain a large fraction of cells in either S, G2/M, and G1 phase, which is also reflected in PI FACS analysis (Figure 4.1 a).

Synchronized cells were fractionated in cytoplasmic, nucleoplasmic, and chromatin-bound fraction [Figure 4.1 b (left)]. Vinculin was used as a cytoplasmic marker, whereas histone 2 B (H2B) and TOP2A were used as markers for chromatin-bound proteins. MYCN is mainly bound to chromatin. Additionally, Aurora-A levels were investigated, showing that total Aurora-A level increase throughout the cell cycle, with least Aurora-A in G1 phase and most in G2/M phase. Besides this, the percentage of cytoplasmic, nucleoplasmic, and chromatin-bound Aurora-A within a cell cycle phase was calculated [Figure 4.1 b (right)]. In G1 phase roughly 50% of Aurora-A is cytoplasmic, whereas in S phase most Aurora-A is bound to chromatin. The fraction of Aurora-A bound to chromatin is lower in G2/M and more Aurora-A is cytoplasmic compared to S phase. This observation also reflects the amount of Aurora-A shown in the immunoblot. Since TPX2 is the best characterized partner protein for Aurora-A and is known to recruit Aurora-A to chromatin in mitosis (Kufer et al., 2002), the amount of TPX2 throughout the cell cycle was analyzed. TPX2 is completely absent in G1 phase and in S phase there is only a faint band visible. TPX2 level increases in the chromatin-bound fraction in G2/M phase.

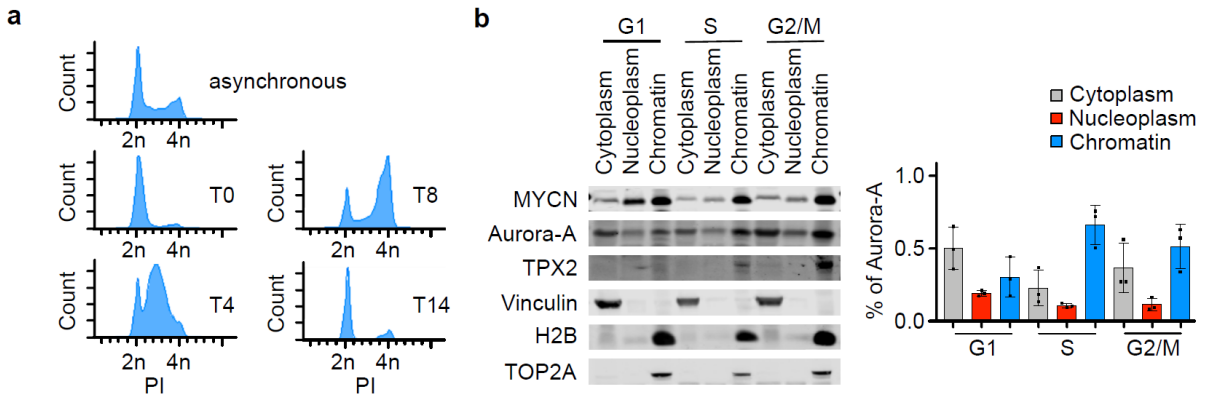

Figure 4.1: Aurora-A is bound to chromatin in a cell cycle dependent manner.
a. PI FACS analysis of IMR-5 cells blocked at the G1/S boundary using thymidine (T0). Asynchronous cells are shown as controls. Cells were released for 4 h (T4) into S phase, for 8 h (T8) into G2/M phase, and for 14 h (T14) into G1 phase (n=3; n in all subsequent figures the number of biological replicates).
b. Fractionation of G1, S, and G2/M synchronized *MYCN*-amplified IMR-5 cells. (left): Immunoblots of equal aliquots of each fraction were investigated for the indicated proteins. Vinculin, histone 2 B (H2B), and TOP2A were used as fractionation controls (n=3). (right): Quantitation of distribution of Aurora-A amount in each cell cycle phase. Shown is the mean ± standard deviation (S.D.; n=3).
Parts of this Figure were published in similar form in Roeschert et al., 2021.

4.1.2 Chromatin association of Aurora-A in S phase is MYCN-dependent

Since the association of Aurora-A with MYCN is S phase-specific (Büchel et al., 2017) and the binding of Aurora-A to chromatin was additionally observed in S phase, the next step was to investigate the role of MYCN in this process. Therefore, IMR-5 cells were treated for 4 h with 10058-F4, a compound that dissociates MYCN and MAX and thereby prevents MYCN association with chromatin (Wang et al., 2007). A MYCN chromatin immunoprecipitation (ChIP) was performed upon 4 h incubation with 100 µM 10058-F4 (Figure 4.2 a). On all target genes analyzed, MYCN levels decreased upon inhibitor treatment by 50%. The intergenic region was used as biological negative control, since no MYCN is bound there. Additionally, IgG was used as a control for unspecific chromatin binding.

A fractionation of IMR-5 cells under the same conditions and an immunoblot of indicated proteins was performed [Figure 4.2 b (left)]. Vinculin was used as a cytoplasmic marker, whereas TOP2A was used as a marker for chromatin-bound proteins. Total MYCN level, as well as MYCN associated with chromatin, decreased upon treatment with 10058-F4. Aurora-A is as previously seen mostly bound to chromatin, but chromatin-associated levels drop when treated with 10058-F4. The amount of chromatin-bound TOP2A, MYCN, and Aurora-A compared to the total level in each condition was quantified [Figure 4.2 b (right)]. TOP2A bound to chromatin is not affected by treatment with 10058-F4. MYCN levels are reduced to 40% and chromatin-bound Aurora-A is reduced by 50% upon inhibition of MYCN/MAX hetero-dimerization.

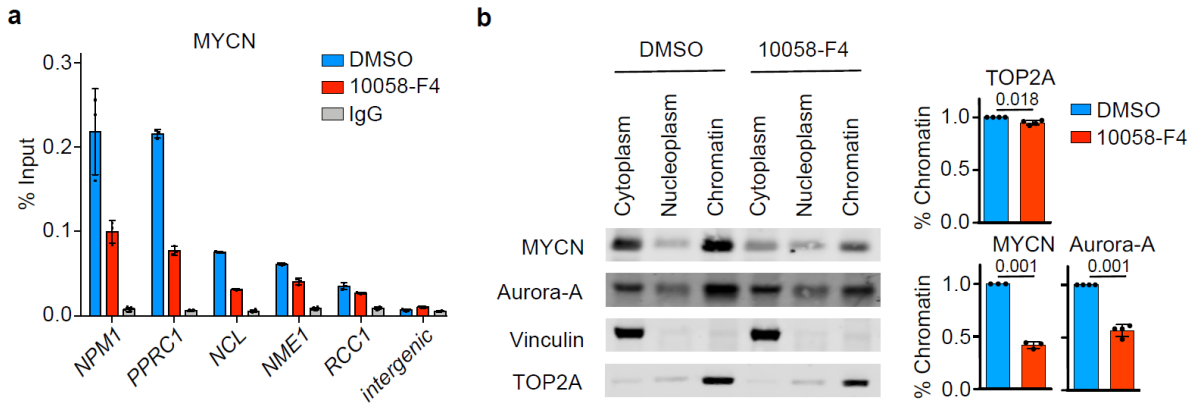

Figure 4.2: Aurora-A association with chromatin is MYCN-dependent.
a. MYCN ChIP at indicated loci treated for 4 h with 100 µM 10058-F4 in asynchronous IMR-5 cells. IgG was used as control for antibody specificity. Error bars indicate S.D. of technical triplicates from a representative experiment (n=3).
b. Fractionation of IMR-5 cells synchronized in S phase and treated for 4 h with 100 µM 10058-F4. (left): Immunoblots of indicated proteins. Vinculin and TOP2A were used as fractionation controls (n=3). (right): Quantitation of relative levels of chromatin-bound proteins. Shown is the mean ± S.D., p-values were calculated using paired two-tailed t-test relative to DMSO (n=3).
Parts of this Figure were published in similar form in Roeschert et al., 2021.

4.1.3 Aurora-A is unphosphorylated in S phase

The phosphorylation status of Aurora-A on T288, usually associated with the activation of its kinase activity, was next assessed in different cell cycle phases. Cells were synchronized using double thymidine block as described before, adding one sample that was treated with nocodazole to enrich for mitotic cells. Synchronization efficiency was analyzed using PI FACS (Figure 4.3 a).

Cells were harvested in different cell cycle phases and phosphorylation of Aurora-A on T288 was determined by immunoblotting (Figure 4.3 b). S10 phosphorylated of histone H3 (pH3S10), a marker for cells in mitosis (Goto et al., 1999), drastically increased in cells treated with nocodazole, which is in line with the robust enrichment in G2/M phase shown by the PI FACS profile. Total Aurora-A levels increase throughout the cell cycle phases analyzed, phosphorylation of T288 on Aurora-A changes during cell cycle. In S phase this phosphorylation could not be detected. This phosphorylation mark is increasing in G2 phase and peaks in mitosis.

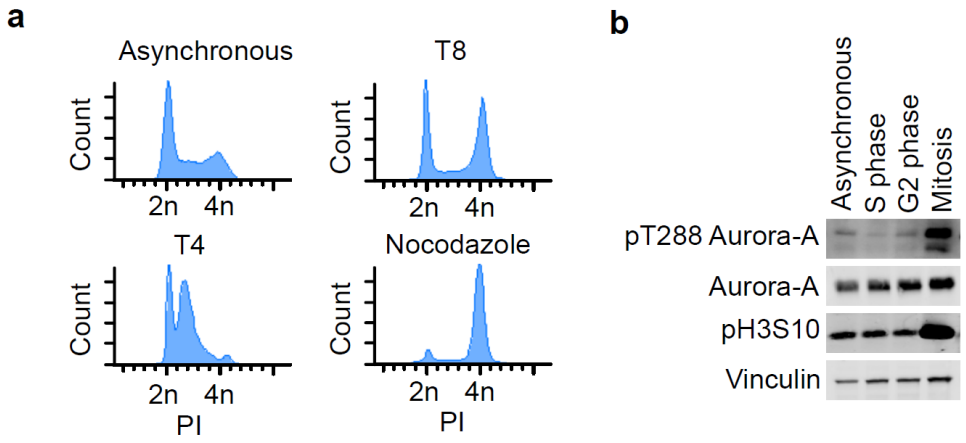

Figure 4.3: Aurora-A is unphosphorylated in S phase.
a. PI FACS analysis of IMR-5 cells. Asynchronous cells as well as cells synchronized using double thymidine block and released for 4 h into S phase, for 8 h into G2/M phase, or using nocodazole in mitosis were assessed (n=2).
b. Immunoblots of indicated proteins from RIPA lysates of asynchronous or synchronized IMR-5 cells in indicated cell cycle phase. Vinculin was used as loading control (n=2).
Parts of this Figure were published in similar form in Roeschert et al., 2021.

Collectively, the results illustrate that Aurora-A is mainly localized to chromatin in S phase and this association is stabilized by MYCN. Additionally, it could be shown that Aurora-A is not phosphorylated on T288 in S phase which is usually considered as a sign for the activity of the kinase.

4.2 Identification of MYCN-dependent Aurora-A substrates in S phase

Previous work showed that MYCN can lead to an activation of Aurora-A (Richards et al., 2016). Considering that the interaction between the two proteins takes place in S phase and that no Aurora-A S phase-specific substrates have been identified so far, an unbiased phosphoproteomic analysis was performed using two Aurora-A inhibitors in S phase-synchronized cells. Additionally, the phosphoproteomic analysis was also performed upon dissociation of MYCN from chromatin in S phase to identify MYCN-dependent substrates. Finally, the role of pH3S10, already described as Aurora-A substrate, in S phase was further investigated.

4.2.1 Identification of Aurora-A substrates in S phase

To identify substrates of Aurora-A in S phase, the chromatin-bound fraction of IMR-5 cells synchronized in S phase, treated with different Aurora-A inhibitors were analyzed by mass-spectrometry (MS). Proteomic and phosphoproteomic analysis was performed to analyze changes on protein level or phosphorylation status upon inhibition of Aurora-A in S phase.

Therefore, IMR-5 cells were synchronized using double thymidine block. At the timepoint of release, cells were treated with 1 µM MLN8237, 1 µM MK5108, or DMSO as control. MK5108 is a pure catalytic inhibitor of Aurora-A, whereas MLN8237 is partially disrupting the conformation and additionally inhibiting the catalytic activity (further explained in 1.4.6). After 4 h, when most IMR-5 cells reached S phase, cells were harvested and fractionated. Equal amount of each fraction was loaded on a Bis-Tris gel and immunoblotting was performed (Figure 4.4 a). Tubulin alpha chain (Tubulin), TFIIIC2, and topoisomerase II a (TOP2A) were used as fractionation controls. Tubulin is mainly present in the cytoplasm, TFIIIC2 is present in all fractions, and TOP2A is mainly bound to chromatin in all samples. Aurora-A is present in the nucleoplasm and fractions of proteins bound to chromatin, whereas MYCN can be found in all fractions, but mainly in cytoplasm and chromatin-bound. Interestingly, inhibition of Aurora-A does not influence neither the level nor the localization of these proteins.

Proteomic analysis of chromatin-bound samples revealed 3193 proteins found at least in two out of three replicates in all conditions (Figure 4.4 b). The volcano plot shows the mean of $\log_2$ fold change (FC) of the three replicates treated with MLN8237 and the three replicates treated with MK5108 both compared to DMSO stratified to the p-value. On the left side, all proteins are displayed which are less abundant bound to chromatin upon treatment. The majority of proteins do not change abundance significantly. Proteins considered as hits were chosen by $\log_2$ FC, p-value < 0.05, and found in at least two out of three replicates of each condition. Less abundant proteins were defined as having a $\log_2$ FC < -2.0, whereas more abundant proteins had a $\log_2$ FC >2.0.

The Venn diagrams summarize all hits of proteins found less (Figure 4.4 c) or more (Figure 4.4 d) abundant upon Aurora-A inhibition.

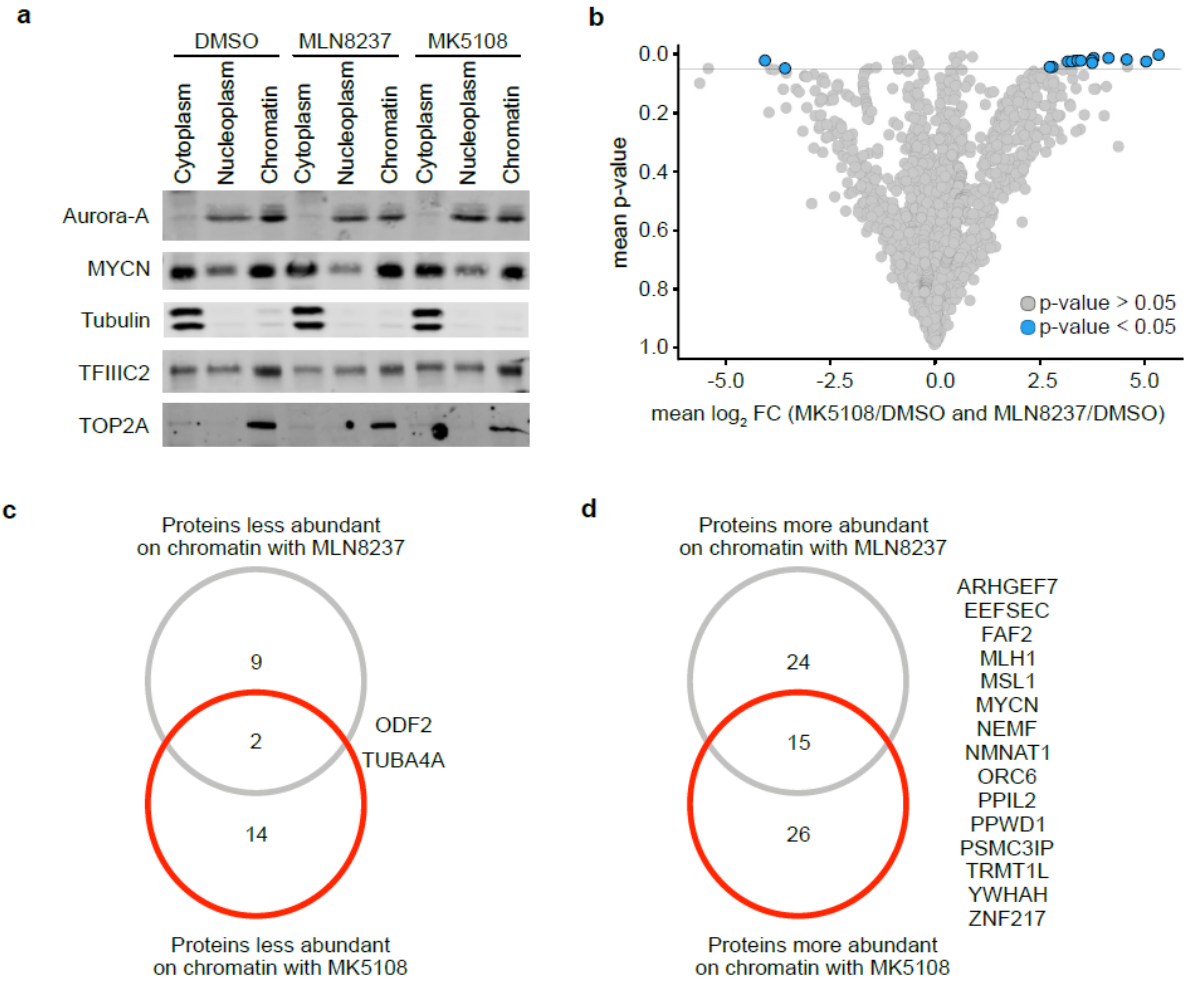

Figure 4.4: Proteomics upon Aurora-A inhibition using two different inhibitors.
a. Immunoblot of S phase-synchronized IMR-5 cells treated for 4 h with 1 µM MLN8237, 1 µM MK5108, or DMSO as control. After harvesting, cells were fractionated, and equal amounts of fractions were loaded to Bis-Tris gel. Immunoblot was performed and indicated proteins were analyzed. Tubulin, TFIIIC2, and TOP2A were used as loading controls (n=3).
b. Volcano plot showing the mean of all proteins found in at least two out of three replicates for each condition. Samples were treated as described in (a). p-value and $\log_2$ fold change (FC) was calculated between DMSO-treated and MLN8237- or MK5108-treated samples. Mean of p-value and mean $\log_2$ FC was calculated by the mean of both individual values. Blue dots represent all proteins, which show a p-value < 0.05 with both inhibitors, all other proteins are shown as grey dots. The black line represents p-value of 0.05 (n=3).
c. Venn diagram depicting the overlap between proteins less abundant on chromatin upon treatment with MLN8237 and MK5108. Proteins were chosen, when found in at least two out of three replicates for all conditions, p-value < 0.05, and $\log_2$ FC compared to DMSO < -2.0.
d. Venn diagram depicting the overlap between proteins more abundant on chromatin upon treatment with MLN8237 and MK5108. Proteins were chosen, when found in at least two out of three replicates for all conditions, p-value < 0.05, and $\log_2$ FC compared to DMSO > 2.0.

Treatment with MLN8237 revealed 11 proteins whereas treatment with MK5108 resulted in 16 proteins significantly less abundant bound to chromatin. Two proteins were found to be less abundant with both inhibitors and are therefore marked in blue on the left side of the volcano plot (Figure 4.4 b).

On the right side of the volcano plot (Figure 4.4 b) proteins are shown in blue, which are found to be significantly more abundant when Aurora-A is inhibited on chromatin. 39 proteins were found more abundant bound to chromatin upon MLN8237-treatment, 41 proteins were found more abundant bound to chromatin upon MK5108-treatment, with an overlap of 15 proteins.

Additionally, phosphoproteomic analysis of chromatin-bound proteins in S phase-synchronized IMR-5 cells treated for 4 h with MLN8237 (Figure 4.5 a) or MK5108 (Figure 4.5 b) were performed. Phosphosites were filtered, according to the localization probability of the identified phosphosite. Phosphosites with localization probabilities > 0.75 were considered. Shown is the mean of all phosphosites, found in at least two out of three replicates. Within the volcano plot the x-axis displays the $\log_2$ FC of MLN8237 compared to DMSO ranging from -1.0 to 1.0. All sites in the negative range of the fold change are less phosphorylated when Aurora-A is inhibited, representing putative targets. Grey dots represent phosphosites (p-value > 0.15) displaying a non-statistically significant change in MLN8237- and MK5108-treated samples compared to DMSO. Blue dots depicted instead statistically significant changes (p-value < 0.15) with both inhibitors compared to DMSO.
Figure 4.5 c shows the comparison between the phosphoproteomics using MLN8237 and MK5108. Each dot represents one phosphosite found in both analysis in at least two out of three replicates. The color of the dot indicates the amino acid which got phosphorylated (blue: serine, green: threonine, red: tyrosine). The black line depicts the diagonal, where all phosphosites are found regulated by both inhibitors similarly. Except for a few outlier phosphosites, the majority of all phosphosites are in proximity to this line, suggesting that both inhibitors regulate phosphorylation of a similar sets of phosphosites.
To identify putative Aurora-A targets, the phosphosites which were less phosphorylated using both Aurora-A inhibitors were compared (Figure 4.5 d). The cut-off for less phosphorylated was arbitrarily set to $\log_2$ FC < -0.2 with both inhibitors. 205 phosphosites were less phosphorylated (p-value < 0.15) when treated with MLN8237 and 196 phosphosites showed less phosphorylation (p-value < 0.15) upon treatment with MK5108. The two inhibitors share 73 phosphosites showing less phosphorylation (Figure 4.5 d). Table 7.1 summarizes important information about the 73 phosphosites, which were found on 60 different proteins.

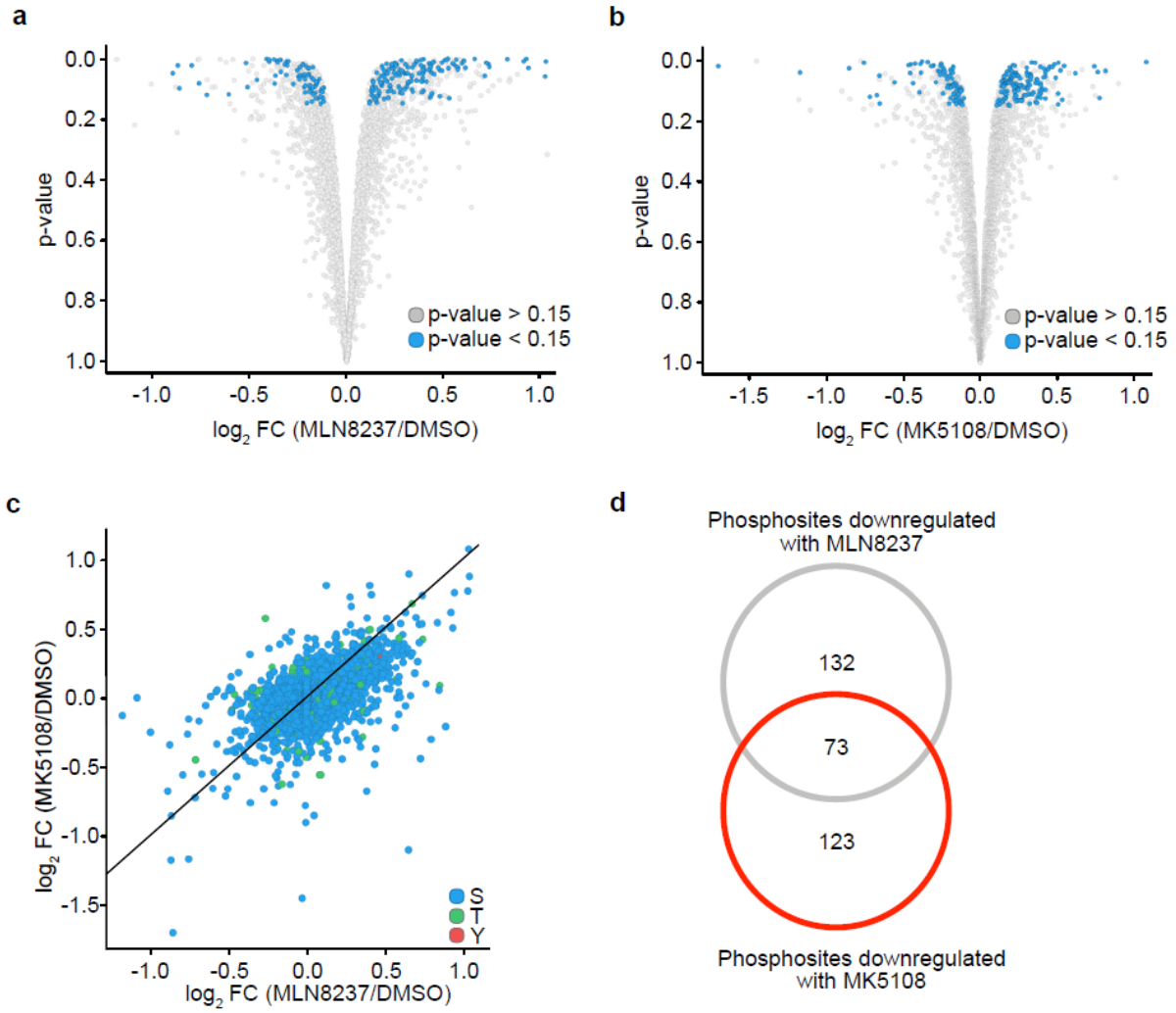

Figure 4.5: Phosphoproteomics upon Aurora-A inhibition.
a. Volcano plot showing the mean of all phosphosites found at least in two out of three replicates for each condition. Phosphosites were investigated from chromatin-bound fraction of S phase-synchronized IMR-5 cells, treated for 4 h with 1 µM MLN8237 and DMSO as control. Log_2 FC was calculated between DMSO- and MLN8237-treated samples. Blue dots represent all phosphosites, which show a p-value < 0.15 in samples treated with MLN8237 and in samples treated with MK5108, all other phosphosites are shown in grey (n=3).
b. Volcano plot similar to (a) of cells treated with 1 µM MK5108 (n=3).
c. Dot plot showing the comparison between the phosphoproteomic analysis of MLN8237- and MK5108-treated samples. Blue, green, and red dots represent phosphorylation on serine, threonine, and tyrosine, respectively. The black line represents the diagonal.
d. Venn diagram depicting the overlap between the phosphosites less phosphorylated upon treatment with MLN8237 and MK5108. Phosphosites were chosen, when found in at least two out of three replicates for each condition, p-value < 0.15, and log_2 FC compared to DMSO < -0.15.

To characterize the pathways in which the 60 putative Aurora-A substrates are involved, a GO Term analysis using DAVID was performed (Figure 4.6 a). The web-based program investigates the enrichment of the potential substrates over all proteins identified as chromatin-bound in the proteomic analysis. Seven GO Terms were significantly ($p < 0.06$) enriched for putative Aurora-A substrates. Four GO Terms are related to mRNA processing or splicing (#1, #2, #3, and #5), two GO Terms to chromatin organization (#4 and #6), and one GO Term to

transcription (#7). Indicating that splicing, chromatin organization, and transcription might be impacted by Aurora-A in S phase.

Figure 4.6 b shows to which significant enriched GO Term the putative Aurora-A substrates belong. 32 of the 60 proteins phosphorylated depending on Aurora-A activity in S phase can be found in one or more of the seven significantly enriched GO Terms. All other proteins were not annotated or the GO Term to which they belong was not significantly enriched. 20 of the 32 proteins are found in GO Term #7 (regulation of transcription). Some proteins like RBM15B or DDX20 are found in five out of seven GO Terms, whereas others like ATAD2 or ATRX are just found in one GO Term.

a

#	GO Term	Benjamini
1	RNA processing	8.5e-3
2	RNA splicing	1.4e-2
3	mRNA processing	2.0e-2
4	Chromatin organization	2.7e-2
5	mRNA metabolic process	2.9e-2
6	Chromosome organization	3.3e-2
7	Regulation of transcription	5.8e-2

b

Gene name	Found in GO Term						
	#1	#2	#3	#4	#5	#6	#7
ADAR	x		x		x		
ATAD2							x
ATRX							x
BCLAF1							x
BPTF				x		x	x
C11orf30				x		x	x
CDK11A							x
DACH1							x
DEK							x
DDX20	x	x	x		x		x
HUWE1				x		x	
LEO1				x		x	x
MCM2				x		x	x
MPHOSPH8				x		x	
MSH6						x	
NCOA5							x
NOLC1	x						
PPIG	x	x					
PRPF4B	x	x	x		x		
RBM15							x
RBM15B	x	x	x		x		x
RRP9	x						
SAFB2							x
SF3B2	x	x	x		x		
SMARCA4				x		x	x
SMARCAD1				x		x	x
SRRM1	x	x	x		x		
SRRM2	x	x	x		x		
THOC2	x	x	x		x		
TP53BP1							x
YY1							x
ZNF687							x

Figure 4.6: Aurora-A substrates in S phase show a strong connection to splicing, chromatin organization, and transcription.
a. Significant GO Terms analyzed by DAVID. 73 phosphosites which are less phosphorylated upon Aurora-A inhibition, were investigated compared to the whole proteome found chromatin-bound in all replicates. GO Terms with Benjamini < 0.06 are shown.
b. Proteins having a phosphosite less phosphorylated upon Aurora-A inhibition which are found in one of the 7 GO Terms from (a). Gene names as well as in which GO Term they were found is depicted.
Parts of this Figure were published in similar form in Roeschert et al., 2021.

4.2.2 Phosphoproteomics upon MYCN inhibition

To determine if proteins phosphorylated by Aurora-A in S phase are also dependent on MYCN, a further phosphoproteomic analysis of chromatin-bound proteins was performed upon MYCN inhibition and compared with the previous phosphoproteomic analysis upon Aurora-A inhibition. If MYCN is activating Aurora-A on chromatin, then removal of MYCN from chromatin would also lead to less active Aurora-A. To investigate the phosphoproteome upon removal of MYCN from chromatin, IMR-5 cells were synchronized and released in the presence of 100 µM 10058-F4 inhibitor. To ensure that after 4 h the majority of cells are enriched in S phase, a PI FACS was performed (Figure 4.7 a). Indeed, FACS analysis revealed that short-term treatment with 10058-F4 does not change the number of cells entering S phase.

Proteomic analysis under the same conditions revealed 2683 proteins bound to chromatin in IMR-5 cells (Figure 4.7 b). For the analysis, proteins were considered that were found in all replicates and all conditions and that showed an abundance greater than 7.5 for the $\log_{10}$ sum (DMSO and 10058-F4) in both replicates. The more often a peptide is found, the greater the $\log_{10}$ sum of DMSO- and 10058-F4-treated sample is. 42 proteins could be identified being more abundant on chromatin upon 10058-F4 treatment [FC (DMSO vs 10058-F4) > 1.2 for both replicates, with a mean FC > 1.5], while 94 proteins were less abundant [FC (DMSO vs 10058-F4) < 0.8 for both replicates, with a mean FC < 0.5)].

For example, Aurora-A was found less abundant upon treatment with 10058-F4. In contrast, Aurora-B does not show any regulation dependent on MYCN-binding to chromatin.

Under the same conditions a phosphoproteomic analysis was performed (Figure 4.7 c). Phosphosites were filtered, according to the localization probability of the identified phosphosite. Phosphosites with localization probabilities > 0.75 were considered. Additionally, the phosphosite must be identified in all conditions in all replicates with a $\log_{10}$ sum in both replicates greater than 7.5. When applying all the criteria to the analysis, 3124 phosphosites were identified in the MYCN-dependent phosphoproteomic analysis. In spite of a remarkable variability between the two replicates, 310 phosphosites showed less phosphorylation ($\log_2$ FC < -0.4) and153 phosphosites showed an increased phosphorylation in both replicates upon removal of MYCN from chromatin ($\log_2$ FC > 0.4).

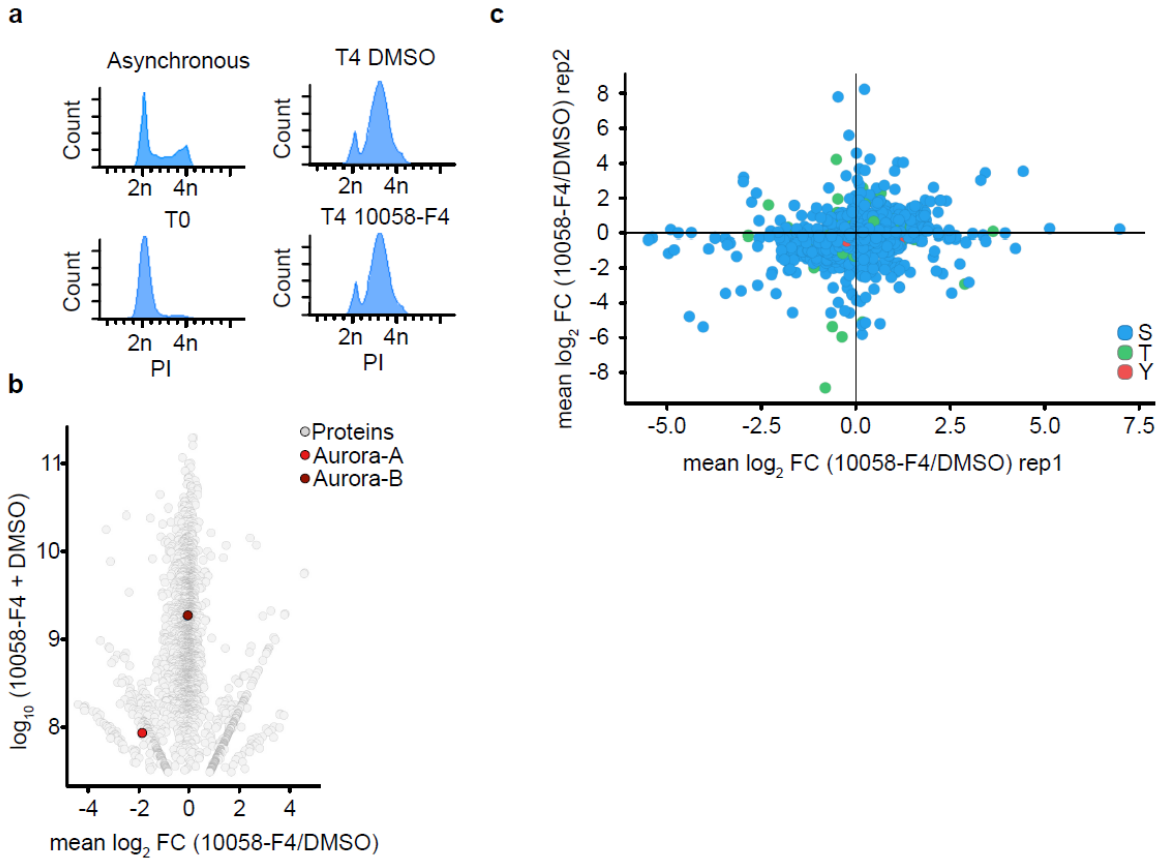

Figure 4.7: Proteomic and phosphoproteomics upon removal of MYCN from chromatin.
a. PI FACS analysis of IMR-5 cells. Asynchronous cells are shown as controls. IMR-5 cells were synchronized at the G1/S boundary by a double thymidine block (T0) and released from the block for 4 h in S phase while treatment with 100 µM 10058-F4 or DMSO as control (n=3).
b. Volcano plot showing proteomic analysis of S phase-synchronized chromatin-bound proteins upon treatment for 4 h with 100 µM 10058-F4. IMR-5 cells were synchronized using double thymidine block and upon release treated for 4 h with 100 µM 10058-F4. The samples were fractionated, and chromatin-bound fraction was assessed for proteomic analysis. The volcano plot displays the mean log_2 FC (10058-F4 compared to DMSO) of both replicates and the mean log_{10} sum of 10058-F4 and DMSO for two replicates. The proteins which were shown are found in all replicates. One grey dot represents one protein, colored dots are Aurora-A (light red) and Aurora-B (dark red;n=2).
c. Dot plot of phosphoproteomic analysis of S phase-synchronized chromatin-bound proteins upon treatment for 4 h with 100 µM 10058-F4. IMR-5 cells were synchronized using double thymidine block and upon release treated for 4 h with 100 µM 10058-F4. The samples were fractionated, and chromatin-bound fraction was assessed for phosphoproteomic analysis. The plot shows the comparison between log_2 FC of 10058-F4 with DMSO from one replicate (rep1) compared to the other replicate (rep2). Each dot represents one phosphosite, the color indicates which phosphosite is phosphorylated. Serine, threonine, and tyrosine are shown in blue, green, and red, respectively (n=2).

To investigate MYCN-dependent Aurora-A substrates, an overlap of phosphosites between Aurora-A inhibition and removal of MYCN from chromatin was performed (Figure 4.8 a). 310 phosphosites were found less phosphorylated when samples were treated with 10058-F4 (Figure 4.7). 73 phosphosites were found less phosphorylated upon treatment with both Aurora-A inhibitors (Figure 4.5, Table 7.1). 8 phosphosites were found to be less phosphorylated in all conditions.

Figure 4.8 b summarizes the common hits. Within the sequence the bold amino acid (AA) is the phosphorylated site. Since the consensus sequence for Aurora-A substrates in mitosis is

published (R/K R/K X S/T; followed by no proline; Kettenbach et al., 2011), the AA sequence from the putative MYCN-dependent Aurora-A substrates were investigated regarding the consensus sequence. Red indicates an AA which is not compatible with the Aurora-A consensus sequence, whereas green indicates an AA which is compatible with the consensus sequence.

Since MAP1B and SORT1 have no known function in the nucleus, they were excluded in all further experiments, which were carried out.

a

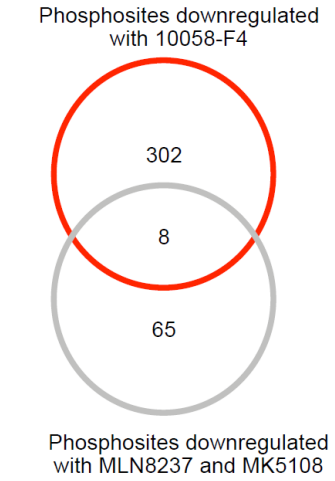

b

Gene name	Protein name	AA	Site	Sequence
ATAD2	ATPase family AAA domain-containing protein 2	S	1243	RNN**S**NTC
ATRX	Transcriptional regulator ATRX	S	731	NSD**S**DEM
DEK	DEK	S	307	EDS**S**DDE
MAP1B	Microtubule-associated protein 1B	S	1396	KVL**S**PLR
MSH6	DNA mismatch repair protein Msh6	S	261	IGG**S**DVE
SF3B2	Splicing factor 3B subunit 2	S	307	LGQ**S**ASE
SMARCAD1	SWI/SNF-related matrix-associated actin-dependent regulator of chromatin subfamily A containing DEAD/H box 1	T	54	RAN**T**PDS
SORT1	Sortilin	S	825	HDD**S**DED

Figure 4.8: Phosphosites downregulated upon MYCN and Aurora-A inhibition.
a. Venn diagram showing the overlap between the combined targets of Aurora-A inhibition and removal of MYCN from chromatin. Phosphoproteomics of chromatin-bound proteins in S phase-synchronized IMR-5 cells treated for 4 h with 1 µM MLN8237, 1 µM MK5108, or DMSO as control. Phosphosites downregulated with both inhibitors, as explained in Figure 4.5 d. Phosphoproteomics of chromatin-bound proteins in S phase-synchronized IMR-5 cells treated for 4 h with 100 µM 10058-F4. Phosphosites downregulated in two experiments as explained in Figure 4.7. b. List of overlapping phosphosites is shown. Gene name, Protein name, the amino acid (AA) which is phosphorylated, the position in the protein, and the target sequence is shown. Regarding the usual preferred consensus sequence of this kinase, amino acids shown in red are incompatible residues and in green are compatible residue for phosphorylation by Aurora-A.

4.2.3 Putative substrates of Aurora-A are in close proximity to MYCN and Aurora-A

To phosphorylate substrates, a kinase has to be in close proximity. The proximity of identified proteins to Aurora-A or MYCN was therefore investigated as a first indication of their nature of MYCN-dependent substrates of Aurora-A. A proximity ligation assay (PLA) between Aurora-A or MYCN and the six hits was performed. Each green dot represents proximity between the two proteins. Green dots could be observed in all combinations tested (Figure 4.9). ATAD2, SF3B2, and SMARCAD1 showed a lot of PLA dots when tested with Aurora-A in the nucleus (Figure 4.9 a). Conversely, ATRX, DEK, and MSH6 only show a few dots per nucleus when tested in PLA together with Aurora-A. PLA dots were also observed for all hits in combination with MYCN in the nucleus, though to a different extent (Figure 4.9 b). SF3B2 and SMARCAD1 showed also together with MYCN a high number of PLA dots. ATAD2, ATRX, DEK, and MSH6 show only a few dots per nucleus when tested in PLA together with MYCN.

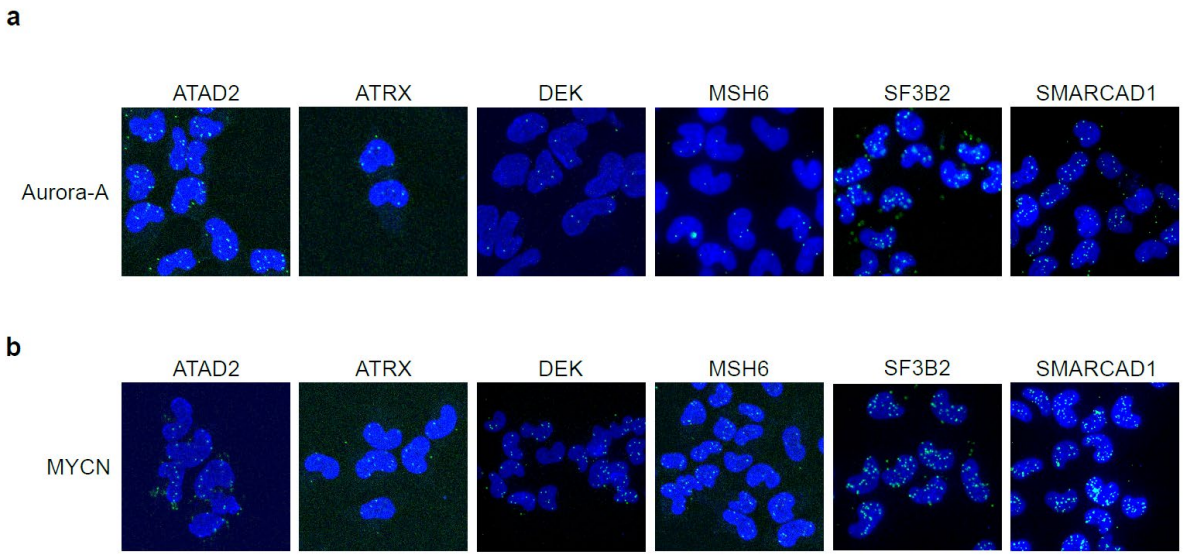

Figure 4.9: Aurora-A and MYCN are in proximity to putative substrates in IMR-5 cells.
a. Pictures of PLA performed with Aurora-A in combination with ATAD2, ATRX, DEK, MSH6, SF3B2, and SMARCAD1. Untreated IMR-5 cells were fixed, PLA was performed, and pictures were analyzed using the SP2 Leica microscope. Representative pictures are shown (n=3).
b. Pictures of PLA performed with MYCN in combination with ATAD2, ATRX, DEK, MSH6, SF3B2, and SMARCAD1. Untreated IMR-5 cells were fixed, PLA was performed, and pictures were analyzed using the SP2 Leica microscope. Representative pictures are shown (n=3).

4.2.4 Aurora-A phosphorylates histone 3 in S phase

One published target for Aurora kinases in mitosis is pH3S10 (Crosio et al., 2002). Since histone tails are not covered by phosphoproteomic analysis upon tryptic digestion, none of those modifications were found in the phosphoproteomic analysis (Figure 4.5). Thus, H3S10 phosphorylation was further investigated using immunofluorescence. To distinguish S phase cells, EdU – which is incorporated into duplicating DNA and therefore specific for S phase cells -was added to IMR-5 cells 30 min prior fixation. Cells were stained with pH3S10 and nuclei were counterstained with Hoechst (Figure 4.10 a). EdU incorporation shows that all cells are in different stages of S phase. Interestingly, pH3S10 staining in S phase appears spot-like. The picture suggests that the number of spots increases during S phase. In the merge picture one can see, that pH3S10 spots are not close to areas of EdU incorporation, indicating that those are two distinct events.

To evaluate the influence of Aurora-A on pH3S10, IMR-5 cells were treated with 100 nM MLN8237 for 8 h or DMSO as a control. To gain information about pH3S10 throughout the cell cycle, cells were incubated with EdU 30 min before harvesting, later stained for cyclin B1, and finally counterstained with Hoechst (Figure 4.10 b). G1 phase cells display negative staining for EdU (red staining) and cyclin B1 (orange staining). S phase cells are EdU-positive. G2 phase cells display cytoplasmic cyclin B1. Mitotic cells display nuclear cyclin B1 (Heald et al.,

1993). Different mitotic phases were differentiated by Hoechst staining. Example pictures for each cell cycle phase are shown in Figure 4.10 b (top panel).

While G1 phase cells show no staining for pH3S10 (green staining), S phase cells show pH3S10 spots, as already seen in Figure 4.10 a. Upon treatment with Aurora-A inhibitor pH3S10 spots disappear. As S phase cells, G2 phase cells show pH3S10 spots which decrease upon inhibition of Aurora-A. Cells in Pro-, Meta-, and Anaphase show a strong pH3S10 staining without indication of a spot-like structure. The quantitation of pH3S10 in different cell cycle phases is shown in Figure 4.10 b (lower panel).

In S and G2 phase, spots were counted using the Harmony® High-Content Analysis software. pH3S10 spots disappear in S phase upon inhibition with Aurora-A. Also, G2 phase cells show a reduction in pH3S10 spots, albeit the effect is not as strong as in S phase. Since mitotic cells show a staining of pH3S10 throughout the nucleus and no dots, the pH3S10 intensity was used as measure to calculate differences. Inhibition of Aurora-A did not change the intensity of the pH3S10 staining in any mitotic cell cycle phase.

Low doses of MLN8237 inhibit the catalytic functions of Aurora-A, whereas increasing amounts disrupts the Aurora-A/MYCN complex formation, leading to a degradation of MYCN (Otto et al., 2009). To further investigate whether the kinase activity alone is required for H3S10 phosphorylation or the Aurora-A/MYCN complex has any impact on pH3S10 staining the same experiment was performed using 1 µM MLN8237 (Figure 4.10 c). The quantitation shows pH3S10 spots in S and G2 phase and pH3S10 intensity in mitotic cell cycle phases. The pH3S10 spots are reduced upon Aurora-A inhibition in S and G2 phase, whereas intensity of pH3S10 does not change in any mitotic cell phase, mirroring the treatment with 100 nM MLN8237 (Figure 4.10 b).

Additionally, IMR-5 cells were treated with the catalytic Aurora-A inhibitor MK5108 (1 µM). Figure 4.10 d shows the quantitation of pH3S10 spots in S phase comparing inhibition with MK5108 (1 µM) and MLN8237 (100 nM). Inhibition of Aurora-A with MK5108 also reduces the amount of pH3S10 spots, albeit much weaker than inhibition with MLN8237.

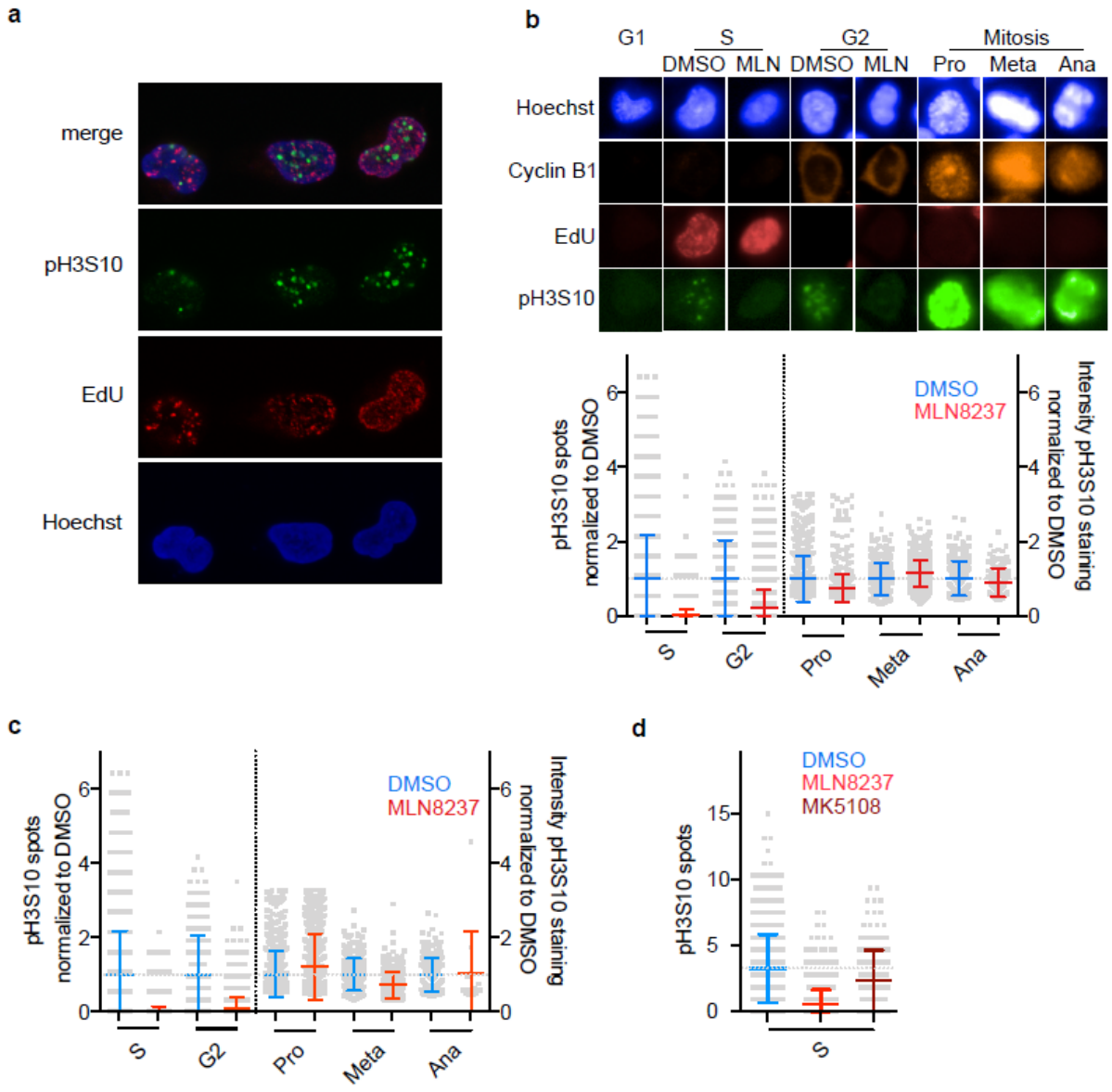

Figure 4.10: Aurora-A phosphorylates H3S10 in S phase.
a. Pictures of Immunofluorescence showing IMR-5 cells, incubated for 30 min with 1 µM EdU, and subsequently fixed. The cells were stained with pH3S10 with Alexa Fluor 488, EdU with Alexa Fluor 647, and Hoechst. Pictures were taken at SP2 Leica microscope (n=2).
b. IMR-5 cells were treated for 8 h with 100 nM MLN8237 or DMSO as control. 30 min before fixation cells were incubated with 1 µM EdU. Cells were stained with pH3S10, cyclin B1, EdU, and nuclei were counterstained with Hoechst to distinguish cell cycle phases. (Top) Example pictures of IMR-5 cells demonstrating how cell cycle phases were chosen. (Bottom) Quantitation of pH3S10 spots in S and G2 phase or intensity in different phases of mitosis. Error bars show mean ± S.D. (n=3).
c. Quantitation of pH3S10 staining upon treatment with 1 µM MLN8237. Cells were stained and analyzed as explained in (b). Error bars show mean ± S.D. (n=3).
d. Quantitation of pH3S10 staining upon treatment for 8 h with 100 nM MLN8237 and 1 µM MK5108. S phase cells were identified by EdU incorporation. pH3S10 spots in S phase were analyzed using the Operetta® High-Content Imaging System. Error bars show mean ± S.D. (n=3).
Parts of this Figure were published in similar form in Roeschert et al., 2021.

To investigate chromatin-bound pH3S10, a ChIP for pH3S10 in S phase-synchronized IMR-5 cells treated for 4 h with 100 nM MLN8237 was performed (Figure 4.11). IgG was used as a control for unspecific chromatin binding. IgG control did not show any qPCR signal at all loci

tested. DMSO-treated cells show an increase in pH3S10 signal on promoters as well as in the intergenic and centrosomal region. When Aurora-A is inhibited the pH3S10 signal is drastically decreased on all loci tested.

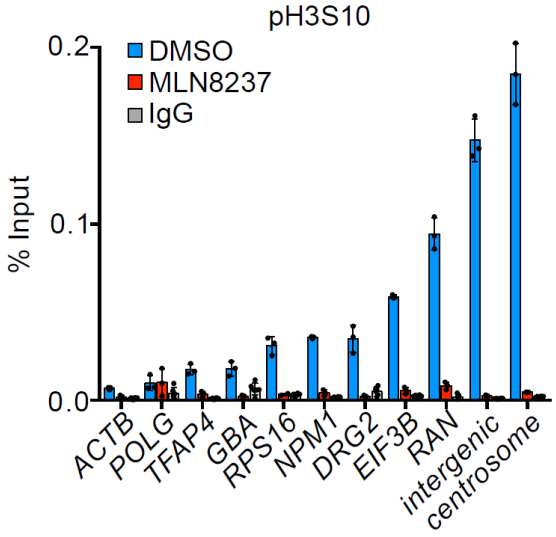

Figure 4.11: Aurora-A phosphorylates H3S10 on chromatin in S phase.
ChIP of pH3S10 from S phase-synchronized IMR-5 cells treated for 4 h with 1 µM MLN8237 or DMSO as control at indicated loci. IgG was used as negative control. Error bars indicate S.D. of technical triplicates from a representative experiment (n=3).
This Figure was published in similar form in Roeschert et al., 2021.

To genetically investigate the relationship between Aurora-A and pH3S10, we used IMR-5 cells expressing a doxycycline-inducible construct harboring either Aurora-A WT or Aurora-A T217D mutant. The empty vector (EV) was used as a control. The T217D mutant is resistant to MLN8237-treatment (Brockmann et al., 2013). Upon 24 h of Aurora-A expression, cells were treated for 8 h with 100 nM MLN8237. EdU was incorporated for 30 min and cells were stained with pH3S10, EdU, cyclin B1, and Hoechst. Example pictures are shown in Figure 4.12 a. The spot-like structure of S phase cells is not visible anymore upon treatment with MLN8237. When Aurora-A WT is overexpressed, the intensity of the pH3S10 signal is increased but is still completely abolished upon treatment with MLN8237. Overexpression of Aurora-A T217D results in an increased pH3S10 signal, which results in a pan-staining all over the nucleus compared to IMR-5 cells expressing EV. The signal is reduced but still strongly present upon MLN8237-treatment.

The quantitation of EdU-positive S phase cells is depicted in Figure 4.12 b, reflecting the observation in the example pictures. The intensity of pH3S10 signal increases when Aurora-A is overexpressed and further increases upon expression of Aurora-A T217D. Upon challenging the cells with MLN8237, the cells expressing Aurora-A WT reduce the pH3S10 intensity to levels seen with IMR-5 EV. Aurora-A T217D cells, show a reduction in pH3S10 intensity, albeit the intensity is still stronger than seen with overexpression of Aurora-A WT.

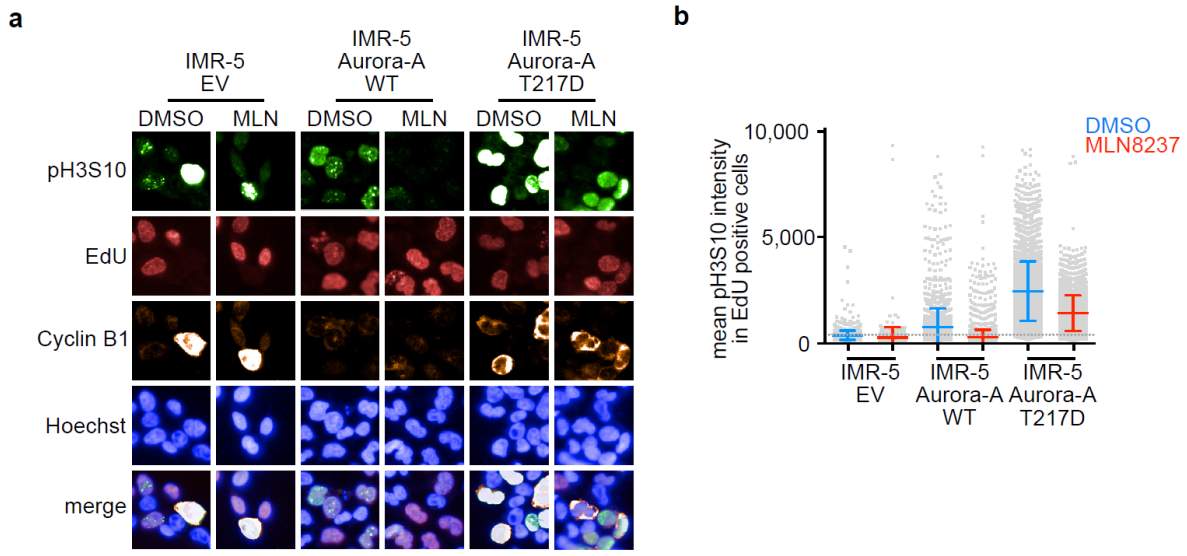

Figure 4.12: pH3S10 staining upon overexpression of Aurora-A WT and T217D mutant.
a. Example pictures of IMR-5 cells expressing empty vector (EV), Aurora-A WT, or Aurora-A T217D mutant treated for 8 h with 100 nM MLN8237 or DMSO as control. Cells incorporate EdU for 30 min and were stained for pH3S10, EdU, cyclin B1, and Hoechst (n=3).
b. Quantitation of pH3S10 intensity in EdU-positive S phase cells from (a;n=3).

Aurora-B, another member of the Aurora family of kinases is also known to phosphorylate H3S10 (Richie & Golden, 2005). To test if this is cell cycle-specific and to exclude off-target effects of MLN8237, immunofluorescence comparing treatment for 8 h with 100 nM MLN8237 and 100 nM AZD1152, a well-characterized Aurora-B inhibitor, was performed. Cells incorporate EdU and were stained with cyclin B1 to distinguish cell cycle phases. The quantitation of pH3S10 shows that Aurora-B has the strongest effect in mitosis, where it completely abolishes the pH3S10 signal (Figure 4.13 a). The influence of Aurora-B inhibition on pH3S10 in S and G2 phase was instead very mild. This was contrary to Aurora-A inhibition, where the strongest effects on pH3S10 were seen in S and G2 phase but not in mitosis.

Histone 3 can harbor post-translational modifications on several residues. Another specific modification in mitosis is phosphorylation on threonine 3 (pH3T3; Polioudaki et al., 2004). To investigate effects on pH3T3, IMR-5 cells were treated for 8 h with 100 nM Aurora-A (MLN8237) and Aurora-B (AZD1152) inhibitor. Immunofluorescence was performed staining cyclin B1 and upon EdU incorporation to distinguish cell cycle phases. Quantitation of pH3T3 intensity is shown in Figure 4.13 b, c, and d. In IMR-5 cells treated with DMSO no signal was observed in G1- and S phase but the signal massively increases in G2/M phase, indicating that the pH3T3 modification is indeed mitosis-specific (Figure 4.13 c). Inhibition with MLN8237 decreases the pH3T3 signal in G2/M phase, whereas treatment with Aurora-B inhibitor drastically reduces pH3T3 signal close to background level (Figure 4.13 d), indicating a role for Aurora-B in the phosphorylation of H3T3.

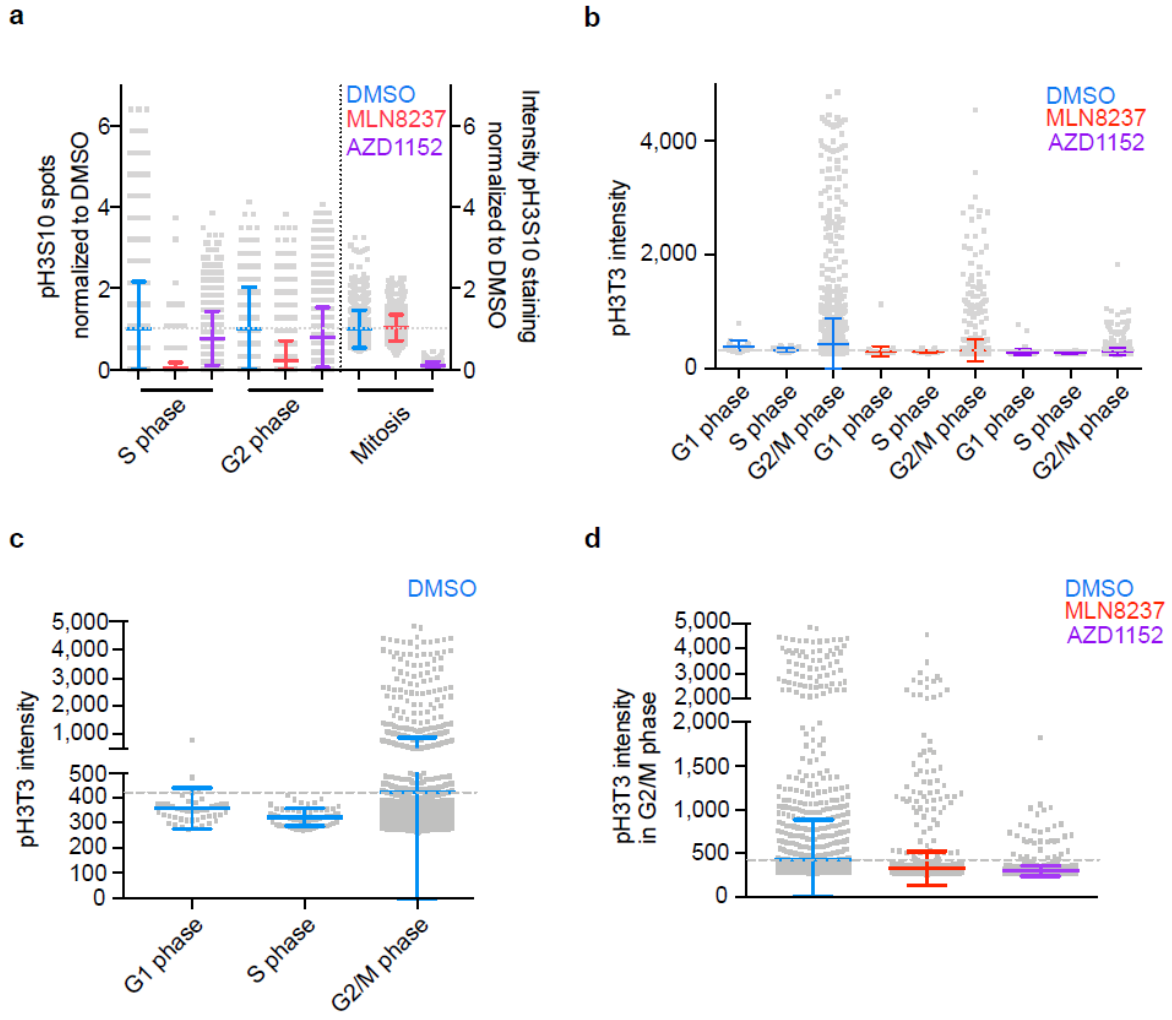

Figure 4.13: Aurora-B does not contribute to H3S10 phosphorylation in S phase, neither is H3T3 phosphorylation affected by Aurora kinases in S phase.
a. Quantitation of pH3S10 immunofluorescence staining. IMR-5 cells were treated for 8 h with 100 nM MLN8237, 100 nM AZD1152, or DMSO as control. 1 µM EdU was incorporated for 30 min before fixation. Cells were stained for pH3S10, further counterstained for cyclin B1, and EdU incorporated to distinguish cell cycle phases. pH3S10 spots were counted in S and G2 phase cells and pH3S10 intensity was calculated in mitotic cells. Values from different experiments were normalized to DMSO control. Each grey dot represents one cell. Shown is the mean ± S.D. (n=3).
b. Quantitation of pH3T3 immunofluorescence staining. IMR-5 cells were treated for 8 h with 100 nM MLN8237, 100 nM AZD1152, or DMSO as control. 1 µM EdU was incorporated for 30 min before fixation. Cells were stained for cyclin B1, EdU incorporation to distinguish cell cycle phases, and pH3T3. pH3T3 intensity was analyzed using the Harmony® High-Content Analysis software, each dot represents one cell. Shown is the mean ± S.D. (n=3).
c. Quantitation of pH3T3 immunofluorescence staining. IMR-5 cells were stained for cyclin B1, EdU incorporation to distinguish cell cycle phases, and pH3T3. pH3T3 intensity was analyzed using the Harmony® High-Content Analysis software, each dot represents one cell. Shown is the mean ± S.D. (n=3).
d. Quantitation pf pH3T3 immunofluorescence staining. IMR-5 cells were treated for 8 h with 100 nM MLN8237, 100 nM AZD1152, or DMSO as control. G2/M phase cells were identified by cyclin B1 staining. pH3T3 intensity was analyzed using Harmony® High-Content Analysis software, each dot represents one cell. Shown is the mean ± S.D. (n=3).
Parts of this Figure were published in similar form in Roeschert et al., 2021.

4.2.5 pH3S10 is also regulated MYCN-dependent

To investigate whether pH3S10 is also regulated by MYCN in S phase, SH-EP cells were used. SH-EP cells are neuroblastoma cells which express MYC instead of MYCN endogenously. Upon stable expression or acute induction of MYCN, SH-EP cells switch their expression from MYC to MYCN, as shown previously (Herold et al., 2019) and in Figure 4.14 a. Interestingly, MYC-to-MYCN switch takes place both upon stable expression of MYCN wild type (WT) or a MYCN T58A mutant. The MYCN mutant cannot get phosphorylated by GSK3 on this modified residue and can thereby not be recognized by the E3 ligase SCF^{FBXW7}, rendering MYCN resistant to proteasomal degradation (Sjostrom et al., 2005).

To analyze pH3S10 signal in S phase, SH-EP cells expressing MYCN WT or T58A mutant were treated for 8 h with 100 nM MLN8237 or DMSO as control. Cells were EdU-incorporated and pH3S10-stained as described above. pH3S10 intensity was quantified using the Harmony® High-Content Analysis software (Figure 4.14 b). pH3S10 staining intensity was increased upon expression of MYCN WT and, to a greater extent, of MYCN T58A. Upon inhibition of Aurora-A in all cell lines there is a decrease of pH3S10 staining in S phase. However, the decrease is much stronger for SH-EP cells expressing MYCN WT or T58A mutant.

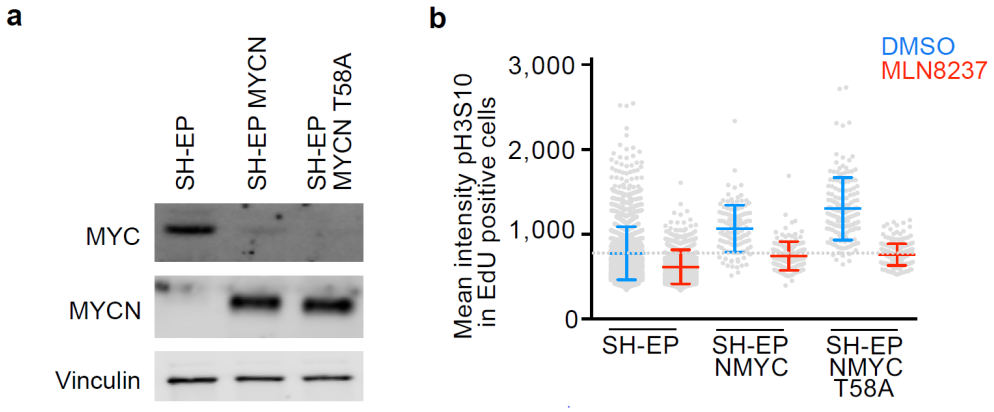

Figure 4.14: MYCN levels influence pH3S10.
a. Immunoblots of indicated proteins from *MYC*-amplified neuroblastoma cell line SH-EP with and without a plasmid that stably expresses MYCN WT or T58A mutant. Vinculin was used as a loading control (n=3).
b. Quantitation of pH3S10 IF in EdU positive SH-EP cells expressing no plasmid, MYCN wild-type (WT) or MYCN T58A mutant. Cells were treated for 8 h with 100 nM MLN8237 or DMSO as control. Mean intensity of pH3S10 was quantified using the Operetta® High-Content Imaging System. Shown is the mean ± S.D. (n=3).
Parts of this Figure were published in similar form in Roeschert et al., 2021.

Taken together, the results indicate that Aurora-A - albeit being unphosphorylated at T288 – is active in S phase. 73 phosphosites of chromatin-bound proteins were found to be regulated by Aurora-A. Those putative targets in S phase are involved in processes like splicing, chromatin modification, and transcription. 8 phosphosites were found to be regulated by MYCN-activated Aurora-A. All putative substrates tested show PLA signals with MYCN and Aurora-A.
Additionally, genetic and pharmacological interference with Aurora-A revealed that catalytic activity of Aurora-A is required to phosphorylate H3S10 in S phase. This residue is phosphorylated in a MYCN-dependent manner. Off-target effects regarding Aurora-B can be ruled out and additional mitotic modifications tested (pH3T3) do not play a role in S phase.

4.3 Aurora-A regulates H3 deposition and thereby prevents transcription-replication conflicts in S phase

Since Aurora-A is MYCN-dependently bound to chromatin in S phase and phosphorylates H3S10, the affected downstream pathways were further investigated. Pathways in which putative Aurora-A targets are involved were investigated including histone composition, splicing, and transcription.

4.3.1 Aurora-A leads to incorporation of H3.3

Aurora-A phosphorylates H3S10 in S phase and changes in post-translational modification of histone tail can rearrange chromatin structure (Bannister & Kouzarides, 2011). Therefore, two histone H3 isoforms were further analyzed depending on Aurora-A activity. H3.3 is replication-independently incorporated and is associated with flexible exchange. H3.1 is a bulk histone incorporated replication-dependently and associated with non-flexible exchange (Tagami et al., 2004).

ChIP-seq experiments of total H3 (measuring H3.1 and H3.3 isoforms) and of the isoform H3.3 upon MLN8237-treatment in S phase-synchronized IMR-5 cells were performed. Density plots of total H3 and H3.3 ChIP-seqs centered around the first nucleosome (Figure 4.15 a) display a nucleosome-free region in front of the first nucleosome. Upon inhibition of Aurora-A, total H3 is more, whereas H3.3 is less incorporated, indicating that H3.1 increases. H3.3 incorporation was stratified for highly MYCN-bound promoters (Figure 4.15 b) and promoters not bound by MYCN (Figure 4.15 c). Comparable results were obtained for H3.3 incorporation on all genes (Figure 4.15 a) and on genes highly bound by MYCN (Figure 4.15 b). On promoters with low MYCN binding limited nucleosome-free region was detected, indicated by the comparable low drop in signal before the first nucleosome. However, the H3.3 incorporation was still more pronounced when Aurora-A is active. Those results are reflected in browser tracks on example genes for high (*NCL*) and low (*COL5A2*) MYCN occupancy (Figure 4.15 d).

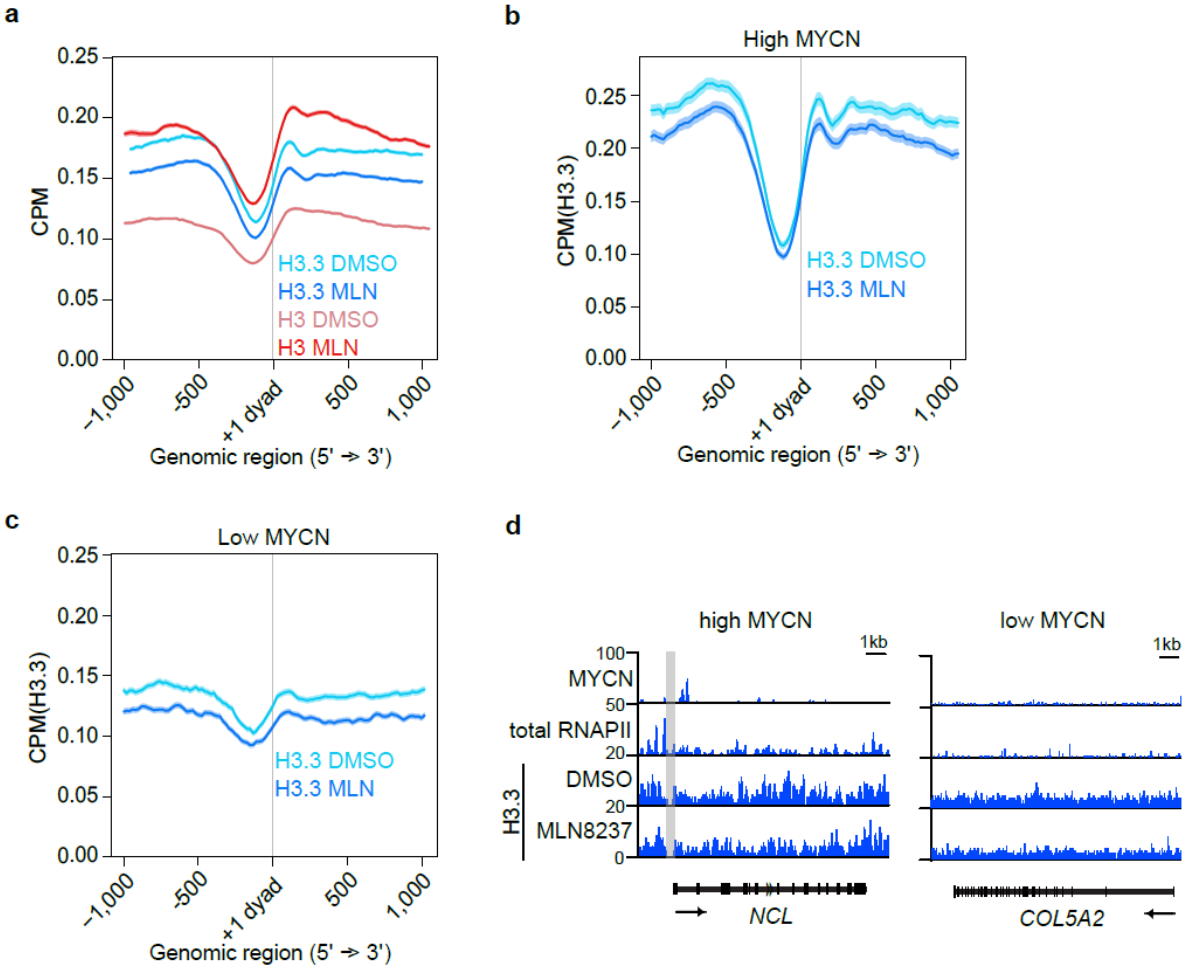

Figure 4.15: Aurora-A favors incorporation of H3.3.
a. Density plot of H3 and H3.3 ChIP-seqs in S phase-synchronized IMR-5 cells treated for 4 h with 1 µM MLN8237. The signal is centered on the first nucleosome ("+1 dyad") located downstream of the TSS (n=14,340 genes; n=2). H3 ChIP-seq was performed by Dr. Gabriele Büchel.
b. Density plot as in (a) for histone H3.3 for 3,000 expressed genes with highest MYCN promoter occupancy. Shading is ± Standard error of the mean (S.E.M.; n=2).
c. Density plot as in (b) for histone H3.3 for 3,000 expressed genes with lowest MYCN promoter occupancy. Shading is ± S.E.M..
d. Browser tracks of H3.3 ChIP-seq (a) on genes with high (*NCL*) and low (*COL5A2*) MYCN occupancy. Grey bar represents nucleosome free region.
Parts of this Figure were published in similar form in Roeschert et al., 2021.

4.3.2 Aurora-A inhibition impairs RNAPII function

Incorporation of different histone isoforms and changes in post-translational modifications of histones are often associated with changes in transcription. Therefore, transcription by RNA polymerase II (RNAPII) upon Aurora-A inhibition was investigated. Different stages of transcription are characterized by different phosphorylation patterns of the heptameric repeat of the C-terminal domain (CTD) of RNAPII. For example, elongating RNAPII can be identified by its serine 2 phosphorylation (RNAPII pSer2). First, ChIP-seq of total RNAPII was performed in S phase-synchronized cells treated with Aurora-A inhibitors. The metagene analysis over the whole gene showed the characteristic distribution for RNAPII (Figure 4.16 a). Total RNAPII

peaks around the TSS and remains stable throughout the gene. When comparing DMSO- and MLN8237-treated samples, the RNAPII peak at the TSS is nearly the same whereas less RNAPII is found in the gene body upon Aurora-A inhibition using MLN8237. MK5108-treatment shows an increase in RNAPII at the TSS and displays the same amount of RNAPII throughout the gene body.

The traveling ratio, defined as occupancy at the TSS + 300 bp divided by the occupancy throughout the whole gene (Reppas et al., 2006), was then calculated to determine the impact of Aurora-A inhibition on transcription. The ratio indicates whether RNAPII moves slower or faster upon treatment. The traveling ratio of every gene was calculated for MLN8237- (Figure 4.16 b) and MK5108- (Figure 4.16 c) treated samples compared to DMSO and shown in a kernel density plot. In this plot, every dot represents one gene: the more the dots divert from the diagonal (dashed line), the more the traveling ratio changes between the samples. Samples treated with MLN8237 showed a shift of the blue cloud of dots towards the y-axis, indicating slower transcription upon Aurora-A inhibition. The same can be observed when investigating the samples treated with MK5108. This result demonstrated that Aurora-A is required for proper transcription in S phase.

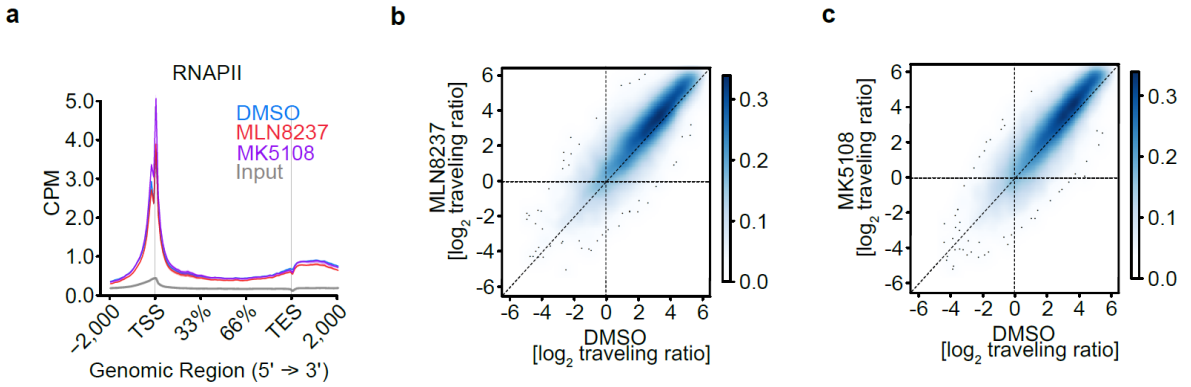

Figure 4.16: Aurora-A inhibition impairs RNAPII functionality.
a. Metagene plot illustrating distribution of the total RNAPII ChIP-seq signal within transcribed regions of all expressed genes (n=17,533) in S phase-synchronized IMR-5 cells treated for 4 h with 1 µM MLN8237, 1µM MK5108, or DMSO as control (n=2).
b. 2D Kernel density plot showing RNAPII traveling ratio in S phase-synchronized cells treated for 4 h with 1 µM MLN8237 or DMSO as control (n=2).
c. 2D Kernel density plot showing RNAPII traveling ratio in S phase-synchronized cells treated for 4 h with 1 µM MK5108 or DMSO as control (n=2).
Parts of this Figure were published in similar form in Roeschert et al., 2021.

To better investigate the effect of Aurora-A on elongating RNAPII, a ChIP-seq of RNAPII pSer2 in IMR-5 cells treated as indicated before was performed. A metagene analysis performed on all expressed genes shows characteristic occupancy throughout the gene body with an increase at the TES (Figure 4.17 a). A massive increase around the TSS in samples treated with MLN8237, and a clear but weaker increase in samples treated with MK5108 compared to DMSO was observed. For samples treated with MLN8237, an increase in occupancy is also

observed throughout the gene body. This finding indicates that Aurora-A inhibition leads to a stalling or slowing down of RNAPII when phosphorylated on Ser2. To identify whether this phenotype is MYCN-dependent the genes were stratified by MYCN occupancy on promoters. This revealed that accumulation of RNAPII pSer2 correlates with MYCN occupancy (Figure 4.17 b). The more MYCN is bound the more RNAPII pSer2 is observed.

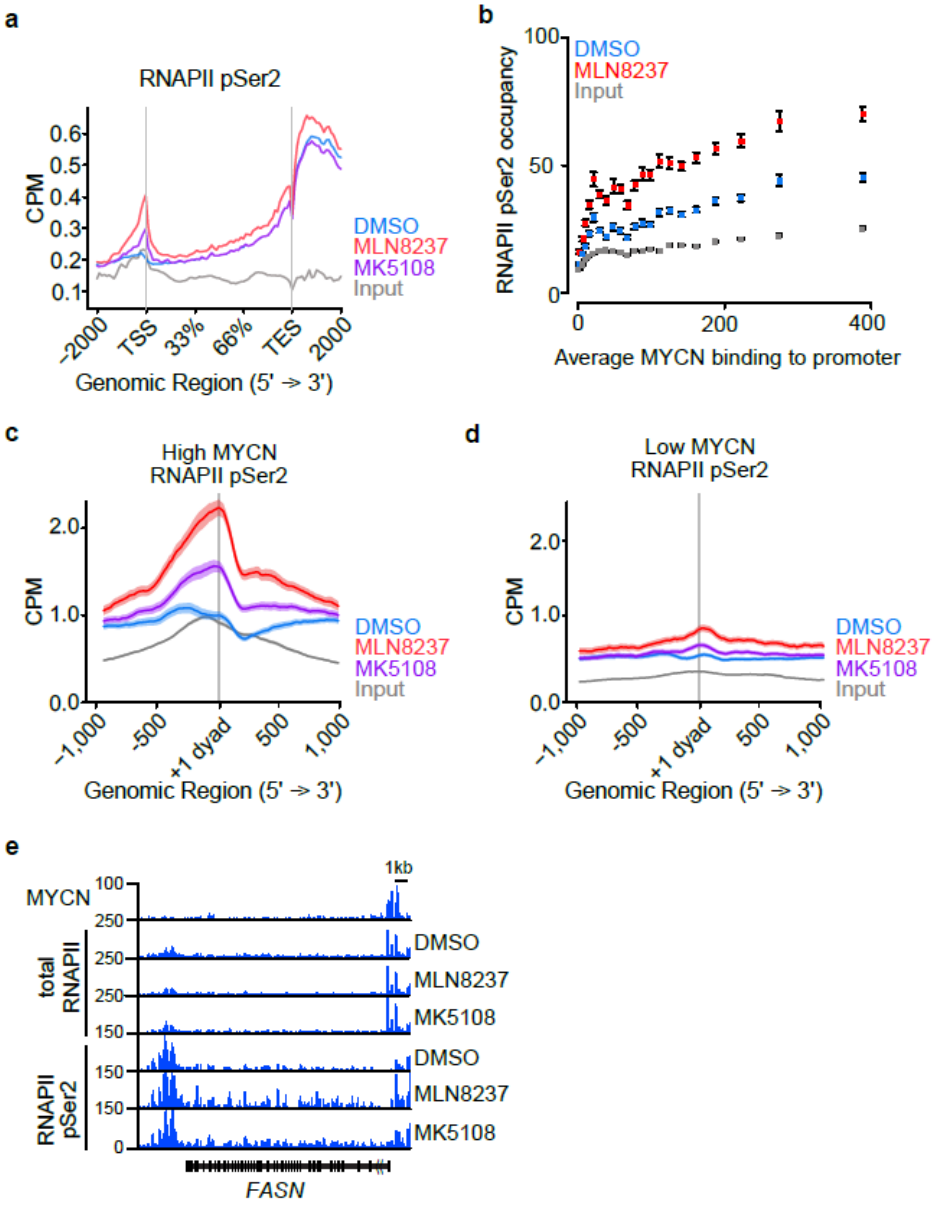

Figure 4.17: Aurora-A prevents elongation defects of RNAPII.
a. Metagene plot illustrating distribution of RNAPII pSer2 ChIP-seq signal within transcribed regions of all expressed genes (n=17,533) in S phase-synchronized IMR-5 cells treated for 4 h with 1 µM MLN8237, 1 µM MK5108, or DMSO as control (n=2).
b. Bin plots of average RNAPII pSer2 ChIP-seq occupancy downstream of the TSS from S phase-synchronized IMR-5 cells treated for 2 h with 1 µM MLN8237 or DMSO. Genes were ordered by MYCN occupancy. Bins contain 3,000 genes each.
c. Data set of (a) is filtered for the 3,000 expressed genes with highest MYCN promoter occupancy. The signal is centered on the first nucleosome ("+1 dyad") located within 300 nt downstream of the TSS. Shading is ± S.E.M..
d. Data set of (a) is filtered for the 3,000 expressed genes with lowest MYCN promoter occupancy. The signal is centered on the first nucleosome ("+1 dyad") located within 300 nt downstream of the TSS. Shading is ± S.E.M..
e. Browser tracks of RNAPII pSer2 ChIP-seq (a) at MYCN target gene *FASN*.
Parts of this Figure were published in similar form in Roeschert et al., 2021.

Considering that Aurora-A promotes a change in histone composition and that RNAPII pSer2 ChIP-seq peak is localized close to the TSS, a new read density plot was centered around the first nucleosome and stratified for 3,000 genes with highest (Figure 4.17 c) and lowest MYCN binding (Figure 4.17 d). At genes with high MYCN occupancy Aurora-A caused stalling of RNAPII pSer2 at the first nucleosome. This increase is higher upon treatment with MLN8237 than with MK5108 which is also reflected in the browser track of a MYCN target gene (Figure 4.17 e). On genes with low MYCN occupancy, there is no effect in RNAPII pSer2 signal.

4.3.3 Short-term inhibition of Aurora-A does not impact gene expression in S phase

To investigate whether gene expression is changed upon Aurora-A inhibition, RNA-seq was performed on S phase-synchronized IMR-5 cells upon 4 h treatment with 1 µM MLN8237. Gene-Set enrichment analysis (GSEA) was performed. The five most regulated Hallmark gene sets are shown (Figure 4.18 a). Solely, the “Hallmark_UV_Response_DN” (Figure 4.18 b) was significantly enriched in the IMR-5 cells treated with Aurora-A inhibitor, indicating that short-term inhibition of Aurora-A in S phase does not impact total mRNA level.

a

Gene Set	NES	q-Value
Hallmark_UV_Response_DN	1.61	0.048
Hallmark_Mitotic_Spindle	1.56	0.119
Hallmark_Protein_Secretion	1.53	0.137
Hallmark_Hedgehog_Signaling	1.48	0.172
Hallmark_G2M_Checkpoint	1.36	0.498

b

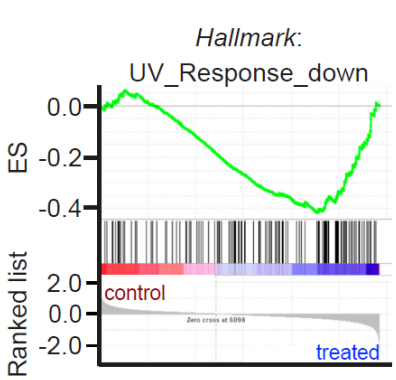

Figure 4.18: Short-term inhibition of Aurora-A does not impact gene expression in S phase.
a. Table of the first five hallmark gene sets mostly downregulated upon treatment with Aurora-A inhibitor. The gene sets were identified from GSEA analysis of mRNA-seq of S phase-synchronized IMR-5 cells treated for 4 h with 1 µM MLN8237 or DMSO; NES (normalized enrichment score; n=3).
b. GSEA signature showing response of a hallmark gene set indicating UV response down in S phase-synchronized IMR-5 cells treated for 4 h with DMSO as control or 1 µM MLN8237 as treated (n=3).

4.3.4 Aurora-A inhibition impairs global splicing in S phase

Investigation of phosphoproteomics upon Aurora-A inhibition in S phase revealed 78 phosphosites downregulated with both inhibitors (Figure 4.5). GO Term analysis revealed that a major affected pathway is splicing (Figure 4.6). Therefore, the influence of Aurora-A on splicing was further investigated. To assess this question, IMR-5 cells were synchronized in S, G2/M, and G1 phase. 4 h before harvest cells were treated with 1 µM MLN8237, 1 µM MK5108, 1 µM Pladienolide B (PlaB), or DMSO as control. PlaB is a well-characterized splicing inhibitor

that acts by sequestering the SF3B1 protein (Effenberger et al., 2014). Unbound SF3B1 is part of the U2 spliceosomal subunit and gets hyperphosphorylated upon splicing activation. SF3B1 hyperphosphorylation can be considered as a marker for productive splicing (Girard et al., 2012). Total level and two phosphorylation-specific sites of SF3B1 were investigated by immunoblotting (Figure 4.19 a). Total SF3B1 does not change throughout cell cycle or upon treatment with any inhibitor. The phosphorylation of T313 and T328 is especially high in G1 and G2 phase, when investigating DMSO-treated cells. Upon treatment with PlaB, regardless of the cell cycle the phosphorylation of T313 and T328 is completely abolished. The effect of PlaB is in line with the literature. Treatment with MLN8237 and MK5108 has no influence on phosphorylated SF3B1 in G1 and G2/M phase but reduces phosphorylation of SF3B1 in S phase. The quantitation of total, pT313, and pT328 SF3B1 level in S phase is shown in Figure 4.19 b reveals the same results already observed by representative immunoblot.

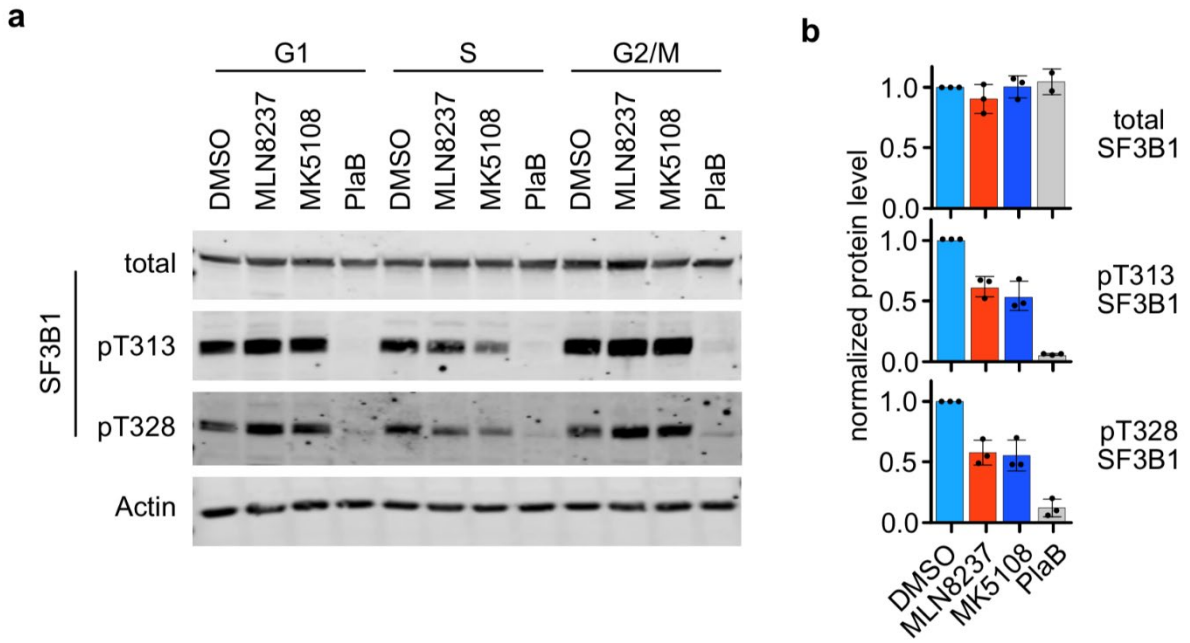

Figure 4.19: Aurora-A is needed for splicing in S phase.
a. Immunoblots of synchronized IMR-5 cells that were treated for 4 h with 1 µM MLN8237, 1 µM MK5108, 1 µM PlaB, or DMSO as control. Cells were synchronized by double thymidine block and released for 4 h, 8 h, or 14 h into S, G2/M, or G1 phase, respectively, harvested by scraping and lysed using RIPA buffer. Actin was used as loading control. Total protein level of SF3B1 as well as phosphorylation on T313 and T328 were investigated (n=3). b. Quantitation of total SF3B1 or SF3B1 phosphorylated on T313 or T328 in S phase-synchronized IMR-5 cells, treated for 4 h with 1 µM MLN8237, 1 µM MK5108, 1 µM PlaB, or DMSO as control. Error bars indicate mean ± S.D. (n=3).
Parts of this Figure were published in similar form in Roeschert et al., 2021.

To further assess whether global splicing is impaired a 4-thio-uridine-sequencing (4sU-seq) was performed. IMR-5 cells were synchronized and treated with 1 µM MLN8237, 1 µM MK5108, 1 µM PlaB, or DMSO as control at the timepoint of release. After 2 h a 15 min pulse with 500 µM 4sU was performed (Figure 4.20 a). One sample (pulse) was harvested directly after the pulse. This enables an overview on actively transcribed gene loci (that incorporate

4sU) regardless of RNA processing. All other samples were incubated for 2 further hours (chase) and then harvested, allowing to appreciate the status of RNA processing. RNA with incorporated 4sU was pulled down and sequenced. Reads were divided in different read categories as described in Cossa et al., 2020 (Figure 4.20 b).

Reads were divided in three groups: mature mRNA (grey), non-spliced pre-mRNA (blue), and RNA without coding sequence (red). Mature mRNA reads can either be found spanning one exon (exonic) or two exons (spliced). Reads of non-spliced pre-mRNA harbor sequences spanning exon and intron (exon-intron or intron-exon) or only intron (intronic). Reads without coding sequence can be reads found at the transcription start site (TSS), at the transcription end site (TES), at the read through after the TES (TES-RT), or in intergenic (intergenic) sequences.

Figure 4.20 c shows the mean percentage of reads found in three replicates for each group. In the pulse sample, a lot of intronic reads (64.5%) and only a few spliced reads (3.3%) or exonic reads (14.9%) were found. In the DMSO-treated sample, intronic reads (41.0%) are reduced, whereas spliced reads (9.9%) and exonic reads (39.2%) are increased. When cells are treated with PlaB, the percentage of reads reflect the pulse sample, since splicing cannot occur. When cells are treated with Aurora-A inhibitor MLN8237 or MK5108 intronic reads are increased whereas spliced reads and exonic reads are decreased compared to DMSO control. The effect of Aurora-A inhibitors was significant albeit much weaker than observed with the splicing inhibitor or in the pulsed sample.

a

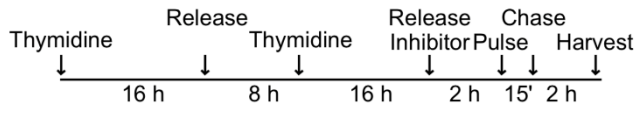

b

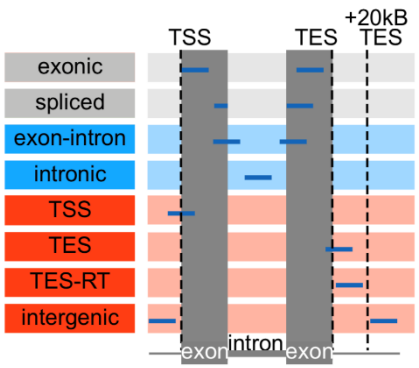

c

Sample	Spliced reads	Exonic	Exon intron overlap	Intergenic	Intronic
Pulse	3.3	14.9	2.9	17.2	64.5
DMSO	9.9	39.2	2.3	17.0	41.0
MLN8237	8.9	35.3	2.3	16.5	45.5
MK5108	8.7	36.3	2.3	15.7	45.4
PlaB	2.4	15.0	3.8	15.5	64.0

Figure 4.20: Aurora-A inhibition impairs global splicing.
a. Diagram showing the setup of the 4sU-seq experiment. IMR-5 cells were S phase-synchronized. The cells were treated at time of release from thymidine block with 1 µM MLN8237, 1 µM MK5108, 1 µM PlaB, or DMSO as control. After 2 h cells were pulsed for 15 min with 500 µM 4sU and further chased for 2 h before harvesting.
b. Definition of read categories for (c). Blue lines show the region where the reads mapped to. Three categories are distinguished by color: grey (exonic and spliced) represents mature mRNA, blue (exon-intron and intronic) represents non-spliced pre-mRNA, and red (TSS, TES, TES-RT, and intergenic) represents RNA without coding sequence. TSS: transcription start site, TES: transcription end site, RT: read through.
c. Mean percentage of reads recovered in each category described in (b), from experiments set up as described in (a; n=3). Paired t-test and Wilcoxon matched-pairs signed rank test was performed, indicating that all treatments (PlaB, MK5108, and MLN8237) significantly reduce the percentage of spliced reads relative to DMSO control (p-value < 0.0001).
Parts of this Figure were published in similar form in Roeschert et al., 2021.

4.3.5 Aurora-A prevents transcription-replication conflicts

Results presented so far indicate that Aurora-A inhibition causes stalling of elongating RNAPII in S phase. Considering the concomitant DNA replication, it is therefore conceivable that one of the functions of Aurora-A in S phase is to prevent transcription-replication conflicts in S phase, as already proposed (Büchel et al., 2017). Therefore, a PLA was performed, investigating the proximity between proliferating cell nuclear antigen (PCNA), the DNA clamp behind the replication machinery and RNAPII (Figure 4.21 a). IMR-5 cells were incubated for 8 h with indicated inhibitors and PLA was performed. Nuclei were counterstained with Hoechst. Green dots represent proximity between PCNA and RNAPII. Number of PLA spots increases when cells are treated with Aurora-A inhibitors as compared to DMSO. Additionally, cells were treated with two different transcription inhibitors, NVP-2 and flavopiridol (FP). When transcription is inhibited very few PLA spots were detected. Quantification of the PLA signal reveals an increase by 1.5-fold upon treatment with 100 nM MLN8237 and 2-fold upon 1 µM MLN8237-treatment compared to DMSO control (Figure 4.21 b). When IMR-5 cells are treated with MK5108, PLA signal increases to 1.5-fold, comparable to 100 nM MLN8237. NVP-2 and FP treatment decreased the PLA signal to less than 0.5-fold. The technical control combining only one antibody for both proteins showed no signal at all, indicating that the primary antibody alone does not create a PLA signal.

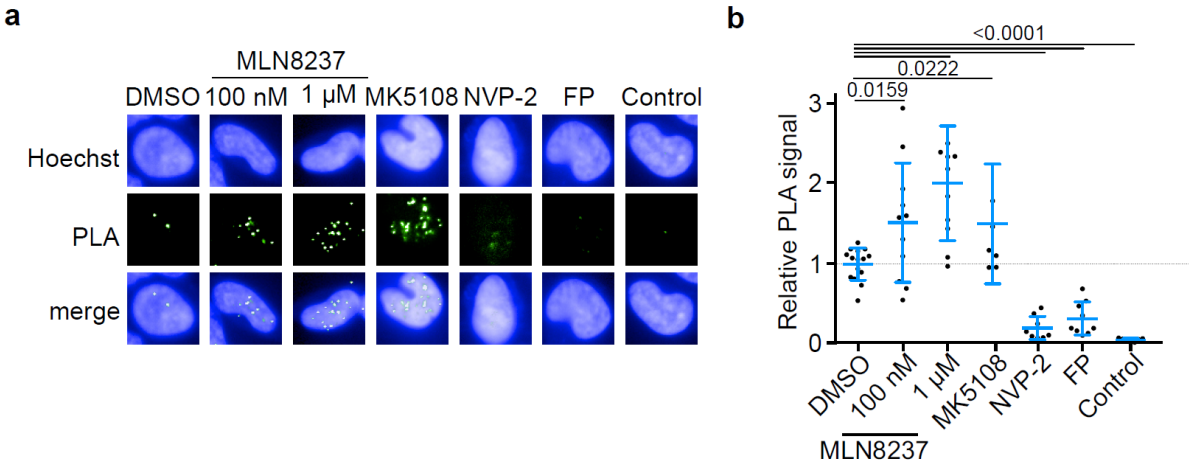

Figure 4.21: Aurora-A prevents transcription-replication conflicts.
a. Pictures of PLA between total RNAPII and PCNA. IMR-5 cells were treated for 8 h with 100 nM and 1 µM MLN8237, 1 µM MK5108, 200 nM NVP-2, 200 nM Flavopiridol (FP), and DMSO as control. IMR-5 cells were fixed, PLA was performed, and nuclei were counterstained with Hoechst. Control is a technical control for the reliability of the PLA signal, therefore only one primary antibody was used in cells treated for 8 h with 1 µM MLN8237, PLA was performed according to manufacturer´s protocol. Example pictures were taken with Operetta® High-Content Imaging System (n=3).
b. Quantitation of results of PLA signal between RNAPII and PCNA in asynchronous IMR-5 cells shown in (a). Each dot represents mean PLA signal of all cells in one well compared to solvent control. Shown is the mean ± S.D., p-values were calculated using unpaired two-tailed t-test relative to DMSO (n=3).
Parts of this Figure were published in similar form in Roeschert et al., 2021.

4.3.6 RNase H1 induction stabilizes Nucleosome +1

It was demonstrated that Aurora-A prevents the formation of DNA-RNA hybrids termed R-loops (Roeschert et al., 2021). This is in keeping with the observations that Aurora-A inhibition impairs splicing (Figure 4.19 and Figure 4.20), if considering that defective splicing induces accumulation of nascent RNA that can bind DNA and form R-loops. This aspect was further addressed by expressing a RNase H1 construct, an enzyme able to resolve R-loops, in a doxycycline (Dox)-inducible manner (Figure 4.22 a). The HA antibody was used to specifically detect HA-tagged overexpressed RNase H1. A clear band is detectable when cells were treated with Dox, whereas no HA-signal was observed in EtOH-treated cells. The functionality of the HA-RNase H1 activity was controlled by performing a DRIP (Roeschert et al., 2021).

Cells were synchronized after induction of RNase H1. PI FACS profiles reveal that overexpression of RNase H1 has no influence on S phase-synchronization efficacy (Figure 4.22 b).

Since Aurora-A inhibition affects H3.3 occupancy, the consequences of removal of R-loops for nucleosome composition were investigated. Therefore, H3.3 ChIP-seq was performed in S phase-synchronized IMR-5 cells, pre-treated for 24 h with doxycycline to induce RNase H1 or EtOH as control. A density plot was centered around the first nucleosome, showing an increased incorporation of H3.3 around the first nucleosome upon overexpression of RNase H1 (Figure 4.22 c). H3.3 deposition is promoted by Aurora-A and counteracted by R-loop formation.

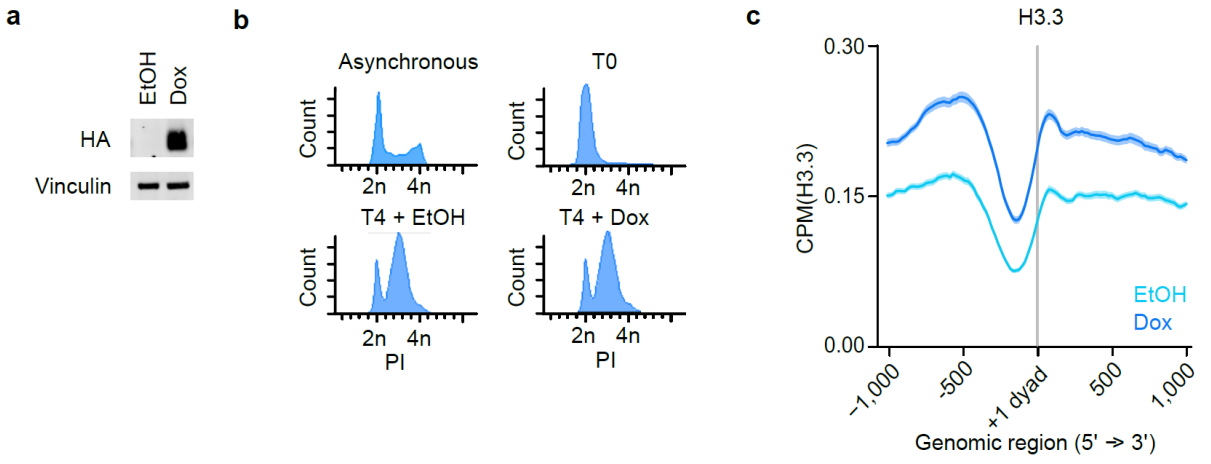

Figure 4.22: RNase H1 induction stabilizes Nucleosome +1.
a. Immunoblot demonstrating induction of HA-RNase H1 in IMR-5 cells with doxycycline-inducible HA-RNase H1. IMR-5 cells were treated for 24 h with doxycycline (Dox) to induce HA-RNase H1 or EtOH to demonstrate no induction. Vinculin was used as loading control. HA was used to detect HA-RNase H1 (n=3).
b. PI FACS analysis of IMR-5 cells expressing doxycycline-inducible RNase H1 synchronized by a double thymidine block (T0). Asynchronous cells are shown as controls. Cells were released from the block for 4 h into S phase. RNase H1 expression was induced 24 h before release from thymidine block due to the addition of Dox (n=3).
c. Density plot of H3.3 ChIP-seq signal in S phase-synchronized RNase H1-IMR-5 cells treated for 24 h with Dox to induce expression of RNase H1 or EtOH (as control). The signal is centered on the first nucleosome ("+1 dyad"; n=14,340 genes) located within 300 nt downstream of the TSS (n=2).
Parts of this Figure were published in similar form in Roeschert et al., 2021.

4.3.7 RNase H1 induction leads to stalling of RNAPII but does not increase transcription-replication conflicts

To analyze effects of RNase H1 expression on RNAPII, ChIP-seqs of total RNAPII and RNAPII pSer2 were performed. Therefore, IMR-5 cells were S phase-synchronized using thymidine block and pre-treated with doxycycline for 24 h to express RNase H1 or EtOH as control. Density plots of total RNAPII ChIP-seq centered around the TSS (Figure 4.23 a) as well as browser tracks of MYCN-bound genes (Figure 4.23 b) show normal RNAPII distribution in cells treated with EtOH. Figure 4.23 c shows a density plot of RNAPII pSer2 ChIP-seq centered around the first nucleosome. The density plots and browser tracks show that both forms of RNAPII are highly enriched when RNase H1 is expressed. This indicates that removal of R-loops results in stalling of RNAPII around the first nucleosome.

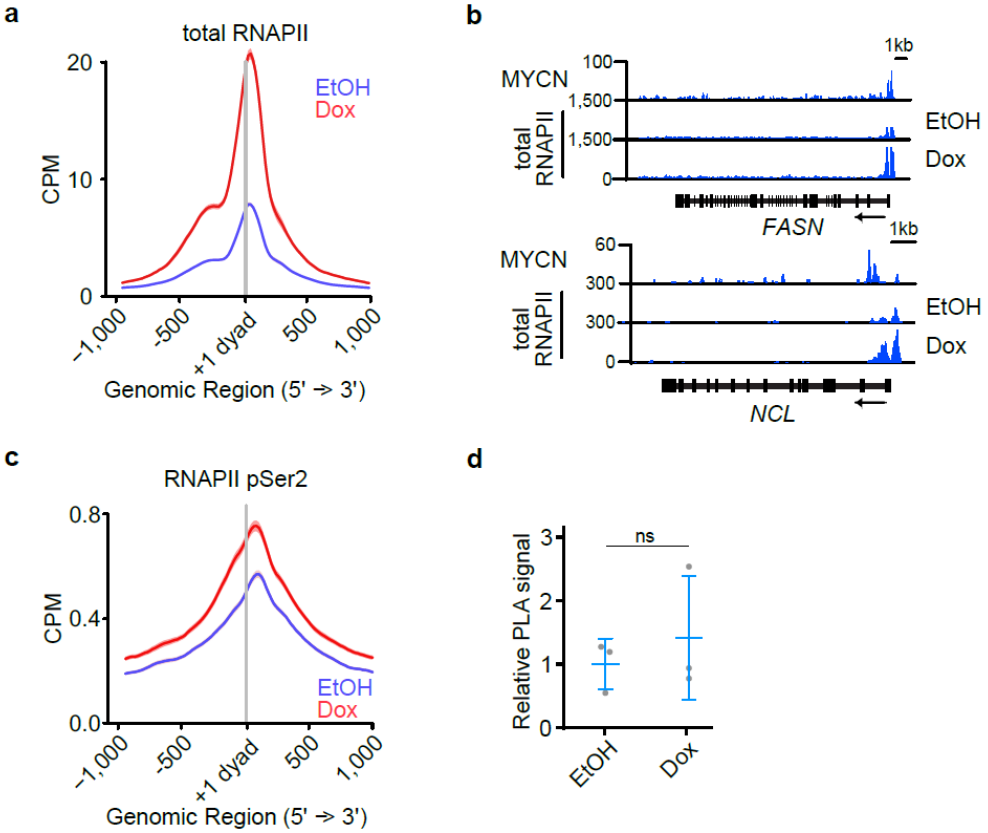

Figure 4.23: RNase H1 overexpression leads to stalling of RNAPII, which does not result in transcription-replication conflicts.
a. Density plot of ChIP-seq signal for total RNAPII in IMR-5 cells inducible expressing RNase H1, synchronized by double thymidine block into S phase. The cells were treated for 24 h with 1 µg/µl doxycycline (Dox) to induce RNase H1 expression or EtOH (as control). The signal is centered on the first nucleosome ("+1 dyad") located within 300 nt downstream of the TSS for 3,000 expressed genes with highest MYCN promoter occupancy (n=2).
b. Browser tracks of total RNAPII ChIP-seqs from (a) at MYCN target genes *FASN* and *NCL*.
c. Density plot of ChIP-seq signal for RNAPII pSer2 in IMR-5 cells inducible expressing RNase H1, synchronized by double thymidine block into S phase. The cells were treated for 24 h with 1 µg/µl Dox or EtOH. The signal is centered on the first nucleosome ("+1 dyad") located within 300 nt downstream of the TSS (n=14,340 genes; n=2).
d. Quantitation of RNAPII and PCNA PLA signals in asynchronous IMR-5 cells expressing inducible RNase H1, treated for 24 h with Dox or EtOH. Each dot represents mean PLA signal of all cells in one well compared to solvent control. Shown is the mean ± S.D., p-value was calculated using unpaired two-tailed t-test relative to DMSO control (n=3).
Parts of this Figure were published in similar form in Roeschert et al., 2021.

Stalling of RNAPII can cause problems with ongoing replication. Therefore, PLA between PCNA and total RNAPII in IMR-5 cells with overexpression of RNase H1 was performed to investigate whether transcription-replication conflicts occur (Figure 4.23 d). Expression of RNase H1 does not change the number of transcription-replication conflicts. Therefore, it can be concluded that formation of R-loops does not contribute to transcription-replication conflicts. Taken together the results indicate that Aurora-A promotes H3.3 incorporation into the first nucleosome, whereas it prevents the incorporation of bulk histone H3.1. Inhibition of Aurora-A leads to stalling of the elongating form of RNAPII, but short-term inhibition does not impact mRNA levels measured by RNA-seq. Furthermore, the analyses of SF3B1 phosphorylation and or nascent RNA suggest a role – direct or indirect – of Aurora-A in regulating splicing activity. Additionally, Aurora-A prevents the formation of transcription-replication conflicts. Finally, resolution of R-loops by overexpression of RNase H1 results in an increased incorporation and therefore stabilization of the first nucleosome. Additionally, overexpression of RNase H1 leads to a stalling of the total as well as the elongating form of RNAPII but has no impact on the formation of transcription-replication conflicts.

4.4 Aurora-A inhibition activates ATR

4.4.1 Aurora-A inhibition induces ATR activation

Previously published data indicated that Aurora-A inhibition induces the activation of ATR, as measured by the phosphorylation of ATR targets S33 on RPA32 or S345 on CHK1 (Büchel et al., 2017; Shiotani et al., 2013). Additionally, stalled replication forks which occur e.g., at transcription-replication conflicts can activate ATR (Hamperl & Cimprich, 2016). To verify if transcription-replication conflicts observed upon Aurora-A inhibition (Figure 4.21) are directly inducing downstream activation of ATR, pS33 RPA32 upon Aurora-A inhibition in S phase was investigated.

An immunofluorescence was performed on IMR-5 cells treated for 8 h with different concentrations of MLN8237, ranging from 100 nM to 10 µM. The mean intensity of pS33 of RPA32 of all EdU positive S phase cells is shown (Figure 4.24). This result indicates that 100 nM MLN8237 which is sufficient to inhibit the catalytic activity of Aurora-A does not induce phosphorylation of RPA32. Increasing the concentration of MLN8237 results in phosphorylation of RPA32. In line with literature, this shows that inhibition of Aurora-A induces ATR activation in a dose-dependent manner.

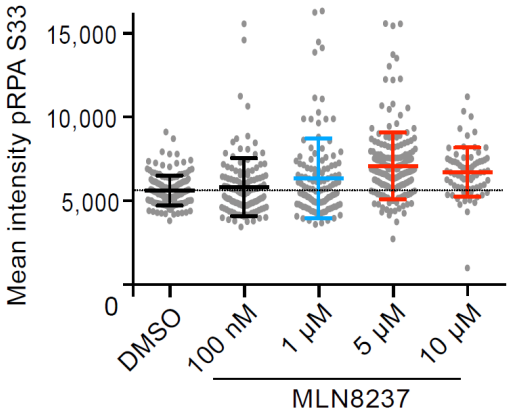

Figure 4.24: Aurora-A inhibition induces ATR activation.
IMR-5 cells were treated for 8 h with different concentrations of Aurora-A inhibitor MLN8237 (range from 100 nM to 10 µM) or DMSO as control. 30 min before fixation cells were incubated with 1 µM EdU, cells were fixed, stained for pRPA32 S33, and for EdU. Shown is the mean intensity in EdU positive cells in each condition ± S.D.; each dot represents one cell. Statistically significant differences to DMSO control are indicated in blue ($p=0.0004$) and red ($p<0.0001$; n=3).
This Figure was published in similar form in Roeschert et al., 2021.

4.4.2 Aurora-A substrate SF3B2 prevents ATR activation

Since it is known that Aurora-A inhibition causes activation of ATR and that inhibition of splicing using PlaB can also enhance sensitivity of cells to ATR inhibition (Nguyen et al., 2018). One identified substrate of MYCN-activated Aurora-A is SF3B2 which has a known function in splicing. IMR-5 cells were transfected with a siRNA pool targeting SF3B2 for 24 h or 48 h and

mRNA expression of *SF3B2* gene was tested (Figure 4.25 a). Since siRNA treatment for 24 h was more efficient, all further experiments were performed 24 h after siRNA transfection.

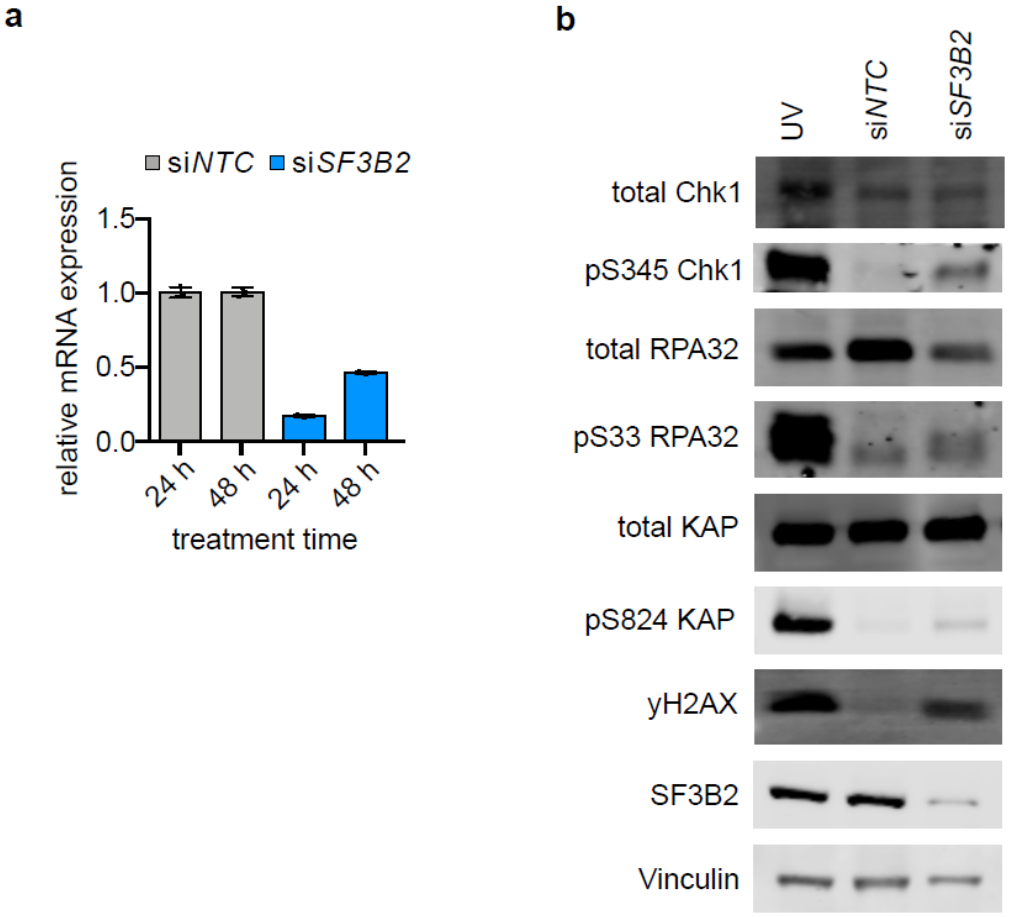

Figure 4.25: SF3B2, a potential Aurora-A substrate in S phase, prevents ATR activation.
a. IMR-5 cells were transfected with siRNA pools targeting SF3B2 or control for 24 h or 48 h. Relative mRNA expression of *SF3B2* was investigated. Error bars indicate S.D. of technical triplicates (n=1).
b. Immunoblot of DNA damage markers in IMR-5 cells transfected with si*NTC* or si*SF3B2* for 24 h. UV light was used as positive control for induction of DNA damage and applied for 60 s to untransfected IMR-5 cells, which were further incubated for 1 h at 37 °C. Cells were harvested and lysed using RIPA. Indicated proteins were investigated on immunoblot. Vinculin was used as loading control and SF3B2 was used to validate that siRNA treatment worked (n=2).

IMR-5 cells were transfected with si*NTC* and si*SF3B2* for 24 h. IMR-5 cells exposed to UV light were used as positive control for induction of DNA damage. Immunoblotting of indicated proteins involved in DNA damage response was performed (Figure 4.25 b). General DNA damage was investigated by γH2AX. Additionally, phosphorylation of S824 on KAP1 (a marker for ATM activation) as well as phosphorylation of S345 on Chk1 or S33 on RPA32 (markers for ATR activation), were assessed.

Treatment with si*SF3B2* resulted in a drastic decrease in SF3B2 protein level, indicating that the siRNA treatment worked. Exposure to UV light led to a drastic increase of all tested DNA damage markers. Transfection with si*SF3B2* resulted in an increase of γH2AX, a general

marker for DNA damage. Additionally, phosphorylation of KAP1 is slightly increased, while pS345 Chk1 and pS33 RPA32 are increased upon treatment with si*SF3B2*. This indicates that absence of SF3B2 activates ATR more strongly than ATM.

4.4.3 Combined Aurora-A and ATR inhibition leads to apoptosis in a MYCN-dependent manner

Since Aurora-A inhibition results in an activation of ATR (Büchel et al., 2017, Figure 4.24), it is conceivable that a combination of Aurora-A and ATR inhibitors results in a likely synergistic effect. Therefore, two *MYCN*-amplified neuroblastoma cell lines were treated for 36 h with single agent, the combination (1 µM AZD6738, 100 nM MLN8237), or DMSO as control. Crystal violet staining visualizes the cell growth after treatment in IMR-5 cells (Figure 4.26 a) and NGP cells (Figure 4.26 b). Cells treated with DMSO grow to a full dish. Treatment with AZD6738 already mildly decreases cell growth. MLN8237 drastically reduces cell growth and this is even enhanced when cells are treated with the combination. NGP cells reflect the result of IMR-5 cells, indicating that both *MYCN*-amplified neuroblastoma cells react in the same way to the treatment with the inhibitor.

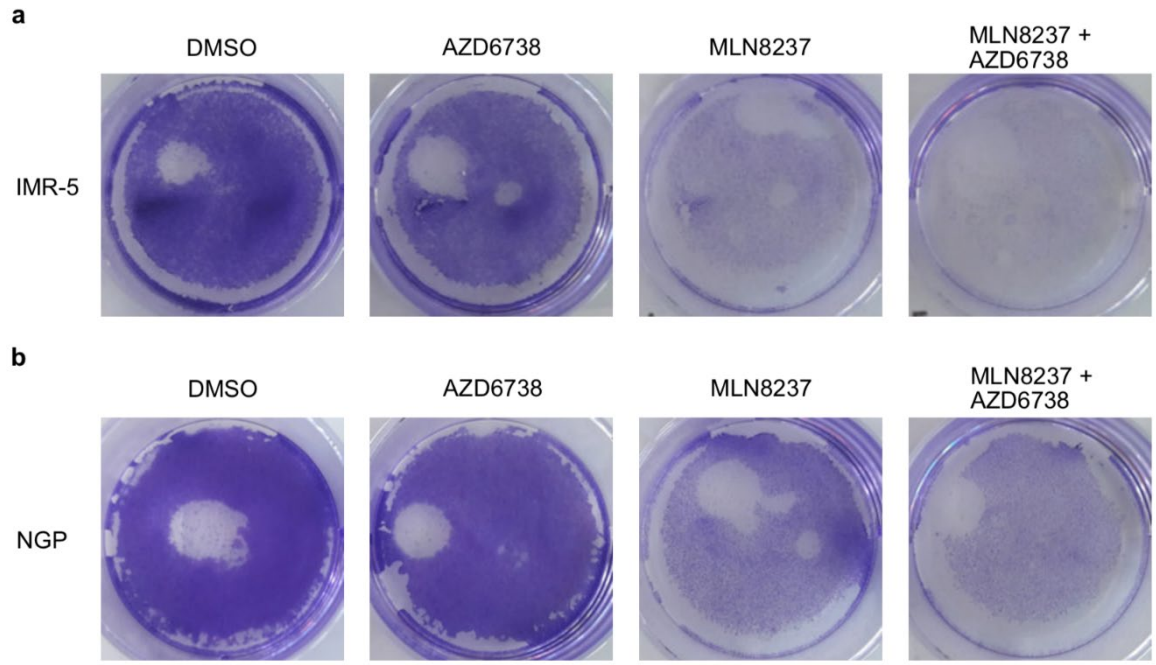

Figure 4.26: Crystal violet staining reflects growth deficiency upon combinatorial treatment in two *MYCN*-amplified neuroblastoma cells.
a. *MYCN*-amplified IMR-5 cells were treated for 36 h with 1 µM AZD6738, 100 nM MLN8237, a combination, or DMSO as control (n=3).
b. *MYCN*-amplified NGP cells were treated for 36 h with 1 µM AZD6738, 100 nM MLN8237, a combination, or DMSO as control (n=3).

To better understand the reasons of the differential growth upon AZD6738- and MLN8237-treatment, apoptosis and cell cycle behavior were assessed. Apoptosis was first investigated using Annexin V/PI FACS in six different neuroblastoma cell lines. Three *MYCN* non-amplified (SH-EP, SK-NAS, SH-SY5Y) and three *MYCN*-amplified (IMR-5, NGP, IMR-32) neuroblastoma cell lines were treated with single inhibitor or combination (100 nM MLN8237, 1 µM AZD6738) or DMSO for 48 h (Figure 4.27 a). *MYCN* non-amplified cells are not affected by treatment with inhibitors or combination. IMR-5 and NGP cells show the same pattern. They display nearly no apoptosis when treated with DMSO or AZD6738, while treatment with MLN8237 induces apoptosis and the combination of both inhibitors further increases apoptosis. IMR-32 cells show a similar trend, although a relatively high number of apoptotic cells is already present upon DMSO- or AZD6738-treatment. Still, treatment of IMR-32 cells with MLN8237 increased apoptosis and this further increased upon combinatorial treatment.
Upon investigation of synergism*, MYCN* non-amplified cell lines show no synergistic effect upon combinatorial treatment, whereas two *MYCN*-amplified cell lines showed synergism (Table 7.2).

To test if Aurora-A catalytic function is important for this apoptotic phenotype upon combination treatment the experiment was repeated using MK5108 (Figure 4.27 b). IMR-5 cells treated with MK5108 show an increase in apoptosis, albeit weaker than upon treatment with 100 nM MLN8237. Consistently with the MLN8237 result in IMR-5 cells, there is a further increase of apoptosis when treated with MK5108 and AZD6738, indicating synergism (Table 7.2).
To test that it is an Aurora-A-specific effect, IMR-5 cells which express doxycycline-inducible Aurora-A WT or T217D mutant (which is not affected by treatment with MLN8237) were employed (Brockmann et al., 2013). Doxycycline was added 24 h before inhibitor treatment. The results of the Annexin V/PI FACS revealed that without expression of Aurora-A, cells behave comparable as seen before (Figure 4.27 c). When Aurora-A WT is overexpressed, Aurora-A inhibition results in less apoptosis, whereas the increase in apoptotic cells is still present, when combinatorial treatment was applied. When Aurora-A T217D mutant is overexpressed, there is no increased apoptosis observable upon MLN8237 and only mild increase upon combinatorial treatment, which indicates no synergism (Table 7.2).

The Chk1 kinase is a downstream target of ATR. Therefore, it was tested if inhibiting Chk1 together with Aurora-A has similar effects. IMR-5 cells were treated for 24 h and 48 h with 1 µM CHIR-124, a selective Chk1 inhibitor, 100 nM MLN8237, combination of both, or DMSO as control (Figure 4.27 d). DMSO treatment has no effect on apoptosis in IMR-5 cells. Inhibition of Chk1 increases the amounts of apoptotic cells after 24 h. Inhibition of Aurora-A for 24 h is

well tolerable for IMR-5 cells and only mildly increases the amount of apoptosis. Combinatorial treatment increased the amounts of apoptotic cells. In contrast to ATR inhibition, Chk1 inhibition as single agent for 48 h already induced a lot of apoptosis in IMR-5 cells. Incubation with the combination for 24 h revealed a slight synergistic effect, whereas 48 h treatment resulted in no synergistic effect (Table 7.2).

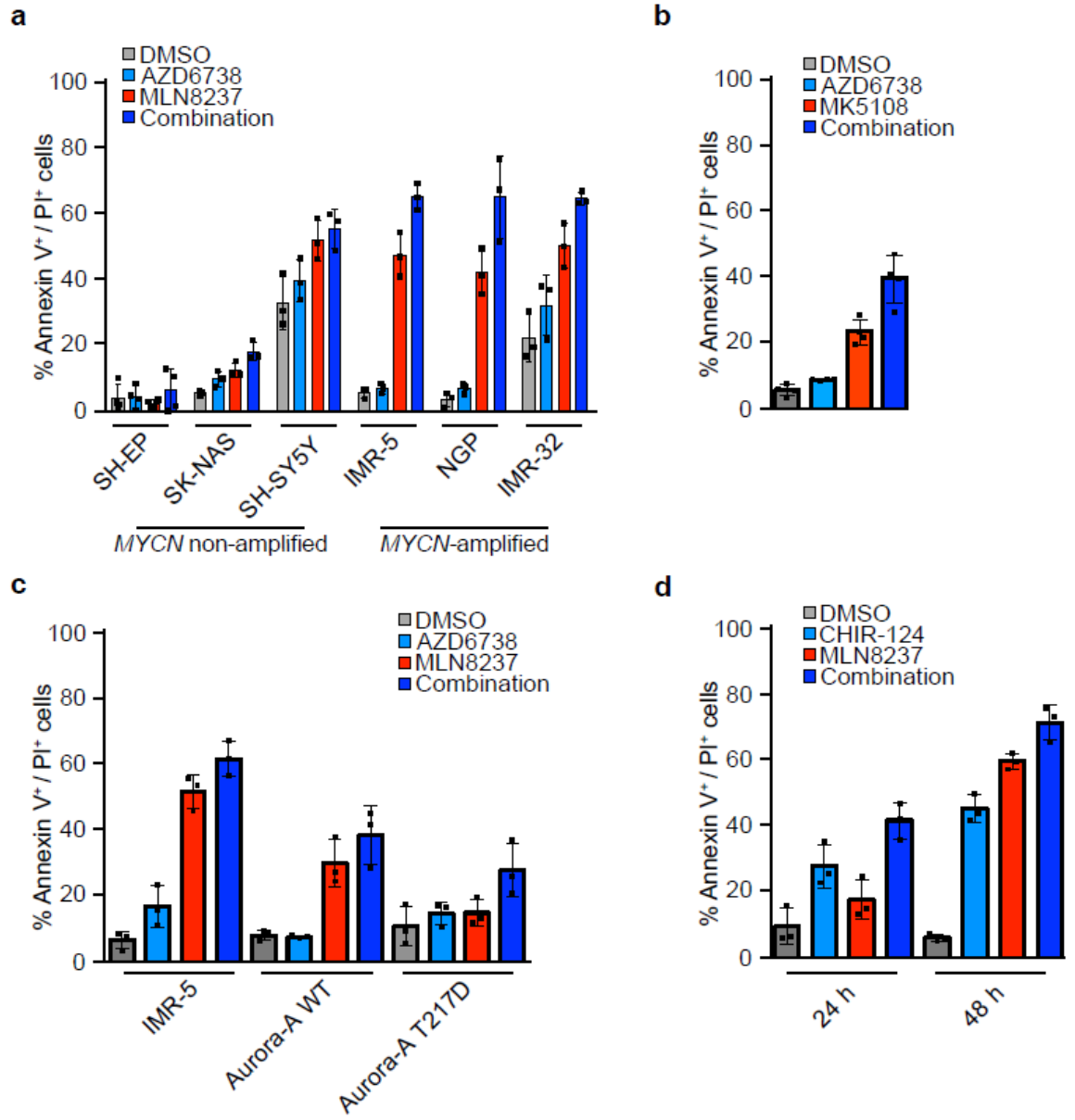

Figure 4.27: Combinatorial treatment enhances apoptosis in a MYCN-dependent manner.
a. Annexin V/PI FACS analysis of six neuroblastoma cell lines, treated for 48 h with 1 µM AZD6738, 100 nM MLN8237, a combination, or DMSO as control. SH-EP, SK-NAS, and SH-SY5Y are *MYCN* non-amplified neuroblastoma cell lines, whereas IMR-5, NGP, and IMR-32 are *MYCN*-amplified neuroblastoma cell lines. Shown is the mean ± S.D. (n=3).
b. Annexin V/PI FACS analysis in IMR-5 cells treated for 48 h with 1 µM AZD6738, 1 µM MK5108, a combination, or DMSO as control. Shown is the mean ± S.D. (n=4).
c. Annexin V/PI FACS analysis of IMR-5 cells, IMR-5 cells expressing inducible Aurora-A WT, or an inducible Aurora-A T217D mutant. Expression was induced for 24 h prior 48 h treatment with 1 µM AZD6738, 100 nM MLN8237, a combination or DMSO as control. Shown is the mean ± S.D. (n=3).
d. Annexin V/PI FACS analysis in IMR-5 cells treated for 24 h or 48 h with 1 µM CHIR-124, 100 nM MLN8237, a combination, or DMSO as control. Shown is the mean ± S.D. (n=3).
Parts of this Figure were published in similar form in Roeschert et al., 2021.

In parallel to apoptosis analyses, cell cycle behavior upon MLN8237/AZD6738 combination was also investigated. Aurora-A has an important role in entry into mitosis, therefore inhibition of Aurora-A is expected to result in a cell cycle arrest at the border between G2 and mitosis (Brockmann et al., 2013). Activation of ATR results in a checkpoint activation in S or G2 phase and therefore results in a S or G2 arrest (Saldivar et al., 2017). IMR-5 cells were synchronized and at the timepoint of release treated with different inhibitors (1 µM AZD6738, 100 nM MLN8237, or a combination) or DMSO as control. The samples were harvested after 2 h, 4 h, 6 h, 8 h, 10 h, or 11 h and cells in different cell cycle phases were measured using PI FACS (Figure 4.28).

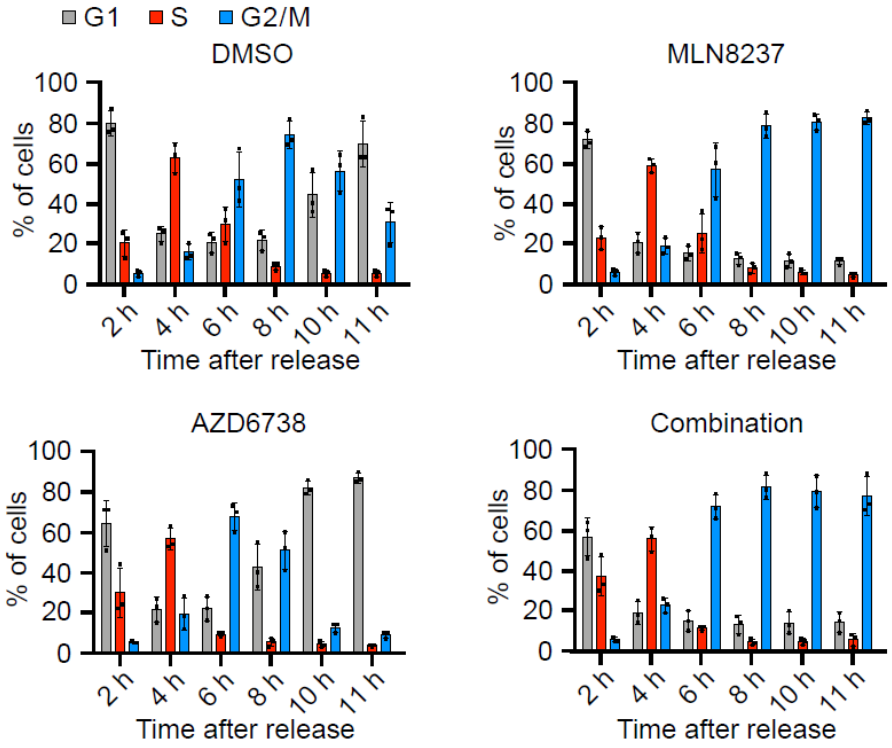

Figure 4.28: Combinatorial treatment enhances cell cycle speed and induces cell cycle arrest.
IMR-5 cells were synchronized using double thymidine block. At the time of release cells were treated with 1 µM AZD6738, 100 nM MLN8237, their combination, or DMSO as control. Cells were harvested for PI FACS after 2 h, 4 h, 6 h, 8 h, 10 h, and 11 h. The amounts of cells in G1 (grey), S (red), and G2/M (blue) phase were quantified by PI FACS. Shown is the mean ± S.D. (n=3).

IMR-5 cells treated with DMSO display a usual cell cycle distribution. Most cells were released for 2 h into G1, for 4 h into S, 6 h and 8 h into G2/M, and 10 h and 11 h into G1 phase. Upon treatment with 100 nM MLN8237 the cells released for more than 6 h arrested in G2/M phase, in line with published data (Brockmann et al., 2013). IMR-5 cells released in the presence of AZD6738 showed an accelerated cell cycle speed. This phenotype is especially present after 8 h, when most DMSO-treated cells are in G2/M and AZD6738-treated cells already reached the next G1 phase. When cells were released and incubated with the combination of ATR and Aurora-A inhibitors, the cells showed accelerated cell cycle speed. After 2 h already a

significant number of cells reached S phase and after 6 h most cells reached G2/M phase and arrested in the cell cycle.

4.4.4 RNase H1 induction does not prevent apoptosis

Upon simultaneous inhibition of Aurora-A and ATR, *MYCN*-amplified neuroblastoma cells undergo apoptosis. To investigate the role of R-loops in this process, IMR-5 cells expressing a doxycycline-inducible RNase H1 were used. As demonstrated in Figure 4.22, pre-treatment for 24 h with doxycycline results in expression of RNase H1. IMR-5 cells pre-treated for 24 h with EtOH or Dox, followed by 48 h treatment with 1 µM AZD6738, 100 nM MLN8237, combination, or DMSO as control, were stained with Annexin V/PI (Figure 4.29 a). As previously shown (Figure 4.27 a), DMSO and AZD6738-treatment does not influence levels of apoptosis in IMR-5 cells. Apoptosis levels increase upon inhibition of Aurora-A and further elevate when cells were co-treated with an ATR inhibitor. There was no difference in apoptosis upon overexpression of RNase H1. Therefore, removal of R-loops does not impact apoptosis levels upon inhibition of Aurora-A and ATR.

Additionally, a PI FACS analysis was performed to investigate the contribution of R-loops resolution to the cell cycle phenotype observed upon combinatorial treatment (Figure 4.29 b). Asynchronously growing IMR-5 cells with inducible RNase H1 were pre-treated for 24 h with EtOH or Dox and treated for 8 h or 24 h with 1 µM AZD6738, 100 nM MLN8237, their combination, or DMSO. Cells treated with DMSO show a majority of cells in G1 phase, as well as an equal distribution of the non-G1 phase cells between S and G2/M phase. This distribution neither change upon prolongation of DMSO treatment nor with overexpression of RNase H1. Treatment for 8 h with AZD6738 increased the amounts of cells in G1 phase compared to DMSO treatment. G1 phase cells increase even further upon 24 h treatment. Upon 8 h treatment with MLN8237 most cells are in G2/M phase, which can also be observed upon 24 h treatment. Upon treatment with the combination for 8 h an arrest of the majority of cells in G2/M phase was observed, this arrest was enhanced when treatment was prolonged to 24 h. The same percentages were measured when RNase H1 was overexpressed. The results indicate that RNase H1 expression does not alter the cell cycle phenotype induced by Aurora-A or ATR inhibition.

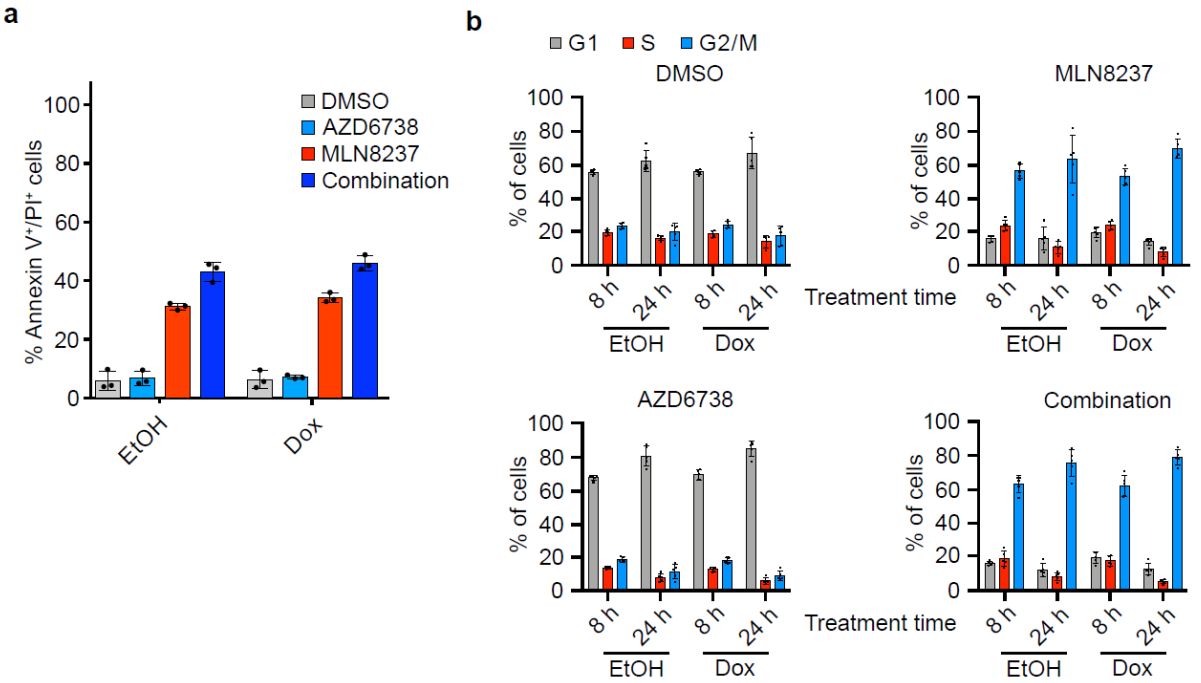

Figure 4.29: RNase H1 overexpression does not affect apoptosis or cell cycle.
a. Annexin V/PI FACS of IMR-5 cells expressing doxycycline-inducible RNase H1. 1 µg/ml Dox or EtOH was added 24 h before start of the experiment. After pre-treatment, cells were incubated for 48 h with 1 µM AZD6738, 100 nM MLN8237, combination, or DMSO as control. Annexin V/PI FACS was performed and measured on FACSCanto™II. Shown is the mean ± S.D. (n=3).
b. PI FACS of IMR-5 cells expressing inducible RNase H1. 1 µg/ml Dox or EtOH was added 24 h before start of the experiment. After pre-treatment, cells were incubated with 1 µM AZD6738, 100 nM MLN8237, combination, or DMSO as control. Cells were treated for 8 h or 24 h and harvested for PI FACS. The amounts of cells in G1 (grey), S (red), and G2/M (blue) phase were quantified by FACS. Shown is the mean ± S.D. (n=3).

4.4.5 PARP1 prevents the formation of transcription-replication conflicts

PARP1 is activated at stalled replication forks to stabilize them, similarly to ATR (Ronson et al., 2018). To investigate whether PARP1 and ATR have similar functions in addition to Aurora-A inhibition, the effect of PARP1 on transcription-replication conflicts as well as apoptosis in *MYCN*-amplified neuroblastoma cells were investigated.

Therefore, transcription-replication conflicts were measured by PLA between PCNA and RNAPII upon inhibition of PARP1 using 1 µM Olaparib for 8 h (Figure 4.30 a). The result shows that transcription-replication conflicts occur more often upon PARP1 inhibition, comparably to results obtained for Aurora-A inhibition (Figure 4.21).

As a next step the effect of combinatorial inhibition of PARP1 and Aurora-A on apoptosis of *MYCN*-amplified neuroblastoma was investigated (Figure 4.30 b). 24 h treatment of any inhibitor does not result in an increased apoptosis of IMR-5 cells. Treatment for 48 h increases apoptosis for all single agents and even more cells undergo apoptosis when treated with both inhibitors. Combinatorial treatment with Olaparib and MLN8237 does not result in a synergistic effect in this experiment (Table 7.2).

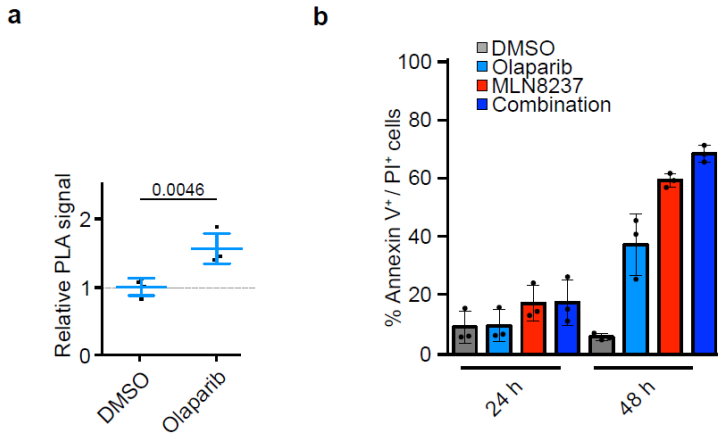

Figure 4.30: Effect of PARP1 inhibition on transcription-replication conflicts and apoptosis.
a. Quantitation of transcription-replication conflicts measured by PLA between PCNA and RNAPII. IMR-5 cells were treated for 8 h with 1 µM Olaparib or DMSO as control. PLA was performed and results were quantified with the Operetta® High-Content Imaging System. P-values analyzed using unpaired t-test (n=3).
b. Annexin V/PI FACS of IMR-5 cells upon 24 h or 48 h treatment with 100 nM MLN8237, 1 µM Olaparib, or combination (n=3).
Parts of this Figure were published in similar form in Roeschert et al., 2021.

Taken together, Aurora-A inhibition as well as knockdown of the putative Aurora-A target SF3B2 in S phase result in the activation of ATR. Combinatorial treatment of Aurora-A and ATR inhibitors results in a synergistic reduction of cell growth. This can be due to increased apoptosis of *MYCN*-amplified neuroblastoma cells as well as an accelerated cell cycle speed resulting in a G2/M arrest. The synergistic effect of apoptosis can be seen additionally by using another inhibitor of Aurora-A and a slightly synergistic effect is also observable upon inhibition of CHK1, the downstream kinase of ATR. The apoptotic phenotype can be rescued by expression of a mutant Aurora-A which does not respond to inhibitor treatment. Overexpression of RNase H1 does not rescue the apoptotic phenotype, neither impact the cell cycle arrest.

PARP inhibition increased the number of transcription-replication conflicts but showed no synergism on neuroblastoma cells when combined with Aurora-A inhibition.

5 Discussion

5.1 Aurora-A is MYCN-dependent bound to chromatin in S phase

Aurora-A is a widely studied kinase in G2/M phase. However, recent literature suggested a role for Aurora-A in S phase. Aurora-A mainly interacts with MYCN in S phase of the cell cycle (Büchel et al., 2017) and MYCN induces auto-phosphorylation of Aurora-A *in vitro*, indicating a coactivator function (Richards et al., 2016). However, nothing is known regarding the subcellular localization of this complex.

The investigation of subcellular localization of Aurora-A throughout the cell cycle revealed that total Aurora-A levels increased from G1 to G2/M phase (Figure 4.1 b), which is in line with literature (Kimura et al., 1997). Additionally, the subcellular localization of Aurora-A changes throughout the cell cycle. Aurora-A is mainly cytoplasmic in G1 phase, whereas in S phase it is mainly chromatin-bound. G2/M phase revealed similar amounts of cytoplasmic and chromatin-bound Aurora-A. TPX2 is the known chromatin anchor for Aurora-A (Kufer et al., 2002), which is widely expressed in G2/M phase, while it is almost absent in G1 and S phase (Hsu et al., 2017). This suggests that association of Aurora-A with chromatin in S phase cannot be mediated by TPX2. Since Aurora-A needs a cofactor to bind chromatin, there has to be another protein fulfilling this function in S phase. From previous work, it is known that MYCN specifically interacts with Aurora-A in S phase (Büchel et al., 2017) and MYCN showed binding to chromatin throughout the cell cycle.

To investigate the MYCN-dependency of Aurora-A association to chromatin in S phase, 10058-F4 was used. 10058-F4 is a compound preventing the hetero-dimerization of MYCN with MAX and thereby association to chromatin (Wang et al., 2007), as confirmed by a MYCN ChIP which showed reduced MYCN binding (Figure 4.2 a).

A comparable result was also obtained from fractionation experiments (Figure 4.2 b). Besides the reduction of MYCN binding to chromatin also total MYCN levels decreased upon 10058-F4 treatment. This can be explained as stability of MYCN is regulated by chromatin binding, since the loss of this association results in a proteasomal degradation (Mathsyaraja et al., 2019). Upon 10058-F4 treatment also chromatin binding of Aurora-A was decreased, arguing that Aurora-A was stabilized by MYCN on chromatin.

Since 10058-F4 interferes not only with MYCN/MAX but also with other BR-HLH-LZ proteins, the specificity for MYCN using siRNA or shRNA is desirable. Nevertheless, this approach was not pursued since MYCN also drives the transcription of Aurora-A (den Hollander et al., 2010; Shang et al., 2009) and therefore long-term knockdown of MYCN would automatically result in a reduction of levels of Aurora-A as well as other proteins. Therefore, interpretation of direct or indirect effects would be impossible. Additionally, *MYCN*-amplified cell lines have 100 x fold higher MYCN levels and therefore siRNA and shRNA only moderately reduce MYCN levels

(Schwab et al., 2003) and due to the *MYCN*-amplification also establishing an auxin inducible degron system would be highly challenging.

5.2 Aurora-A is unphosphorylated in S phase

Aurora-A is usually in an inactive conformation until the binding of a coactivator which enables a conformational change resulting in kinase activation. The most studied coactivator for Aurora-A is TPX2, which results in a hyperactivation of Aurora-A when localized to spindle poles which can be assessed by the auto-phosphorylation of Aurora-A at T288 (Zeng et al., 2010). MYCN was identified as a protein that can activate Aurora-A which leads to its auto-phosphorylation *in vitro* (Richards et al., 2016).

By immunoblot, auto-phosphorylation of Aurora-A throughout cell cycle was investigated (Figure 4.3 b). In mitosis, there is a massive increase of auto-phosphorylated Aurora-A which is in line with published data, showing that complex formation with TPX2 at the spindle poles results in auto-phosphorylation (Zheng et al., 2010). In S phase Aurora-A is unphosphorylated which indicates that even though auto-phosphorylation of Aurora-A is visible when activated by MYCN *in vitro*, this is not observed in cells.

However, auto-phosphorylation of Aurora-A cannot predict whether the kinase is active or not but enhances the activity of the kinase two-fold (Dodson & Bayliss, 2012). Already other publication showed that in mitosis Aurora-A is additionally active on the spindle itself but is only auto-phosphorylated on T288 at the spindle poles. At the spindle, Aurora-A is kept unphosphorylated by protein phosphatase 6 (PPP6) which prevents hyper-activation of Aurora-A to ensure proper spindle assembly (Zeng et al., 2010). Therefore, the activity of Aurora-A cannot be measured only by investigating the phosphorylation status.

Additionally, it is possible that cells need unphosphorylated Aurora-A which is less active to balance kinase activity which might reflect a fine-tuning mechanism.

Collectively, the results suggest the activity of Aurora-A in a MYCN-dependent manner in S phase. To gain further insights, a systematic analysis of putative Aurora-A targets was pursued.

5.3 Investigation of MYCN-dependent Aurora-A substrates in S phase

Aurora-A substrates as well as the consensus sequence for preferred phosphorylation sites have been already studied previously (Kettenbach et al., 2011). However, no studies focused on Aurora-A substrates in S phase. Therefore, MYCN-dependent Aurora-A substrates in S phase were further investigated.

5.3.1 Aurora-A substrates in S phase

Approximately 3,200 chromatin-bound proteins were identified in S phase in a mass-spectrometry (MS) analysis (Figure 4.4 b) which is in line with publications where 3,100 proteins bound to chromatin were identified (Ginno et al., 2018). Of the chromatin-bound proteins only a very small subset changed abundance upon inhibition of Aurora-A. MYCN was one of the proteins identified showing enhanced binding to chromatin. MLH1, PPIL2, PSMC3IP, TRMT1L, and ZNF217 were also found more abundant and it is published that they are MYC interaction partners (Heidelberger et al., 2018; Kalkat et al., 2018; Koch et al., 2007). Therefore, it seems reasonable to believe that the effects are indirect due to elevated levels of MYCN on chromatin. However, elevated protein levels of MYCN were not observed in immunoblot analysis (Figure 4.4 a). This is possible, as MS analysis is more sensitive for small changes whereas immunoblot needs a more robust change to identify differences in protein amount. As the key question was the change in phosphorylated proteins, the results of the proteomic analysis and the pathways in which the proteins are involved were not further investigated.

To identify phosphorylation changes on proteins, phosphoproteomic analysis was performed under the same conditions described for proteomic analysis (Figure 4.5). The two Aurora-A inhibitors used show high correlation of the regulated phosphosites (Figure 4.5 c), although the mode of action of the inhibitors is slightly different. MK5108 is a pure catalytic inhibitor, whereas MLN8237 inhibits the catalytic activity and additionally disrupts the Aurora-A/MYCN complex, when used in higher concentrations (Gustafson et al., 2014; Brockmann et al., 2013). With MLN8237 treatment slightly more phosphosites are downregulated compared to MK5108 treatment, which is in line with publications, demonstrating that MLN8237 is the more potent inhibitor (Brockmann et al., 2013). 73 phosphosites were downregulated with both inhibitors and were therefore considered as putative Aurora-A targets in S phase (Table 7.1).

Interestingly, the proteins bearing these sites revealed enrichment in mediators of “mRNA processing” and Aurora-A has been already implicated in processes related to splicing for example in regulating alternative splicing, which results in the expression of isoforms that prevent apoptosis (Moore et al., 2010). Additionally, recent literature demonstrated that

Aurora-A localizes to nuclear speckles, where splicing occurs, and that Aurora-A can interact and phosphorylate proteins involved in splicing *in vitro*. Thereby, long-term inhibition (24 h) of Aurora-A in G1, G2, and M phase regulates alternative splicing of 505 genes (Damodaran et al., 2020). The impact of Aurora-A in S phase on the pathways mRNA processing and transcription were further investigated (see 5.4). And as the aim was to investigate MYCN-dependent Aurora-A targets, the hits were further filtered and the results which were obtained will be discussed below (see 5.3.2).

Besides the downregulated phosphosites, also upregulated phosphosites upon Aurora-A inhibition were identified. This could be indirect downstream effects when processes like transcription and mRNA processing are altered. However, those sites were not further investigated.

5.3.2 MYCN-dependent Aurora-A targets identified by MS

To identify MYCN-dependent Aurora-A substrates a MS of chromatin-bound proteins in S phase was performed upon 10058-F4 treatment. Short-term removal of MYCN from chromatin did not impair cell cycle progression (Figure 4.7 a). In the proteomic analysis 3,124 proteins were identified as chromatin-bound, which is comparable to the results obtained with Aurora-A inhibitors and literature (Ginno et al., 2018). Aurora-A was found to be less abundant bound to chromatin when MYCN was not present (Figure 4.7 b) reflecting previous results indicating that MYCN is the anchor for Aurora-A in S phase. The other family member Aurora-B does not change abundance when MYCN cannot bind chromatin, indicating that this complex formation on chromatin is Aurora-A-specific.

Additionally, a phosphoproteomic analysis was performed (Figure 4.7 c). Although the replicates display variability, 310 phosphosites could be unequivocally identified as less phosphorylated upon MYCN removal from chromatin (Figure 4.8 a). Comparing the MYCN- with the Aurora-A-dependent phosphosites in S phase revealed 8 phosphosites less phosphorylated in both conditions. This suggests that those sites are MYCN-dependent Aurora-A targets (Figure 4.8 b). The proteins on which the phosphosites were identified are ATAD2, ATRX, DEK, MAP1B, MSH6, SF3B2, SMARCAD1, and SORT1. Even though MAP1B and SORT1 show staining in the nucleus (ProteinAtlas), they have no known function there. Therefore, those two proteins were excluded in all further experiments.

ATAD2 is the only hit, where the phosphorylated residue is included in a *bona fide* Aurora-A consensus sequence (Kettenbach et al., 2011). Nevertheless, binding of MYCN could change the accessibility to the binding pocket and therefore also change the preferred phosphorylation sequence. For other kinases, it was reported that small oncogene-induced mutations can result in an increased substrate repertoire, indicating that changes in binding pockets can indeed

result in a different preference for the phosphorylation sequence (Creixell et al., 2015). Additionally, the consensus sequence is preferred by a kinase but does not exclude that other sequences can be phosphorylated as well (Sardon et al., 2010). For all these reasons, also other phosphosites could be indeed targeted by Aurora-A.

A further investigation revealed that all proteins show proximity to MYCN and Aurora-A. This was more evident for ATAD2, SF3B2, and SMARCAD1 and weaker for ATRX, DEK, and MSH6 when tested with Aurora-A. Interestingly, ATRX was reported to interact with Aurora-A directly in a reconstituted complex, corroborating the results observed in the PLA (Kamran et al., 2017). When tested with MYCN, SF3B2 and SMARCAD1 showed a high number of PLA spots, whereas ATAD2, ATRX, DEK, and MSH6 showed weaker signal. SF3B2, SMARCAD1, ATAD2, and MSH6 have been identified in several high-throughput MS analyses as interaction partner of MYC (Heidelberger et al., 2018; Ewing et al., 2007; Koch et al., 2007). SF3B2 was additionally identified in a Proximity Label MS of MYC (Kalkat et al., 2018) and the interaction with ATAD2 has been further studied by a reconstituted complex revealing that those proteins indeed interact directly (Ciró et al., 2009). The overall interaction network has been summarized in Figure 5.1.

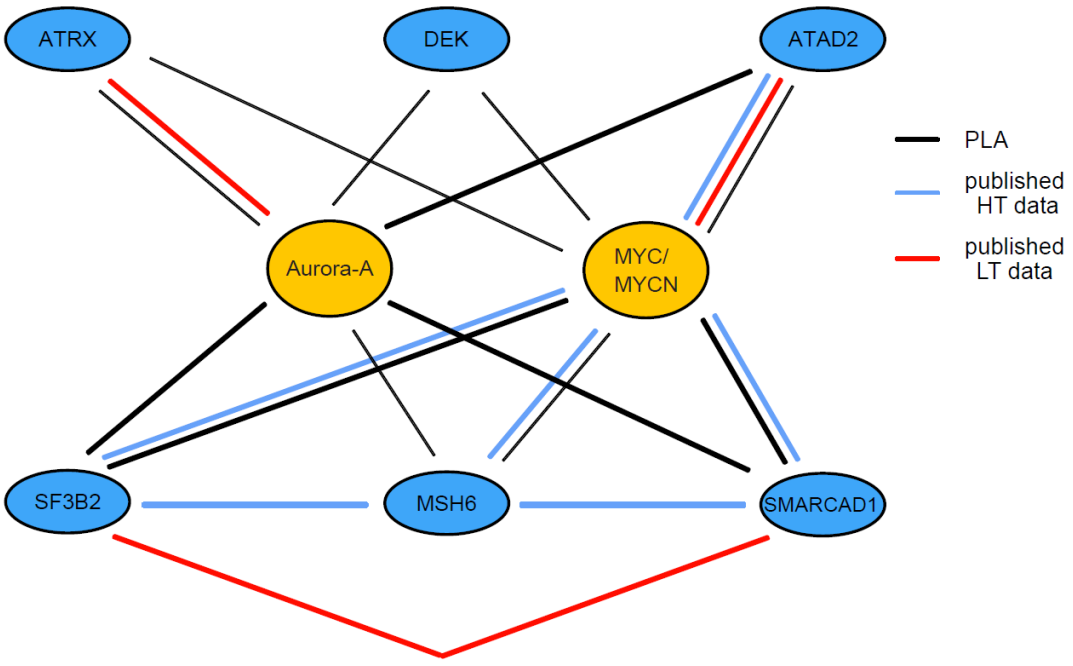

Figure 5.1:Schematic network of protein interaction with MYCN and Aurora-A.
Putative MYCN-dependent Aurora-A targets are depicted in blue. The color of the line indicates whether interaction was identified in PLA (black) high-throughput (HT; blue) or low-throughput (LT; red) data. Thickness of line indicates a lot (thick) or little (thin) PLA signal.

All proteins except for DEK have been implicated in either interacting with MYC or Aurora-A. However, most MS studies from literature have investigated MYC- and not MYCN-interacting proteins. As a kinase does not need a robust interaction with a protein to phosphorylate it, it is

also possible that those proteins would not be found in a high-throughput MS analysis. Furthermore, some of the proteins have been identified to interact with each other e.g., SMARCAD1 showed interaction with SF3B2 and MSH6 (Rowbotham et al., 2011). How the function of these proteins could be involved in the processes regulated by Aurora-A in S phase will be discussed below (see 5.4).

Peptides spanning the found phosphorylation site on ATRX, MAP1B, and MSH6 were incubated with purified Aurora-A and were assessed in an *in vitro* phosphorylation assay (data not shown here, done by Mark Richards, Richard Bayliss Lab, Faculty of Biological Sciences, University of Leeds, UK). The *in vitro* assay revealed that Aurora-A alone cannot phosphorylate indicated phosphosites. It is possible, that Aurora-A in complex with MYCN is required to phosphorylate those targets or that the phosphorylation is not a direct Aurora-A phosphorylation site. Therefore, further experiments are needed.

5.3.3 H3S10 is a MYCN-dependent Aurora-A target

Among the published Aurora-A targets is serine 10 of histone H3 (H3S10). Considering that histone tails cannot be covered by MS analysis using tryptic digest (Liigand et al., 2019), the effect of Aurora-A on pH3S10 was further investigated in small-scale experiments. The phosphorylation of H3S10 has several published roles. It is a known mark for condensed heterochromatin and thereby a marker for mitotic cells. Additionally, studies showed that pH3S10 enhances transcription and thereby marks euchromatin (reviewed in Sawicka & Seiser, 2012). One reason for this could be a difference in time during cell cycle and the kinase which phosphorylates this residue. The published function of H3S10 phosphorylation by Aurora-A is to prevent H3K9 di-methylation by G9a, a methyltransferase adding a methyl-group on this residue and thereby inactivating gene expression (Kim et al., 2016).

Interestingly, besides the published mitotic high intensity staining, pH3S10 displays a spot-like pattern in S and G2 phase (Figure 4.10 a, b). Aurora-A inhibition reduces the spot-like pattern, suggesting that Aurora-A targets pH3S10 mainly in S phase. Thereby, MK5108 showed reduced efficacy compared to MLN8237 as already discussed above.

To genetically validate this finding, a comparison between wild type (WT) and a MLN8237-resistent Aurora-A mutant (T217D) was performed. Overexpression of the mutant does not enhance Aurora-A levels compared to WT overexpression, but drastically enhances auto-phosphorylation, indicating that the mutant is much more active than Aurora-A WT (Brockmann et al., 2013). In line with this data, overexpression of Aurora-A WT results in increased pH3S10 in S phase, which is even further enhanced upon expression of Aurora-A T217D mutant. Consistently, MLN8237 treatment abolished pH3S10 signal – but not in T217D expressing cells (Figure 4.12). Further experiments with siRNA or shRNA experiments could not be

performed, because long-term treatment results in an arrest of cells in G2/M phase (Brockmann et al., 2013). Still, the available results indicate that pH3S10 is a target of Aurora-A in S phase.

Beyond Aurora-A, more than 10 kinases are known to phosphorylate H3S10, including Aurora-B (Monier et al., 2007; Crosio et al., 2002). To rule out the contribution of Aurora-B to the described phenotype, an Aurora-B inhibitor was used. Aurora-B regulates pH3S10 levels in mitosis but does not influence its level in S or G2 phase (Figure 4.13 a). This finding is in keeping with the literature were Aurora-B is reported as a mitotic kinase for pH3S10 (Crosio et al., 2002).

Importantly, the decrease of pH3S10 immunofluorescence signal was also confirmed by ChIP experiments (Figure 4.11), indicating additionally that the post-translational modification on the histone is added while on chromatin. Global pH3S10 distribution was investigated by ChIP-seq and revealed that the signal is drastically reduced globally upon Aurora-A inhibition in S phase (Roeschert et al., 2021).

Furthermore, H3S10 phosphorylation is MYCN-dependent, as assessed by the comparison of SH-EP cells which are *MYCN* non-amplified neuroblastoma cells and SH-EP cells expressing MYCN WT or a non-degradable MYCN mutant (MYCN T58A; Sjostrom et al., 2005). Upon stable expression of MYCN or MYCN T58A, the cells change their expression from MYC to MYCN (Herold et al., 2019; Figure 4.14 a). Immunofluorescence revealed that MYCN overexpression and to an even higher level MYCN T58A overexpression increased the pH3S10 signal in S phase, while Aurora-A inhibition decreased it (Figure 4.14 b).

All these finding support the idea that MYCN recruits Aurora-A to chromatin, where it gets activated and phosphorylates H3S10.

Mechanistically, this can also be mediated by the chromatin remodeler SMARCAD1 which was one of the identified MYCN-dependent Aurora-A substrates. SMARCAD1 mediates gene silencing by heterochromatin maintenance and can recruit G9a, a methyltransferase which can di-methylate H3K9 (Yu et al., 2011). This recruitment is counteracted by Aurora-A activity (Kim et al., 2016). In this perspective, the phosphorylation of the identified Aurora-A dependent SMARCAD1 site could prevent its binding to DNA, reducing G9a recruitment and further enhancing H3S10 phosphorylation (Figure 5.2). This model warrants further investigation.

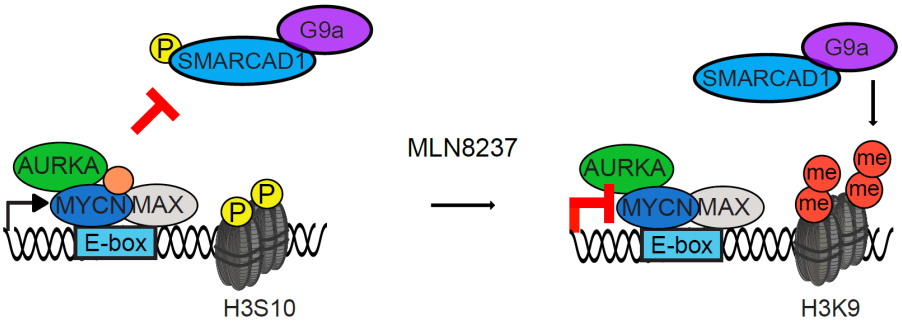

Figure 5.2: Model of Aurora-A counteracting G9a activity to prevent transcriptional repression. Aurora-A substrates are depicted in light blue.

5.4 Pathways regulated by Aurora-A in S phase

Aurora-A phosphorylates multiple substrates in S phase and many of them are involved in different pathways. As no specific function for Aurora-A in S phase is yet described processes like histone incorporation, transcription, and mRNA processing were further investigated to develop a broader understanding of Aurora-A´s function in S phase.

5.4.1 Aurora-A leads to incorporation of H3.3

As Aurora-A was identified as a kinase phosphorylating H3S10 in S phase, chromatin occupancy of H3.1 and H3.3, the two most expressed isoforms of histone H3 in neuroblastoma cells, which can both be phosphorylated on S10, was further investigated.

Upon inhibition of Aurora-A, H3.3 ChIP-seq signal decreased, whereas H3 ChIP-seq signal increased (Figure 4.15 a). Since the H3 ChIP measured H3.1 and H3.3 isoforms and the H3.3 ChIP is specific for the H3.3 isoform, it is likely that the H3.1 isoform is enriched whereas the H3.3 isoform is reduced upon inhibition of Aurora-A. Interestingly, the effect is more pronounced on genes with higher MYCN occupancy (Figure 4.15 b compared to c).

Those results support the hypothesis that Aurora-A facilitates the incorporation of H3.3. H3.3 is considered as a flexible histone, indicating that the DNA is easier accessible. This could also promote transcription.

Different proteins account for the incorporation of those histone isoforms. Scaffolding chaperons like HIRA have been identified in specifically incorporating H3.3 into promoters and gene bodies of actively transcribed genes as well as regulatory elements (Ray-Gallet et al., 2011; Goldberg et al., 2010). The DAXX-ATRX complex was also identified as a H3.3-specific incorporation complex. However, compared to HIRA, the incorporation of H3.3 by DAXX-ATRX is specific to telomeric regions and pericentric heterochromatin (Lewis et al., 2010). The incorporation does not require replication and is associated with flexible exchange on highly transcribed genes. H3.1 instead is considered as the “canonical” H3 histone, which is incorporated during replication and cannot be flexibly exchanged (Tagami et al., 2004).

Since Aurora-A is not known to bind to DNA nor to histones, it is likely that a substrate of Aurora-A is required for the incorporation. One of the proteins identified as MYCN-dependent Aurora-A target is DEK. DEK is known to regulate the pool of free and nucleosomal H3.3 in a cell (Ivanauskiene et al., 2014; Sawatsubashi et al., 2010). Knock-out of DEK has been implicated in enhanced, uncontrolled loading of H3.3 by HIRA as well as by the DAXX-ATRX complex, resulting in fragile telomers. Therefore, DEK is considered as a safeguard in regulating amount and incorporation of H3.3 (Ivanauskiene et al., 2014). This suggests that Aurora-A phosphorylates DEK in S phase to regulate the amount of free H3.3, which can be incorporated by specific histone chaperons (Figure 5.3).

The two MYCN-dependent Aurora-A substrates ATRX and ATAD2 have been identified as histone chaperons. ATRX is a known H3.3 chaperone, but also ATAD2 was identified as a histone chaperone for H3/H4 heterodimers (Cho et al., 2019). However, the preferred isoforms for H3 or H4 were not further investigated. Therefore, phosphorylation of MYCN-activated Aurora-A on ATAD2 or ATRX could contribute to the deposition of H3.3 to DNA (Figure 5.3). All these hypotheses need further investigation.

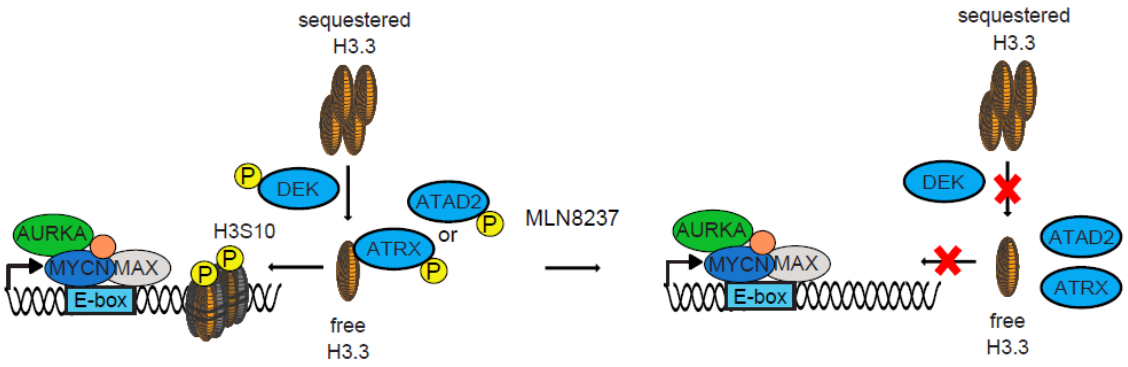

Figure 5.3: Contribution of MYCN-activated Aurora-A substrates in H3.3 incorporation.
Substrates are shown in light blue.

Besides this, ATRX is also a protein often found mutated in neuroblastoma (Cheung et al., 2012). ATRX mutations almost-always lead to a truncation of the protein associated with loss of function. Additionally, it was identified that ATRX mutations are mutually exclusive with *MYCN*-amplification (Zeineldin et al., 2020), indicating a specific role for unperturbed ATRX function upon high levels of MYCN.

ATRX positions H3.3 to prevent the formation of G-quadruplex (G4) structures, known to interfere with transcription and replication (Clynes et al., 2013; Clynes & Gibbons, 2013). This function of ATRX is specifically well reported at telomeres, which are associated with high G4 density (Clynes et al., 2015). However, G4 structures are also often found in promoters of genes (Marsico et al., 2019). When transcription is enhanced by MYCN overexpression, it is important to prevent the formation of those structures with could otherwise lead to problems during transcription and replication. Therefore, the relevance of ATRX function upon *MYCN*-amplification could very well fit to the model, that ATRX is a histone chaperone required to deposit H3.3 into DNA after MYCN-dependent transcription.

5.4.2 Aurora-A inhibition impairs RNAPII function

Another process in which some of the putative Aurora-A targets are involved is transcription. Therefore, the influence of Aurora-A on the behavior of RNAPII in S phase was investigated. To determine whether transcription is impacted a ChIP-seq of total RNAPII and elongating

RNAPII (RNAPII pSer2) upon Aurora-A inhibition was performed (Figure 4.16 and Figure 4.17). Intriguingly, treatment with MLN8237 or MK5108 yielded slightly different results. MLN8237 induced a reduction of RNAPII occupancy throughout the gene body, whereas MK5108 increased the occupancy of RNAPII at the TSS and showed the comparable amount throughout the gene body as the DMSO control. Importantly, both inhibitors resulted in a slower transcription of RNAPII, indicated by the travelling ratio. H3S10 phosphorylation has been implicated to promote pause-release of RNAPII (Jonkers & Lis, 2015; Ivaldi et al., 2007), suggesting that the dynamics of phosphorylation of H3S10 by Aurora-A is linked to ongoing transcription.

Aurora-A inhibition induced a re-distribution also of elongating RNAPII, with an increased occupancy both at the TSS and throughout the gene body, indicating that elongating RNAPII is stalling or slowing down. The accumulation at the TSS, correlates with a broad zone around the first nucleosome, where the biggest effect is observed (Figure 4.17 c).

However, the TSS as well as the pause site, the first nucleosome, and the exon-intron boundary are in proximity to each other, making distinction complicated (Cossa et al., 2020). Since phosphorylated RNAPII was analyzed it is rather unlikely that the accumulation occurs at the TSS. Additionally, the phosphorylation of RNAPII indicates that CDK9 is active ruling out stalling at the pause site (Jonkers et al., 2014). Since there were effects on histone incorporation as well as splicing observed it is also possible that the stalling or accumulation of RNAPII occurs at the exon-intron boundary. However, the effects on global histone incorporation were stronger than on global splicing and therefore it is reasonable to suggest that the stalling occurs at the first nucleosome.

Furthermore, those effects were stratified by MYCN occupancy at the promoters. This analysis revealed that on highly MYCN-bound genes the levels of RNAPII pSer2 increased and consecutively the stalling effect is more pronounced. On genes with low MYCN occupancy, there is no effect in RNAPII pSer2 signal. This is not surprising, as promoters bound by MYC are also co-occupied by RNAPII and the genes are considered as highly transcribed (Walz et al., 2014).

5.4.3 Aurora-A impacts RNA processing in S phase

To investigate the impact of Aurora-A on gene expression in S phase, RNA-seq was performed. Short-term treatment with Aurora-A inhibitor in S phase results in minor changes in gene expression (Figure 4.18). RNA-seq measures the steady state level of mRNA expression. Therefore, it is possible, that Aurora-A either does not influence expression of genes or that the timepoint chosen was too short to investigate changes. mRNAs have a half-life between 10 min and several hours (Shyu et al., 1989). Another information which can be

derived from RNA-seq data is whether alternative splicing occurs. Long-term inhibition of Aurora-A has been implicated in regulating alternative splicing of proteins involved in apoptosis (Moore et al., 2010). However, upon short-term Aurora-A inhibition no major changes in alternative splicing occurred (data not shown).

Among the most affected phosphosites upon Aurora-A inhibition are several proteins involved in RNA processing. Therefore, splicing activity upon Aurora-A inhibition was assessed.

The SF3B1 protein is hyper-phosphorylated during assembly of the active spliceosome and phosphorylated SF3B1 is a marker for active splicing (Girard et al., 2012). Interestingly, Aurora-A inhibition reduced SF3B1 phosphorylation by 50% in S phase (Figure 4.19). Other cell cycle phases showed no change or a slight increase in spliceosome assembly upon Aurora-A inhibition. To further elucidate whether spliceosome assembly is also functionally connected to less spliced mRNA, nascent RNA was investigated upon Aurora-A inhibition. The positive control PlaB showed the expected results, as splicing cannot occur and the PlaB-treated cells mimic the pulse sample, which was also already previously described (Cossa et al., 2020). Aurora-A inhibition results in a decrease of spliced and exonic reads and an increase in intronic reads compared to the control. However, the result on global splicing was not as strong as suggested by the results of phosphorylated SF3B1. Therefore, it is likely that Aurora-A does not regulate all spliceosomes, indicating that not all genes are affected similarly.

So far, no stratification of genes which are most affected by Aurora-A inhibition was determined. One possibility is that gene length plays a role whether or not the genes are affected. Another option is that the gene function determines if the gene is still transcribed in S phase and therefore affected by Aurora-A inhibition. It has been shown that in S phase two main groups of genes are transcribed. The first group of genes is involved in DNA damage response and the second group is required for progression of S phase (Meryet-Figuiere et al., 2014). DNA damage genes are known to be long genes that have more exons and could be therefore differently affected by Aurora-A inhibition (Krajewska et al., 2019). Besides this, the longest genes have been shown to be transcribed throughout a whole cell cycle and harbor hots spots of DNA breaks called common fragile sites, often associated with transcription-replication conflicts and R-loop formation (Helmrich et al., 2011). So, stratification could indeed reveal which genes are less spliced upon Aurora-A inhibition.

Splicing and transcription are processes which are coupled in a cell and splicing factors are also known to directly interact with RNAPII (Lin et al., 2008). The majority of genes are at least partially spliced already during transcription (Merkhofer et al., 2014). The two processes regulate each other, as it is known that inhibition of transcription affects splicing but also that impairment of splicing results in stalling of RNAPII at the first exon-intron boundary (Cossa et al., 2020; Saldi et al., 2016). Additionally, knock-down of splicing factors results in reduced

transcription (Lin et al., 2008). Therefore, on the one hand Aurora-A´s impact on transcription elongation indirectly accounts for the effects which were observed in splicing or on the other hand it is also possible that Aurora-A directly regulates splicing. The latter possibility would be supported by the observation that SF3B2 and DEK, two factors which were identified as MYCN-dependent Aurora-A targets additionally have a strong implication to splicing.

DEK is known to interact with components of the spliceosome and is required for the proper 3´splice site choice (Kress & Guthrie, 2006). DEK could also regulate the observed phenotypes in splicing. However, this is unlikely, as DEK has no role in spliceosome assembly, which is disturbed upon inhibition of Aurora-A.

SF3B2 is part of the U2 spliceosomal subunit (Brosi et al., 1993) which is required for branch point binding, assembly facilitation, and spliceosome activation (Sun, 2020). Recent work showed that mutations in splicing factors result in stalled RNAPII and lead to the formation of R-loops which as a consequence can activate ATR (Chen et al., 2018; Nguyen et al., 2018). Knockdown of SF3B2 results in the activation of ATR more prominent than ATM (Figure 4.25). Therefore, it is possible that MYCN-activated Aurora-A phosphorylates SF3B2 which results in proper splicing and prevents stalling of RNAPII and R-loop formation. Therefore, unphosphorylated SF3B2 could activate ATR. Indeed, inhibition of splicing using PlaB results in stalling of RNAPII (Kindgren et al., 2019) as well as in increased R-loop formation (Roeschert et al., 2021; Cossa et al., 2020). Whether these events could depend on SF3B2 will be subject of further analyses (Figure 5.4).

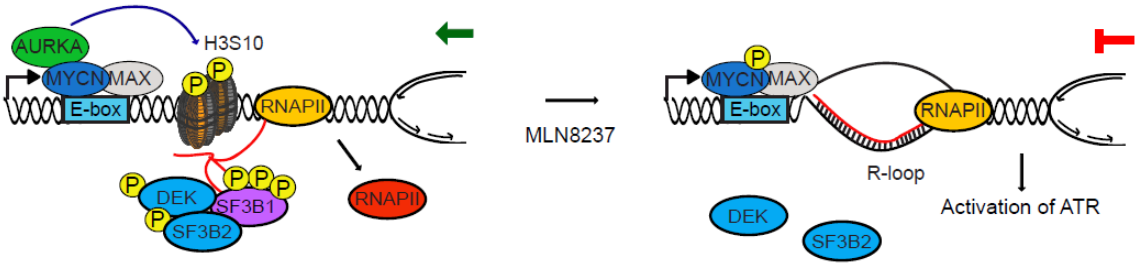

Figure 5.4: Contribution of MYCN-activated Aurora-A substrates in splicing.
Substrates are shown in light blue.

Besides the two putative targets of Aurora-A, Aurora-A itself can co-localize to nuclear speckles, where splicing occurs. And several other factors like SRSF1, SRSF3, and SRSF7 which are also involved in splicing have been recently identified as Aurora-A targets *in vitro* (Damodaran et al., 2020). Phosphosites of those proteins were also identified less phosphorylated upon Aurora-A inhibition however not significantly downregulated with both inhibitors (data not shown). A related protein SRSF5 was identified significantly less phosphorylated with both Aurora-A inhibitors (Table 7.1). Therefore, it is also possible that

Aurora-A directly regulates splicing, which as consequence indirectly affects transcription elongation.
Whether the effect of Aurora-A on splicing in S phase is direct or indirect remains elusive and needs to be further investigated.

5.4.4 Aurora-A prevents transcription-replication conflicts

Our previous work suggested that Aurora-A is involved in the establishment of transcription-replication conflicts (Büchel et al., 2017). To prove this hypothesis, a PLA between PCNA and total RNAPII, two major members of the replication and transcription machinery, respectively was performed to investigate the occurrence of transcription-replication conflicts (Okamoto et al., 2019). To ensure specificity, a technical control for this assay was conducted using only single antibodies and this did not result in a measurable signal, indicating that the assay is trustable.
Catalytic inhibition of Aurora-A using low doses of MLN8237 or MK5108 results in a 1.5-fold increase in transcription-replication conflicts. Increasing MLN8237 concentrations (i.e., which also leads to the disruption of the Aurora-A/MYCN complex) enhances the number of transcription-replication conflicts, indicating that catalytic activity of Aurora-A is only partially required for those conflicts. This is in line with the observation that the Aurora-A/MYCN complex is required to recruit de-capping factors, leading to transcription termination (Roeschert et al., 2021). Therefore, it is reasonable to suggest that disruption of the complex formation enhances stalling of RNAPII which results in increased transcription-replication conflicts.
As an internal control to show that transcription-replication conflicts need transcription to occur two different CDK9 inhibitors were used. Flavopiridol which leads to a stalling of RNAPII on nearly all genes (Chao & Price, 2001), as well as the more specific CDK9 inhibitor NVP-2 (Olson et al., 2018), result in a decreased number of transcription-replication conflicts. The data indicate that active transcription is required to form those conflicts and that stalling of RNAPII per se does not result in transcription-replication conflicts. However, it is also possible that it is a stochiometric principle, since stalling of RNAPII upon inhibitor treatment, reduces levels of RNAPII compared to unperturbed cells, the chance of a replication fork to collide with a stalled RNAPII decreases. As seen with CRISPR knock-out of CDK9 results in stalling of RNAPII and additionally prevents re-initiation of RNAPII, resulting in less RNAPII on chromatin (Shao & Zeitlinger, 2017). This assay is therefore not able to clearly state whether active transcription is needed to induce transcription-replication conflicts or not.
Recent work showed, that when the replication machinery is stalled, PCNA gets ubiquitinated followed by its removal from chromatin by ATAD5 to initiate replication restart (Park et al., 2019). The kinetics of this process remains to be elucidated. However, this can indicate that

the transcription-replication conflicts measured by PCNA with RNAPII underestimate the number of conflicts that in fact occur. Since the attempt of solving the problem leads to the removal of PCNA. One way of investigating this further, could be to perform the PLA between other subunits of the replication machinery like RAD9 or RAD1 and RNAPII (Delacroix et al., 2007).

Besides the observation of transcription-replication conflicts, Aurora-A inhibition also results in the activation of ATR (Büchel et al., 2017; see 5.3.5) and the formation of R-loops (Roeschert et al., 2021). Therefore, it is likely that the conflicts that occur are head-on collisions and not co-transcriptional conflicts (Hamperl et al., 2017).

5.4.5 Aurora-A inhibition induces ATR activation

It was already published that inhibition of Aurora-A induced ATR activation (Büchel et al., 2017), but the underlying mechanisms remained elusive. Interestingly, ATR gets activated in S phase only upon the addition of large amounts of Aurora-A inhibitor (Figure 4.21). As it is known that low doses of MLN8237 are required to inhibit catalytic activity, whereas higher doses are needed to disrupt the Aurora-A/MYCN complex (Brockmann et al., 2013), it is likely that disruption of the Aurora-A/MYCN complex is required for the enhanced activation of ATR. The function of ATR is to sense stressed and stalled replication forks (Saldivar et al., 2017). Stalling of the replication fork can occur due to conflicts between transcription and replication (Hamperl et al., 2017). Aurora-A inhibition induces transcription-replication conflicts (see 5.3.4) and the number of conflicts increases using higher amounts of Aurora-A inhibitors which result in disruption of the Aurora-A/MYCN complex.

Additionally, the requirement of high concentrations of Aurora-A inhibitor to activate ATR can be explained by the basal activity of ATR in S phase, which is needed to quickly resolve problems during replication that can occur mainly at common fragile sites (Casper et al., 2002). Therefore, some stalled replication forks can easily be repaired by the already active ATR kinases without resulting in measurable differences in ATR downstream targets (Cortez et al., 2001). Only if the stalled replication forks exceed the capable number for already active ATR kinases the difference is measurable. Therefore, it is likely that the effect is underestimated. As Aurora-A/MYCN complex disruption also results in reduced fork progression, this could explain why ATR activation is especially pronounced under these conditions (Roeschert et al., 2021).

Additionally, two MYCN-dependent Aurora-A substrates ATAD2 and ATRX, have both been shown to regulate replication. ATAD2 localizes to nascent DNA and is required for PCNA loading (Koo et al., 2016). ATRX is involved in NHEJ as well as HR and prevents DNA damage accompanied by replication fork progression (George et al., 2020; Huh et al., 2016;

Koschmann et al., 2016). Therefore, phosphorylation of ATAD2 or ATRX could regulate the coordination of replication with transcription. And if the two proteins cannot be phosphorylated this could enhance the stalling of replication forks which result in ATR activation (Figure 5.5). Also, these hypotheses require further accurate analysis.

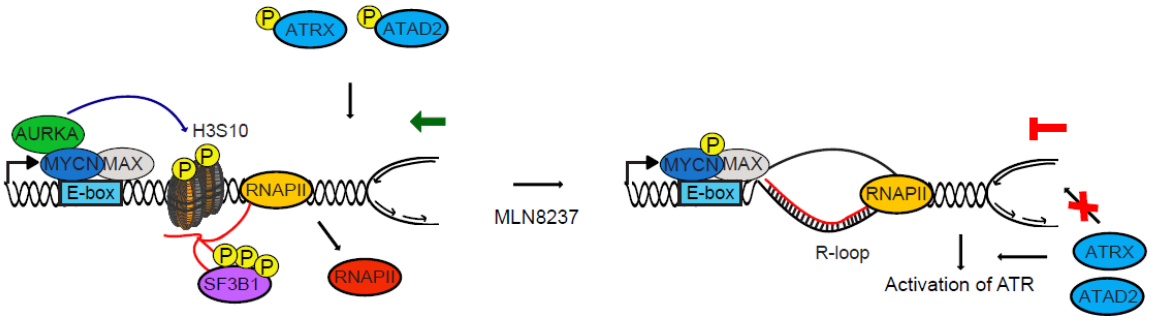

Figure 5.5: Contribution of MYCN-activated Aurora-A substrates in replication fork progression and transcription-replication conflicts.
Substrates are shown in light blue.

5.4.6 Summary of processes regulated by Aurora-A in S phase

All pathways regulated by Aurora-A in S phase are summarized in the model shown in Figure 5.6. As the Aurora-A inhibitor MLN8237 can interfere with catalytic activity as well as with complex formation of the Aurora-A/MYCN complex when used in higher amounts, the processes which require catalytic activity or complex formation are summarized in Table 5.1.

Aurora-A phosphorylates H3S10 in S phase. The incorporation of H3.3 counteracts the R-loop formation and co-transcriptional splicing can occur. Therefore, transcription can get terminated before colliding with a replication fork, preventing transcription-replication conflicts. If Aurora-A is inhibited, H3S10 cannot be phosphorylated and H3.3 cannot get incorporated. Therefore, a promoter-proximal R-loop is forming which also results in stalling of RNAPII. As transcription cannot get terminated before collision with a replication fork this leads to head-on collisions of the transcription- and replication machinery, measurable as transcription-replication conflicts. These conflicts are co-occurring with replication fork stalling which results in activation of ATR.

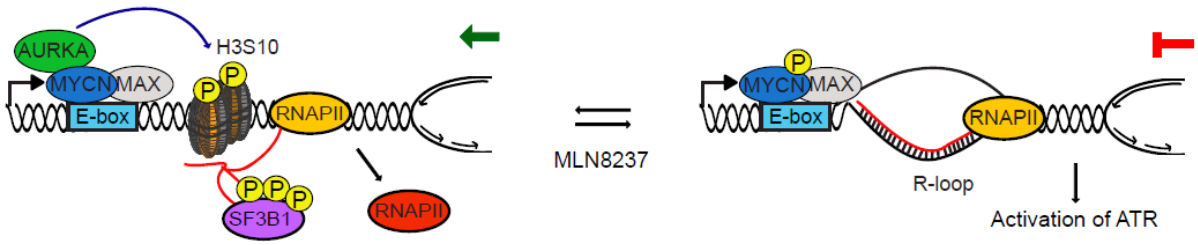

Figure 5.6: Model of pathways regulated by Aurora-A in S phase.
Parts of this Figure were published in similar form in Roeschert et al., 2021.

Not all effects observed are only relying on the catalytic activity of Aurora-A. Low doses of MLN8237 result in catalytic inhibition of Aurora-A, whereas high doses of MLN8237 leads to a disruption of the Aurora-A/MYCN complex (Brockmann et al., 2013). Therefore, those two scenarios can be distinguished and the results for Aurora-A's function in S phase are summarized (Table 5.1). Catalytic activity of Aurora-A is required for phosphorylation of H3S10 in S phase. High-throughput data were only performed with high doses of Aurora-A inhibitors, therefore no statements on the requirement of the catalytic activity of Aurora-A on H3.3 incorporation, RNAPII stalling, and splicing can be made. Transcription-replication conflicts can be observed already when catalytic activity is inhibited and increase when the complex formation is impaired. One reason for this could be that the recruitment of de-capping factors requires intact formation of the Aurora-A/MYCN complex (Roeschert et al., 2021). Therefore, it is likely that RNAPII stalling occurs already when catalytic activity is impaired and increases further when complex formation is disrupted. ATR activation depends on complex disruption which is in line with the enhanced transcription-replication conflicts observed under these conditions.

Table 5.1: Summary of processes regulated by Aurora-A and whether catalytic activity or complex disruption is required. The symbol indicates whether the process was not analyzed (?), showed no phenotype (-), showed a phenotype (+), or showed an enhanced phenotype as (++).

Process	Catalytic activity	Aurora-A/MYCN complex disruption
pH3S10	+	+
H3.3 incorporation	?	+
Stalling of RNAPII	?	+
Splicing	?	+
Transcription-replication conflicts	+	++
Recruitment of de-capping factors	-	+
ATR activation	-	+

5.5 RNase H1 overexpression does not rescue Aurora-A inhibition

Aurora-A prevents head-on collisions of RNAPII and the replication machinery and interfering with Aurora-A using siRNA as well as inhibitors results in an accumulation of R-loops at actively transcribed genes (Roeschert et al., 2021). R-loops are RNA/DNA hybrids that can be “unscheduled” which are potential genomic threats when not resolved or “regulatory” which influence gene expression, transcription termination, DNA repair, and repair of short telomers (Niehrs & Luke, 2020). R-loops can be resolved by helicases like SETX, DHX9, AQR, BLM (reviewed in Crossley et al., 2019), or nucleases like RNase H1 that specifically degrades the RNA in this hybrid (Nowotny et al., 2008).

Interestingly, expression of an inducible RNase H1 construct indicated that resolved R-loops in S phase result in an increased incorporation of the histone H3.3, as measured by ChIP-seq (Figure 4.22 c). Furthermore, ChIP-seqs of total RNAPII and RNAPII pSer2 revealed that overexpression of RNase H1 results in the accumulation of total RNAPII as well as of RNAPII pSer2 (Figure 4.23 a, c). While Aurora-A inhibition results in stalling of elongating RNAPII, overexpression of RNase H1 mainly leads to accumulation of unphosphorylated RNAPII. Therefore, the stalling upon R-loop removal occurs at the TSS, pause-site, exon-intron boundary, or as suggested at the first nucleosome, as all those elements are in proximity to each other (Cossa et al., 2020).

Aurora-A promotes, whereas R-loops counteract the deposition of H3.3. However, stabilization of the first nucleosome can lead to stalling of RNAPII. In this view, Aurora-A can balance these processes and its regulation has to be finely controlled. This could also explain why Aurora-A is not phosphorylated in S phase (Figure 5.7).

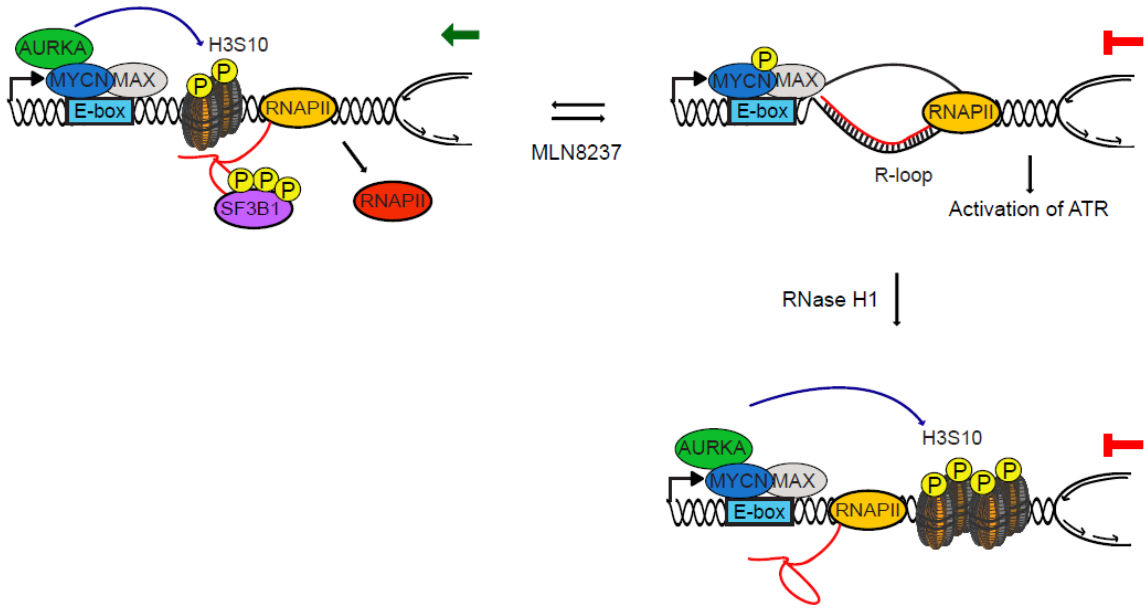

Figure 5.7: Model how resolved R-loops interfere with pathways regulated by Aurora-A in S phase.

Additionally, overexpression of RNase H1 has no impact on the formation of transcription-replication conflicts (Figure 4.23 d). Therefore, R-loops which can be removed by RNase H1 do not result in transcription-replication conflicts. Since RNase H1 does not remove all R-loop structures it is possible that the helicases like SETX play a role in this process. SUMOylated SETX can interact with the exosome facilitating the termination of nascent transcripts (Richard et al., 2013). Additionally, recent data suggested that SETX is recruited by BRCA1 to DNA, where the complex is required to resolve R-loop mediated DNA damage. This indicates a regulatory function of SETX in transcription termination (Hatchi et al., 2015). To fully exclude that R-loops play a role in transcription-replication conflicts, SETX and the other helicases would need to be tested.

Considering that the combinatorial treatment results in an increase of apoptotic cells, the dependence of the phenotype on R-loops was assessed (Figure 4.29 a). RNase H1 overexpression did not result in a decreased amount of apoptosis. Therefore, R-loops seem not to be the driving force for cells to undergo apoptosis. Additionally, no change in cell cycle speed or arrest was observed upon induction of R-loops, indicating that R-loop formation resolved by RNase H1 does also not change cell cycle speed (Figure 4.29 b).

5.6 Improved therapeutic options for *MYCN*-amplified neuroblastoma

Aurora-A was originally found in a synthetic lethality screen of *MYCN*-amplified neuroblastoma, where it is required to maintain MYCN levels (Otto et al., 2009), indicating a critical role for Aurora-A in neuroblastoma. Treatment of neuroblastoma in mice with MLN8237 showed reduced tumor growth and an increase in overall survival (Brockmann et al., 2013). However, due to the dose-limiting toxicity the treatment had massive side-effects. Therefore, an improved therapy using synergistic drugs would be beneficial, as side-effects and drug toxicity could be reduced.

5.6.1 Combined Aurora-A and ATR inhibition

As Aurora-A inhibition results in transcription-replication conflicts which activate the kinase ATR, *MYCN*-amplified neuroblastoma cells were treated with Aurora-A and ATR inhibitors (Figure 4.26). This treatment resulted in a decreased cell number and correlated both to G2/M phase arrest and apoptosis potentiation upon combinatorial treatment.

The apoptosis assay was performed in three *MYCN* non-amplified and three *MYCN*-amplified cell lines, revealing that the observed apoptosis upon Aurora-A and combinatorial inhibition is MYCN-specific (Figure 4.27 a). Consistently, synergism (according to the Bliss method) between Aurora-A and ATR inhibitor could only be seen in *MYCN*-amplified neuroblastoma cell lines (Table 7.2). This was verified with another Aurora-A inhibitor, MK5108 (Figure 4.27 b). The combination of MK5108 with AZD6738 also significantly increased the number of apoptotic cells, revealing that both Aurora-A inhibitors together with ATR inhibitor resulted in synergism in *MYCN*-amplified neuroblastoma. To further validate that this effect is Aurora-A-specific, genetic validation experiments were performed (Figure 4.27 d). Aurora-A WT overexpression resulted in decreased apoptosis upon Aurora-A inhibition, while Aurora-A T217D mutant was resistant to MLN8237-treatment (Brockmann et al., 2013). Therefore, inhibition with MLN8237 did not show any apoptosis and only a slight increase in apoptosis upon combinatorial treatment. However, this slight increase does not reflect synergism.

To further validate that this effect is ATR-dependent, CHK1 (a downstream target of ATR) was inhibited (Liu et al., 2000). CHK1 inhibition resulted in an increased apoptosis after 48 h. The combinatorial inhibition after 24 h resulted in a synergistic increase in apoptosis. After 48 h no synergism was observed, which is possible due to the high amounts of apoptosis in the single agent treatment. To verify that this is a synergistic effect more experiments with different concentration of both inhibitors would be needed. As for 24 h a slightly synergistic effect could be observed it is likely that with optimization the two inhibitors show synergism.

Together, the results indicate that the combination of Aurora-A and ATR inhibitor, showed synergism in *MYCN*-amplified neuroblastoma cells. This synergism is Aurora-A- and ATR-

specific, as different inhibitors, genetic interference, and downstream targets revealed similar results. However, the molecular mechanism for the apoptosis induction remains unclear. It is conceivable that cells accumulate damage during S phase, due to the transcription-replication conflicts, which are usually repaired by the function of ATR. It is possible, that if both proteins cannot fulfill their jobs, this can induce pro-apoptotic proteins which result in the increased apoptosis observed.

This indicates that indeed this combination enables a therapeutic window. As shown in Roeschert et al. (2021), the combinatorial therapy results in a decreased tumor burden and a prolonged survival of all treated mice. Additionally, 25% of the mice were cured from neuroblastoma.

5.6.2 Combined Aurora-A and PARP1 inhibition

Similarly to ATR, PARP1 is activated at stalled replication forks to stabilize them in response to replication stress (Ronson et al., 2018). PARP1 is active during S phase and interacts with the replication machinery (Dantzer et al., 1998). To investigate whether PARP1 and ATR have similar functions also in addition to Aurora-A inhibition the effect of PARP1 inhibition on *MYCN*-amplified neuroblastoma cells was further assessed.

Like MLN8237 (Figure 4.27), the PARP1 inhibitor Olaparib results in an increased number of transcription-replication conflicts (Figure 4.30 a). As PARP1 is implicated in regulating transcription as well as replication, it is not surprising that inhibition of this protein may result in unregulated transcription and replication which leads to the formation of such conflicts (Kraus & Lis, 2003).

As a next step the effect of combinatorial inhibition of PARP1 and Aurora-A on apoptosis of *MYCN*-amplified neuroblastoma cells was investigated (Figure 4.30 b). Even though there is no synergistic effect in this experiment (Table 7.2), treatment for 48 h increases apoptosis for all single agents, which is in line with literature (King et al., 2020) and even more cells undergo apoptosis when treated with both inhibitors. To clearly investigate synergism, both inhibitors need to be tested with various concentrations.

The combination was also tested in TH-MYCN mice and revealed a decrease in tumor growth and increased number of apoptotic cells (Roeschert et al., 2021). This indicated that also combinatorial inhibition of Aurora-A and PARP1 could constitute a therapeutic window for *MYCN*-amplified neuroblastoma.

PARP1 inhibitors are already in clinical trials for several types of cancer, including prostate, pancreatic, and breast cancer (reviewed in Slade, 2020). PARP1 inhibition is especially beneficial in cancers with elevated replication stress as seen for cancer types with mutated proteins in DNA repair pathways (e.g., *BRCA1* or *BRCA2*). As Aurora-A leads to increased

replication stress, which synergizes with PARP1 inhibition, this is in line with published data that it enables benefits for tumor therapy (Pillay et al., 2019).

5.6.3 Clinical relevance of findings on therapy of neuroblastoma patients

So far, the standard of care therapy for neuroblastoma is chemotherapy using a mix of several chemotherapeutics (American Cancer Society). Targeted cancer therapy could be beneficial for patients for the following reasons:

First, there is genomic evidence that targeting Aurora-A could be beneficial for tumor treatment since overexpression of Aurora-A correlates with a poor prognosis of neuroblastoma patients (Shang et al., 2009). Thus, elevated Aurora-A levels contribute to several non-mitotic roles of the kinase not observed under physiological conditions (Pugacheva et al., 2007). This would indicate that targeting non-physiological functions of Aurora-A could reduce the off-target effects for non-cancer cells.

Second, Aurora-A was identified in a synthetic lethality screen for *MYCN*-amplified tumors (Otto et al., 2009), indicating that Aurora-A is especially important for the survival of *MYCN*-amplified cells. As MYCN is even in children usually not expressed in most tissues (Knoepfler et al., 2002), this is an additional hint that mainly cancer cells would be affected by the treatment.

Third, the side-effects for chemotherapy are enormous (American Cancer Society). Especially, fast proliferating cells are targeted by chemotherapy like immune cells. Besides this fact, neuroblastoma patients are very young and most of their stem cells from different origins are proliferating in order to organize organ or body growth (Williams et al., 2006). Besides the side-effects in targeting also other fast proliferating cells, it is also very well reported that chemotherapy is able to induce new mutations which could further lead to other types of cancer or malignancies (Fruman & O'Brien, 2017).

Fourth, using a synergistic approach enables the reduction of amount of inhibitor used to a degree, where side-effects from single agent treatment is minimized (Roeschert et al., 2021).

Fifth, the combinatorial treatment resulted in an arrest of cells in G2/M phase. Problems during replication can accumulate mutations which lead to chromosomal instability. Chromosomal instability as well as the ability to exit mitosis can result in massive chromosome rearrangements which lead to genomic complexity of a tumor (Umbreit et al., 2020). Thus, the arrest of cells in G2/M phase is beneficial since chromosome instability cannot result in heterogeneity of tumors which enable tolerance to anti-cancer treatments.

Therefore, targeted therapy for neuroblastoma patients using Aurora-A and ATR or PARP1 inhibitors is a valuable new approach which could be beneficial for patients.

6 Bibliography

Abid Ali, F., Douglas, M. E., Locke, J., Pye, V. E., Nans, A., Diffley, J. F. X., & Costa, A. (2017). Cryo-EM structure of a licensed DNA replication origin. *Nat Commun, 8*(1), 2241. doi:10.1038/s41467-017-02389-0

Adhikari, B., Bozilovic, J., Diebold, M., Schwarz, J. D., Hofstetter, J., Schroder, M., . . . Wolf, E. (2020). PROTAC-mediated degradation reveals a non-catalytic function of AURORA-A kinase. *Nat Chem Biol*. doi:10.1038/s41589-020-00652-y

Akhtar, M. S., Heidemann, M., Tietjen, J. R., Zhang, D. W., Chapman, R. D., Eick, D., & Ansari, A. Z. (2009). TFIIH kinase places bivalent marks on the carboxy-terminal domain of RNA polymerase II. *Mol Cell, 34*(3), 387-393. doi:10.1016/j.molcel.2009.04.016

Alfieri, C., Zhang, S., & Barford, D. (2017). Visualizing the complex functions and mechanisms of the anaphase promoting complex/cyclosome (APC/C). *Open Biol, 7*(11). doi:10.1098/rsob.170204

American Cancer Society: URL: http//www.cancer.org/ : (01.12.2020)

American Cancer Society (2014): Special Section: Cancer in Children & Adolescents. Cancer Facts & Figures 2014, pp 25-42.

Amin, M., Minton, S. E., LoRusso, P. M., Krishnamurthi, S. S., Pickett, C. A., Lunceford, J., . . . Lockhart, A. C. (2016). A phase I study of MK-5108, an oral aurora a kinase inhibitor, administered both as monotherapy and in combination with docetaxel, in patients with advanced or refractory solid tumors. *Invest New Drugs, 34*(1), 84-95. doi:10.1007/s10637-015-0306-7

Arnold, H. K., & Sears, R. C. (2006). Protein phosphatase 2A regulatory subunit B56alpha associates with c-myc and negatively regulates c-myc accumulation. *Mol Cell Biol, 26*(7), 2832-2844. doi:10.1128/MCB.26.7.2832-2844.2006

Asghar, U., Witkiewicz, A. K., Turner, N. C., & Knudsen, E. S. (2015). The history and future of targeting cyclin-dependent kinases in cancer therapy. *Nat Rev Drug Discov, 14*(2), 130-146. doi:10.1038/nrd4504

Atchley, W. R., & Fitch, W. M. (1995). Myc and Max: molecular evolution of a family of proto-oncogene products and their dimerization partner. *Proc Natl Acad Sci U S A, 92*(22), 10217-10221. doi:10.1073/pnas.92.22.10217

Aygun, O., Svejstrup, J., & Liu, Y. (2008). A RECQ5-RNA polymerase II association identified by targeted proteomic analysis of human chromatin. *Proc Natl Acad Sci U S A, 105*(25), 8580-8584. doi:10.1073/pnas.0804424105

Bachetti, T., Di Paolo, D., Di Lascio, S., Mirisola, V., Brignole, C., Bellotti, M., . . . Perri, P. (2010). PHOX2B-mediated regulation of ALK expression: in vitro identification of a functional relationship between two genes involved in neuroblastoma. *PLoS One, 5*(10). doi:10.1371/journal.pone.0013108

Baluapuri, A., Wolf, E., & Eilers, M. (2020). Target gene-independent functions of MYC oncoproteins. *Nat Rev Mol Cell Biol, 21*(5), 255-267. doi:10.1038/s41580-020-0215-2

Bannister, A. J., & Kouzarides, T. (2011). Regulation of chromatin by histone modifications. *Cell Res, 21*(3), 381-395. doi:10.1038/cr.2011.22

Barr, P. M., Li, H., Spier, C., Mahadevan, D., LeBlanc, M., Ul Haq, M., . . . Friedberg, J. W. (2015). Phase II Intergroup Trial of Alisertib in Relapsed and Refractory Peripheral T-Cell Lymphoma and Transformed Mycosis Fungoides: SWOG 1108. *J Clin Oncol, 33*(21), 2399-2404. doi:10.1200/JCO.2014.60.6327

Batty, P., & Gerlich, D. W. (2019). Mitotic Chromosome Mechanics: How Cells Segregate Their Genome. *Trends Cell Biol, 29*(9), 717-726. doi:10.1016/j.tcb.2019.05.007

Bavetsias, V., & Linardopoulos, S. (2015). Aurora Kinase Inhibitors: Current Status and Outlook. *Front Oncol, 5*, 278. doi:10.3389/fonc.2015.00278

Bellanger, J. M., & Gonczy, P. (2003). TAC-1 and ZYG-9 form a complex that promotes microtubule assembly in C. elegans embryos. *Curr Biol, 13*(17), 1488-1498. doi:10.1016/s0960-9822(03)00582-7

Benson, E. K., Mungamuri, S. K., Attie, O., Kracikova, M., Sachidanandam, R., Manfredi, J. J., & Aaronson, S. A. (2014). p53-dependent gene repression through p21 is mediated by recruitment of E2F4 repression complexes. *Oncogene, 33*(30), 3959-3969. doi:10.1038/onc.2013.378

Bentley, D. L. (2014). Coupling mRNA processing with transcription in time and space. *Nat Rev Genet, 15*(3), 163-175. doi:10.1038/nrg3662

Bernstein, B. E., Humphrey, E. L., Erlich, R. L., Schneider, R., Bouman, P., Liu, J. S., . . . Schreiber, S. L. (2002). Methylation of histone H3 Lys 4 in coding regions of active genes. *Proc Natl Acad Sci U S A, 99*(13), 8695-8700. doi:10.1073/pnas.082249499

Bertolin, G., Bulteau, A. L., Alves-Guerra, M. C., Burel, A., Lavault, M. T., Gavard, O., . . . Tramier, M. (2018). Aurora kinase A localises to mitochondria to control organelle dynamics and energy production. *Elife, 7*. doi:10.7554/eLife.38111

Bertolin, G., & Tramier, M. (2020). Insights into the non-mitotic functions of Aurora kinase A: more than just cell division. *Cell Mol Life Sci, 77*(6), 1031-1047. doi:10.1007/s00018-019-03310-2

Blackwell, T. K., Kretzner, L., Blackwood, E. M., Eisenman, R. N., & Weintraub, H. (1990). Sequence-specific DNA binding by the c-Myc protein. *Science, 250*(4984), 1149-1151. doi:10.1126/science.2251503

Boeva, V., Louis-Brennetot, C., Peltier, A., Durand, S., Pierre-Eugene, C., Raynal, V., . . . Janoueix-Lerosey, I. (2017). Heterogeneity of neuroblastoma cell identity defined by transcriptional circuitries. *Nat Genet, 49*(9), 1408-1413. doi:10.1038/ng.3921

Bolstad, B. M., Irizarry, R. A., Astrand, M., & Speed, T. P. (2003). A comparison of normalization methods for high density oligonucleotide array data based on variance and bias. *Bioinformatics, 19*(2), 185-193. doi:10.1093/bioinformatics/19.2.185

Boos, D., Frigola, J., & Diffley, J. F. (2012). Activation of the replicative DNA helicase: breaking up is hard to do. *Curr Opin Cell Biol, 24*(3), 423-430. doi:10.1016/j.ceb.2012.01.011

Bourdeaut, F., Trochet, D., Janoueix-Lerosey, I., Ribeiro, A., Deville, A., Coz, C., . . . Delattre, O. (2005). Germline mutations of the paired-like homeobox 2B (PHOX2B) gene in neuroblastoma. *Cancer Lett, 228*(1-2), 51-58. doi:10.1016/j.canlet.2005.01.055

Bown, N., Cotterill, S., Lastowska, M., O'Neill, S., Pearson, A. D., Plantaz, D., . . . Van Roy, N. (1999). Gain of chromosome arm 17q and adverse outcome in patients with neuroblastoma. *N Engl J Med, 340*(25), 1954-1961. doi:10.1056/NEJM199906243402504

Brockmann, M., Poon, E., Berry, T., Carstensen, A., Deubzer, H. E., Rycak, L., . . . Eilers, M. (2013). Small molecule inhibitors of aurora-a induce proteasomal degradation of N-myc in childhood neuroblastoma. *Cancer Cell, 24*(1), 75-89. doi:10.1016/j.ccr.2013.05.005

Brosi, R., Gröning, K., Behrens, S. E., Lührmann, R., & Krämer, A. (1993). Interaction of mammalian splicing factor SF3a with U2 snRNP and relation of its 60-kD subunit to yeast PRP9. *Science, 262*(5130), 102-105. doi:10.1126/science.8211112

Büchel, G., Carstensen, A., Mak, K. Y., Roeschert, I., Leen, E., Sumara, O., . . . Eilers, M. (2017). Association with Aurora-A Controls N-MYC-Dependent Promoter Escape and Pause Release of RNA Polymerase II during the Cell Cycle. *Cell Rep, 21*(12), 3483-3497. doi:10.1016/j.celrep.2017.11.090

Cadoret, J. C., Meisch, F., Hassan-Zadeh, V., Luyten, I., Guillet, C., Duret, L., . . . Prioleau, M. N. (2008). Genome-wide studies highlight indirect links between human replication origins and gene regulation. *Proc Natl Acad Sci U S A, 105*(41), 15837-15842. doi:10.1073/pnas.0805208105

Callan, H. G. (1974). DNA replication in the chromosomes of eukaryotes. *Cold Spring Harb Symp Quant Biol, 38*, 195-203. doi:10.1101/sqb.1974.038.01.023

Caren, H., Kryh, H., Nethander, M., Sjoberg, R. M., Trager, C., Nilsson, S., . . . Martinsson, T. (2010). High-risk neuroblastoma tumors with 11q-deletion display a poor prognostic, chromosome instability phenotype with later onset. *Proc Natl Acad Sci U S A, 107*(9), 4323-4328. doi:10.1073/pnas.0910684107

Carlsen, N. L. (1990). The new International Neuroblastoma Staging System: some critical notes. *J Clin Oncol, 8*(5), 935-936. doi:10.1200/JCO.1990.8.5.935

Casper, A. M., Nghiem, P., Arlt, M. F., & Glover, T. W. (2002). ATR regulates fragile site stability. *Cell, 111*(6), 779-789. doi:10.1016/s0092-8674(02)01113-3

Chacon Simon, S., Wang, F., Thomas, L. R., Phan, J., Zhao, B., Olejniczak, E. T., . . . Fesik, S. W. (2020). Discovery of WD Repeat-Containing Protein 5 (WDR5)-MYC Inhibitors Using Fragment-Based Methods and Structure-Based Design. *J Med Chem, 63*(8), 4315-4333. doi:10.1021/acs.jmedchem.0c00224

Chan, C. S., & Botstein, D. (1993). Isolation and characterization of chromosome-gain and increase-in-ploidy mutants in yeast. *Genetics, 135*(3), 677-691. Retrieved from https://www.ncbi.nlm.nih.gov/pubmed/8293973

Chao, S. H., & Price, D. H. (2001). Flavopiridol inactivates P-TEFb and blocks most RNA polymerase II transcription in vivo. *J Biol Chem, 276*(34), 31793-31799. doi:10.1074/jbc.M102306200

Charron, J., Malynn, B. A., Fisher, P., Stewart, V., Jeannotte, L., Goff, S. P., . . . Alt, F. W. (1992). Embryonic lethality in mice homozygous for a targeted disruption of the N-myc gene. *Genes Dev, 6*(12A), 2248-2257. doi:10.1101/gad.6.12a.2248

Chen, E. Y., Tan, C. M., Kou, Y., Duan, Q., Wang, Z., Meirelles, G. V., . . . Ma'ayan, A. (2013). Enrichr: interactive and collaborative HTML5 gene list enrichment analysis tool. *BMC Bioinformatics, 14*, 128. doi:10.1186/1471-2105-14-128

Chen, H., Liu, H., & Qing, G. (2018). Targeting oncogenic Myc as a strategy for cancer treatment. *Signal Transduct Target Ther, 3*, 5. doi:10.1038/s41392-018-0008-7

Chen, L., Chen, J. Y., Huang, Y. J., Gu, Y., Qiu, J., Qian, H., . . . Fu, X. D. (2018). The Augmented R-Loop Is a Unifying Mechanism for Myelodysplastic Syndromes Induced by High-Risk Splicing Factor Mutations. *Mol Cell, 69*(3), 412-425.e416. doi:10.1016/j.molcel.2017.12.029

Chen, Y., Takita, J., Choi, Y. L., Kato, M., Ohira, M., Sanada, M., . . . Ogawa, S. (2008). Oncogenic mutations of ALK kinase in neuroblastoma. *Nature, 455*(7215), 971-974. doi:10.1038/nature07399

Cheng, M., Olivier, P., Diehl, J. A., Fero, M., Roussel, M. F., Roberts, J. M., & Sherr, C. J. (1999). The p21(Cip1) and p27(Kip1) CDK 'inhibitors' are essential activators of cyclin D-dependent kinases in murine fibroblasts. *EMBO J, 18*(6), 1571-1583. doi:10.1093/emboj/18.6.1571

Cheung, N. K., Zhang, J., Lu, C., Parker, M., Bahrami, A., Tickoo, S. K., . . . St Jude Children's Research Hospital-Washington University Pediatric Cancer Genome, P. (2012). Association of age at diagnosis and genetic mutations in patients with neuroblastoma. *JAMA, 307*(10), 1062-1071. doi:10.1001/jama.2012.228

Cheung, P., Allis, C. D., & Sassone-Corsi, P. (2000). Signaling to chromatin through histone modifications. *Cell, 103*(2), 263-271. doi:10.1016/s0092-8674(00)00118-5

Chipumuro, E., Marco, E., Christensen, C. L., Kwiatkowski, N., Zhang, T., Hatheway, C. M., . . . George, R. E. (2014). CDK7 inhibition suppresses super-enhancer-linked oncogenic transcription in MYCN-driven cancer. *Cell, 159*(5), 1126-1139. doi:10.1016/j.cell.2014.10.024

Cho, C., Jang, J., Kang, Y., Watanabe, H., Uchihashi, T., Kim, S. J., . . . Song, J. J. (2019). Structural basis of nucleosome assembly by the Abo1 AAA+ ATPase histone chaperone. *Nat Commun, 10*(1), 5764. doi:10.1038/s41467-019-13743-9

Choi, S. H., Wright, J. B., Gerber, S. A., & Cole, M. D. (2010). Myc protein is stabilized by suppression of a novel E3 ligase complex in cancer cells. *Genes Dev, 24*(12), 1236-1241. doi:10.1101/gad.1920310

Ciró, M., Prosperini, E., Quarto, M., Grazini, U., Walfridsson, J., McBlane, F., . . . Helin, K. (2009). ATAD2 is a novel cofactor for MYC, overexpressed and amplified in aggressive tumors. *Cancer Res, 69*(21), 8491-8498. doi:10.1158/0008-5472.Can-09-2131

Clynes, D., Jelinska, C., Xella, B., Ayyub, H., Scott, C., Mitson, M., . . . Gibbons, R. J. (2015). Suppression of the alternative lengthening of telomere pathway by the chromatin remodelling factor ATRX. *Nat Commun, 6*, 7538. doi:10.1038/ncomms8538

Clynes, D., & Gibbons, R. J. (2013). ATRX and the replication of structured DNA. *Curr Opin Genet Dev, 23*(3), 289-294. doi:10.1016/j.gde.2013.01.005

Clynes, D., Higgs, D. R., & Gibbons, R. J. (2013). The chromatin remodeller ATRX: a repeat offender in human disease. *Trends Biochem Sci, 38*(9), 461-466. doi:10.1016/j.tibs.2013.06.011

Cohn, S. L., Pearson, A. D., London, W. B., Monclair, T., Ambros, P. F., Brodeur, G. M., . . . Force, I. T. (2009). The International Neuroblastoma Risk Group (INRG) classification system: an INRG Task Force report. *J Clin Oncol, 27*(2), 289-297. doi:10.1200/JCO.2008.16.6785

Compe, E., & Egly, J. M. (2012). TFIIH: when transcription met DNA repair. *Nat Rev Mol Cell Biol, 13*(6), 343-354. doi:10.1038/nrm3350

Cortez, D., Guntuku, S., Qin, J., & Elledge, S. J. (2001). ATR and ATRIP: partners in checkpoint signaling. *Science, 294*(5547), 1713-1716. doi:10.1126/science.1065521

Cowling, V. H., Chandriani, S., Whitfield, M. L., & Cole, M. D. (2006). A conserved Myc protein domain, MBIV, regulates DNA binding, apoptosis, transformation, and G2 arrest. *Mol Cell Biol, 26*(11), 4226-4239. doi:10.1128/MCB.01959-05

Cossa, G., Roeschert, I., Prinz, F., Baluapuri, A., Silveira Vidal, R., Schulein-Volk, C., . . . Eilers, M. (2020). Localized Inhibition of Protein Phosphatase 1 by NUAK1 Promotes Spliceosome Activity and Reveals a MYC-Sensitive Feedback Control of Transcription. *Mol Cell, 77*(6), 1322-1339 e1311. doi:10.1016/j.molcel.2020.01.008

Cox, J., Hein, M. Y., Luber, C. A., Paron, I., Nagaraj, N., & Mann, M. (2014). Accurate proteome-wide label-free quantification by delayed normalization and maximal peptide ratio extraction, termed MaxLFQ. *Mol Cell Proteomics, 13*(9), 2513-2526. doi:10.1074/mcp.M113.031591

Creixell, P., Schoof, E. M., Simpson, C. D., Longden, J., Miller, C. J., Lou, H. J., . . . Linding, R. (2015). Kinome-wide decoding of network-attacking mutations rewiring cancer signaling. *Cell, 163*(1), 202-217. doi:10.1016/j.cell.2015.08.056

Crosio, C., Fimia, G. M., Loury, R., Kimura, M., Okano, Y., Zhou, H., . . . Sassone-Corsi, P. (2002). Mitotic phosphorylation of histone H3: spatio-temporal regulation by mammalian Aurora kinases. *Mol Cell Biol, 22*(3), 874-885. doi:10.1128/mcb.22.3.874-885.2002

Crossley, M. P., Bocek, M., & Cimprich, K. A. (2019). R-Loops as Cellular Regulators and Genomic Threats. *Mol Cell, 73*(3), 398-411. doi:10.1016/j.molcel.2019.01.024

Damodaran, A. P., Gavard, O., Gagné, J.-P., Rogalska, M. E., Mancini, E., Courtheoux, T., . . . Prigent, C. (2020). Aurora-A phosphorylates splicing factors and regulates alternative splicing. In: bioRxiv.

Dantzer, F., Nasheuer, H. P., Vonesch, J. L., de Murcia, G., & Ménissier-de Murcia, J. (1998). Functional association of poly(ADP-ribose) polymerase with DNA polymerase alpha-primase complex: a link between DNA strand break detection and DNA replication. *Nucleic Acids Res, 26*(8), 1891-1898. doi:10.1093/nar/26.8.1891

Dauch, D., Rudalska, R., Cossa, G., Nault, J. C., Kang, T. W., Wuestefeld, T., . . . Zender, L. (2016). A MYC-aurora kinase A protein complex represents an actionable drug target in p53-altered liver cancer. *Nat Med, 22*(7), 744-753. doi:10.1038/nm.4107

Davis, A. C., Wims, M., Spotts, G. D., Hann, S. R., & Bradley, A. (1993). A null c-myc mutation causes lethality before 10.5 days of gestation in homozygotes and reduced fertility in heterozygous female mice. *Genes Dev, 7*(4), 671-682. doi:10.1101/gad.7.4.671

Delacroix, S., Wagner, J. M., Kobayashi, M., Yamamoto, K., & Karnitz, L. M. (2007). The Rad9-Hus1-Rad1 (9-1-1) clamp activates checkpoint signaling via TopBP1. *Genes Dev, 21*(12), 1472-1477. doi:10.1101/gad.1547007

Delmore, J. E., Issa, G. C., Lemieux, M. E., Rahl, P. B., Shi, J., Jacobs, H. M., . . . Mitsiades, C. S. (2011). BET bromodomain inhibition as a therapeutic strategy to target c-Myc. *Cell, 146*(6), 904-917. doi:10.1016/j.cell.2011.08.017

den Hollander, J., Rimpi, S., Doherty, J. R., Rudelius, M., Buck, A., Hoellein, A., . . . Keller, U. (2010). Aurora kinases A and B are up-regulated by Myc and are essential for maintenance of the malignant state. *Blood, 116*(9), 1498-1505. doi:10.1182/blood-2009-11-251074

DePamphilis, M. L. (1993). Origins of DNA replication in metazoan chromosomes. *J Biol Chem, 268*(1), 1-4. Retrieved from https://www.ncbi.nlm.nih.gov/pubmed/8416916

Devaiah, B. N., Case-Borden, C., Gegonne, A., Hsu, C. H., Chen, Q., Meerzaman, D., . . . Singer, D. S. (2016). BRD4 is a histone acetyltransferase that evicts nucleosomes from chromatin. *Nat Struct Mol Biol, 23*(6), 540-548. doi:10.1038/nsmb.3228

Dewar, J. M., & Walter, J. C. (2017). Mechanisms of DNA replication termination. *Nat Rev Mol Cell Biol, 18*(8), 507-516. doi:10.1038/nrm.2017.42

Dimitrova, D. S., & Gilbert, D. M. (1999). The spatial position and replication timing of chromosomal domains are both established in early G1 phase. *Mol Cell, 4*(6), 983-993. doi:10.1016/s1097-2765(00)80227-0

Ding, L., Cao, J., Lin, W., Chen, H., Xiong, X., Ao, H., . . . Cui, Q. (2020). The Roles of Cyclin-Dependent Kinases in Cell-Cycle Progression and Therapeutic Strategies in Human Breast Cancer. *Int J Mol Sci, 21*(6). doi:10.3390/ijms21061960

Dodson, C. A., & Bayliss, R. (2012). Activation of Aurora-A kinase by protein partner binding and phosphorylation are independent and synergistic. *J Biol Chem, 287*(2), 1150-1157. doi:10.1074/jbc.M111.312090

Dodson, C. A., Kosmopoulou, M., Richards, M. W., Atrash, B., Bavetsias, V., Blagg, J., & Bayliss, R. (2010). Crystal structure of an Aurora-A mutant that mimics Aurora-B bound to MLN8054: insights into selectivity and drug design. *Biochem J, 427*(1), 19-28. doi:10.1042/BJ20091530

Du, W., Amarachintha, S., Wilson, A. F., & Pang, Q. (2016). Hyper-active non-homologous end joining selects for synthetic lethality resistant and pathological Fanconi anemia hematopoietic stem and progenitor cells. *Sci Rep, 6*, 22167. doi:10.1038/srep22167

Dubois, N. C., Adolphe, C., Ehninger, A., Wang, R. A., Robertson, E. J., & Trumpp, A. (2008). Placental rescue reveals a sole requirement for c-Myc in embryonic erythroblast survival and hematopoietic stem cell function. *Development, 135*(14), 2455-2465. doi:10.1242/dev.022707

DuBois, S. G., Kalika, Y., Lukens, J. N., Brodeur, G. M., Seeger, R. C., Atkinson, J. B., . . . Matthay, K. K. (1999). Metastatic sites in stage IV and IVS neuroblastoma correlate with age, tumor biology, and survival. *J Pediatr Hematol Oncol, 21*(3), 181-189. doi:10.1097/00043426-199905000-00005

Durlacher, C. T., Li, Z. L., Chen, X. W., He, Z. X., & Zhou, S. F. (2016). An update on the pharmacokinetics and pharmacodynamics of alisertib, a selective Aurora kinase A inhibitor. *Clin Exp Pharmacol Physiol, 43*(6), 585-601. doi:10.1111/1440-1681.12571

Dutertre, S., Cazales, M., Quaranta, M., Froment, C., Trabut, V., Dozier, C., . . . Ducommun, B. (2004). Phosphorylation of CDC25B by Aurora-A at the centrosome contributes to the G2-M transition. *J Cell Sci, 117*(Pt 12), 2523-2531. doi:10.1242/jcs.01108

Eberhardy, S. R., & Farnham, P. J. (2001). c-Myc mediates activation of the cad promoter via a post-RNA polymerase II recruitment mechanism. *J Biol Chem, 276*(51), 48562-48571. doi:10.1074/jbc.M109014200

Eckschlager, T., Pilat, D., Kodet, R., Dahbiova, R., Stankova, J., Jasinska, J., & Hrusak, O. (1996). DNA ploidy in neuroblastoma. *Neoplasma, 43*(1), 23-26. Retrieved from https://www.ncbi.nlm.nih.gov/pubmed/8843955

Effenberger, K. A., Anderson, D. D., Bray, W. M., Prichard, B. E., Ma, N., Adams, M. S., . . . Jurica, M. S. (2014). Coherence between cellular responses and in vitro splicing inhibition for the anti-tumor drug pladienolide B and its analogs. *J Biol Chem, 289*(4), 1938-1947. doi:10.1074/jbc.M113.515536

Eick, D., & Geyer, M. (2013). The RNA polymerase II carboxy-terminal domain (CTD) code. *Chem Rev, 113*(11), 8456-8490. doi:10.1021/cr400071f

Ewing, R. M., Chu, P., Elisma, F., Li, H., Taylor, P., Climie, S., . . . Figeys, D. (2007). Large-scale mapping of human protein-protein interactions by mass spectrometry. *Mol Syst Biol, 3*, 89. doi:10.1038/msb4100134

Eyers, P. A., Erikson, E., Chen, L. G., & Maller, J. L. (2003). A novel mechanism for activation of the protein kinase Aurora A. *Curr Biol, 13*(8), 691-697. doi:10.1016/s0960-9822(03)00166-0

Farag, S. S. (2011). The potential role of Aurora kinase inhibitors in haematological malignancies. *Br J Haematol, 155*(5), 561-579. doi:10.1111/j.1365-2141.2011.08898.x

Fellmann, C., Hoffmann, T., Sridhar, V., Hopfgartner, B., Muhar, M., Roth, M., . . . Zuber, J. (2013). An optimized microRNA backbone for effective single-copy RNAi. *Cell Rep, 5*(6), 1704-1713. doi:10.1016/j.celrep.2013.11.020

Filippakopoulos, P., Qi, J., Picaud, S., Shen, Y., Smith, W. B., Fedorov, O., . . . Bradner, J. E. (2010). Selective inhibition of BET bromodomains. *Nature, 468*(7327), 1067-1073. doi:10.1038/nature09504

Follis, A. V., Hammoudeh, D. I., Daab, A. T., & Metallo, S. J. (2009). Small-molecule perturbation of competing interactions between c-Myc and Max. *Bioorg Med Chem Lett, 19*(3), 807-810. doi:10.1016/j.bmcl.2008.12.025

Fong, C. T., Dracopoli, N. C., White, P. S., Merrill, P. T., Griffith, R. C., Housman, D. E., & Brodeur, G. M. (1989). Loss of heterozygosity for the short arm of chromosome 1 in human neuroblastomas: correlation with N-myc amplification. *Proc Natl Acad Sci U S A, 86*(10), 3753-3757. doi:10.1073/pnas.86.10.3753

Frank, S. R., Parisi, T., Taubert, S., Fernandez, P., Fuchs, M., Chan, H. M., . . . Amati, B. (2003). MYC recruits the TIP60 histone acetyltransferase complex to chromatin. *EMBO Rep, 4*(6), 575-580. doi:10.1038/sj.embor.embor861

Franks, L. M., Bollen, A., Seeger, R. C., Stram, D. O., & Matthay, K. K. (1997). Neuroblastoma in adults and adolescents: an indolent course with poor survival. *Cancer, 79*(10), 2028-2035. doi:10.1002/(sici)1097-0142(19970515)79:10<2028::aid-cncr26>3.0.co;2-v

Fruman, D. A., & O'Brien, S. (2017). A targeted treatment with off-target risks. *Nature, 542*(7642), 424-425. doi:10.1038/nature21504

Fujii, Y., Yada, M., Nishiyama, M., Kamura, T., Takahashi, H., Tsunematsu, R., . . . Nakayama, K. I. (2006). Fbxw7 contributes to tumor suppression by targeting multiple proteins for ubiquitin-dependent degradation. *Cancer Sci, 97*(8), 729-736. doi:10.1111/j.1349-7006.2006.00239.x

Fujinaga, K., Irwin, D., Huang, Y., Taube, R., Kurosu, T., & Peterlin, B. M. (2004). Dynamics of human immunodeficiency virus transcription: P-TEFb phosphorylates RD and dissociates negative effectors from the transactivation response element. *Mol Cell Biol, 24*(2), 787-795. doi:10.1128/mcb.24.2.787-795.2004

Fujita, T., Igarashi, J., Okawa, E. R., Gotoh, T., Manne, J., Kolla, V., . . . Brodeur, G. M. (2008). CHD5, a tumor suppressor gene deleted from 1p36.31 in neuroblastomas. *J Natl Cancer Inst, 100*(13), 940-949. doi:10.1093/jnci/djn176

Gartlgruber, M., Sharma, A. K., Quintero, A., Dreidax, D., Jansky, S., Park, Y.-G., . . . Westermann, F. (2020). Super enhancers define regulatory subtypes and cell identity in neuroblastoma. *Nature Cancer*. doi:10.1038/s43018-020-00145-w

Gavet, O., & Pines, J. (2010). Progressive activation of CyclinB1-Cdk1 coordinates entry to mitosis. *Dev Cell, 18*(4), 533-543. doi:10.1016/j.devcel.2010.02.013

George, R. E., Sanda, T., Hanna, M., Frohling, S., Luther, W., 2nd, Zhang, J., . . . Look, A. T. (2008). Activating mutations in ALK provide a therapeutic target in neuroblastoma. *Nature, 455*(7215), 975-978. doi:10.1038/nature07397

George, S. L., Lorenzi, F., King, D., Hartlieb, S., Campbell, J., Pemberton, H., . . . Chesler, L. (2020). Therapeutic vulnerabilities in the DNA damage response for the treatment of ATRX mutant neuroblastoma. *EBioMedicine, 59*, 102971-102971. doi:10.1016/j.ebiom.2020.102971

Giet, R., McLean, D., Descamps, S., Lee, M. J., Raff, J. W., Prigent, C., & Glover, D. M. (2002). Drosophila Aurora A kinase is required to localize D-TACC to centrosomes and to regulate astral microtubules. *J Cell Biol, 156*(3), 437-451. doi:10.1083/jcb.200108135

Giet, R., Uzbekov, R., Cubizolles, F., Le Guellec, K., & Prigent, C. (1999). The Xenopus laevis aurora-related protein kinase pEg2 associates with and phosphorylates the kinesin-related protein XlEg5. *J Biol Chem, 274*(21), 15005-15013. doi:10.1074/jbc.274.21.15005

Gilbert, D. M., Takebayashi, S. I., Ryba, T., Lu, J., Pope, B. D., Wilson, K. A., & Hiratani, I. (2010). Space and time in the nucleus: developmental control of replication timing and chromosome architecture. *Cold Spring Harb Symp Quant Biol, 75*, 143-153. doi:10.1101/sqb.2010.75.011

Gilburt, J. A. H., Sarkar, H., Sheldrake, P., Blagg, J., Ying, L., & Dodson, C. A. (2017). Dynamic Equilibrium of the Aurora A Kinase Activation Loop Revealed by Single-Molecule Spectroscopy. *Angewandte Chemie (International ed. in English), 56*(38), 11409-11414. doi:10.1002/anie.201704654

Ginno, P. A., Burger, L., Seebacher, J., Iesmantavicius, V., & Schübeler, D. (2018). Cell cycle-resolved chromatin proteomics reveals the extent of mitotic preservation of the genomic regulatory landscape. *Nature Communications, 9*(1), 4048. doi:10.1038/s41467-018-06007-5

Girard, C., Will, C. L., Peng, J., Makarov, E. M., Kastner, B., Lemm, I., . . . Luhrmann, R. (2012). Post-transcriptional spliceosomes are retained in nuclear speckles until splicing completion. *Nat Commun, 3*, 994. doi:10.1038/ncomms1998

Glover-Cutter, K., Larochelle, S., Erickson, B., Zhang, C., Shokat, K., Fisher, R. P., & Bentley, D. L. (2009). TFIIH-associated Cdk7 kinase functions in phosphorylation of C-terminal domain Ser7 residues, promoter-proximal pausing, and termination by RNA polymerase II. *Mol Cell Biol, 29*(20), 5455-5464. doi:10.1128/MCB.00637-09

Goldberg, A. D., Banaszynski, L. A., Noh, K. M., Lewis, P. W., Elsaesser, S. J., Stadler, S., . . . Allis, C. D. (2010). Distinct factors control histone variant H3.3 localization at specific genomic regions. *Cell, 140*(5), 678-691. doi:10.1016/j.cell.2010.01.003

Goto, H., Tomono, Y., Ajiro, K., Kosako, H., Fujita, M., Sakurai, M., . . . Inagaki, M. (1999). Identification of a novel phosphorylation site on histone H3 coupled with mitotic chromosome condensation. *J Biol Chem, 274*(36), 25543-25549. doi:10.1074/jbc.274.36.25543

Grant, R., Abdelbaki, A., Bertoldi, A., Gavilan, M. P., Mansfeld, J., Glover, D. M., & Lindon, C. (2018). Constitutive regulation of mitochondrial morphology by Aurora A kinase depends on a predicted cryptic targeting sequence at the N-terminus. *Open Biol, 8*(6). doi:10.1098/rsob.170272

Grim, J. E., Gustafson, M. P., Hirata, R. K., Hagar, A. C., Swanger, J., Welcker, M., . . . Clurman, B. E. (2008). Isoform- and cell cycle-dependent substrate degradation by the Fbw7 ubiquitin ligase. *J Cell Biol, 181*(6), 913-920. doi:10.1083/jcb.200802076

Grunberg, S., & Hahn, S. (2013). Structural insights into transcription initiation by RNA polymerase II. *Trends Biochem Sci, 38*(12), 603-611. doi:10.1016/j.tibs.2013.09.002

Guo, C., White, P. S., Weiss, M. J., Hogarty, M. D., Thompson, P. M., Stram, D. O., . . . Maris, J. M. (1999). Allelic deletion at 11q23 is common in MYCN single copy neuroblastomas. *Oncogene, 18*(35), 4948-4957. doi:10.1038/sj.onc.1202887

Guo, J., Li, T., Schipper, J., Nilson, K. A., Fordjour, F. K., Cooper, J. J., . . . Price, D. H. (2014). Sequence specificity incompletely defines the genome-wide occupancy of Myc. *Genome Biol, 15*(10), 482. doi:10.1186/s13059-014-0482-3

Gustafson, W. C., Meyerowitz, J. G., Nekritz, E. A., Chen, J., Benes, C., Charron, E., . . . Weiss, W. A. (2014). Drugging MYCN through an allosteric transition in Aurora kinase A. *Cancer Cell, 26*(3), 414-427. doi:10.1016/j.ccr.2014.07.015

Hallberg, B., & Palmer, R. H. (2016). The role of the ALK receptor in cancer biology. *Annals of Oncology, 27*, iii4-iii15. doi:https://doi.org/10.1093/annonc/mdw301

Hamperl, S., Bocek, M. J., Saldivar, J. C., Swigut, T., & Cimprich, K. A. (2017). Transcription-Replication Conflict Orientation Modulates R-Loop Levels and Activates Distinct DNA Damage Responses. *Cell, 170*(4), 774-786.e719. doi:10.1016/j.cell.2017.07.043

Hamperl, S., & Cimprich, K. A. (2016). Conflict Resolution in the Genome: How Transcription and Replication Make It Work. *Cell, 167*(6), 1455-1467. doi:10.1016/j.cell.2016.09.053

Hannak, E., Kirkham, M., Hyman, A. A., & Oegema, K. (2001). Aurora-A kinase is required for centrosome maturation in Caenorhabditis elegans. *J Cell Biol, 155*(7), 1109-1116. doi:10.1083/jcb.200108051

Haren, L., Remy, M. H., Bazin, I., Callebaut, I., Wright, M., & Merdes, A. (2006). NEDD1-dependent recruitment of the gamma-tubulin ring complex to the centrosome is necessary for centriole duplication and spindle assembly. *J Cell Biol, 172*(4), 505-515. doi:10.1083/jcb.200510028

Harlen, K. M., & Churchman, L. S. (2017). The code and beyond: transcription regulation by the RNA polymerase II carboxy-terminal domain. *Nat Rev Mol Cell Biol, 18*(4), 263-273. doi:10.1038/nrm.2017.10

Harrington, J. J., & Lieber, M. R. (1994). Functional domains within FEN-1 and RAD2 define a family of structure-specific endonucleases: implications for nucleotide excision repair. *Genes Dev, 8*(11), 1344-1355. doi:10.1101/gad.8.11.1344

Hartwell, L. H., & Weinert, T. A. (1989). Checkpoints: controls that ensure the order of cell cycle events. *Science, 246*(4930), 629-634. doi:10.1126/science.2683079

Hatchi, E., Skourti-Stathaki, K., Ventz, S., Pinello, L., Yen, A., Kamieniarz-Gdula, K., . . . Livingston, D. M. (2015). BRCA1 recruitment to transcriptional pause sites is required for R-loop-driven DNA damage repair. *Mol Cell, 57*(4), 636-647. doi:10.1016/j.molcel.2015.01.011

Heald, R., McLoughlin, M., & McKeon, F. (1993). Human wee1 maintains mitotic timing by protecting the nucleus from cytoplasmically activated Cdc2 kinase. *Cell, 74*(3), 463-474. doi:10.1016/0092-8674(93)80048-j

Heidelberger, J. B., Voigt, A., Borisova, M. E., Petrosino, G., Ruf, S., Wagner, S. A., & Beli, P. (2018). Proteomic profiling of VCP substrates links VCP to K6-linked ubiquitylation and c-Myc function. *EMBO Rep, 19*(4). doi:10.15252/embr.201744754

Heller, R. C., Kang, S., Lam, W. M., Chen, S., Chan, C. S., & Bell, S. P. (2011). Eukaryotic origin-dependent DNA replication in vitro reveals sequential action of DDK and S-CDK kinases. *Cell, 146*(1), 80-91. doi:10.1016/j.cell.2011.06.012

Helmrich, A., Ballarino, M., & Tora, L. (2011). Collisions between replication and transcription complexes cause common fragile site instability at the longest human genes. *Mol Cell, 44*(6), 966-977. doi:10.1016/j.molcel.2011.10.013

Herold, S., Kalb, J., Büchel, G., Ade, C. P., Baluapuri, A., Xu, J., . . . Eilers, M. (2019). Recruitment of BRCA1 limits MYCN-driven accumulation of stalled RNA polymerase. *Nature, 567*(7749), 545-549. doi:10.1038/s41586-019-1030-9

Hirota, T., Kunitoku, N., Sasayama, T., Marumoto, T., Zhang, D., Nitta, M., . . . Saya, H. (2003). Aurora-A and an interacting activator, the LIM protein Ajuba, are required for mitotic commitment in human cells. *Cell, 114*(5), 585-598. doi:10.1016/s0092-8674(03)00642-1

Ho, Y. S., Duh, J. S., Jeng, J. H., Wang, Y. J., Liang, Y. C., Lin, C. H., . . . Lin, J. K. (2001). Griseofulvin potentiates antitumorigenesis effects of nocodazole through induction of apoptosis and G2/M cell cycle arrest in human colorectal cancer cells. *Int J Cancer, 91*(3), 393-401. doi:10.1002/1097-0215(200002)9999:9999<::aid-ijc1070>3.0.co;2-#

Hoehner, J. C., Gestblom, C., Hedborg, F., Sandstedt, B., Olsen, L., & Pahlman, S. (1996). A developmental model of neuroblastoma: differentiating stroma-poor tumors' progress along an extra-adrenal chromaffin lineage. *Lab Invest, 75*(5), 659-675. Retrieved from https://www.ncbi.nlm.nih.gov/pubmed/8941212

Hong, X., O'Donnell, J. P., Salazar, C. R., Van Brocklyn, J. R., Barnett, K. D., Pearl, D. K., . . . Lehman, N. L. (2014). The selective Aurora-A kinase inhibitor MLN8237 (alisertib) potently inhibits proliferation of glioblastoma neurosphere tumor stem-like cells and

potentiates the effects of temozolomide and ionizing radiation. *Cancer Chemother Pharmacol, 73*(5), 983-990. doi:10.1007/s00280-014-2430-z
Hsu, C. W., Chen, Y. C., Su, H. H., Huang, G. J., Shu, C. W., Wu, T. T., & Pan, H. W. (2017). Targeting TPX2 Suppresses the Tumorigenesis of Hepatocellular Carcinoma Cells Resulting in Arrested Mitotic Phase Progression and Increased Genomic Instability. *J Cancer, 8*(8), 1378-1394. doi:10.7150/jca.17478
Hu, W., Kavanagh, J. J., Deaver, M., Johnston, D. A., Freedman, R. S., Verschraegen, C. F., & Sen, S. (2005). Frequent overexpression of STK15/Aurora-A/BTAK and chromosomal instability in tumorigenic cell cultures derived from human ovarian cancer. *Oncol Res, 15*(1), 49-57. doi:10.3727/096504005775082101
Huh, M. S., Ivanochko, D., Hashem, L. E., Curtin, M., Delorme, M., Goodall, E., . . . Picketts, D. J. (2016). Stalled replication forks within heterochromatin require ATRX for protection. *Cell Death Dis, 7*(5), e2220. doi:10.1038/cddis.2016.121
Huang, C. H., Lujambio, A., Zuber, J., Tschaharganeh, D. F., Doran, M. G., Evans, M. J., . . . Lowe, S. W. (2014). CDK9-mediated transcription elongation is required for MYC addiction in hepatocellular carcinoma. *Genes Dev, 28*(16), 1800-1814. doi:10.1101/gad.244368.114
Huang da, W., Sherman, B. T., & Lempicki, R. A. (2009). Systematic and integrative analysis of large gene lists using DAVID bioinformatics resources. *Nat Protoc, 4*(1), 44-57. doi:10.1038/nprot.2008.211
Huang, M., & Weiss, W. A. (2013). Neuroblastoma and MYCN. *Cold Spring Harbor perspectives in medicine, 3*(10), a014415. doi:10.1101/cshperspect.a014415
Hurlin, P. J., Zhou, Z. Q., Toyo-oka, K., Ota, S., Walker, W. L., Hirotsune, S., & Wynshaw-Boris, A. (2003). Deletion of Mnt leads to disrupted cell cycle control and tumorigenesis. *EMBO J, 22*(18), 4584-4596. doi:10.1093/emboj/cdg442
Ikegaki, N., Shimada, H., & International Neuroblastoma Pathology, C. (2019). Subgrouping of Unfavorable Histology Neuroblastomas With Immunohistochemistry Toward Precision Prognosis and Therapy Stratification. *JCO Precis Oncol, 3*. doi:10.1200/PO.18.00312
Ilves, I., Petojevic, T., Pesavento, J. J., & Botchan, M. R. (2010). Activation of the MCM2-7 helicase by association with Cdc45 and GINS proteins. *Mol Cell, 37*(2), 247-258. doi:10.1016/j.molcel.2009.12.030
Isola, J. J., Kallioniemi, O. P., Chu, L. W., Fuqua, S. A., Hilsenbeck, S. G., Osborne, C. K., & Waldman, F. M. (1995). Genetic aberrations detected by comparative genomic hybridization predict outcome in node-negative breast cancer. *Am J Pathol, 147*(4), 905-911. Retrieved from https://www.ncbi.nlm.nih.gov/pubmed/7573366
Ivaldi, M. S., Karam, C. S., & Corces, V. G. (2007). Phosphorylation of histone H3 at Ser10 facilitates RNA polymerase II release from promoter-proximal pausing in Drosophila. *Genes & development, 21*(21), 2818-2831. doi:10.1101/gad.1604007
Ivanauskiene, K., Delbarre, E., McGhie, J. D., Küntziger, T., Wong, L. H., & Collas, P. (2014). The PML-associated protein DEK regulates the balance of H3.3 loading on chromatin and is important for telomere integrity. *Genome Res, 24*(10), 1584-1594. doi:10.1101/gr.173831.114
Izumi, T., & Maller, J. L. (1993). Elimination of cdc2 phosphorylation sites in the cdc25 phosphatase blocks initiation of M-phase. *Mol Biol Cell, 4*(12), 1337-1350. doi:10.1091/mbc.4.12.1337
Jang, Y. J., Ma, S., Terada, Y., & Erikson, R. L. (2002). Phosphorylation of threonine 210 and the role of serine 137 in the regulation of mammalian polo-like kinase. *J Biol Chem, 277*(46), 44115-44120. doi:10.1074/jbc.M202172200
Janoueix-Lerosey, I., Lequin, D., Brugieres, L., Ribeiro, A., de Pontual, L., Combaret, V., . . . Delattre, O. (2008). Somatic and germline activating mutations of the ALK kinase receptor in neuroblastoma. *Nature, 455*(7215), 967-970. doi:10.1038/nature07398

Jonkers, I., Kwak, H., & Lis, J. T. (2014). Genome-wide dynamics of Pol II elongation and its interplay with promoter proximal pausing, chromatin, and exons. *Elife, 3*, e02407. doi:10.7554/eLife.02407

Jonkers, I., & Lis, J. T. (2015). Getting up to speed with transcription elongation by RNA polymerase II. *Nat Rev Mol Cell Biol, 16*(3), 167-177. doi:10.1038/nrm3953

Jung, L. A., Gebhardt, A., Koelmel, W., Ade, C. P., Walz, S., Kuper, J., . . . Eilers, M. (2017). OmoMYC blunts promoter invasion by oncogenic MYC to inhibit gene expression characteristic of MYC-dependent tumors. *Oncogene, 36*(14), 1911-1924. doi:10.1038/onc.2016.354

Kalkat, M., Resetca, D., Lourenco, C., Chan, P. K., Wei, Y., Shiah, Y. J., . . . Penn, L. Z. (2018). MYC Protein Interactome Profiling Reveals Functionally Distinct Regions that Cooperate to Drive Tumorigenesis. *Mol Cell, 72*(5), 836-848 e837. doi:10.1016/j.molcel.2018.09.031

Kamran, M., Long, Z. J., Xu, D., Lv, S. S., Liu, B., Wang, C. L., . . . Liu, Q. (2017). Aurora kinase A regulates Survivin stability through targeting FBXL7 in gastric cancer drug resistance and prognosis. *Oncogenesis, 6*(2), e298. doi:10.1038/oncsis.2016.80

Kashatus, D. F., Lim, K. H., Brady, D. C., Pershing, N. L., Cox, A. D., & Counter, C. M. (2011). RALA and RALBP1 regulate mitochondrial fission at mitosis. *Nat Cell Biol, 13*(9), 1108-1115. doi:10.1038/ncb2310

Katayama, H., Sasai, K., Kawai, H., Yuan, Z. M., Bondaruk, J., Suzuki, F., . . . Sen, S. (2004). Phosphorylation by aurora kinase A induces Mdm2-mediated destabilization and inhibition of p53. *Nat Genet, 36*(1), 55-62. doi:10.1038/ng1279

Kato, G. J., Barrett, J., Villa-Garcia, M., & Dang, C. V. (1990). An amino-terminal c-myc domain required for neoplastic transformation activates transcription. *Mol Cell Biol, 10*(11), 5914-5920. doi:10.1128/mcb.10.11.5914

Kettenbach, A. N., Schweppe, D. K., Faherty, B. K., Pechenick, D., Pletnev, A. A., & Gerber, S. A. (2011). Quantitative phosphoproteomics identifies substrates and functional modules of Aurora and Polo-like kinase activities in mitotic cells. *Sci Signal, 4*(179), rs5. doi:10.1126/scisignal.2001497

Kim, D., Pertea, G., Trapnell, C., Pimentel, H., Kelley, R., & Salzberg, S. L. (2013). TopHat2: accurate alignment of transcriptomes in the presence of insertions, deletions and gene fusions. *Genome Biol, 14*(4), R36. doi:10.1186/gb-2013-14-4-r36

Kim, S. R., Kim, K. B., Chae, Y. C., Park, J. W., & Seo, S. B. (2016). H3S10 phosphorylation-mediated transcriptional regulation by Aurora kinase A. *Biochem Biophys Res Commun, 469*(1), 22-28. doi:10.1016/j.bbrc.2015.11.063

Kim, T. K., Ebright, R. H., & Reinberg, D. (2000). Mechanism of ATP-dependent promoter melting by transcription factor IIH. *Science, 288*(5470), 1418-1422. doi:10.1126/science.288.5470.1418

Kimura, M., Kotani, S., Hattori, T., Sumi, N., Yoshioka, T., Todokoro, K., & Okano, Y. (1997). Cell cycle-dependent expression and spindle pole localization of a novel human protein kinase, Aik, related to Aurora of Drosophila and yeast Ipl1. *J Biol Chem, 272*(21), 13766-13771. doi:10.1074/jbc.272.21.13766

Kindgren, P., Ivanov, M., & Marquardt, S. (2019). Native elongation transcript sequencing reveals temperature dependent dynamics of nascent RNAPII transcription in Arabidopsis. *Nucleic Acids Research, 48*(5), 2332-2347. doi:10.1093/nar/gkz1189

King, D., Li, X. D., Almeida, G. S., Kwok, C., Gravells, P., Harrison, D., . . . Bryant, H. E. (2020). MYCN expression induces replication stress and sensitivity to PARP inhibition in neuroblastoma. *Oncotarget, 11*(23), 2141-2159. doi:10.18632/oncotarget.27329

Kinzel, D., Boldt, K., Davis, E. E., Burtscher, I., Trumbach, D., Diplas, B., . . . Lickert, H. (2010). Pitchfork regulates primary cilia disassembly and left-right asymmetry. *Dev Cell, 19*(1), 66-77. doi:10.1016/j.devcel.2010.06.005

Knoepfler, P. S., Cheng, P. F., & Eisenman, R. N. (2002). N-myc is essential during neurogenesis for the rapid expansion of progenitor cell populations and the inhibition of neuronal differentiation. *Genes Dev, 16*(20), 2699-2712. doi:10.1101/gad.1021202

Knott, S. R. V., Viggiani, C. J., & Aparicio, O. M. (2009). To promote and protect: Coordinating DNA replication and transcription for genome stability. *Epigenetics, 4*(6), 362-365. doi:10.4161/epi.4.6.9712

Koch, H. B., Zhang, R., Verdoodt, B., Bailey, A., Zhang, C. D., Yates, J. R., 3rd, . . . Hermeking, H. (2007). Large-scale identification of c-MYC-associated proteins using a combined TAP/MudPIT approach. *Cell Cycle, 6*(2), 205-217. doi:10.4161/cc.6.2.3742

Kohl, N. E., Kanda, N., Schreck, R. R., Bruns, G., Latt, S. A., Gilbert, F., & Alt, F. W. (1983). Transposition and amplification of oncogene-related sequences in human neuroblastomas. *Cell, 35*(2 Pt 1), 359-367. doi:10.1016/0092-8674(83)90169-1

Kollareddy, M., Zheleva, D., Dzubak, P., Brahmkshatriya, P. S., Lepsik, M., & Hajduch, M. (2012). Aurora kinase inhibitors: progress towards the clinic. *Invest New Drugs, 30*(6), 2411-2432. doi:10.1007/s10637-012-9798-6

Koniaras, K., Cuddihy, A. R., Christopoulos, H., Hogg, A., & O'Connell, M. J. (2001). Inhibition of Chk1-dependent G2 DNA damage checkpoint radiosensitizes p53 mutant human cells. *Oncogene, 20*(51), 7453-7463. doi:10.1038/sj.onc.1204942

Koo, S. J., Fernández-Montalván, A. E., Badock, V., Ott, C. J., Holton, S. J., von Ahsen, O., . . . Gorjánácz, M. (2016). ATAD2 is an epigenetic reader of newly synthesized histone marks during DNA replication. *Oncotarget, 7*(43), 70323-70335. doi:10.18632/oncotarget.11855

Koopman, G., Reutelingsperger, C. P., Kuijten, G. A., Keehnen, R. M., Pals, S. T., & van Oers, M. H. (1994). Annexin V for flow cytometric detection of phosphatidylserine expression on B cells undergoing apoptosis. *Blood, 84*(5), 1415-1420. Retrieved from https://www.ncbi.nlm.nih.gov/pubmed/8068938

Koschmann, C., Calinescu, A. A., Nunez, F. J., Mackay, A., Fazal-Salom, J., Thomas, D., . . . Castro, M. G. (2016). ATRX loss promotes tumor growth and impairs nonhomologous end joining DNA repair in glioma. *Sci Transl Med, 8*(328), 328ra328. doi:10.1126/scitranslmed.aac8228

Koyama, H., Zhuang, T., Light, J. E., Kolla, V., Higashi, M., McGrady, P. W., . . . Brodeur, G. M. (2012). Mechanisms of CHD5 Inactivation in neuroblastomas. *Clin Cancer Res, 18*(6), 1588-1597. doi:10.1158/1078-0432.CCR-11-2644

Krajewska, M., Dries, R., Grassetti, A. V., Dust, S., Gao, Y., Huang, H., . . . George, R. E. (2019). CDK12 loss in cancer cells affects DNA damage response genes through premature cleavage and polyadenylation. *Nature Communications, 10*(1), 1757. doi:10.1038/s41467-019-09703-y

Kraus, W. L., & Lis, J. T. (2003). PARP goes transcription. *Cell, 113*(6), 677-683. doi:10.1016/s0092-8674(03)00433-1

Kress, T. L., & Guthrie, C. (2006). Molecular biology. Accurate RNA siting and splicing gets help from a DEK-hand. *Science, 312*(5782), 1886-1887. doi:10.1126/science.1130324

Krishna, T. S., Kong, X. P., Gary, S., Burgers, P. M., & Kuriyan, J. (1994). Crystal structure of the eukaryotic DNA polymerase processivity factor PCNA. *Cell, 79*(7), 1233-1243. doi:10.1016/0092-8674(94)90014-0

Kufer, T. A., Sillje, H. H., Korner, R., Gruss, O. J., Meraldi, P., & Nigg, E. A. (2002). Human TPX2 is required for targeting Aurora-A kinase to the spindle. *J Cell Biol, 158*(4), 617-623. doi:10.1083/jcb.200204155

Kunitoku, N., Sasayama, T., Marumoto, T., Zhang, D., Honda, S., Kobayashi, O., . . . Hirota, T. (2003). CENP-A phosphorylation by Aurora-A in prophase is required for enrichment of Aurora-B at inner centromeres and for kinetochore function. *Dev Cell, 5*(6), 853-864. doi:10.1016/s1534-5807(03)00364-2

Langmead, B., Trapnell, C., Pop, M., & Salzberg, S. L. (2009). Ultrafast and memory-efficient alignment of short DNA sequences to the human genome. *Genome Biol, 10*(3), R25. doi:10.1186/gb-2009-10-3-r25

Langston, L. D., Zhang, D., Yurieva, O., Georgescu, R. E., Finkelstein, J., Yao, N. Y., . . . O'Donnell, M. E. (2014). CMG helicase and DNA polymerase epsilon form a functional

15-subunit holoenzyme for eukaryotic leading-strand DNA replication. *Proc Natl Acad Sci U S A, 111*(43), 15390-15395. doi:10.1073/pnas.1418334111
Leeuwen, F. N., Kain, H. E., Kammen, R. A., Michiels, F., Kranenburg, O. W., & Collard, J. G. (1997). The guanine nucleotide exchange factor Tiam1 affects neuronal morphology; opposing roles for the small GTPases Rac and Rho. *J Cell Biol, 139*(3), 797-807. doi:10.1083/jcb.139.3.797
Lewis, L. M., Edwards, M. C., Meyers, Z. R., Talbot, C. C., Jr., Hao, H., Blum, D., . . . Errington, T. M. (2018). Replication Study: Transcriptional amplification in tumor cells with elevated c-Myc. *Elife, 7*. doi:10.7554/eLife.30274
Lewis, P. W., Elsaesser, S. J., Noh, K. M., Stadler, S. C., & Allis, C. D. (2010). Daxx is an H3.3-specific histone chaperone and cooperates with ATRX in replication-independent chromatin assembly at telomeres. *Proc Natl Acad Sci U S A, 107*(32), 14075-14080. doi:10.1073/pnas.1008850107
Liberzon, A., Subramanian, A., Pinchback, R., Thorvaldsdottir, H., Tamayo, P., & Mesirov, J. P. (2011). Molecular signatures database (MSigDB) 3.0. *Bioinformatics, 27*(12), 1739-1740. doi:10.1093/bioinformatics/btr260
Liigand, P., Kaupmees, K., & Kruve, A. (2019). Influence of the amino acid composition on the ionization efficiencies of small peptides. *J Mass Spectrom, 54*(6), 481-487. doi:10.1002/jms.4348
Liigand, P., Kaupmees, K., & Kruve, A. (2019). Influence of the amino acid composition on the ionization efficiencies of small peptides. *J Mass Spectrom, 54*(6), 481-487. doi:10.1002/jms.4348
Lim, K. H., Brady, D. C., Kashatus, D. F., Ancrile, B. B., Der, C. J., Cox, A. D., & Counter, C. M. (2010). Aurora-A phosphorylates, activates, and relocalizes the small GTPase RalA. *Mol Cell Biol, 30*(2), 508-523. doi:10.1128/MCB.00916-08
Lim, S. K., & Gopalan, G. (2007a). Antizyme1 mediates AURKAIP1-dependent degradation of Aurora-A. *Oncogene, 26*(46), 6593-6603. doi:10.1038/sj.onc.1210482
Lim, S. K., & Gopalan, G. (2007b). Aurora-A kinase interacting protein 1 (AURKAIP1) promotes Aurora-A degradation through an alternative ubiquitin-independent pathway. *Biochem J, 403*(1), 119-127. doi:10.1042/BJ20061272
Lin, C. Y., Lovén, J., Rahl, P. B., Paranal, R. M., Burge, C. B., Bradner, J. E., . . . Young, R. A. (2012). Transcriptional amplification in tumor cells with elevated c-Myc. *Cell, 151*(1), 56-67. doi:10.1016/j.cell.2012.08.026
Lin, S., Coutinho-Mansfield, G., Wang, D., Pandit, S., & Fu, X. D. (2008). The splicing factor SC35 has an active role in transcriptional elongation. *Nat Struct Mol Biol, 15*(8), 819-826. doi:10.1038/nsmb.1461
Lindon, C., Grant, R., & Min, M. (2015). Ubiquitin-Mediated Degradation of Aurora Kinases. *Front Oncol, 5*, 307. doi:10.3389/fonc.2015.00307
Lipford, J. R., & Bell, S. P. (2001). Nucleosomes positioned by ORC facilitate the initiation of DNA replication. *Mol Cell, 7*(1), 21-30. doi:10.1016/s1097-2765(01)00151-4
Littlepage, L. E., Wu, H., Andresson, T., Deanehan, J. K., Amundadottir, L. T., & Ruderman, J. V. (2002). Identification of phosphorylated residues that affect the activity of the mitotic kinase Aurora-A. *Proc Natl Acad Sci U S A, 99*(24), 15440-15445. doi:10.1073/pnas.202606599
Liu, Q., Kaneko, S., Yang, L., Feldman, R. I., Nicosia, S. V., Chen, J., & Cheng, J. Q. (2004). Aurora-A abrogation of p53 DNA binding and transactivation activity by phosphorylation of serine 215. *J Biol Chem, 279*(50), 52175-52182. doi:10.1074/jbc.M406802200
Liu, Y., Vidanes, G., Lin, Y. C., Mori, S., & Siede, W. (2000). Characterization of a Saccharomyces cerevisiae homologue of Schizosaccharomyces pombe Chk1 involved in DNA-damage-induced M-phase arrest. *Mol Gen Genet, 262*(6), 1132-1146. doi:10.1007/pl00008656
Lorenzin, F., Benary, U., Baluapuri, A., Walz, S., Jung, L. A., von Eyss, B., . . . Wolf, E. (2016). Different promoter affinities account for specificity in MYC-dependent gene regulation. *Elife, 5*. doi:10.7554/eLife.15161

Lovén, J., Orlando, D. A., Sigova, A. A., Lin, C. Y., Rahl, P. B., Burge, C. B., . . . Young, R. A. (2012). Revisiting global gene expression analysis. *Cell, 151*(3), 476-482. doi:10.1016/j.cell.2012.10.012

Lu, L. Y., Wood, J. L., Ye, L., Minter-Dykhouse, K., Saunders, T. L., Yu, X., & Chen, J. (2008). Aurora A is essential for early embryonic development and tumor suppression. *J Biol Chem, 283*(46), 31785-31790. doi:10.1074/jbc.M805880200

Lu, Y., Hu, Z., Mangala, L. S., Stine, Z. E., Hu, X., Jiang, D., . . . Dang, C. V. (2018). MYC Targeted Long Noncoding RNA DANCR Promotes Cancer in Part by Reducing p21 Levels. *Cancer Res, 78*(1), 64-74. doi:10.1158/0008-5472.CAN-17-0815

Luders, J., Patel, U. K., & Stearns, T. (2006). GCP-WD is a gamma-tubulin targeting factor required for centrosomal and chromatin-mediated microtubule nucleation. *Nat Cell Biol, 8*(2), 137-147. doi:10.1038/ncb1349

Ma, T., Van Tine, B. A., Wei, Y., Garrett, M. D., Nelson, D., Adams, P. D., . . . Harper, J. W. (2000). Cell cycle-regulated phosphorylation of p220(NPAT) by cyclin E/Cdk2 in Cajal bodies promotes histone gene transcription. *Genes Dev, 14*(18), 2298-2313. doi:10.1101/gad.829500

MacNeill, S. (2012). Composition and dynamics of the eukaryotic replisome: a brief overview. *Subcell Biochem, 62*, 1-17. doi:10.1007/978-94-007-4572-8_1

Mahajan, P. B. (1994). Modulation of transcription of rRNA genes by rapamycin. *Int J Immunopharmacol, 16*(9), 711-721. doi:10.1016/0192-0561(94)90091-4

Malumbres, M., & Barbacid, M. (2001). To cycle or not to cycle: a critical decision in cancer. *Nat Rev Cancer, 1*(3), 222-231. doi:10.1038/35106065

Malynn, B. A., de Alboran, I. M., O'Hagan, R. C., Bronson, R., Davidson, L., DePinho, R. A., & Alt, F. W. (2000). N-myc can functionally replace c-myc in murine development, cellular growth, and differentiation. *Genes Dev, 14*(11), 1390-1399. Retrieved from https://www.ncbi.nlm.nih.gov/pubmed/10837031

Mandriota, S. J., Valentijn, L. J., Lesne, L., Betts, D. R., Marino, D., Boudal-Khoshbeen, M., . . . Gumy-Pause, F. (2015). Ataxia-telangiectasia mutated (ATM) silencing promotes neuroblastoma progression through a MYCN independent mechanism. *Oncotarget, 6*(21), 18558-18576. doi:10.18632/oncotarget.4061

Manfredi, M. G., Ecsedy, J. A., Chakravarty, A., Silverman, L., Zhang, M., Hoar, K. M., . . . Sells, T. B. (2011). Characterization of Alisertib (MLN8237), an investigational small-molecule inhibitor of aurora A kinase using novel in vivo pharmacodynamic assays. *Clin Cancer Res, 17*(24), 7614-7624. doi:10.1158/1078-0432.CCR-11-1536

Marahrens, Y., & Stillman, B. (1992). A yeast chromosomal origin of DNA replication defined by multiple functional elements. *Science, 255*(5046), 817-823. doi:10.1126/science.1536007

Maris, J. M., Hogarty, M. D., Bagatell, R., & Cohn, S. L. (2007). Neuroblastoma. *Lancet, 369*(9579), 2106-2120. doi:10.1016/S0140-6736(07)60983-0

Maris, J. M., & Matthay, K. K. (1999). Molecular biology of neuroblastoma. *J Clin Oncol, 17*(7), 2264-2279. doi:10.1200/JCO.1999.17.7.2264

Marsico, G., Chambers, V. S., Sahakyan, A. B., McCauley, P., Boutell, J. M., Antonio, M. D., & Balasubramanian, S. (2019). Whole genome experimental maps of DNA G-quadruplexes in multiple species. *Nucleic Acids Research, 47*(8), 3862-3874. doi:10.1093/nar/gkz179

Martin, D. E., Soulard, A., & Hall, M. N. (2004). TOR regulates ribosomal protein gene expression via PKA and the Forkhead transcription factor FHL1. *Cell, 119*(7), 969-979. doi:10.1016/j.cell.2004.11.047

Marumoto, T., Hirota, T., Morisaki, T., Kunitoku, N., Zhang, D., Ichikawa, Y., . . . Saya, H. (2002). Roles of aurora-A kinase in mitotic entry and G2 checkpoint in mammalian cells. *Genes Cells, 7*(11), 1173-1182. doi:10.1046/j.1365-2443.2002.00592.x

Marumoto, T., Honda, S., Hara, T., Nitta, M., Hirota, T., Kohmura, E., & Saya, H. (2003). Aurora-A kinase maintains the fidelity of early and late mitotic events in HeLa cells. *J Biol Chem, 278*(51), 51786-51795. doi:10.1074/jbc.M306275200

Marumoto, T., Zhang, D., & Saya, H. (2005). Aurora-A - a guardian of poles. *Nat Rev Cancer, 5*(1), 42-50. doi:10.1038/nrc1526
Masai, H., Matsumoto, S., You, Z., Yoshizawa-Sugata, N., & Oda, M. (2010). Eukaryotic chromosome DNA replication: where, when, and how? *Annu Rev Biochem, 79*, 89-130. doi:10.1146/annurev.biochem.052308.103205
Massimino, M., Biassoni, V., Gandola, L., Garre, M. L., Gatta, G., Giangaspero, F., . . . Rutkowski, S. (2016). Childhood medulloblastoma. *Crit Rev Oncol Hematol, 105*, 35-51. doi:10.1016/j.critrevonc.2016.05.012
Mathsyaraja, H., Freie, B., Cheng, P. F., Babaeva, E., Catchpole, J. T., Janssens, D., . . . Eisenman, R. N. (2019). Max deletion destabilizes MYC protein and abrogates Emicro-Myc lymphomagenesis. *Genes Dev, 33*(17-18), 1252-1264. doi:10.1101/gad.325878.119
Matsuo, N., Terao, M., Nabeshima, Y., & Hoshino, M. (2003). Roles of STEF/Tiam1, guanine nucleotide exchange factors for Rac1, in regulation of growth cone morphology. *Mol Cell Neurosci, 24*(1), 69-81. doi:10.1016/s1044-7431(03)00122-2
Matsuoka, S., Rotman, G., Ogawa, A., Shiloh, Y., Tamai, K., & Elledge, S. J. (2000). Ataxia telangiectasia-mutated phosphorylates Chk2 in vivo and in vitro. *Proc Natl Acad Sci U S A, 97*(19), 10389-10394. doi:10.1073/pnas.190030497
McMahon, S. B., Van Buskirk, H. A., Dugan, K. A., Copeland, T. D., & Cole, M. D. (1998). The novel ATM-related protein TRRAP is an essential cofactor for the c-Myc and E2F oncoproteins. *Cell, 94*(3), 363-374. doi:10.1016/s0092-8674(00)81479-8
McMahon, S. B., Wood, M. A., & Cole, M. D. (2000). The essential cofactor TRRAP recruits the histone acetyltransferase hGCN5 to c-Myc. *Mol Cell Biol, 20*(2), 556-562. doi:10.1128/mcb.20.2.556-562.2000
Meerbrey, K. L., Hu, G., Kessler, J. D., Roarty, K., Li, M. Z., Fang, J. E., . . . Elledge, S. J. (2011). The pINDUCER lentiviral toolkit for inducible RNA interference in vitro and in vivo. *Proc Natl Acad Sci U S A, 108*(9), 3665-3670. doi:10.1073/pnas.1019736108
Melichar, B., Adenis, A., Lockhart, A. C., Bennouna, J., Dees, E. C., Kayaleh, O., . . . Schusterbauer, C. (2015). Safety and activity of alisertib, an investigational aurora kinase A inhibitor, in patients with breast cancer, small-cell lung cancer, non-small-cell lung cancer, head and neck squamous-cell carcinoma, and gastro-oesophageal adenocarcinoma: a five-arm phase 2 study. *Lancet Oncol, 16*(4), 395-405. doi:10.1016/S1470-2045(15)70051-3
Meraldi, P., Honda, R., & Nigg, E. A. (2002). Aurora-A overexpression reveals tetraploidization as a major route to centrosome amplification in p53-/- cells. *EMBO J, 21*(4), 483-492. doi:10.1093/emboj/21.4.483
Merkhofer, E. C., Hu, P., & Johnson, T. L. (2014). Introduction to cotranscriptional RNA splicing. *Methods in molecular biology (Clifton, N.J.), 1126*, 83-96. doi:10.1007/978-1-62703-980-2_6
Meryet-Figuiere, M., Alaei-Mahabadi, B., Ali, M. M., Mitra, S., Subhash, S., Pandey, G. K., . . . Kanduri, C. (2014). Temporal separation of replication and transcription during S-phase progression. *Cell cycle (Georgetown, Tex.), 13*(20), 3241-3248. doi:10.4161/15384101.2014.953876
Min, M., Mayor, U., & Lindon, C. (2013). Ubiquitination site preferences in anaphase promoting complex/cyclosome (APC/C) substrates. *Open Biol, 3*(9), 130097. doi:10.1098/rsob.130097
Minn, A. J., Boise, L. H., & Thompson, C. B. (1996). Expression of Bcl-xL and loss of p53 can cooperate to overcome a cell cycle checkpoint induced by mitotic spindle damage. *Genes Dev, 10*(20), 2621-2631. doi:10.1101/gad.10.20.2621
Molenaar, J. J., Koster, J., Zwijnenburg, D. A., van Sluis, P., Valentijn, L. J., van der Ploeg, I., . . . Versteeg, R. (2012). Sequencing of neuroblastoma identifies chromothripsis and defects in neuritogenesis genes. *Nature, 483*(7391), 589-593. doi:10.1038/nature10910

Monier, K., Mouradian, S., & Sullivan, K. F. (2007). DNA methylation promotes Aurora-B-driven phosphorylation of histone H3 in chromosomal subdomains. *J Cell Sci, 120*(Pt 1), 101-114. doi:10.1242/jcs.03326

Moore, M. J., Wang, Q., Kennedy, C. J., & Silver, P. A. (2010). An alternative splicing network links cell-cycle control to apoptosis. *Cell, 142*(4), 625-636. doi:10.1016/j.cell.2010.07.019

Mori, D., Yamada, M., Mimori-Kiyosue, Y., Shirai, Y., Suzuki, A., Ohno, S., . . . Hirotsune, S. (2009). An essential role of the aPKC-Aurora A-NDEL1 pathway in neurite elongation by modulation of microtubule dynamics. *Nat Cell Biol, 11*(9), 1057-1068. doi:10.1038/ncb1919

Mori, D., Yano, Y., Toyo-oka, K., Yoshida, N., Yamada, M., Muramatsu, M., . . . Hirotsune, S. (2007). NDEL1 phosphorylation by Aurora-A kinase is essential for centrosomal maturation, separation, and TACC3 recruitment. *Mol Cell Biol, 27*(1), 352-367. doi:10.1128/MCB.00878-06

Mori, S., & Shirahige, K. (2007). Perturbation of the activity of replication origin by meiosis-specific transcription. *J Biol Chem, 282*(7), 4447-4452. doi:10.1074/jbc.M609671200

Moroz, V., Machin, D., Faldum, A., Hero, B., Iehara, T., Mosseri, V., . . . London, W. B. (2011). Changes over three decades in outcome and the prognostic influence of age-at-diagnosis in young patients with neuroblastoma: a report from the International Neuroblastoma Risk Group Project. *Eur J Cancer, 47*(4), 561-571. doi:10.1016/j.ejca.2010.10.022

Mosse, Y. P., Fox, E., Teachey, D. T., Reid, J. M., Safgren, S. L., Carol, H., . . . Weigel, B. J. (2019). A Phase II Study of Alisertib in Children with Recurrent/Refractory Solid Tumors or Leukemia: Children's Oncology Group Phase I and Pilot Consortium (ADVL0921). *Clin Cancer Res, 25*(11), 3229-3238. doi:10.1158/1078-0432.CCR-18-2675

Mosse, Y. P., Laudenslager, M., Khazi, D., Carlisle, A. J., Winter, C. L., Rappaport, E., & Maris, J. M. (2004). Germline PHOX2B mutation in hereditary neuroblastoma. *Am J Hum Genet, 75*(4), 727-730. doi:10.1086/424530

Mosse, Y. P., Laudenslager, M., Longo, L., Cole, K. A., Wood, A., Attiyeh, E. F., . . . Maris, J. M. (2008). Identification of ALK as a major familial neuroblastoma predisposition gene. *Nature, 455*(7215), 930-935. doi:10.1038/nature07261

Muller, H., Schmidt, D., Steinbrink, S., Mirgorodskaya, E., Lehmann, V., Habermann, K., . . . Lange, B. M. (2010). Proteomic and functional analysis of the mitotic Drosophila centrosome. *EMBO J, 29*(19), 3344-3357. doi:10.1038/emboj.2010.210

Muncan, V., Sansom, O. J., Tertoolen, L., Phesse, T. J., Begthel, H., Sancho, E., . . . Clarke, A. R. (2006). Rapid loss of intestinal crypts upon conditional deletion of the Wnt/Tcf-4 target gene c-Myc. *Mol Cell Biol, 26*(22), 8418-8426. doi:10.1128/MCB.00821-06

Muse, G. W., Gilchrist, D. A., Nechaev, S., Shah, R., Parker, J. S., Grissom, S. F., . . . Adelman, K. (2007). RNA polymerase is poised for activation across the genome. *Nat Genet, 39*(12), 1507-1511. doi:10.1038/ng.2007.21

Nair, S. K., & Burley, S. K. (2003). X-ray structures of Myc-Max and Mad-Max recognizing DNA. Molecular bases of regulation by proto-oncogenic transcription factors. *Cell, 112*(2), 193-205. doi:10.1016/s0092-8674(02)01284-9

Nau, M. M., Brooks, B. J., Battey, J., Sausville, E., Gazdar, A. F., Kirsch, I. R., . . . Minna, J. D. (1985). L-myc, a new myc-related gene amplified and expressed in human small cell lung cancer. *Nature, 318*(6041), 69-73. doi:10.1038/318069a0

NB97, Neuroblastomstudie (2002)

Nesbit, C. E., Tersak, J. M., & Prochownik, E. V. (1999). MYC oncogenes and human neoplastic disease. *Oncogene, 18*(19), 3004-3016. doi:10.1038/sj.onc.1202746

Ngan, E. S. (2015). Heterogeneity of neuroblastoma. *Oncoscience, 2*(10), 837-838. doi:10.18632/oncoscience.216

Nguyen, H. D., Leong, W. Y., Li, W., Reddy, P. N. G., Sullivan, J. D., Walter, M. J., . . . Graubert, T. A. (2018). Spliceosome Mutations Induce R Loop-Associated Sensitivity to ATR

Inhibition in Myelodysplastic Syndromes. *Cancer Res, 78*(18), 5363-5374. doi:10.1158/0008-5472.CAN-17-3970
Nguyen, H. G., Chinnappan, D., Urano, T., & Ravid, K. (2005). Mechanism of Aurora-B degradation and its dependency on intact KEN and A-boxes: identification of an aneuploidy-promoting property. *Mol Cell Biol, 25*(12), 4977-4992. doi:10.1128/MCB.25.12.4977-4992.2005
Nicol, J. W., Helt, G. A., Blanchard, S. G., Jr., Raja, A., & Loraine, A. E. (2009). The Integrated Genome Browser: free software for distribution and exploration of genome-scale datasets. *Bioinformatics, 25*(20), 2730-2731. doi:10.1093/bioinformatics/btp472
Nie, Z., Hu, G., Wei, G., Cui, K., Yamane, A., Resch, W., . . . Levens, D. (2012). c-Myc is a universal amplifier of expressed genes in lymphocytes and embryonic stem cells. *Cell, 151*(1), 68-79. doi:10.1016/j.cell.2012.08.033
Niehrs, C., & Luke, B. (2020). Regulatory R-loops as facilitators of gene expression and genome stability. *Nature Reviews Molecular Cell Biology, 21*(3), 167-178. doi:10.1038/s41580-019-0206-3
Nigg, E. A. (1995). Cyclin-dependent protein kinases: key regulators of the eukaryotic cell cycle. *Bioessays, 17*(6), 471-480. doi:10.1002/bies.950170603
Nigg, E. A. (2001). Mitotic kinases as regulators of cell division and its checkpoints. *Nat Rev Mol Cell Biol, 2*(1), 21-32. doi:10.1038/35048096
Nikonova, A. S., Astsaturov, I., Serebriiskii, I. G., Dunbrack, R. L., Jr., & Golemis, E. A. (2013). Aurora A kinase (AURKA) in normal and pathological cell division. *Cell Mol Life Sci, 70*(4), 661-687. doi:10.1007/s00018-012-1073-7
Nowacki, S., Skowron, M., Oberthuer, A., Fagin, A., Voth, H., Brors, B., . . . Fischer, M. (2008). Expression of the tumour suppressor gene CADM1 is associated with favourable outcome and inhibits cell survival in neuroblastoma. *Oncogene, 27*(23), 3329-3338. doi:10.1038/sj.onc.1210996
Nowotny, M., Cerritelli, S. M., Ghirlando, R., Gaidamakov, S. A., Crouch, R. J., & Yang, W. (2008). Specific recognition of RNA/DNA hybrid and enhancement of human RNase H1 activity by HBD. *EMBO J, 27*(7), 1172-1181. doi:10.1038/emboj.2008.44
Okamoto, Y., Abe, M., Itaya, A., Tomida, J., Ishiai, M., Takaori-Kondo, A., . . . Takata, M. (2019). FANCD2 protects genome stability by recruiting RNA processing enzymes to resolve R-loops during mild replication stress. *Febs j, 286*(1), 139-150. doi:10.1111/febs.14700
Okuda, M., Horn, H. F., Tarapore, P., Tokuyama, Y., Smulian, A. G., Chan, P. K., . . . Fukasawa, K. (2000). Nucleophosmin/B23 is a target of CDK2/cyclin E in centrosome duplication. *Cell, 103*(1), 127-140. doi:10.1016/s0092-8674(00)00093-3
Olson, C. M., Jiang, B., Erb, M. A., Liang, Y., Doctor, Z. M., Zhang, Z., . . . Gray, N. S. (2018). Pharmacological perturbation of CDK9 using selective CDK9 inhibition or degradation. *Nat Chem Biol, 14*(2), 163-170. doi:10.1038/nchembio.2538
Otto, T., Horn, S., Brockmann, M., Eilers, U., Schuttrumpf, L., Popov, N., . . . Eilers, M. (2009). Stabilization of N-Myc is a critical function of Aurora A in human neuroblastoma. *Cancer Cell, 15*(1), 67-78. doi:10.1016/j.ccr.2008.12.005
Otto, T., & Sicinski, P. (2017). Cell cycle proteins as promising targets in cancer therapy. *Nat Rev Cancer, 17*(2), 93-115. doi:10.1038/nrc.2016.138
Park, S. H., Kang, N., Song, E., Wie, M., Lee, E. A., Hwang, S., . . . Myung, K. (2019). ATAD5 promotes replication restart by regulating RAD51 and PCNA in response to replication stress. *Nature Communications, 10*(1), 5718. doi:10.1038/s41467-019-13667-4
Pattyn, A., Morin, X., Cremer, H., Goridis, C., & Brunet, J. F. (1999). The homeobox gene Phox2b is essential for the development of autonomic neural crest derivatives. *Nature, 399*(6734), 366-370. doi:10.1038/20700
Peifer, M., Hertwig, F., Roels, F., Dreidax, D., Gartlgruber, M., Menon, R., . . . Fischer, M. (2015). Telomerase activation by genomic rearrangements in high-risk neuroblastoma. *Nature, 526*(7575), 700-704. doi:10.1038/nature14980

Peng, J., Marshall, N. F., & Price, D. H. (1998). Identification of a cyclin subunit required for the function of Drosophila P-TEFb. *J Biol Chem, 273*(22), 13855-13860. doi:10.1074/jbc.273.22.13855

Petersen, B. O., Lukas, J., Sorensen, C. S., Bartek, J., & Helin, K. (1999). Phosphorylation of mammalian CDC6 by cyclin A/CDK2 regulates its subcellular localization. *EMBO J, 18*(2), 396-410. doi:10.1093/emboj/18.2.396

Pillay, N., Tighe, A., Nelson, L., Littler, S., Coulson-Gilmer, C., Bah, N., . . . Taylor, S. S. (2019). DNA Replication Vulnerabilities Render Ovarian Cancer Cells Sensitive to Poly(ADP-Ribose) Glycohydrolase Inhibitors. *Cancer Cell, 35*(3), 519-533.e518. doi:10.1016/j.ccell.2019.02.004

Pinyol, R., Scrofani, J., & Vernos, I. (2013). The role of NEDD1 phosphorylation by Aurora A in chromosomal microtubule nucleation and spindle function. *Curr Biol, 23*(2), 143-149. doi:10.1016/j.cub.2012.11.046

Plotnikova, O. V., Nikonova, A. S., Loskutov, Y. V., Kozyulina, P. Y., Pugacheva, E. N., & Golemis, E. A. (2012). Calmodulin activation of Aurora-A kinase (AURKA) is required during ciliary disassembly and in mitosis. *Mol Biol Cell, 23*(14), 2658-2670. doi:10.1091/mbc.E11-12-1056

Plotnikova, O. V., Pugacheva, E. N., Dunbrack, R. L., & Golemis, E. A. (2010). Rapid calcium-dependent activation of Aurora-A kinase. *Nat Commun, 1*, 64. doi:10.1038/ncomms1061

Polioudaki, H., Markaki, Y., Kourmouli, N., Dialynas, G., Theodoropoulos, P. A., Singh, P. B., & Georgatos, S. D. (2004). Mitotic phosphorylation of histone H3 at threonine 3. *FEBS Lett, 560*(1-3), 39-44. doi:10.1016/S0014-5793(04)00060-2

Porrua, O., & Libri, D. (2015). Transcription termination and the control of the transcriptome: why, where and how to stop. *Nat Rev Mol Cell Biol, 16*(3), 190-202. doi:10.1038/nrm3943

Prendergast, G. C., & Ziff, E. B. (1991). Methylation-sensitive sequence-specific DNA binding by the c-Myc basic region. *Science, 251*(4990), 186-189. doi:10.1126/science.1987636

ProteinAtlas: URL: http//www.proteinatlas.org/ : (10.01.2021)

Pugacheva, E. N., Jablonski, S. A., Hartman, T. R., Henske, E. P., & Golemis, E. A. (2007). HEF1-dependent Aurora A activation induces disassembly of the primary cilium. *Cell, 129*(7), 1351-1363. doi:10.1016/j.cell.2007.04.035

Pulverer, B. J., Fisher, C., Vousden, K., Littlewood, T., Evan, G., & Woodgett, J. R. (1994). Site-specific modulation of c-Myc cotransformation by residues phosphorylated in vivo. *Oncogene, 9*(1), 59-70. Retrieved from https://www.ncbi.nlm.nih.gov/pubmed/8302604

Qi, W., Cooke, L. S., Liu, X., Rimsza, L., Roe, D. J., Manziolli, A., . . . Mahadevan, D. (2011). Aurora inhibitor MLN8237 in combination with docetaxel enhances apoptosis and anti-tumor activity in mantle cell lymphoma. *Biochemical pharmacology, 81*(7), 881-890. doi:10.1016/j.bcp.2011.01.017

Qiu, S., Liu, J., & Xing, F. (2017). Antizyme inhibitor 1: a potential carcinogenic molecule. *Cancer Sci, 108*(2), 163-169. doi:10.1111/cas.13122

Quinlan, A. R. (2014). BEDTools: The Swiss-Army Tool for Genome Feature Analysis. *Curr Protoc Bioinformatics, 47*, 11 12 11-34. doi:10.1002/0471250953.bi1112s47

Raabe, E. H., Laudenslager, M., Winter, C., Wasserman, N., Cole, K., LaQuaglia, M., . . . Maris, J. M. (2008). Prevalence and functional consequence of PHOX2B mutations in neuroblastoma. *Oncogene, 27*(4), 469-476. doi:10.1038/sj.onc.1210659

Ray-Gallet, D., Woolfe, A., Vassias, I., Pellentz, C., Lacoste, N., Puri, A., . . . Almouzni, G. (2011). Dynamics of histone H3 deposition in vivo reveal a nucleosome gap-filling mechanism for H3.3 to maintain chromatin integrity. *Mol Cell, 44*(6), 928-941. doi:10.1016/j.molcel.2011.12.006

Ray Chaudhuri, A., & Nussenzweig, A. (2017). The multifaceted roles of PARP1 in DNA repair and chromatin remodelling. *Nat Rev Mol Cell Biol, 18*(10), 610-621. doi:10.1038/nrm.2017.53

Reboutier, D., Troadec, M. B., Cremet, J. Y., Fukasawa, K., & Prigent, C. (2012). Nucleophosmin/B23 activates Aurora A at the centrosome through phosphorylation of serine 89. *J Cell Biol, 197*(1), 19-26. doi:10.1083/jcb.201107134

Reppas, N. B., Wade, J. T., Church, G. M., & Struhl, K. (2006). The transition between transcriptional initiation and elongation in E. coli is highly variable and often rate limiting. *Mol Cell, 24*(5), 747-757. doi:10.1016/j.molcel.2006.10.030

Richard, P., Feng, S., & Manley, J. L. (2013). A SUMO-dependent interaction between Senataxin and the exosome, disrupted in the neurodegenerative disease AOA2, targets the exosome to sites of transcription-induced DNA damage. *Genes Dev, 27*(20), 2227-2232. doi:10.1101/gad.224923.113

Richards, M. W., Burgess, S. G., Poon, E., Carstensen, A., Eilers, M., Chesler, L., & Bayliss, R. (2016). Structural basis of N-Myc binding by Aurora-A and its destabilization by kinase inhibitors. *Proc Natl Acad Sci U S A, 113*(48), 13726-13731. doi:10.1073/pnas.1610626113

Richie, C. T., & Golden, A. (2005). Chromosome segregation: Aurora B gets Tousled. *Curr Biol, 15*(10), R379-382. doi:10.1016/j.cub.2005.05.009

Ries, L. A. G., & SEER Program (National Cancer Institute (U.S.)). (1999). *Cancer incidence and survival among children and adolescents : United States SEER program 1975-1995 /[edited by Lynn A. Gloecker Ries ... et al.]*. Bethesda, MD: National Cancer Institute, SEER Program.

Ritchie, M. E., Phipson, B., Wu, D., Hu, Y., Law, C. W., Shi, W., & Smyth, G. K. (2015). limma powers differential expression analyses for RNA-sequencing and microarray studies. *Nucleic Acids Res, 43*(7), e47. doi:10.1093/nar/gkv007

Roderwieser, A., Sand, F., Walter, E., Fischer, J., Gecht, J., Bartenhagen, C., . . . Fischer, M. (2019). Telomerase Is a Prognostic Marker of Poor Outcome and a Therapeutic Target in Neuroblastoma. *JCO Precision Oncology*(3), 1-20. doi:10.1200/po.19.00072

Roeschert, I., Poon, E., Henssen, A. G., Dorado Garcia, H., Gatti, M., Giansanti, C., . . . Büchel, G., Eilers, M. (2021). Combined inhibition of Aurora-A and ATR kinases results in regression of MYCN-amplified neuroblastoma. *Nature Cancer*. doi:10.1038/s43018-020-00171-8

Roghi, C., Giet, R., Uzbekov, R., Morin, N., Chartrain, I., Le Guellec, R., . . . Prigent, C. (1998). The Xenopus protein kinase pEg2 associates with the centrosome in a cell cycle-dependent manner, binds to the spindle microtubules and is involved in bipolar mitotic spindle assembly. *J Cell Sci, 111 (Pt 5)*, 557-572. Retrieved from https://www.ncbi.nlm.nih.gov/pubmed/9454730

Ronson, G. E., Piberger, A. L., Higgs, M. R., Olsen, A. L., Stewart, G. S., McHugh, P. J., . . . Lakin, N. D. (2018). PARP1 and PARP2 stabilise replication forks at base excision repair intermediates through Fbh1-dependent Rad51 regulation. *Nat Commun, 9*(1), 746. doi:10.1038/s41467-018-03159-2

Rosenthal, A., Kumar, S., Hofmeister, C., Laubach, J., Vij, R., Dueck, A., . . . Stewart, A. K. (2016). A Phase Ib Study of the combination of the Aurora Kinase Inhibitor Alisertib (MLN8237) and Bortezomib in Relapsed Multiple Myeloma. *British journal of haematology, 174*(2), 323-325. doi:10.1111/bjh.13765

Rowbotham, S. P., Barki, L., Neves-Costa, A., Santos, F., Dean, W., Hawkes, N., . . . Mermoud, J. E. (2011). Maintenance of silent chromatin through replication requires SWI/SNF-like chromatin remodeler SMARCAD1. *Mol Cell, 42*(3), 285-296. doi:10.1016/j.molcel.2011.02.036

Ruffner, H., & Verma, I. M. (1997). BRCA1 is a cell cycle-regulated nuclear phosphoprotein. *Proc Natl Acad Sci U S A, 94*(14), 7138-7143. doi:10.1073/pnas.94.14.7138

Sabò, A., Kress, T. R., Pelizzola, M., de Pretis, S., Gorski, M. M., Tesi, A., . . . Amati, B. (2014). Selective transcriptional regulation by Myc in cellular growth control and lymphomagenesis. *Nature, 511*(7510), 488-492. doi:10.1038/nature13537

Saito-Ohara, F., Imoto, I., Inoue, J., Hosoi, H., Nakagawara, A., Sugimoto, T., & Inazawa, J. (2003). PPM1D is a potential target for 17q gain in neuroblastoma. *Cancer Res, 63*(8), 1876-1883. Retrieved from https://www.ncbi.nlm.nih.gov/pubmed/12702577

Saldi, T., Cortazar, M. A., Sheridan, R. M., & Bentley, D. L. (2016). Coupling of RNA Polymerase II Transcription Elongation with Pre-mRNA Splicing. *J Mol Biol, 428*(12), 2623-2635. doi:10.1016/j.jmb.2016.04.017

Saldivar, J. C., Cortez, D., & Cimprich, K. A. (2017). The essential kinase ATR: ensuring faithful duplication of a challenging genome. *Nat Rev Mol Cell Biol, 18*(10), 622-636. doi:10.1038/nrm.2017.67

Sano, H., Bonadio, J., Gerbing, R. B., London, W. B., Matthay, K. K., Lukens, J. N., & Shimada, H. (2006). International neuroblastoma pathology classification adds independent prognostic information beyond the prognostic contribution of age. *Eur J Cancer, 42*(8), 1113-1119. doi:10.1016/j.ejca.2005.11.031

Sanso, M., Levin, R. S., Lipp, J. J., Wang, V. Y., Greifenberg, A. K., Quezada, E. M., . . . Fisher, R. P. (2016). P-TEFb regulation of transcription termination factor Xrn2 revealed by a chemical genetic screen for Cdk9 substrates. *Genes Dev, 30*(1), 117-131. doi:10.1101/gad.269589.115

Sardon, T., Pache, R. A., Stein, A., Molina, H., Vernos, I., & Aloy, P. (2010). Uncovering new substrates for Aurora A kinase. *EMBO Rep, 11*(12), 977-984. doi:10.1038/embor.2010.171

Sasai, K., Parant, J. M., Brandt, M. E., Carter, J., Adams, H. P., Stass, S. A., . . . Sen, S. (2008). Targeted disruption of Aurora A causes abnormal mitotic spindle assembly, chromosome misalignment and embryonic lethality. *Oncogene, 27*(29), 4122-4127. doi:10.1038/onc.2008.47

Sausen, M., Leary, R. J., Jones, S., Wu, J., Reynolds, C. P., Liu, X., . . . Hogarty, M. D. (2013). Integrated genomic analyses identify ARID1A and ARID1B alterations in the childhood cancer neuroblastoma. *Nat Genet, 45*(1), 12-17. doi:10.1038/ng.2493

Sawatsubashi, S., Murata, T., Lim, J., Fujiki, R., Ito, S., Suzuki, E., . . . Kato, S. (2010). A histone chaperone, DEK, transcriptionally coactivates a nuclear receptor. *Genes Dev, 24*(2), 159-170. doi:10.1101/gad.1857410

Sawicka, A., & Seiser, C. (2012). Histone H3 phosphorylation - a versatile chromatin modification for different occasions. *Biochimie, 94*(11), 2193-2201. doi:10.1016/j.biochi.2012.04.018

Schaub, F. X., Dhankani, V., Berger, A. C., Trivedi, M., Richardson, A. B., Shaw, R., . . . Cancer Genome Atlas, N. (2018). Pan-cancer Alterations of the MYC Oncogene and Its Proximal Network across the Cancer Genome Atlas. *Cell Syst, 6*(3), 282-300 e282. doi:10.1016/j.cels.2018.03.003

Schmittgen, T. D., & Livak, K. J. (2008). Analyzing real-time PCR data by the comparative C(T) method. *Nat Protoc, 3*(6), 1101-1108. doi:10.1038/nprot.2008.73

Schnepp, R. W., Khurana, P., Attiyeh, E. F., Raman, P., Chodosh, S. E., Oldridge, D. A., . . . Diskin, S. J. (2015). A LIN28B-RAN-AURKA Signaling Network Promotes Neuroblastoma Tumorigenesis. *Cancer Cell, 28*(5), 599-609. doi:10.1016/j.ccell.2015.09.012

Schukur, L., Zimmermann, T., Niewoehner, O., Kerr, G., Gleim, S., Bauer-Probst, B., . . . Thoma, C. R. (2020). Identification of the HECT E3 ligase UBR5 as a regulator of MYC degradation using a CRISPR/Cas9 screen. *Scientific Reports, 10*(1), 20044. doi:10.1038/s41598-020-76960-z

Schulte, J. H., & Eggert, A. (2015). Neuroblastoma. *Crit Rev Oncog, 20*(3-4), 245-270. doi:10.1615/critrevoncog.2015014033

Schulze, A., Zerfass, K., Spitkovsky, D., Middendorp, S., Berges, J., Helin, K., . . . Henglein, B. (1995). Cell cycle regulation of the cyclin A gene promoter is mediated by a variant E2F site. *Proc Natl Acad Sci U S A, 92*(24), 11264-11268. doi:10.1073/pnas.92.24.11264

Schvartzman, J. B., Krimer, D. B., & Van't Hof, J. (1984). The effects of different thymidine concentrations on DNA replication in pea-root cells synchronized by a protracted 5-fluorodeoxyuridine treatment. *Exp Cell Res, 150*(2), 379-389. doi:10.1016/0014-4827(84)90581-0

Schwab, M., Westermann, F., Hero, B., & Berthold, F. (2003). Neuroblastoma: biology and molecular and chromosomal pathology. *Lancet Oncol, 4*(8), 472-480. doi:10.1016/s1470-2045(03)01166-5

Schwartz, D., & Rotter, V. (1998). p53-dependent cell cycle control: response to genotoxic stress. *Semin Cancer Biol, 8*(5), 325-336. doi:10.1006/scbi.1998.0095

Seeger, R. C., Brodeur, G. M., Sather, H., Dalton, A., Siegel, S. E., Wong, K. Y., & Hammond, D. (1985). Association of multiple copies of the N-myc oncogene with rapid progression of neuroblastomas. *N Engl J Med, 313*(18), 1111-1116. doi:10.1056/NEJM198510313131802

Seki, A., Coppinger, J. A., Jang, C. Y., Yates, J. R., & Fang, G. (2008). Bora and the kinase Aurora a cooperatively activate the kinase Plk1 and control mitotic entry. *Science, 320*(5883), 1655-1658. doi:10.1126/science.1157425

Sen, S., Zhou, H., Zhang, R. D., Yoon, D. S., Vakar-Lopez, F., Ito, S., . . . Czerniak, B. (2002). Amplification/overexpression of a mitotic kinase gene in human bladder cancer. *J Natl Cancer Inst, 94*(17), 1320-1329. doi:10.1093/jnci/94.17.1320

Sever-Chroneos, Z., Angus, S. P., Fribourg, A. F., Wan, H., Todorov, I., Knudsen, K. E., & Knudsen, E. S. (2001). Retinoblastoma tumor suppressor protein signals through inhibition of cyclin-dependent kinase 2 activity to disrupt PCNA function in S phase. *Mol Cell Biol, 21*(12), 4032-4045. doi:10.1128/MCB.21.12.4032-4045.2001

Shang, X., Burlingame, S. M., Okcu, M. F., Ge, N., Russell, H. V., Egler, R. A., . . . Nuchtern, J. G. (2009). Aurora A is a negative prognostic factor and a new therapeutic target in human neuroblastoma. *Mol Cancer Ther, 8*(8), 2461-2469. doi:10.1158/1535-7163.MCT-08-0857

Shao, W., & Zeitlinger, J. (2017). Paused RNA polymerase II inhibits new transcriptional initiation. *Nat Genet, 49*(7), 1045-1051. doi:10.1038/ng.3867

Sheiness, D., & Bishop, J. M. (1979). DNA and RNA from uninfected vertebrate cells contain nucleotide sequences related to the putative transforming gene of avian myelocytomatosis virus. *J Virol, 31*(2), 514-521. doi:10.1128/JVI.31.2.514-521.1979

Shen, L., Shao, N., Liu, X., & Nestler, E. (2014). ngs.plot: Quick mining and visualization of next-generation sequencing data by integrating genomic databases. *BMC Genomics, 15*, 284. doi:10.1186/1471-2164-15-284

Shi, J., & Vakoc, C. R. (2014). The mechanisms behind the therapeutic activity of BET bromodomain inhibition. *Mol Cell, 54*(5), 728-736. doi:10.1016/j.molcel.2014.05.016

Shimada, H., Ambros, I. M., Dehner, L. P., Hata, J., Joshi, V. V., Roald, B., . . . Castleberry, R. P. (1999). The International Neuroblastoma Pathology Classification (the Shimada system). *Cancer, 86*(2), 364-372. Retrieved from https://www.ncbi.nlm.nih.gov/pubmed/10421273

Shimada, H., Chatten, J., Newton, W. A., Jr., Sachs, N., Hamoudi, A. B., Chiba, T., . . . Misugi, K. (1984). Histopathologic prognostic factors in neuroblastic tumors: definition of subtypes of ganglioneuroblastoma and an age-linked classification of neuroblastomas. *J Natl Cancer Inst, 73*(2), 405-416. doi:10.1093/jnci/73.2.405

Shimomura, T., Hasako, S., Nakatsuru, Y., Mita, T., Ichikawa, K., Kodera, T., . . . Iwasawa, Y. (2010). MK-5108, a highly selective Aurora-A kinase inhibitor, shows antitumor activity alone and in combination with docetaxel. *Mol Cancer Ther, 9*(1), 157-166. doi:10.1158/1535-7163.MCT-09-0609

Shiotani, B., Nguyen, H. D., Hakansson, P., Marechal, A., Tse, A., Tahara, H., & Zou, L. (2013). Two distinct modes of ATR activation orchestrated by Rad17 and Nbs1. *Cell Rep, 3*(5), 1651-1662. doi:10.1016/j.celrep.2013.04.018

Shyu, A. B., Greenberg, M. E., & Belasco, J. G. (1989). The c-fos transcript is targeted for rapid decay by two distinct mRNA degradation pathways. *Genes Dev, 3*(1), 60-72. doi:10.1101/gad.3.1.60

Siegel, R. L., Miller, K. D., & Jemal, A. (2019). Cancer statistics, 2019. *CA Cancer J Clin, 69*(1), 7-34. doi:10.3322/caac.21551

Sjostrom, S. K., Finn, G., Hahn, W. C., Rowitch, D. H., & Kenney, A. M. (2005). The Cdk1 complex plays a prime role in regulating N-myc phosphorylation and turnover in neural precursors. *Dev Cell, 9*(3), 327-338. doi:10.1016/j.devcel.2005.07.014

Slade, D. (2020). PARP and PARG inhibitors in cancer treatment. *Genes Dev, 34*(5-6), 360-394. doi:10.1101/gad.334516.119

Soucek, L., & Evan, G. I. (2010). The ups and downs of Myc biology. *Curr Opin Genet Dev, 20*(1), 91-95. doi:10.1016/j.gde.2009.11.001

Soucek, L., Helmer-Citterich, M., Sacco, A., Jucker, R., Cesareni, G., & Nasi, S. (1998). Design and properties of a Myc derivative that efficiently homodimerizes. *Oncogene, 17*(19), 2463-2472. doi:10.1038/sj.onc.1202199

Soucek, L., Jucker, R., Panacchia, L., Ricordy, R., Tato, F., & Nasi, S. (2002). Omomyc, a potential Myc dominant negative, enhances Myc-induced apoptosis. *Cancer Res, 62*(12), 3507-3510. Retrieved from https://www.ncbi.nlm.nih.gov/pubmed/12067996

Soucek, L., Nasi, S., & Evan, G. I. (2004). Omomyc expression in skin prevents Myc-induced papillomatosis. *Cell Death Differ, 11*(9), 1038-1045. doi:10.1038/sj.cdd.4401443

Soucek, L., Whitfield, J., Martins, C. P., Finch, A. J., Murphy, D. J., Sodir, N. M., . . . Evan, G. I. (2008). Modelling Myc inhibition as a cancer therapy. *Nature, 455*(7213), 679-683. doi:10.1038/nature07260

Soucek, L., Whitfield, J. R., Sodir, N. M., Masso-Valles, D., Serrano, E., Karnezis, A. N., . . . Evan, G. I. (2013). Inhibition of Myc family proteins eradicates KRas-driven lung cancer in mice. *Genes Dev, 27*(5), 504-513. doi:10.1101/gad.205542.112

Sporbert, A., Domaing, P., Leonhardt, H., & Cardoso, M. C. (2005). PCNA acts as a stationary loading platform for transiently interacting Okazaki fragment maturation proteins. *Nucleic Acids Res, 33*(11), 3521-3528. doi:10.1093/nar/gki665

Staller, P., Peukert, K., Kiermaier, A., Seoane, J., Lukas, J., Karsunky, H., . . . Eilers, M. (2001). Repression of p15INK4b expression by Myc through association with Miz-1. *Nat Cell Biol, 3*(4), 392-399. doi:10.1038/35070076

Stanton, B. R., Perkins, A. S., Tessarollo, L., Sassoon, D. A., & Parada, L. F. (1992). Loss of N-myc function results in embryonic lethality and failure of the epithelial component of the embryo to develop. *Genes Dev, 6*(12A), 2235-2247. doi:10.1101/gad.6.12a.2235

Subramanian, A., Tamayo, P., Mootha, V. K., Mukherjee, S., Ebert, B. L., Gillette, M. A., . . . Mesirov, J. P. (2005). Gene set enrichment analysis: a knowledge-based approach for interpreting genome-wide expression profiles. *Proc Natl Acad Sci U S A, 102*(43), 15545-15550. doi:10.1073/pnas.0506580102

Sugimoto, K., Urano, T., Zushi, H., Inoue, K., Tasaka, H., Tachibana, M., & Dotsu, M. (2002). Molecular dynamics of Aurora-A kinase in living mitotic cells simultaneously visualized with histone H3 and nuclear membrane protein importinalpha. *Cell Struct Funct, 27*(6), 457-467. doi:10.1247/csf.27.457

Sun, C. (2020). The SF3b complex: splicing and beyond. *Cellular and Molecular Life Sciences, 77*(18), 3583-3595. doi:10.1007/s00018-020-03493-z

Sur, S., & Agrawal, D. K. (2016). Phosphatases and kinases regulating CDC25 activity in the cell cycle: clinical implications of CDC25 overexpression and potential treatment strategies. *Molecular and cellular biochemistry, 416*(1-2), 33-46. doi:10.1007/s11010-016-2693-2

Tagami, H., Ray-Gallet, D., Almouzni, G., & Nakatani, Y. (2004). Histone H3.1 and H3.3 complexes mediate nucleosome assembly pathways dependent or independent of DNA synthesis. *Cell, 116*(1), 51-61. doi:10.1016/s0092-8674(03)01064-x

Taguchi, S., Honda, K., Sugiura, K., Yamaguchi, A., Furukawa, K., & Urano, T. (2002). Degradation of human Aurora-A protein kinase is mediated by hCdh1. *FEBS Lett, 519*(1-3), 59-65. doi:10.1016/s0014-5793(02)02711-4

Tang, A., Gao, K., Chu, L., Zhang, R., Yang, J., & Zheng, J. (2017). Aurora kinases: novel therapy targets in cancers. *Oncotarget, 8*(14), 23937-23954. doi:10.18632/oncotarget.14893

Tesi, A., de Pretis, S., Furlan, M., Filipuzzi, M., Morelli, M. J., Andronache, A., . . . Sabò, A. (2019). An early Myc-dependent transcriptional program orchestrates cell growth during B-cell activation. *EMBO Rep, 20*(9), e47987. doi:10.15252/embr.201947987

Thomas, L. R., Foshage, A. M., Weissmiller, A. M., Popay, T. M., Grieb, B. C., Qualls, S. J., . . . Tansey, W. P. (2016). Interaction of MYC with host cell factor-1 is mediated by the evolutionarily conserved Myc box IV motif. *Oncogene, 35*(27), 3613-3618. doi:10.1038/onc.2015.416

Thomas, L. R., Wang, Q., Grieb, B. C., Phan, J., Foshage, A. M., Sun, Q., . . . Tansey, W. P. (2015). Interaction with WDR5 promotes target gene recognition and tumorigenesis by MYC. *Mol Cell, 58*(3), 440-452. doi:10.1016/j.molcel.2015.02.028

Tillery, M. M. L., Blake-Hedges, C., Zheng, Y., Buchwalter, R. A., & Megraw, T. L. (2018). Centrosomal and Non-Centrosomal Microtubule-Organizing Centers (MTOCs) in Drosophila melanogaster. *Cells, 7*(9). doi:10.3390/cells7090121

Trochet, D., Bourdeaut, F., Janoueix-Lerosey, I., Deville, A., de Pontual, L., Schleiermacher, G., . . . Amiel, J. (2004). Germline mutations of the paired-like homeobox 2B (PHOX2B) gene in neuroblastoma. *Am J Hum Genet, 74*(4), 761-764. doi:10.1086/383253

Trumpp, A., Refaeli, Y., Oskarsson, T., Gasser, S., Murphy, M., Martin, G. R., & Bishop, J. M. (2001). c-Myc regulates mammalian body size by controlling cell number but not cell size. *Nature, 414*(6865), 768-773. doi:10.1038/414768a

Tsai, M. Y., Wiese, C., Cao, K., Martin, O., Donovan, P., Ruderman, J., . . . Zheng, Y. (2003). A Ran signalling pathway mediated by the mitotic kinase Aurora A in spindle assembly. *Nat Cell Biol, 5*(3), 242-248. doi:10.1038/ncb936

Umbreit, N. T., Zhang, C. Z., Lynch, L. D., Blaine, L. J., Cheng, A. M., Tourdot, R., . . . Pellman, D. (2020). Mechanisms generating cancer genome complexity from a single cell division error. *Science, 368*(6488). doi:10.1126/science.aba0712

Vader, G., & Lens, S. M. (2008). The Aurora kinase family in cell division and cancer. *Biochim Biophys Acta, 1786*(1), 60-72. doi:10.1016/j.bbcan.2008.07.003

Valentijn, L. J., Koster, J., Zwijnenburg, D. A., Hasselt, N. E., van Sluis, P., Volckmann, R., . . . Versteeg, R. (2015). TERT rearrangements are frequent in neuroblastoma and identify aggressive tumors. *Nat Genet, 47*(12), 1411-1414. doi:10.1038/ng.3438

van Groningen, T., Koster, J., Valentijn, L. J., Zwijnenburg, D. A., Akogul, N., Hasselt, N. E., . . . Versteeg, R. (2017). Neuroblastoma is composed of two super-enhancer-associated differentiation states. *Nat Genet, 49*(8), 1261-1266. doi:10.1038/ng.3899

Vandesompele, J., Baudis, M., De Preter, K., Van Roy, N., Ambros, P., Bown, N., . . . Speleman, F. (2005). Unequivocal delineation of clinicogenetic subgroups and development of a new model for improved outcome prediction in neuroblastoma. *J Clin Oncol, 23*(10), 2280-2299. doi:10.1200/JCO.2005.06.104

Vaughn, J. P., Davis, P. L., Jarboe, M. D., Huper, G., Evans, A. C., Wiseman, R. W., . . . Marks, J. R. (1996). BRCA1 expression is induced before DNA synthesis in both normal and tumor-derived breast cells. *Cell Growth Differ, 7*(6), 711-715. Retrieved from https://www.ncbi.nlm.nih.gov/pubmed/8780884

Veerakumarasivam, A., Goldstein, L. D., Saeb-Parsy, K., Scott, H. E., Warren, A., Thorne, N. P., . . . Kelly, J. D. (2008). AURKA overexpression accompanies dysregulation of DNA-damage response genes in invasive urothelial cell carcinoma. *Cell Cycle, 7*(22), 3525-3533. doi:10.4161/cc.7.22.7042

Vo, B. T., Wolf, E., Kawauchi, D., Gebhardt, A., Rehg, J. E., Finkelstein, D., . . . Roussel, M. F. (2016). The Interaction of Myc with Miz1 Defines Medulloblastoma Subgroup Identity. *Cancer Cell, 29*(1), 5-16. doi:10.1016/j.ccell.2015.12.003

von der Lehr, N., Johansson, S., Wu, S., Bahram, F., Castell, A., Cetinkaya, C., . . . Larsson, L. G. (2003). The F-box protein Skp2 participates in c-Myc proteosomal degradation and acts as a cofactor for c-Myc-regulated transcription. *Mol Cell, 11*(5), 1189-1200. doi:10.1016/s1097-2765(03)00193-x

Vos, S. M., Farnung, L., Boehning, M., Wigge, C., Linden, A., Urlaub, H., & Cramer, P. (2018). Structure of activated transcription complex Pol II-DSIF-PAF-SPT6. *Nature, 560*(7720), 607-612. doi:10.1038/s41586-018-0440-4

Waga, S., & Stillman, B. (1998). The DNA replication fork in eukaryotic cells. *Annu Rev Biochem, 67*, 721-751. doi:10.1146/annurev.biochem.67.1.721

Walz, S., Lorenzin, F., Morton, J., Wiese, K. E., von Eyss, B., Herold, S., . . . Eilers, M. (2014). Activation and repression by oncogenic MYC shape tumour-specific gene expression profiles. *Nature, 511*(7510), 483-487. doi:10.1038/nature13473

Wang, H., Hammoudeh, D. I., Follis, A. V., Reese, B. E., Lazo, J. S., Metallo, S. J., & Prochownik, E. V. (2007). Improved low molecular weight Myc-Max inhibitors. *Mol Cancer Ther, 6*(9), 2399-2408. doi:10.1158/1535-7163.MCT-07-0005

Wang, L. L., Teshiba, R., Ikegaki, N., Tang, X. X., Naranjo, A., London, W. B., . . . Shimada, H. (2015). Augmented expression of MYC and/or MYCN protein defines highly aggressive MYC-driven neuroblastoma: a Children's Oncology Group study. *Br J Cancer, 113*(1), 57-63. doi:10.1038/bjc.2015.188

Watanabe, N., Arai, H., Iwasaki, J., Shiina, M., Ogata, K., Hunter, T., & Osada, H. (2005). Cyclin-dependent kinase (CDK) phosphorylation destabilizes somatic Wee1 via multiple pathways. *Proc Natl Acad Sci U S A, 102*(33), 11663-11668. doi:10.1073/pnas.0500410102

Weiss, W. A., Aldape, K., Mohapatra, G., Feuerstein, B. G., & Bishop, J. M. (1997). Targeted expression of MYCN causes neuroblastoma in transgenic mice. *EMBO J, 16*(11), 2985-2995. doi:10.1093/emboj/16.11.2985

Welcker, M., Orian, A., Grim, J. E., Eisenman, R. N., & Clurman, B. E. (2004a). A nucleolar isoform of the Fbw7 ubiquitin ligase regulates c-Myc and cell size. *Curr Biol, 14*(20), 1852-1857. doi:10.1016/j.cub.2004.09.083

Welcker, M., Orian, A., Jin, J., Grim, J. E., Harper, J. W., Eisenman, R. N., & Clurman, B. E. (2004b). The Fbw7 tumor suppressor regulates glycogen synthase kinase 3 phosphorylation-dependent c-Myc protein degradation. *Proc Natl Acad Sci U S A, 101*(24), 9085-9090. doi:10.1073/pnas.0402770101

WHO, W.H.O. World health organization – estimated number of deaths, worldwide, both sex, all ages (2020). URL: http://www.who.int/.: (01.12.2020)

Williams, D. A., Xu, H., & Cancelas, J. A. (2006). Children are not little adults: just ask their hematopoietic stem cells. *J Clin Invest, 116*(10), 2593-2596. doi:10.1172/jci30083

Wilzen, A., Nilsson, S., Sjoberg, R. M., Kogner, P., Martinsson, T., & Abel, F. (2009). The Phox2 pathway is differentially expressed in neuroblastoma tumors, but no mutations were found in the candidate tumor suppressor gene PHOX2A. *Int J Oncol, 34*(3), 697-705. doi:10.3892/ijo_00000196

Winter, G. E., Buckley, D. L., Paulk, J., Roberts, J. M., Souza, A., Dhe-Paganon, S., & Bradner, J. E. (2015). Phthalimide conjugation as a strategy for in vivo target protein degradation. *Science, 348*(6241), 1376-1381. doi:10.1126/science.aab1433

Wittmann, T., Boleti, H., Antony, C., Karsenti, E., & Vernos, I. (1998). Localization of the kinesin-like protein Xklp2 to spindle poles requires a leucine zipper, a microtubule-associated protein, and dynein. *J Cell Biol, 143*(3), 673-685. doi:10.1083/jcb.143.3.673

Wittmann, T., Wilm, M., Karsenti, E., & Vernos, I. (2000). TPX2, A novel xenopus MAP involved in spindle pole organization. *J Cell Biol, 149*(7), 1405-1418. doi:10.1083/jcb.149.7.1405

Wu, J. C., Chen, T. Y., Yu, C. T., Tsai, S. J., Hsu, J. M., Tang, M. J., . . . Huang, C. Y. (2005). Identification of V23RalA-Ser194 as a critical mediator for Aurora-A-induced cellular motility and transformation by small pool expression screening. *J Biol Chem, 280*(10), 9013-9022. doi:10.1074/jbc.M411068200

Xiao, D., Yue, M., Su, H., Ren, P., Jiang, J., Li, F., . . . Qing, G. (2016). Polo-like Kinase-1 Regulates Myc Stabilization and Activates a Feedforward Circuit Promoting Tumor Cell Survival. *Mol Cell, 64*(3), 493-506. doi:10.1016/j.molcel.2016.09.016

Xu, J., Yue, C. F., Zhou, W. H., Qian, Y. M., Zhang, Y., Wang, S. W., . . . Liu, Q. (2014). Aurora-A contributes to cisplatin resistance and lymphatic metastasis in non-small cell lung cancer and predicts poor prognosis. *J Transl Med, 12*, 200. doi:10.1186/1479-5876-12-200

Yamada, T., Yamaguchi, Y., Inukai, N., Okamoto, S., Mura, T., & Handa, H. (2006). P-TEFb-mediated phosphorylation of hSpt5 C-terminal repeats is critical for processive transcription elongation. *Mol Cell, 21*(2), 227-237. doi:10.1016/j.molcel.2005.11.024

Yamaguchi, Y., Takagi, T., Wada, T., Yano, K., Furuya, A., Sugimoto, S., . . . Handa, H. (1999). NELF, a multisubunit complex containing RD, cooperates with DSIF to repress RNA polymerase II elongation. *Cell, 97*(1), 41-51. doi:10.1016/s0092-8674(00)80713-8

Yamamoto, K., Hanada, R., Kikuchi, A., Ichikawa, M., Aihara, T., Oguma, E., . . . Hayashi, Y. (1998). Spontaneous regression of localized neuroblastoma detected by mass screening. *J Clin Oncol, 16*(4), 1265-1269. doi:10.1200/JCO.1998.16.4.1265

Yang, G., Chang, B., Yang, F., Guo, X., Cai, K. Q., Xiao, X. S., . . . Liu, J. (2010). Aurora kinase A promotes ovarian tumorigenesis through dysregulation of the cell cycle and suppression of BRCA2. *Clin Cancer Res, 16*(12), 3171-3181. doi:10.1158/1078-0432.CCR-09-3171

Yin, X., Giap, C., Lazo, J. S., & Prochownik, E. V. (2003). Low molecular weight inhibitors of Myc-Max interaction and function. *Oncogene, 22*(40), 6151-6159. doi:10.1038/sj.onc.1206641

Yu, X., Minter-Dykhouse, K., Malureanu, L., Zhao, W. M., Zhang, D., Merkle, C. J., . . . Chen, J. (2005). Chfr is required for tumor suppression and Aurora A regulation. *Nat Genet, 37*(4), 401-406. doi:10.1038/ng1538

Zeineldin, M., Federico, S., Chen, X., Fan, Y., Xu, B., Stewart, E., . . . Dyer, M. A. (2020). MYCN amplification and ATRX mutations are incompatible in neuroblastoma. *Nat Commun, 11*(1), 913. doi:10.1038/s41467-020-14682-6

Zeitlin, S. G., Shelby, R. D., & Sullivan, K. F. (2001). CENP-A is phosphorylated by Aurora B kinase and plays an unexpected role in completion of cytokinesis. *J Cell Biol, 155*(7), 1147-1157. doi:10.1083/jcb.200108125

Zeng, K., Bastos, R. N., Barr, F. A., & Gruneberg, U. (2010). Protein phosphatase 6 regulates mitotic spindle formation by controlling the T-loop phosphorylation state of Aurora A bound to its activator TPX2. *J Cell Biol, 191*(7), 1315-1332. doi:10.1083/jcb.201008106

Zhang, D., Hirota, T., Marumoto, T., Shimizu, M., Kunitoku, N., Sasayama, T., . . . Saya, H. (2004). Cre-loxP-controlled periodic Aurora-A overexpression induces mitotic abnormalities and hyperplasia in mammary glands of mouse models. *Oncogene, 23*(54), 8720-8730. doi:10.1038/sj.onc.1208153

Zhang, N., Ichikawa, W., Faiola, F., Lo, S. Y., Liu, X., & Martinez, E. (2014). MYC interacts with the human STAGA coactivator complex via multivalent contacts with the GCN5 and TRRAP subunits. *Biochim Biophys Acta, 1839*(5), 395-405. doi:10.1016/j.bbagrm.2014.03.017

Zhang, Q., West-Osterfield, K., Spears, E., Li, Z., Panaccione, A., & Hann, S. R. (2017). MB0 and MBI Are Independent and Distinct Transactivation Domains in MYC that Are Essential for Transformation. *Genes (Basel), 8*(5). doi:10.3390/genes8050134

Zheng, L., & Shen, B. (2011). Okazaki fragment maturation: nucleases take centre stage. *J Mol Cell Biol, 3*(1), 23-30. doi:10.1093/jmcb/mjq048

Zimmerman, K. A., Yancopoulos, G. D., Collum, R. G., Smith, R. K., Kohl, N. E., Denis, K. A., . . . et al. (1986). Differential expression of myc family genes during murine development. *Nature, 319*(6056), 780-783. doi:10.1038/319780a0

Zubiaga, A. M. (2020). Foreword Special Issue Cell Cycle and Regulation. *Genes (Basel), 11*(3). doi:10.3390/genes11030254

7 Appendix

Supplementary data

Table 7.1: Table of overlapping phosphosites. Phosphoproteomics were performed on chromatin-bound proteins in S phase-synchronized IMR-5 cells treated for 4 h with 1 µM MLN8237, 1 µM MK5108, or DMSO as control. Gene name and protein name on which the phosphorylation was found are shown, as well as the localization probability (Loc prob), the likelihood that the phosphorylation is taking place on the site found, and not on an adjacent site. The amino acid (AA) and the position (pos) as well as within which sequence the phosphorylation was found. As an Aurora-A consensus sequence is identified (Kettenbach et al., 2011), the color the AA indicates a sterically unpreferred AA (red) or a sterically preferred AA (green). The counts (cnt) in DMSO (Ctrl), MK5108 (MK) and MLN8237 (MLN) reflects in how many replicates this site was found. Log_2 fold change (logFC) of MK or MLN versus DMSO and p-value (p) calculated for MK and MLN are shown.

Gene name	Protein name	Loc prob	AA	Pos	Sequence	Ctr cnt	MK cnt	MLN cnt	logFC MK	logFC MLN	p MK	p MLN
ADAR	Double-stranded RNA-specific adenosine deaminase	0.98	S	599	TAE**S**QTP	3	3	2	-0.16	-0.17	0.12	0.14
AHCTF1	ELYS	0.98	S	1218	PSP**S**PRG	3	2	3	-0.45	-0.24	0.01	0.06
AHCTF1	ELYS	1.00	S	1541	RNL**S**FNE	3	3	3	-0.38	-0.41	0.00	0.00
ATAD2	ATPase family AAA domain-containing protein 2	1.00	S	1243	RNN**S**NTC	3	2	2	-0.42	-0.39	0.01	0.01
ATRX	Transcriptional regulator ATRX	0.94	S	729	DQN**S**DSD	2	3	2	-0.40	-0.46	0.10	0.07
ATRX	Transcriptional regulator ATRX	1.00	S	731	NSD**S**DEM	2	2	2	-0.32	-0.18	0.02	0.09
BCLAF1	Bcl-2-associated transcription factor 1	1.00	S	222	YSN**S**PRS	2	3	2	-0.18	-0.21	0.11	0.11
BPTF	Nucleosome-remodeling factor subunit BPTF	1.00	S	2465	QGQ**S**PVR	3	3	3	-0.13	-0.19	0.10	0.03
C11orf30	BRCA2-interacting transcriptional repressor EMSY	1.00	S	168	TVK**S**PRP	3	3	3	-0.19	-0.24	0.12	0.07
CASKIN2	Caskin-2	1.00	S	697	**R**SP**S**QES	2	3	2	-0.31	-0.22	0.02	0.05
CDK11A	Cyclin-dependent kinase 11 A	1.00	S	47	KRD**S**LEE	3	3	3	-0.19	-0.22	0.04	0.02
CDK11B	Cycln-dependent kinase 11 B	1.00	S	47	KRD**S**LEE	3	3	3	-0.19	-0.22	0.04	0.02
CDK11B	Cycln-dependent kinase 11 B	1.00	S	752	RGT**S**PRP	3	3	3	-0.13	-0.37	0.14	0.00
CENPU	Centromere protein U	0.98	S	108	KRS**S**DTS	3	3	3	-0.12	-0.12	0.10	0.10
CENPU	Centromere protein U	0.97	S	111	SDT**S**GNE	2	3	2	-0.17	-0.15	0.11	0.13
CLSPN	Claspin	0.94	S	808	GFR**S**PSP	2	3	2	-0.19	-0.18	0.09	0.11
CTNNBL1	Beta-catenin-like protein 1	1.00	S	545	DGR**S**PEF	3	3	3	-0.12	-0.12	0.10	0.11
DACH1	Dachshund hmolog 1	1.00	S	493	DSP**S**PAP	3	3	3	-0.18	-0.33	0.06	0.00
DBN1	Drebrin	0.83	S	337	PTR**S**PSD	2	3	2	-0.39	-0.51	0.04	0.01
DDX20	Probable ATP-dependent RNA helicase DDX20	1.00	S	672	GNK**S**YLE	3	3	3	-0.16	-0.15	0.08	0.09
DEK	DEK	1.00	S	307	EDS**S**DDE	3	3	3	-0.25	-0.12	0.01	0.13
GTF3C1	General transcription factor 3C polypeptide 1	1.00	S	739	EED**S**QGK	2	3	3	-0.20	-0.20	0.14	0.15
HNRNPUL2	Heterogeneous nuclear ribonucleoprotein U-like protein 2	1.00	S	228	RSK**S**PLP	2	3	3	-0.26	-0.21	0.05	0.09
HUWE1	E3 ubiquitin-protein ligase HUWE1	0.99	S	1907	GTA**S**DDE	2	2	2	-0.19	-0.18	0.08	0.09
IWS1	Protein IWS1 homolog	1.00	S	237	ASD**S**ENE	3	3	3	-0.17	-0.34	0.07	0.00
LEO1	RNA polymerase-associated protein LEO1	1.00	S	277	ARG**S**DSE	3	3	3	-0.11	-0.17	0.12	0.03
LIMCH1	LIM and calponin homology domains-containing protein 1	1.00	S	718	KPK**S**PEP	2	3	3	-0.20	-0.14	0.05	0.13
MAP1B	Microtubule-associated protein 1 B	1.00	S	1396	KVL**S**PLR	2	3	3	-0.19	-0.21	0.09	0.07
MCM2	DNA replication licensing factor MCM2	0.99	S	27	LTS**S**PGR	2	2	2	-0.72	-0.72	0.12	0.12
MPHOSPH8	M-phase phosphoprotein 8	1.00	S	136	EAN**S**DSD	3	3	3	-0.18	-0.14	0.04	0.08
MPHOSPH8	M-phase phosphoprotein 8	1.00	S	138	NSD**S**DQQ	3	3	3	-0.15	-0.13	0.09	0.13
MSH6	DNA mismatch repair protein Msh6	1.00	S	261	IGG**S**DVE	3	3	3	-0.20	-0.15	0.05	0.11

NCOA5	Nuclear receptor coactivator 5	0.92	S	9	SRP**S**PTR	3	2	3	-0.65	-0.60	0.14	0.12
NES	Nestin	0.98	S	471	PPL**S**PDH	2	2	3	-1.17	-0.76	0.04	0.08
NOL8	Nuclear protein 8	1.00	T	888	FLE**T**DSE	2	3	2	-0.22	-0.25	0.06	0.04
NOL8	Nuclear protein 8	1.00	S	890	ETD**S**EEE	3	3	3	-0.14	-0.16	0.11	0.07
NOLC1	Nucleolar and coiled-body phosphoprotein 1	1.00	S	643	ADN**S**FDA	3	3	3	-0.23	-0.39	0.04	0.00
PHF14	PHD finger protein 14	1.00	T	287	EEL**T**NDS	3	3	3	-0.17	-0.11	0.02	0.10
PHF14	PHD finger protein 14	0.99	S	290	TND**S**LTL	3	3	3	-0.18	-0.13	0.02	0.07
PHF14	PHD finger protein 14	1.00	S	302	NED**S**LIL	2	2	2	-0.26	-0.31	0.04	0.02
PHF3	PHD finger protein 3	1.00	S	1722	AQN**S**PSV	3	3	3	-0.13	-0.12	0.09	0.11
PPIG	Peptidyl-prolyl cis-trans-isomerase G	1.00	S	254	SKK**S**ASS	3	2	3	-0.14	-0.11	0.12	0.14
PRPF4B	Serine/threonine-protein kinase PRP4 homolog	1.00	T	576	STR**T**RSP	3	3	3	-0.24	-0.20	0.03	0.05
RACGAP1	Rac GTPase-activating protein 1	1.00	S	203	KTR**S**IGS	2	2	3	-0.29	-0.27	0.07	0.08
RAI1	Retinoic acid-induced protein 1	1.00	S	1374	AGG**S**PVG	3	3	3	-0.15	-0.13	0.10	0.15
RBM15	Putative RNA-binding protein 15	1.00	S	659	SPE**S**DRP	2	3	3	-0.25	-0.19	0.02	0.05
RBM15B	Putative RNA-binding protein 15B	1.00	S	562	RRN**S**LEG	3	3	2	-0.34	-0.30	0.00	0.01
RMI1	RecQ-mediated genome instability protein 1	0.82	S	283	TRQ**S**SFE	2	3	3	-0.27	-0.35	0.03	0.01
RRP9	U3 small nucleolar RNA-interacting protein 2	1.00	S	53	SSD**S**ESE	2	2	2	-0.66	-0.51	0.05	0.09
SAFB2	Scaffold attachment factor B2	0.84	S	234	EES**S**ELE	3	2	2	-0.56	-0.79	0.07	0.02
SCARF2	Scavenger receptor class F member 2	1.00	S	653	LSP**S**PER	3	3	3	-0.17	-0.29	0.08	0.01
SF3B2	Splicing factor 3B subunit 2	1.00	S	307	LGQ**S**ASE	3	3	3	-0.12	-0.15	0.14	0.08
SFSWAP	Splicing factor, suppressor of white-apricot homolog	1.00	S	604	DDD**S**DDD	3	3	3	-0.46	-0.36	0.04	0.08
SMARCA4	Transcription activator BRG1	0.99	S	1382	YSD**S**LTE	2	3	3	-0.26	-0.17	0.02	0.06
SMARCAD1	SWI/SNF-related matrix-associated actin-dependent regulator of chromatin subfamily A containing DEAD/H box 1	1.00	T	54	RAN**T**PDS	3	3	3	-0.15	-0.21	0.13	0.05
SMARCAD1	SWI/SNF-related matrix-associated actin-dependent regulator of chromatin subfamily A containing DEAD/H box 1	1.00	S	57	TPD**S**DIT	3	3	3	-0.20	-0.24	0.09	0.05
SON	SON	1.00	S	2029	RRF**S**RSP	3	3	3	-0.18	-0.17	0.08	0.10
SORT1	Sortilin	1.00	S	825	HDD**S**DED	3	3	3	-0.21	-0.30	0.08	0.02
SRRM1	Serine/arginine repetitive matrix protein 1	1.00	S	713	RRQ**S**PSP	3	2	3	-1.70	-0.86	0.02	0.10
SRRM2	Serine/arginine repetitive matrix protein 2	1.00	S	377	HGG**S**PQP	3	3	3	-0.67	-0.89	0.11	0.05
SRRM2	Serine/arginine repetitive matrix protein 2	0.93	S	857	SIT**S**PQA	3	3	3	-0.24	-0.31	0.11	0.05
SRRM2	Serine/arginine repetitive matrix protein 2	1.00	S	992	HSG**S**ISPY	3	3	3	-0.85	-0.87	0.02	0.02
SRRM2	Serine/arginine repetitive matrix protein 2	1.00	S	1541	RSG**S**SQE	3	3	3	-0.39	-0.21	0.01	0.09
SRRM2	Serine/arginine repetitive matrix protein 2	1.00	S	1542	SGS**S**QEL	3	3	3	-0.19	-0.19	0.03	0.03
SRSF5	Serine/arginine-rich splicing factor 5	0.92	S	208	YSR**S**RKS	2	2	2	-0.76	-0.36	0.01	0.06
SYMPK	Symplekin	1.00	S	1243	EER**S**PQT	3	3	3	-0.16	-0.17	0.14	0.12
THOC2	THO complex subunit 2	1.00	S	1514	KHK**S**ESP	2	2	3	-0.47	-0.33	0.01	0.04
TP53BP1	TP53-binding protein 1	1.00	S	500	PKN**S**PED	3	3	3	-0.13	-0.13	0.10	0.11
TUBA1A	Tubulin alpha-1A chain	1.00	S	48	GDD**S**FNT	3	3	3	-0.30	-0.35	0.01	0.01
WDHD1	WD repeat and HMG-box DNA-binding protein 1	1.00	S	868	AED**S**GEA	2	2	2	-0.21	-0.24	0.09	0.07
YY1	Transcriptional repressor protein YY1	1.00	S	118	GDD**S**DGL	2	2	2	-0.17	-0.19	0.13	0.11
ZC3H18	Zinc finger CCCH domain-containing protein 18	1.00	S	78	EPK**S**QDQ	3	3	3	-0.23	-0.21	0.05	0.06
ZNF687	Zinc finger protein 687	1.00	S	266	FKQ**S**PGH	3	3	3	-0.12	-0.20	0.15	0.02

Table 7.2: Calculation of synergism using Bliss analysis. The figure in which the data are shown as well as further information to identify which condition or cell line was used to for synergism analysis. To calculate synergism, the fraction affected (FA) upon drug treatment 1 or 2 was used to calculate the expected FA according to formula: Expected $FA_{12} = FA_1 + FA_2 – (FA_1 * FA_2)$. The calculated expected FA as well as the observed FA from the experiment is listed. The conclusion was grouped in three categories: Synergism (if the observed FA was at least 9% higher than the expected FA), slight synergism (if the observed FA was 1% - 9% higher than expected FA), all other cases were considered as no synergism.

Figure	Cell line	Drug 1	Drug 2	Expected FA	Observed FA	Conclusion
4.24 a	SH-EP	AZD6738	MLN8237	6.4%	6.3%	No Synergism
4.24 a	SK-NAS	AZD6738	MLN8237	21.0%	18.2%	No Synergism
4.24 a	SH-SY5Y	AZD6738	MLN8237	71.2%	55.6%	No Synergism
4.24 a	IMR-5	AZD6738	MLN8237	51.1%	65.3%	Synergism
4.24 a	NGP	AZD6738	MLN8237	46.2%	65.3%	Synergism
4.24 a	IMR-32	AZD6738	MLN8237	66.5%	64.9%	No Synergism
4.24 b	IMR-5	AZD6738	MK5108	29.7%	39.2%	Synergism
4.24 c	IMR-5	AZD6738	MLN8237	59.9%	61.8%	Slight Synergism
4.24 c	IMR-5 Aurora-A WT	AZD6738	MLN8237	35.1%	38.4%	Slight Synergism
4.24 c	IMR-5 Aurora-A T217D	AZD6738	MLN8237	27.3%	27.9%	No Synergism
4.24 d	IMR-5 24 h	CHIR-124	MLN8237	40.2%	41.5%	Slight Synergism
4.24 d	IMR-5 48 h	CHIR-124	MLN8237	77.9%	68.4%	No Synergism
4.27 b	IMR-5 24 h	Olaparib	MLN8237	25.4%	17.7%	No Synergism
4.27 b	IMR-5 48 h	Olaparib	MLN8237	73.4%	68.5%	No Synergism

Abbreviations

Prefixes	
p	pico
n	nano
µ	micro
m	milli
k	kilo

Units	
°C	degree celsius
A	ampere
Da	dalton
g	gram
h	hour
m	meter
min	minute
M	mol/l
s	second
v/v	volume per volume
w/v	weight per volume

Amino acids	Three-letter abbreviation	Single-letter symbol
Alanine	Ala	A
Arginine	Arg	R
Asparagine	Asn	N
Aspartic acid	Asp	D
Cysteine	Cys	C
Glutamine	Gln	Q
Glutamic acid	Glu	E
Glycine	Gly	G
Histidine	His	H
Isoleucine	Ile	I
Leucin	Leu	L
Lysine	Lys	K
Methionine	Met	M
Phenylalanine	Phe	F
Proline	Pro	P
Serine	Ser	S
Threonine	Thr	T
Tryptophan	Trp	W
Tyrosine	Tyr	Y
Valine	Val	V
Variable amino acid	Any	X

Other abbreviations

4sU	4-thio-uridine
4sU-seq	4sU-sequencing
A box	Activation box
AA	Amino acids
ADRN	Adrenergic
ATM	Ataxia telangiectasia mutated
ATR	Ataxia telangiectasia and Rad3-related
APC/C	Anaphase promoting complex/cyclosome
APS	Ammonium persulfate
AZ1	Antizyme 1
B2M	ß-2-microglobulin
BCA	Bicinchoninic assay
BR-HLH-LZ	Basic region helix-loop-helix-leucine zipper
BSA	Bovine serum albumin
CD	Conformation-disrupting
CDC	Cell division cycle
cDNA	Complementary DNA
CDKs	Cyclin-dependent kinases
CDS	Coding sequence
ChIP	Chromatin immunoprecipitation
ChIP-seq	ChIP-sequencing
CNS	Central nervous system
CRCs	Core regulatory circuitries
CTD	C-terminal domain
D box	Destruction box
DLTs	Dose-limiting toxicities
dNTP	Desoxy nucleoside triphosphate
dsDNA	Double-stranded DNA
Dox	Doxycycline
E-boxes	Enhancer-boxes
EdU	5-ethynyl-2'-deoxyuridine
EV	Empty vector
FC	Fold change
FCS	Fetal calf serum
FDR	False discovery rate
FP	Flavopiridol
G4	G-quadruplex
GSEA	Gene set enrichment analysis
HRP	Horseradish peroxidase
IHC	Immunohistochemistry
INPC	International Neuroblastoma Pathology Classification
INSS	International Neuroblastoma Staging System
IP	Immunoprecipitation
LB	Lysogeny broth
LR	Low-risk neuroblastoma
M	Mitosis

MAX	MYC associated factor X
MB	MYC-box
MES	Mesenchymal
MNA	*MYCN*-amplification
mRNA	Messenger RNA
MS	Mass-spectrometry
MTOCs	Microtubule organizing centers
MTS	Mitochondrial targeting sequence
MXD	MAX dimerization
n	Number of independent biological replicates
NHEJ	Non-homologous end joining
NTC	Non-targeting control
ORC	Origin of replication
PARP1	Poly (ADP-ribose) polymerase 1
PAS	Polyadenylation signal
PBS	Phosphate buffered saline
PCNA	Proliferating cell nuclear antigen
PCM	Pericentriolar material
PCR	Polymerase chain reaction
PEI	Polyethylenimine
PI	Propidium iodide
PLA	Proximity ligation assay
PlaB	Pladienolide B
PP	Protein phosphatase
pre-IC	Pre-initiation complex
pre-RC	Pre-replication complex
qPCR	Quantitative PCR
RNAPII	RNA Polymerase II
RNAPII pSer2	RNAPII phosphorylated at Ser2
RNA-seq	RNA-sequencing
RQI	RNA quality indicator
RT	Room temperature
SAC	Spindle assembly checkpoint
S.D.	Standard deviation
S.E.M.	Standard error of the mean
shRNA	Short hairpin RNA
TAE	Tris-Acetate-EDTA
TBS	Tris buffered saline
TBS-T	TBS with Tween 20
TES	Transcription end site
TH	Tyrosine hydroxylase
TSS	Transcription start site
UPS	Ubiquitin proteasome system
WT	Wild type

Table of figures

Table of tables

Acknowledgement

I would like to thank Prof. Dr. Martin Eilers for the opportunity to perform my master and my PhD work in his laboratory. I am grateful to work on this fascinating project. Additionally, I am thankful for the helpful, structured supervision throughout the studies, the fruitful discussions, and suggestions which enabled a constant scientific progress of the project and myself.

Prof. Dr. Manfred Gessler and Prof. Dr. Stefan Knapp I would like to acknowledge for being the members of my thesis committee and for their valuable comments, which helped in progression of the project.

I would especially like to express my profound gratitude to Dr. Gabriele Büchel who worked together with me on this fascinating project. I really appreciate your patient guidance, fruitful discussions, and thank you for sharing your knowledge with me.
Additionally, I would like to thank Dr. Giacomo Cossa who provided a lot of advice and encouragement throughout the whole time and was always willing to discuss any single aspect of the project.
My office and lab mates I would like to acknowledge for the extremely nice time we had together, trying to make the best out of every single day. And without you, Theresa Endres and Bastian Krenz, it would not have been so motivating.
Thanks to Dr. Ursula Eilers and Dr. Christina Schülein-Völk for all the help with the Operetta and all nice conversations while operating the microscope, as well as to Dr. Carsten Ade, Dr. Peter Gallant, and Apoorva Baluapuri for all the help with sequencing and bioinformatics.
Furthermore, I thank all the current and former members from the Eilers lab and the Department for Biochemistry and Molecular Biology for the encouraging working atmosphere, sharing their knowledge, and supporting with their abilities. And here I especially appreciate the fruitful discussions and the strong cooperation with people of the Mensa-group.
Thanks to Gabriele, Giacomo, Christina, and Steffi who proof-read this work and helped with substantial input in improving this thesis.

Thanks to Gabriele, Giacomo, Theresa, Basti, Michi, Carina, Apoorva, Leonie, Daniel, Oli, Jessy, and Sarah for the great time we had, not only in the lab. Thank you for all the evenings and days we spend together, making my time in Würzburg incredibly nice and unforgettable.

Finally, I want to thank my parents, my sister, and my friends for their encouragement and the support throughout my studies.

Publications

Roeschert I.*, Poon E.*, Henssen A.G., Dorado-Garcia H., Gatti M., Giansanti C., Jamin Y., Ade C.P., Gallant P., Schülein-Völk C., Beli P., Richards M., Rosenfeldt M., Altmeyer M., Anderson J., Eggert A., Dobbelstein M., Bayliss R., Chesler L., Büchel G. & Eilers M. (2021): Combined inhibition of Aurora-A and ATR kinases results in regression of *MYCN*-amplified neuroblastoma. *Nature Cancer,* https://doi.org/10.1038/s43018-020-00171-8

Cossa G., **Roeschert I**., Prinz F., Baluapuri A., Vidal R.S., Schülein-Völk C., Chang Y.-C., Ade C.P., Mastrobuoni G., Girard C., Wortmann L., Walz S., Lührmann R., Kempa S., Kuster B., Wolf E., Mumberg D. & Eilers M. (2020): Localized Inhibition of Protein Phosphatase 1 by NUAK1 Promotes Spliceosome Activity and Reveals a MYC-Sensitive Feedback Control of Transcription. *Molecular Cell,* 77 (6), 1322 – 1339.

Büchel G.*, Carstensen A.*, Mak K.-Y.*, **Roeschert I**., Leen E., Sumara O., Hofstetter J., Herold S., Kalb J., Baluapuri A., Poon E., Kwok C., Chesler L., Maric H. M., Rickman D. S., Wolf E., Bayliss R., Walz S. & Eilers M. (2017): Association with Aurora-A controls N-MYC-Dependent Promoter Escape and Pause Release of RNA Polymerase II During the Cell cycle. *Cell reports,* 21, 3483 – 3497.

* authors contributed equally

Affidavit

I hereby confirm that my thesis entitled: “Aurora-A prevents transcription-replication conflicts in *MYCN*-amplified neuroblastoma” is the result of my own work. I did not receive any help or support from commercial consultants. All sources and/or materials are listed and specified in the thesis.

Furthermore, I confirm that this thesis has not yet been submitted as part of another examination process neither in identical nor in similar form.

Place, Date Isabelle Röschert

Eidesstattliche Erklärung

Hiermit erkläre ich an Eides statt, die Dissertation: „Aurora-A verhindert Transkriptions-Replikationskonflikte in *MYCN*-amplifizierten Neuroblastomen” eigenständig, d. h. selbst-ständig und ohne Hilfe eines kommerziellen Promotionsberaters, angefertigt und keine anderen als die von mir angegebenen Quellen und Hilfsmittel verwendet zu haben.

Ich erkläre außerdem, dass die Dissertation weder in gleicher noch in ähnlicher Form bereits in einem anderen Prüfungsverfahren vorgelegt wurde.

Ort, Datum Isabelle Röschert

Curriculum vitae